TECHNISCHE
UNIVERSITÄT
DARMSTADT

TOPOLOGY, SYMMETRY, AND PHASE TRANSITIONS IN LATTICE GAUGE THEORIES

Vom Fachbereich Physik
der Technischen Universität Darmstadt

zur Erlangung des Grades
eines Doktors der Naturwissenschaften (Dr. rer. nat.)

genehmigte Dissertation von
B.Sc. (Hons.) Samuel Ryan Edwards
aus Adelaide, Australien

Darmstadt 2013
D 17

Referent: Priv. Doz. Lorenz von Smekal
Korreferent: Prof. Dr. Jochen Wambach

Tag der Einreichung: 22.04.2013
Tag der Prüfung: 8.05.2013

To Angela.

ABSTRACT

We study connections between global symmetries, topological objects, and phase transitions in non-abelian gauge theories. The characterization of deconfinement as a spontaneous symmetry breaking transition in SU(N) gauge theories with static quarks, and its description in terms of Z_N interfaces, serve as our motivation. We study $2+1$ dimensional SU(N) gauge theories with $N \leq 4$, which are candidates for the exploitation of universality with corresponding N-state Potts models. Exact results from the $2d$ spin systems are used to obtain critical couplings, transition temperatures, exponents, and the behavior of string tensions at criticality. Kramers-Wannier duality emerges between center vortices and electric fluxes at the phase transition for $N \leq 3$, which is inherited from a finite volume self-duality of the $2d$ N-state Potts models. The form of the duality as a discrete Fourier transform over ensembles with interfaces emphasizes the link between confinement and topology in pure SU(N) gauge theories.

We then investigate monopole inducing boundary conditions in SU(N) grand unified theories with an adjoint Higgs field, and find that non-trivial magnetic charge may be enforced but with several restrictions.

Finally, we introduce dynamical quarks and the curious connection between confinement and their fractional electric charge. Owing to a coincidence of quantum numbers in the matter sector, the Standard Model possesses a hidden global center symmetry that is lost when Quantum Chromodynamics (QCD) is treated as an isolated theory. We discuss the topological implications of this symmetry, and investigate their influence on the phase structure of a 2-color lattice model with quarks that carry also a fractional electric charge.

ZUSAMMENFASSUNG

Wir untersuchen den Zusammenhang zwischen globalen Symmetrien, topologischen Objekten und Phasenübergängen in nicht-abelschen Eichtheorien. Dies ist dadurch motiviert, dass in SU(N) Eichtheorien der Deconfinementübergang mit der spontanen Brechung einer globalen Symmetrie assoziiert werden kann. Am Übergang wird die globale $Z_N \in \mathrm{SU}(N)$ Symmetrie gebrochen. Dies geht einher mit der Unterdrückung von Vortexgrenzflächen zwischen verschiedenen Z_N Zentrumssektoren und liefert eine qualitative und quantitative Beschreibung des Phasenübergangs. Wir untersuchen $2+1$ dimensionale SU(N) Eichtheorien mit $N \leq 4$, da diese Kandidaten für die Nutzung von Universalität mit entsprechenden N-Zustands Potts-Modellen sind. Wir nutzen exakte Resultate aus $2d$ Spinsystemen um kritische Kopplungen, Übergangstemperaturen, Exponenten und das asymptotische Verhalten der Stringtension im kritischen Bereich zu berechnen.

Dabei tritt die Kramers-Wannier-Dualität zwischen Zentrumsvortices und elektrischen Flüssen im kritischen Bereich auf. Diese spiegelt die Selbstdualität eines N-Zustands Potts-Modells auf einem Torus wider. Die Eigenschaften der Dualität als Beziehung zwischen Z_N Zentrumssektoren, und ihre Darstellung in den Eichtheorien, unterstreichen die essentielle Verbindung zwischen dem Deconfinementübergang und nicht-trivialer Topologie in SU(N) Eichtheorien.

Danach betrachten wir Monopol induzierende Randbedingungen in SU(N) großen-vereinheitlichten Theorien mit adjungiertem Higgs-Feld und finden, dass nicht-triviale magnetische Ladung dadurch erzwungen werden kann, allerdings mit einigen Einschränkungen.

Zuletzt führen wir dynamische Quarks und die sonderbare Verbindung zwischen Confinement und ihrer gebrochenzahligen elektrischen Ladung ein. Durch einen scheinbar zufälligen Zusammenhang verchiedener Quantenzahlen besitzt das Standardmodell eine versteckte, globale Zentrumssymmetrie. Diese Symmetrie geht verloren, wenn man QCD als isolierte Theorie betrachtet. Wir diskutieren die topologischen Implikationen dieser Symmetrie und untersuchen ihren Einfluss auf das Phasendiagramm eines $2-$Farb Gittermodells mit dynamischen Quarks.

CONTENTS

1

INTRODUCTION

The marriage of Quantum Chromodynamics (QCD) and the electroweak theory of Weinberg, Glashow and Salam [1, 2, 3] is resilient. It has withstood more than thirty years of collider experiments and accommodated multiple generations of fermions. This Standard Model of particle physics must be extended to account for neutrino oscillations [4, 5], dark matter, gravity, and other theoretical puzzles, but this does not inhibit its potency as a low energy effective theory. Even the recent discovery of a 125 GeV particle at the Large Hadron Collider (LHC) is so far consistent with the textbook electroweak paradigm [6, 7].

Yet our theoretical understanding of the Standard Model remains incomplete. This is especially true of QCD, the theory of conspiring quarks and gluons that contribute the vast majority of the mass of ordinary matter. On the one hand, asymptotic freedom indicates that QCD is weakly interacting at high energies [8, 9], allowing one to identify the partons of deep inelastic electron-proton scattering experiments with the quanta of quark and gluon fields. On the other hand, isolated quarks and gluons have never been observed. What's more, the masses of protons and neutrons are much larger than the sum of the current masses of a handful of 'up' and 'down' quarks [10].

> 'Where are the quarks? Why are we so heavy?'

These questions should be explained by the non-linear nature of QCD at low energies. The interactions of quarks and gluons are not mere perturbations to the kinetic terms of the Lagrangian. They are dominant, allowing for the long-range, infra-red (IR) physics behind quark confinement and dynamical mass generation. The pursuit of an understanding of IR QCD dynamics forms a noteworthy contrast with beyond Standard Model endeavors that include extra symmetries or dimensions. They introduce exotic new physics that become relevant under exotic conditions. These conditions may be out of reach of collider experiments. Meanwhile, QCD is challenging us at room temperature.

The complexity of QCD is not diminished as pressure and temperature are increased to the regimes of colliding nuclei or compact stars. In spite of naive expectations from asymptotic freedom, the soup of quarks and gluons produced by the Relativistic Heavy Ion Collider (RHIC) and the Large Hadron Collider (LHC) does not allow for a simplistic interpretation as a phase of weakly interacting, deconfined particles [11]. Indeed, this 'quark-gluon plasma' (QGP) remains strongly coupled. I will refrain from presenting a sketch of the QCD phase diagram at non-zero pressure (chemical potential) and temperature that is commonly inferred from model studies and theoretical arguments. Such a sketch implies that we have a more complete understanding of strong dynamics than we actually do, especially in regimes of large chemical chemical potential where experimental probes and ab initio calculations are lacking.

While waiting on experimental results from RHIC, LHC and the Compressed Baryonic Experiment at FAIR [12], theorists perform their own experiments by pushing and prodding QCD in various ways. There is much to be learned by changing the number of colors or flavors of quarks, the number of spacetime dimensions, and taking diametric extremes such as the limits of massless or infinitely heavy quarks. By keeping track of the similarities and differences, one has a chance of shaking out the most important qualitative features of QCD.

The long range correlations induced by strong interactions prompt one to consider the large scale structure of the fields. Insight may be gained by identifying the dynamically relevant configurations, and determining their fate as QCD and QCD-like theories become weakly interacting at extreme temperatures and pressure. Such fluctuations tend to be topological and permit a semi-classical interpretation. They are objects such as vortices, monopoles, and instantons, which are closely linked with the existence of global symmetries and whether they are realized or spontaneously broken in various thermodynamic phases [13].

Such themes tie together the work presented in this thesis.[1] Lattice field theory is employed throughout as a non-perturbative tool. Not only does it allow for quantitative calculations with well controlled approximations, but its formulation as a statistical system highlights the parallels between gauge theories and spin systems.

Global center symmetry, which is obtained in the limit of static quarks, is of special interest. It allows one to relate the finite temperature deconfinement transition to the spontaneous magnetization of a spin system. For pure SU(3) gauge theory in $3+1$ d, the transition is weakly first order, so an effective description in terms of spins breaks down at some scale. In Chapter 3 we instead study SU(N) gauge theories in $2+1$ d, which have second order transitions for $N < 4$. The goal is to see how far the correspondence with spin systems can take us, and to gain further insight into the universal aspects of the deconfinement transition. Here we are confronted by the Kramers-Wannier duality of N-state Potts models, which are all self-dual in $2d$. This allows for a precision study of the gauge theories, and emphasizes the topological link between of the effective degrees of freedom at criticality: color electric fluxes and the confining fluctuations which are interfaces between between different center sectors of the theory.

In Chapter 4 we take a detour via magnetic monopoles in grand unified theories. In particular, we search for boundary conditions that allow for a non-perturbative lattice study of 't Hooft-Polyakov monopoles in SU(N) gauge theories with an adjoint Higgs field. We find that suitably twisted C-periodic boundary conditions make this possible, but only for even N. Confinement is not a focus here, but is nevertheless related. The center vortex mechanism of confinement in SU(N) gauge theories has been paralleled by the monopole scenario, which attributes confinement to a dual Meissner effect from a condensate of abelian monopoles. Interpreting the monopole inducing boundary conditions in terms of center vortices highlights their close relationship.

1 The work presented in Chapter 3 was obtained in collaboration with Lorenz von Smekal, and has appeared elsewhere in Refs. [14] and [15], and also with Nils Strodthoff in Refs. [16, 17]. The results in Chapter 4 have appeared in Ref. [18], also in collaboration with Dhagash Mehta and Arttu Rajantie. Several of the results in Chapter 5 have been published in Ref. [19, 20] with Andre Sternbeck, and others stem from a collaboration with Jeff Greensite and Kurt Langfeld.

Unification has a long history as an explanation for the relative quantum numbers of the Standard Model matter fields. This ties into Chapter 5, in which we explore the link between the confinement of quarks and their fractional electric charge. Quarks are the only matter fields in the Standard Model with both a confined color charge and fractional electric charge in units of the electron charge. When QCD is studied in isolation, the introduction of dynamical quarks explicitly breaks center symmetry. Deconfinement may no longer be described by spontaneous symmetry breaking with a well-defined order parameter. The fractional electric charge of quarks leads to a hidden global symmetry that combines the centers of the color and electroweak gauge groups and may have non-trivial implications for the phase structure of the Standard Model. Here we are motivated by the potential resurrection of deconfinement as a true phase transition in the presence of dynamical quarks. To that end, we explore conceptual implications of the hidden symmetry in a toy 2-color model of QCD with half-integer electrically charged quarks.

In anticipation of the final resting place of a dissertation, which is in the hands of other students, the style of writing breaks formality so long as precision is not compromised. The intuitive content of the concepts presented here is sometimes obscured by their strict mathematical definition. Hopefully our pedagogical approach will benefit a future reader.

2 GAUGE THEORIES

Before diving into the meat of this thesis, we will briefly review some formal aspects of gauge theories. The intention is to establish conventions, notation, and a context for the subsequent chapters.

2.1 GAUGE INVARIANCE AND GEOMETRY

Remarkably, both of the pillars of modern physics are based on a local symmetry principle. For Einstein's General Relativity the symmetry is diffeomorphism invariance of spacetime itself. For the field theories of the Standard Model, it is an internal gauge symmetry of the field content that lives upon a spacetime background. In each case, the theory is most beautifully formulated using a geometric perspective.

Start with a complex scalar field $\phi(x) \in \mathbb{C}$ for some spin-0 particle with mass m. The free Lagrangian,

$$\mathcal{L} = \frac{1}{2}(\partial_\mu \phi^*)(\partial^\mu \phi) - \frac{1}{2}m^2 \phi^* \phi, \tag{2.1}$$

is invariant under global gauge transformations,

$$\phi(x) \to e^{-ie\theta}\phi(x), \tag{2.2}$$

that map the vector space $\mathbb{C}$ of field values on to itself. The electric charge e tells us how rapidly the phase of ϕ rotates with θ. Demanding invariance under *local* gauge transformations,

$$\phi(x) \to e^{-ie\theta(x)}\phi(x), \tag{2.3}$$

we may imagine that $\phi(x)$ maps to a unique copy of $\mathbb{C}$ at each spacetime point x, and a local gauge transformation is equivalent to a change of basis for the field space. Fiber bundles provide the appropriate framework for a geometric formulation.[1] In the language of fiber bundles, the vector space $\mathbb{C}$ is called the *standard fiber*, while spacetime M is the *base space*. In this case, the fiber bundle is a manifold that locally has the form of a product $M \times \mathbb{C}$ but may have additional non-trivial global structure. The gauge group is comprised of the set of gauge transformations of a fiber on to itself, which is the abelian group U(1) in this case.

The derivative operator compares field values living at different spacetime points, so a consistent way of transporting vectors from one fiber to another is required. Such a *connection* replaces the ordinary derivative with a covariant one,

$$D_\mu \phi = (\partial_\mu + ieA_\mu)\phi, \quad D_\mu \phi^* = (\partial_\mu - ieA_\mu)\phi^*. \tag{2.4}$$

The introduction of a vector potential $A_\mu(x)$ accounts for the infinitesimal change of coordinates (phase) as we move between fibers belonging to neighboring spacetime points.

1 See Ref. [21] for a readable introduction.

Invariance of the Lagrangian requires that the covariant derivative $D_\mu\phi$ transforms like the field ϕ itself under gauge transformations, which justifies its name. This dictates the transformation law for the vector potential,

$$A_\mu(x) \to e^{-ie\theta(x)}[A_\mu(x) - \frac{i}{e}\partial_\mu]e^{ie\theta(x)} = A_\mu(x) + \partial_\mu\theta(x). \tag{2.5}$$

The scalar field ϕ is *parallel transported* along a spacetime path by demanding that its covariant derivative vanishes. Infinitesimally, one adds a correction,

$$ieA_\mu(x)\phi(x), \tag{2.6}$$

when $\phi(x)$ is transported from x to $x + \delta x$. Transportaton along a finite path γ to some point y is an iterative process that compounds the infinitesimal corrections. They exponentiate,

$$\phi(y) = (\mathcal{P}\exp i\int_\gamma eA_\mu dx^\mu)\phi(x), \tag{2.7}$$

where the path ordering $\mathcal{P}$ reminds us that the infinitesimal transportations are performed successively.

If parallel transportation around a closed loop C is non-trivial,

$$\mathcal{P}\exp i\oint_C eA_\mu dx^\mu \neq 1, \tag{2.8}$$

then the connection has *curvature.* This object is called a loop holonomy. It gives the Aharonov-Bohm phase seen by a quanta of ϕ when it traverses the loop C.

The field strength tensor $F_{\mu\nu}(x)$ is an infinitesimal measure of the curvature. It measures the extent to which parallel transport depends on the path taken. Transporting ϕ around a small square with sides of length ϵ in the (μ, ν) -plane gives the holonomy,

$$\approx 1 + ie\epsilon^2 F_{\mu\nu}, \tag{2.9}$$

where the field strength tensor is the 2-form defined by,

$$F_{\mu\nu} = -\frac{i}{e}[D_\mu, D_\nu] = \partial_\mu A_\nu - \partial_\nu A_\mu + ie[A_\mu, A_\nu], \tag{2.10}$$

and the commutator is trivial for electrodynamics. The addition of the gauge invariant term $-\frac{1}{4}F_{\mu\nu}F^{\mu\nu}$ to the Lagrangian encodes the contribution of the curvature of the connection specified by A_μ, the photon field.

Generally, the vector space of matter fields that form the standard fibers may be in any representation of a gauge group. The quarks of QCD belong to the fundamental representation of SU(3). Each Dirac spin component of a quark field ψ transforms as a Grassman valued 3-vector under SU(3) matrix multiplication. Since the covariant derivative acts infinitesimally on the quark field, the gluon vector potential A_μ lives in the Lie algebra, $\mathfrak{su}(3)$. It is a 3×3 matrix spanned by 8 traceless, hermitian generators,

$$\begin{aligned} &A_\mu(x) = A^A_\mu(x)T^A, \qquad \text{with} \\ &[T^A, T^B] = if^{ABC}T^C, \quad \text{tr } T^A T^B = \frac{1}{2}\delta^{AB}. \end{aligned} \tag{2.11}$$

The non-abelian nature of the group SU(3) is expressed in its Lie algebra $\mathfrak{su}(3)$ via the structure constants f^{ABC}, which encode the commutation properties of T^A. The field strength becomes,

$$G_{\mu\nu} = G^A_{\mu\nu} T^A = \partial_\mu A_\nu - \partial_\nu A_\mu + ig[A_\mu, A_\nu], \tag{2.12}$$

with the strong coupling constant g. The Lagrangian contains a sum over quark flavors

$$\mathcal{L}_{\text{QCD}} = \sum_f \bar{\psi}_f \left(i\gamma^\mu D_\mu - m_f \right) \psi_f - \frac{1}{4} G^A_{\mu\nu} G^{A\mu\nu}, \tag{2.13}$$

where the covariant derivative

$$D_\mu q = (\partial_\mu + igA_\mu)q = (\partial_\mu + igA^A_\mu T^A)q, \ A = 1, \ldots, 8, \tag{2.14}$$

is contracted with anticommuting gamma matrices that are normalized by the metric tensor $g_{\mu\nu}$ for Minkowski spacetime,

$$\{\gamma^\mu, \gamma^\nu\} = 2g^{\mu\nu}. \tag{2.15}$$

In addition to a purely kinetic term, the Yang-Mills action for gluons contributes 3 and 4-point self interactions to strong dynamics. There is also a possible CP violating θ-term that is related to tunnelling between different topological sectors via instantons. It is tightly constrained, however, by the experimental upper bound on the electric dipole moment of the neutron [22] and will henceforth be neglected.

The classical equations of motion are derived from stationary points of the action, $S = \int d^4x \mathcal{L}$, with respect to functional variations of the fields. In electrodynamics, variation with respect to the vector potential

$$\delta S = 0 \Rightarrow \partial_\mu \left(\frac{\partial \mathcal{L}}{\partial(\partial_\mu A_\nu)} \right) - \frac{\partial \mathcal{L}}{\partial A_\nu} = 0 \tag{2.16}$$

yields the inhomogeneous Maxwell equations in covariant notation, with source currents constructed from whichever matter fields are included in the Lagrangian. Applying Noether's theorem to global gauge invariance implies that these same currents are conserved. For QCD, the conserved Noether currents contain contributions from the gluon fields. This wrinkle reflects the fact that, in contrast to the photon field, the gluon field is self-coupled and has a color charge of its own.

2.2 QUANTIZATION

For our purposes the path integral formulation is the most convenient quantization scheme. The vacuum expectation value of some operator $O[\text{fields}]$ corresponding to an observable is given by a phase-weighted average over all possible field configurations,

$$\langle O \rangle = \frac{1}{Z} \int \prod_i \mathcal{D}[\text{fields}] O[\text{fields}] e^{iS}, \quad Z = \int \prod_i \mathcal{D}[\text{fields}] e^{iS}. \tag{2.17}$$

Unfortunately, gauge invariance compounds the difficulty of handling this infinite dimensional integral. The same principle that motivates the beautiful geometric formulation of the classical theory becomes a burdensome overcounting upon quantization. Extracting the physically relevant degrees of freedom from the abundance of field configurations and their gauge copies is an extreme technical challenge.

In continuum perturbation theory, quantization may be achieved in a more or less rigorous fashion using the Becchi-Rouet-Stora-Tyutin (BRST) formalism [23]. This necessitates gauge-fixing and the introduction of auxiliary Faddeev-Popov ghosts that must not appear in asymptotic states. The extension to non-perturbative physics is problematic, however, due to Gribov copies and the difficulties of completely fixing the gauge. The rigorous connection between continuum methods in covariant gauges, such as Dyson-Schwinger equations [24, 25, 26] and the Functional Renormalization Group [27, 28], and lattice formulations with manifest gauge invariance, is a work in progress [29, 30]. In this work, lattice field theory is the weapon of choice.

2.3 LATTICE FIELD THEORY

One can make sense of the path integral by discretizing spacetime.[2] The spacing a between lattice points acts as a regulator for short distance UV behavior and, since we are always limited to a finite number of lattice points, the volume provides an IR regulator. Moreover, a finite number of spacetime points and fields entails a finite number of integrals. As the lattice becomes both larger and more densely populated, computations should converge to those in a continuum formulation and provide a practical definition of the path integral. As always, the devil is in the details. The theory must first be distorted in several ways.

Calculations with a finite number of field configurations are hindered by interference from the complex weights e^{iS} in Eq. (2.17). One way to make progress is to abandon Minkowski spacetime by Wick rotating, $t \to it$, to a Euclidean metric. The action picks up the i from the integral over spacetime, so field configurations are now weighted by a Boltzman factor e^{-S}. The path-integral takes the form of a statistical partition function,

$$Z = \int \prod_{\text{fields}} \mathcal{D}[\text{fields}] e^{-S}. \tag{2.18}$$

Given a way to generate n field configurations with a probability distribution $e^{-S[\text{fields}]}$, expectation values may be then be approximated by,

$$\langle O \rangle \simeq \frac{1}{n} \sum_{i=1}^{n} O[\text{fields}]. \tag{2.19}$$

This is feasible when the weight e^{-S} is real. This is, unfortunately, not always the case. The inclusion of a chemical potential μ for fermion fields generally leads to a complex weight, which is referred to as the fermion sign problem. It prevents lattice methods from fully exploring the QCD phase diagram at finite chemical potential.

2 Ref. [31] is our preferred reference for lattice gauge theory.

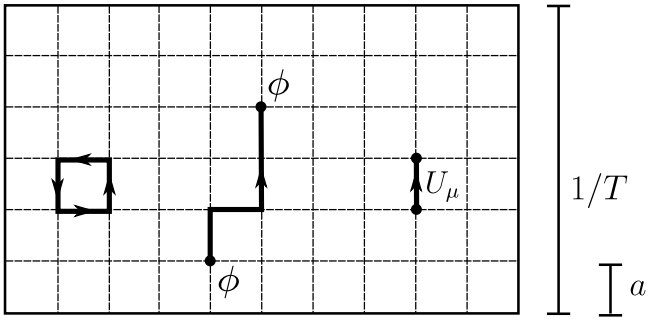

Figure 2.1: Cartoon of the lattice. Links parallel transport the fields ϕ between neighboring spacetime points with lattice spacing a. Plaquettes give the contribution from the field strength tensor, $F_{\mu\nu}$. The inverse of the compact temporal extent determines the temperature T.

2.3.1 *Gauge fields*

Parallel transport of matter fields results in multiplication by a gauge group element, which is built up from successive applications of the Lie algebra valued fields A_μ. As such, it is natural that a lattice formulation is constructed using gauge group elements in place of A_μ. Between neighboring spacetime points x and $x + \hat{\mu}$, with $\hat{\mu}$ in units of the lattice spacing a, one assigns directed group variables, $U_\mu(x)$, that correspond to parallel transport as in Eq. (2.7). In the limit $a \to 0$, the path-ordered exponential is well-approximated by any value for the gauge field along the path,

$$U_\mu(x) \approx \exp[iaA_\mu(x)], \tag{2.20}$$

where the coupling constant g has been absorbed into $A_\mu(x)$.

On the lattice, the curvature of the connection is measured via $a \times a$ square plaquettes. The plaquette in the (μ, ν) plane at x is defined by,

$$\Box_{\mu\nu}(x) = U_\mu(x)U_\nu(x + \hat{\mu})U_{-\mu}(x + \hat{\mu} + \hat{\nu})U_{-\nu}(x + \hat{\nu}), \tag{2.21}$$

where links in the reverse orientation are inverted,

$$U_\mu^\dagger(x) = U_\mu^{-1}(x) = U_{-\mu}(x + \hat{\mu}). \tag{2.22}$$

In the limit $a \to 0$ plaquettes are related to the continuum field strength tensor by,

$$\Box_{\mu\nu} \sim 1 + ia^2 F_{\mu\nu}. \tag{2.23}$$

The contribution of the field strength tensor to the path integral is approximated by a sum over plaquettes to give Wilson's gauge action,

$$S_g = -\sum_{\Box} \frac{\beta}{N} \mathrm{Re}[\mathrm{tr}\, \Box_{\mu\nu}], \tag{2.24}$$

with lattice coupling $\beta = 2N/g^2$ for SU(N). The trace ensures invariance under local gauge transformations $\Omega(x)$,

$$U_\mu(x) \to \Omega^{-1}(x)U_\mu(x)\Omega(x + \hat{\nu}). \tag{2.25}$$

Lattice actions that converge faster than $\mathcal{O}(a^2)$ to the continuum case are constructed by adding operators that are built from larger loops, such as 1×2 rectangles.

The path-integral calls for an integration over gauge field configurations. This means an integration over the gauge group for each link. The measure $dU_\mu(x)$ for a link should be normalizable, and also invariant under gauge transformations, which are just a change of variables. The invariant group measure, or *Haar measure*, is the appropriate choice. The group manifold of SU(2), for example, is isomorphic to the 3-sphere. The Haar measure is then simply the uniform measure on the surface of the sphere inherited from its embedding in $\mathbb{R}^4$. With a measure in hand, one may integrate over each of the finite number of link variables. Expectation values of operators may then be calculated without fixing a gauge.

The most natural operators in lattice theories are loop products of link variables, the analog of the continuum loop holonomies in Eq. (2.8). Gauge invariant loop operators must be closed, both in coordinate and color space. For the latter, this means taking the trace in some representation of the gauge group. Such *Wilson loops* correspond to the parallel transportation of a test charge in the given representation and act as probes of the gauge field fluctuations.

2.3.2 *Matter fields*

So much for the gauge degrees of freedom. Dynamical matter fields are more troublesome.

A single fermion flavor with mass m is described by Dirac spinors $\psi(x)$ and $\bar{\psi}(x)$ living on lattice sites. We will suppress spin and color indices that are summed over in any bilinear expression. Discretization of the fermion action starts with a finite difference approximation for the partial derivative operator,

$$\partial_\mu \psi(x) \to \frac{1}{2a}(\psi(x+\hat{\mu}) - \psi(x-\hat{\mu})). \tag{2.26}$$

Promoting this to a covariant derivative by connecting neighboring sites with parallel transporters $U_\mu(x)$ leads to the naive fermion action,

$$S_F^0 = a^4 \sum_{x,\mu} \bar{\psi}(x)(\gamma_\mu \frac{U_\mu(x)\psi(x+\hat{\mu}) - U_{-\mu}(x)\psi(x-\hat{\mu})}{2a} + m\psi(x)). \tag{2.27}$$

The Euclidean version of the gamma matrices γ_μ satisfy

$$\{\gamma_\mu, \gamma_\nu\} = 2\delta_{\mu\nu}, \tag{2.28}$$

since up and down indices are no longer distinguished. Proceeding naively, we would then integrate over the Grassman fields at each lattice site to include their contribution to the path integral,

$$Z = \int \prod_x \prod_\mu dU_\mu(x) d\psi(x) d\bar{\psi}(x) e^{-S_g - S_F^0}. \tag{2.29}$$

Unfortunately, this doesn't work. The inverse of the bilinear Dirac operator in (2.27) should give the fermion propagator connecting lattice sites. The problem is that

the propagators for fermions pick up poles in momentum space at the edges of the Brillioun zone. For instance, massless fermions pick up a pole at each

$$p_\mu = \pi/a,\ p_\mu \in (-\pi/a, \pi/a], \tag{2.30}$$

in addition to the physical pole at $p_\mu = 0$. These fermion doublers must be removed in the continuum limit.

Wilson suggested the addition of a mass shifting term that vanishes with $1/a$. In compact notation,

$$S_F^0 \to S_F = a^4 \sum_{x,y} \bar{\psi}(x)(1 - \kappa D(x|y)\psi(y), \tag{2.31}$$

where,

$$D(x|y) = \sum_\mu [(1+\gamma_\mu)U_\mu(x)\delta_{y,x+\hat{\mu}} + (1-\gamma_\mu)U_{-\mu}(x)\delta_{y,x-\hat{\mu}}], \tag{2.32}$$

and,

$$\kappa = \frac{1}{2(am+4)}, \tag{2.33}$$

are the hopping matrix and parameter respectively. As $a \to 0$ the fermion doublers become heavy and decouple. The price to pay is that chiral symmetry is explicit broken for any finite lattice spacing. This is a disadvantage that we can live with. A no-go theorem from Nielsen and Ninomiya [32] rules out doubler free lattice actions that are real, local, and have both chiral and translational invariance. One is therefore forced to compromise. Formulations of lattice fermions with better chiral properties, such as domain wall or overlap fermions, require considerable expense and complexity. They are not necessary for our exploratory simulations with dynamical quarks carrying fractional electric charge in Chapter 5.

2.3.3 *Boundary conditions*

In practice, simulations are limited to lattices with a finite physical extent, and the boundary conditions have important consequences.

2.3.3.1 *Temperature*

In the operator formalism, the partition function of a quantum statistical system at finite temperature T is,

$$Z(T) = \text{tr}\ \exp[-\hat{H}/T], \tag{2.34}$$

where $\hat{H}$ is the Hamiltonian. After Wick rotating to imaginary time, $t \to i\tau$, the trace requires translationally invariant boundary conditions (periodic for bosons, anti-periodic for fermions) with respect to the finite temporal extent $1/T$. $Z(T)$ may be then be reexpressed as a functional integral in Euclidean spacetime,

$$Z(T) = \int \prod_{\text{fields}} \mathcal{D}[\text{fields}] e^{-S},\ S = \int_0^{1/T} d\tau \int d^3x \mathcal{L}[\text{fields}]. \tag{2.35}$$

After discretization, this is the thermodynamic limit for taking the spatial volume to infinity for the path-integral calculated on a lattice with a compact temporal

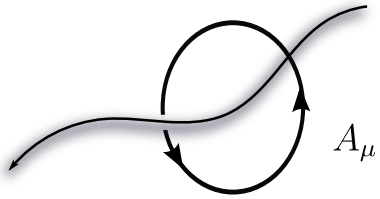

Figure 2.2: Parallel transport of a test charge around a loop measures the enclosed flux, which is described by a loop holonomy as in Eq. (2.8). Symmetries of the action provide the possibility to enforce non-trivial flux on a translationally invariant finite volume.

extent. Any finite lattice whose spatial dimensions are much larger than the longest correlation length in the system is, to a good approximation, in the thermodynamic limit. The temporal extent then fixes the temperature,

$$aN_t = 1/T, \tag{2.36}$$

where N_t is the number of lattice points in the time direction.

This makes the lattice a useful tool for the calculation of thermodynamic quantities and the exploration of the finite temperature phase structure of gauge theories. It is also well-suited for spectroscopy of, e.g., hadron masses at zero temperature, since as $T \to 0$ the lowest lying energy eigenstates that overlap with an operator dominate its expectation value. The trade-off for the ease of access to thermodynamics and spectral properties with a Euclidean metric is that the real-time dynamics are obscured behind the formidable barrier presented by analytic continuation to Minkowski spacetime.

2.3.3.2 *Finite volumes*

The boundary conditions in the spacelike directions should also be translationally invariant. Finite volume surface terms are then avoided, which might otherwise dominate the functional integral. A spacetime torus is the most suitable geometry.

Note, however, that strict periodicity is not required. Boundary conditions are compatible with translational invariance, i.e., the conservation of energy-momentum, so long as they respect the symmetries of the Lagrangian.

Consider, for example, the boundary conditions on the gauge fields, which determine the result of parallel transporting a test charge on some path that wraps around the torus. It is possible for a test charge to measure an Aharonov-Bohm phase (2.8) from enclosed flux as a result of non-trivial boundary conditions, so long as they amount to a symmetry transformation for the dynamic fields that appear in the theory.

For instance, in an SU(N) gauge theory, parallel transporting a fundamental test charge in a closed loop traces out a path on the gauge group manifold of SU(N) that starts from the identity element, according to a path-ordered integral as in (2.8). Taking the trace of the endpoint in SU(N) gives a Wilson loop in the fundamental representation, which corresponds to the gauge invariant Aharonov-Bohm phase picked up by the test charge. Suppose that the loop wraps around one face or cross section of a $1/T \times L^d$ spacetime volume, and that the Aharonov-Bohm phase

picked up by a fundamental test charge is equivalent to a gauge transformation by a Z_N center element,

$$Z_N = \{e^{i2\pi n/N} I,\ n = 0,\ 1, \ldots N-1\} \in \mathrm{SU}(N). \tag{2.37}$$

That is, the field (or wavefunction) ψ belonging to a quark transforms as,

$$\psi \to \mathcal{P} \exp i \oint_C A_\mu dx^\mu \psi = e^{i2\pi n/N} \psi, \tag{2.38}$$

when it is dragged around the loop, in a continuum formulation where A_μ contains the coupling constant g. We may conclude that this cross section is pierced by color flux quantized by Z_N, i.e., a Z_N center vortex.

In the absence of *dynamic* quarks or other fields that represent the center subgroup $Z_N \subset \mathrm{SU}(N)$, such fluxes may be enforced without violating translational invariance or mathematical consistency. First note that there is no issue with multivaluedness if the Lagrangian only contains fields, such as the adjoint gluon field, which transform trivially under $Z_N \subset \mathrm{SU}(N)$ gauge transformations. Parallel transporting a particle in the adjoint representation traces out a closed path in the quotient group $\mathrm{SU}(N)/Z_N$ if the spacetime path encloses Z_N quantized color flux. Particles in the adjoint representation are 'blind' to the flux. From this perspective, the allowed fluxes are determined by the types of closed paths that may be traced out in $\mathrm{SU}(N)/Z_N$. Paths that may be continuously deformed into one another fall into equivalence classes labelled by the first homotopy group,

$$\pi_1(\mathrm{SU}(N)/Z_N) \simeq Z_N, \tag{2.39}$$

which gives a formal topological classification for vortices.

The possibility to construct boundary conditions that enforce non-trivial color flux relies furthermore on the fact that the torus is not simply connected. The Z_N valued jumps in (2.38) for the line integral of A_μ wrapping around a cross section of the finite volume do not necessitate any singularities in the fields. Instead, the system may smoothly interpolate between physically equivalent copies that are related by a Z_N center phase when a loop winds around the torus, which can be kept track of unambiguously via the winding number. From a physical perspective, the fact that the torus is not simply connected means that flux may satisfy a Gauss law while still piercing a finite volume. We may imagine that it closes on itself in the compact directions, or else with mirror fluxes in neighboring volume cells.

The non-perturbative features of gauge theories are often tightly connected with symmetries and the interplay of spacetime and the gauge group via topology. By fixing a theory to a superselection sector with a given vortex or monopole content, it is possible to get a handle on their relevance in various parameter regimes of the theory.

Our description here of boundary conditions and topology only hints at the flavor of the topic. We will have much more to say about topologically non-trivial boundary conditions that induce vortices and magnetic monopoles in Chapter 3 and Chapter 4 respectively. A complete, self-contained review of the mathematics would, however, be at odds with brevity. The interested reader is referred instead to Refs. [21, 33, 34].

3

UNIVERSAL ASPECTS OF CONFINEMENT IN 2 + 1 DIMENSIONS

If quark and gluon fields are the correct building blocks for strongly interacting matter, then QCD must provide an explanation for why we have never observed their quanta as free, individual particles.

> 'They are confined to the interior of hadrons.'

Believing is easy. Deriving confinement from QCD is something else entirely. It is one of the most tenacious problems in all of physics, defying a complete explanation even when we purport to have the underlying model in hand.

It is even difficult to agree on what 'confinement' means. We could take it to mean the absence of color charge from asymptotic gauge invariant quantum states. That is, all of the observed isolated particles are color singlets. This condition is not quite enough, though. It is also satisfied when a theory is in a Higgs phase, in which the charge of a particle is screened by a condensate and dissipates without a Gauss law. In such a case, short range gauge forces ensure that the charge is not observed at long distances. This plasma-style screening is not what one expects from QCD.

Evidently, color charges prefer to form bound states. Bombarding a proton with an energetic electron does not knock out a single quark. Instead it produces more hadrons, which suggests that the color flux of quarks obeys a kind of Gauss law but does not readily spread like electromagnetic flux.

This motivates the idea of a color-electric flux tube between quarks and antiparticles. If the thickness of the tube only weakly depends on the separation distance, then the quark-antiquark potential should be linear at intermediate distance scales. Lattice studies support this, as does the measured angular momentum dependence of meson masses (see Fig. 3.1) [35].

A linear potential would not, by itself, prevent one from isolating a quark an arbitrary distance from other color charges. However, once the flux tube contains enough energy to excite virtual quark pairs from the vacuum it becomes energetically favorable for the tube to break. The energy of the flux tube fuels the production of additional color charges, and one is left with a collection of tightly bound color neutral objects.

It is customary to consider screening by dynamical quarks and the subsequent string-breaking as a separate issue, and to focus on the squeezing of color-electric flux as the most salient aspect of confinement. We may think of the color-electric flux as what is 'confined'. At intermediate distance scales it is justified to ignore quark fluctuations and focus on the gluonic degrees of freedom that direct color flux. Pure Yang-Mills theory, which may only describe *static* fundamental color charges, is therefore an appropriate starting point for understanding confinement.

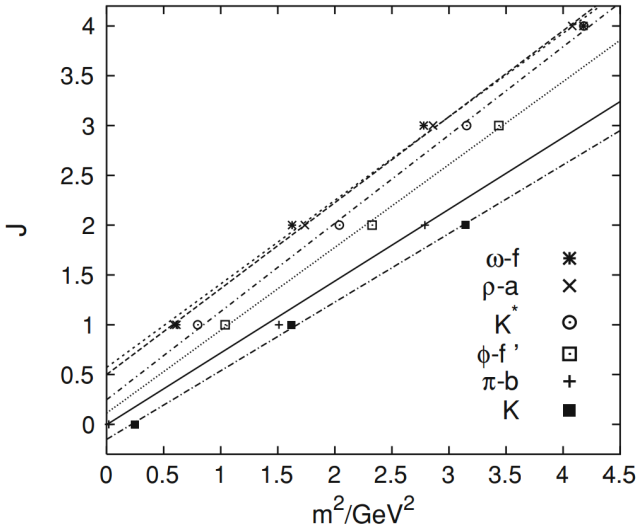

Figure 3.1: The angular momentum dependence of meson masses provides experimental evidence for the formation of an electric flux tube. The linearity of these 'Regge trajectories' is predicted by a spinning-stick model for the flux tube. The figure is from Ref. [35]

So what about asymptotic freedom? The confining mechanism should break down at extreme temperature or pressure, allowing quarks and gluons to take over from hadrons in our intuitive physical picture of mobile (quasi) particles. This is reflected by the breakdown of hadron resonance gas models at high temperature. As more energy is poured into the system, the temperature is restricted to a limiting value by an exponential growth in the density of states [36]. This Hagedorn temperature indicates the temperature scale of deconfinement to be around 160 MeV.

In the limit of static quarks, there is a neat theoretical picture of confinement, originally due to 't Hooft [37]. For pure SU(N) Yang-Mills theory, the finite temperature transition is a true phase transition associated with the spontaneous breakdown of global center symmetry. Spacelike vortices with color-magnetic flux quantized by the Z_N center of SU(N) may be identified as the gauge field fluctuations responsible for the confinement of color-electric flux. They are suppressed with increasing temperature, which eventually results in a spontaneous transition to a deconfined phase.

For the physically relevant case of SU(3) gauge theory in $3+1$ dimensions, this transition is first order. It may be described at criticality by an effective Z_3 spin model, but not perfectly so [38]. Differences in the microscopic physics become relevant at some scale. Reducing the field space via the number of dimensions or colors, however, results in second order transitions that share the universal critical properties of the corresponding spin system (see Fig. 3.2).

In this chapter we study SU(N) gauge theories in $2+1$ d, where SU(2) and SU(3) have second order transitions in the $2d$ Ising and 3-state Potts model universality classes, respectively, and the SU(4) transition is weakly first order at best [39, 40, 41]. We start with a pedagogical review of confinement-deconfinement in pure SU(N) gauge theories from the viewpoint of center vortices and spin interfaces, so as to establish the equivalence of interface inducing 'twisted' boundary conditions

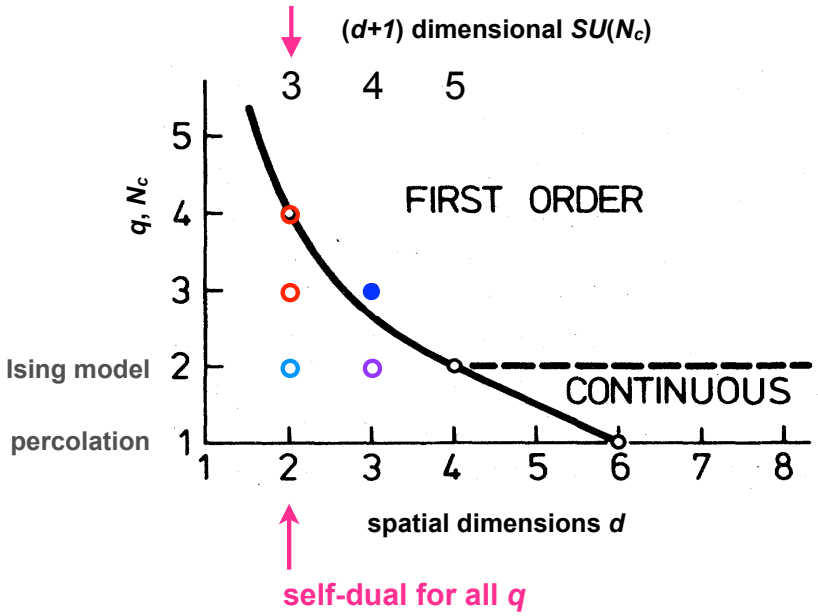

Figure 3.2: Separation line between 1st and 2nd order phase transitions in the q-state Potts models, from [45], and pure SU(N) gauge theories.

in the gauge and spin systems. We then exploit universality to locate the SU(2) phase transition with extreme precision and perform a finite size scaling analysis at criticality. This uncovers a remarkable manifestation of Kramers-Wannier duality between center vortices and the color electric fluxes that they confine, rooted in the self-duality of the $2d$ N-state Potts models.[1]

Our high precision methods apply equally well to SU(3) in $2+1$ d, which we consider briefly before turning to the conundrum of SU(4). There are two riddles here. Scaling that is consistent with the 4-state Potts model has been observed on intermediate lattice volumes [41], despite evidence that the SU(4) transition is first order [39, 40, 41]. Why is the 4-state Potts model favored from the wide class of Z_4 symmetric Ashkin-Teller models? And, what exactly determines the order of a deconfinement transition? It has been conjectured [42, 43, 40, 44] that the change to a first order transition with increasing numbers of colors N develops from a mismatch of degrees of freedom at criticality, namely the glueballs below and deconfined gluon states above T_c. Note, however, that the $2d$ N-state Potts have first order transitions for $N > 4$ (Fig. 3.2), yet cannot have a mismatch of degrees of freedom at criticality because they are self-dual.

1 q is conventionally used to label the number of states of the standard Potts model. We will refer to them as N-state Potts models to match the number of colors in SU(N) gauge theory.

3.1 CONFINEMENT OF COLOR FLUX

Although there are no dynamical sources of fundamental color charge in pure SU(N) gauge theories, static fundamental test charges may still be introduced via traced Wilson loop holonomies,

$$\mathcal{W} = \frac{1}{N}\text{tr}\ \mathcal{P}\exp i\oint_C A_\mu dx^\mu, \tag{3.1}$$

where the trace is required for gauge invariance. Since they tell us how a color charge is parallel transported, these loops are probes of the gauge field fluctuations. Conversely, their expectation value tells us how the system responds to the color flux introduced by the test charge.

A timelike Wilson loop in the fundamental representation is associated with the creation, propagation, and annihilation of a quark-antiquark pair. For large times $\mathcal{T}$, its expectation value gives the potential energy $V(R)$ of a static pair with spatial separation R via [46],

$$\langle \mathcal{W}(R,\mathcal{T})\rangle \sim e^{-V(R)\mathcal{T}}. \tag{3.2}$$

The creation of a confined flux tube implies that the potential should be approximately linear with a string tension σ, $V(R) \sim \sigma R$, which gives an *area law* fall off for large Wilson loops,

$$\langle \mathcal{W}(C)\rangle = \langle \mathcal{W}(R,\mathcal{T})\rangle \sim e^{-\sigma \text{Area}(C)} \quad \text{as} \quad \mathcal{T}\to\infty. \tag{3.3}$$

A timelike Wilson loop therefore serves an order parameter for confinement.

The worldline of a single color charge is singled out by loops that wrap around a compact spacetime direction. The Polyakov loop is such an operator in the time direction,

$$P(\vec{x}) = \frac{1}{N}\text{tr}\ \mathcal{P}\exp i\int_0^{1/T} A_0(\vec{x},0)dt, \tag{3.4}$$

or on the lattice,

$$P(\vec{x}) = \frac{1}{N}\text{tr}\ [U_t(0,\vec{x})U_t(1,\vec{x})\dots U_t(N_t-1,\vec{x})], \tag{3.5}$$

with the product from left to right. It serves as the world line of a static quark at $\vec{x}$ in a system at finite temperature $1/T = aN_t$. The expectation value,

$$\langle P(\vec{x})\rangle = \exp[-F_q], \tag{3.6}$$

gives the free energy per temperature F_q of the color flux of a quark. Confinement implies an infinite free energy in the thermodynamic limit, and hence a vanishing Polyakov loop expectation value. This is a convenient order parameter for our purposes because of its direct relationship with center symmetry.

3.1.1 *Z_N center symmetry*

The vanishing of the Polyakov loop in the confined phase is tied to a global symmetry of pure SU(N) gauge theories. In the absence of dynamical fields that represent the center subgroup,

$$Z_N = \{e^{i2\pi n/N} I; n = 0,\dots,N-1\} \subset \text{SU}(N), \tag{3.7}$$

a constant gauge transformation $z \in Z_N$ has no effect. The constant phases commute and cancel in the transformation law for the gauge fields,

$$A_\mu(x) \to z^*[A_\mu(x) - \frac{i}{g}\partial_\mu]z = A_\mu(x). \tag{3.8}$$

The minimal gauge symmetry is therefore given by the quotient group $\mathrm{SU}(N)/Z_N$. Using $\mathrm{SU}(N)$ results in a redundant description with an an explicit Z_N symmetry.

On the torus, we can define a singular gauge transformation that is periodic in $\mathrm{SU}(N)/Z_N$ but only periodic up to a center phase in $\mathrm{SU}(N)$. A *global center transformation* is such a singular gauge transformation that is non-periodic in the time direction,

$$\Omega(1/T, \vec{x}) = z\Omega(0, \vec{x}),\ z = e^{i2\pi n/N} \in Z_N. \tag{3.9}$$

This is unambiguous if we imagine entering a fresh copy of the system that differs continuously by a Z_N phase when we wind around the torus, as far as a fundamental $\mathrm{SU}(N)$ charge is concerned. The derivative in Eq. (3.8) can then be dropped. Counting the number of windings is not a problem, since the torus is not simply connected. Transformations with $z \neq 1$ correspond to non-contractible loops in $\mathrm{SU}(N)/Z_N$, which are classified by elements of the first homotopy group,

$$\pi_1(\mathrm{SU}(N)/Z_N) = Z_N. \tag{3.10}$$

On the lattice, a global center transformation may be performed by multiplying every link in the final timeslice by the center phase z. The Haar measure is invariant under such a change of variables. So too is the action, since plaquettes pick up an equal number of canceling z and $z*$ phases. When we speak of Z_N center symmetry, we will most often be referring to invariance under these temporal center transformations.

The Polyakov loop counts the winding through center phases. It transforms like,

$$P(\vec{x}) \to zP(\vec{x}). \tag{3.11}$$

When center symmetry is physically realized, configurations in which the Polyakov loop differs by a center phase contribute equally. The expectation value $\langle P(\vec{x})\rangle$ must then vanish, implying an infinite free energy for static quarks. Thus,

$$\langle P(\vec{x})\rangle = \begin{cases} 0, & \text{unbroken } Z_N \text{ symmetry, confined phase.} \\ \text{non-zero}, & \text{broken } Z_N \text{ symmetry, deconfinement phase.} \end{cases} \tag{3.12}$$

3.1.2 *Polyakov loops and spins, interfaces and vortices*

In a landmark paper [38], Svetitsky and Yaffe argued that the spatial components of the gauge fields may be integrated out to give a dimensionally reduced theory of Polyakov loops with short range interactions. Moreover, neighboring loops are ordered at high temperatures by the correspondingly large lattice coupling, which implies the existence of a transition to a deconfined phase.

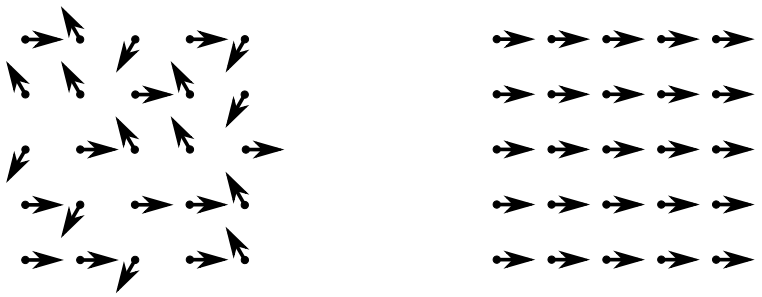

Figure 3.3: Center symmetry is broken in a Z_N symmetric spin or gauge system when it spontaneously orders to a Z_N sector. Equivalently, interfaces between Z_N sectors are suppressed.

A spin model with the same Z_N symmetry then gives an effective description of the gauge theory. Polyakov loops correspond to spins in the sense that their correlators map to one another at T_c. For SU(2) and SU(3) gauge theories, the relevant spin models are nearest neighbor 2 and 3-state Potts models with Hamiltonian,

$$\mathcal{H} = -J \sum_{<s_x,s_y>} \delta(s_x, s_y),\ s_x = e^{i2\pi n/N} \in Z_N,\ J = T/K, \tag{3.13}$$

where the spins are identified with the center phases of SU(N). For SU(N), $N \geq 4$, the coupling J may depend on the relative angle of spins and one must distinguish from a wider class of Z_N symmetric spin systems. From the gauge theory side, this means that there is more than one type of interface between ordered Z_N center sectors.

The Z_N symmetric phase of the spin system is one of disorder. Clusters with a given spin are separated by interfaces that percolate throughout the volume such that the magnetization vanishes. In the gauge theory, the analogous topological defects separate regions in which the Polyakov loop differs by a center phase $z \in Z_N$. This defines a color-magnetic object known as a spacelike center vortex, which is line-like in $2+1$ d or surface-like in $3+1$ d. The flux of a vortex is quantized by the center element $z \in Z_N$. It corresponds to the phase picked up by a fundamental color charge when it is parallel transported around the vortex.

Just as spontaneous magnetization in a Z_N-spin system coincides with the suppression of spin interfaces, the ordering of the Polyakov loop coincides with the suppression of spacelike center vortices. These equivalent descriptions of the symmetry breaking transition set the scene for the formal order-disorder dualities that we will establish later.

The excess free energies of color electric fluxes and spacelike center vortices are complementary order parameters. To make this relationship more precise, we need a way of measuring these free energies. This is possible with topologically nontrivial boundary conditions that exploit global Z_N symmetry.

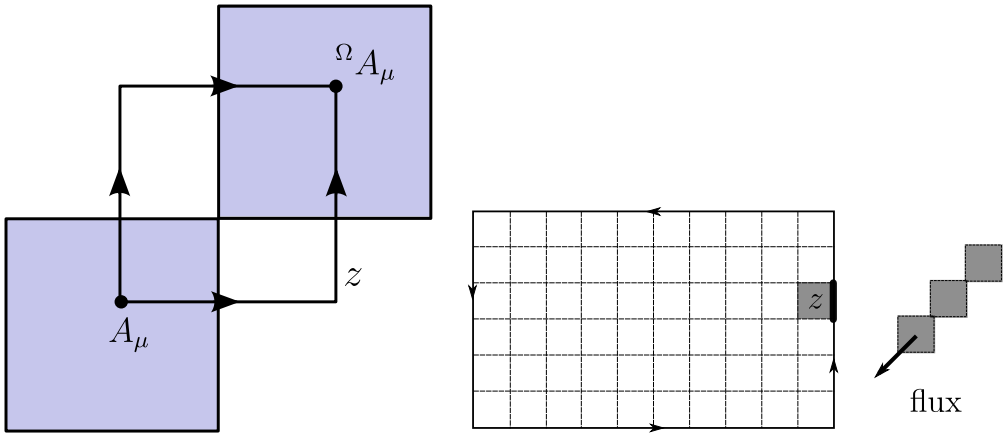

Figure 3.4: Twisted boundary conditions (left) insert an interface, or vortex, between Z_N center sectors, which pierces a cross section of the volume. Shown on the lattice (right). Test charges measure the enclosed center flux when transported around the vortex.

3.2 TWISTED ENSEMBLES

3.2.1 *Interfaces between Z_N sectors*

A spin interface in the N-state Potts model is introduced by choosing boundary conditions that are periodic up to a cyclic shift of the spins,

$$s(\vec{x} + L\hat{\imath}) = e^{i2\pi n/N} s(\vec{x}), \tag{3.14}$$

where L is the number of spins in the $\hat{\imath}$ direction. The system must rotate between Z_N sectors when we wind around the $\hat{\imath}$ direction, which guarantees the existence of an interface that runs in the orthogonal directions. These boundary conditions insert an anti-ferromagnetic seam. The fluctuating system adapts, and the excess free energy compared to the periodic ensemble measures the cost of the interface.

We need the analogous method of forcing an SU(N) gauge system into a mixture of Z_N sectors. This is provided by 't Hooft's twisted boundary conditions [47].

Suppose that we have a compact $1/T \times L^d$ torus. Configurations that are related by local gauge invariance are physically identical, so we only have to impose periodicity up to a gauge transformation $\Omega_\nu(x)$ in each direction. Gauge fields that are separated by the lengths L_μ in the compact directions are then related by,

$$A_\mu(x + L_\nu) = \Omega_\nu^{-1}(x)[A_\mu(x) - \frac{i}{g}\partial_\mu]\Omega_\nu(x), \tag{3.15}$$

or on the lattice,

$$U_\mu(x + L_\nu) = \Omega_\nu^{-1}(x) U_\mu(x) \Omega_\nu(x + \hat{\nu}). \tag{3.16}$$

Successive translations in a (μ, ν)-plane must not depend on the order in which they are applied. Since the gauge fields are blind to global Z_N gauge transformations, the gauge transformations resulting from successive translations may differ by a

constant $z_{\mu\nu}$ center phase. It cancels in the transformation law (3.15). This leads to the cocycle condition,

$$\begin{aligned} &\Omega_\mu(x+L_\nu)\Omega_\nu(x) = z_{\mu\nu}\Omega_\nu(x+L_\mu)\Omega_\nu(x),\ L_\mu \\ &z_{\mu\nu} = \exp\left(2\pi i n_{\mu\nu}/N\right), \text{with } n_{\mu\nu} = -n_{\nu\mu} \in \{0,1,\ldots,N-1\}. \end{aligned} \tag{3.17}$$

Boundary conditions with the same $z_{\mu\nu}$ twist are physically equivalent.

To implement twist on the lattice, one usually chooses transformations $\Omega_\nu(x)$ such that there is one non-periodic link in every (μ,ν)-plane. Consider twist in a (t,i)-plane. The choice,

$$\Omega_t = I,\ \ \Omega_i(t) = \begin{cases} I,\ t=0 \\ z,\ t>0 \end{cases} \tag{3.18}$$

provides non-trivial boundary conditions for a single timelike link in every (t,i)-slice

$$U_t(0,\vec{x}+L\hat{i}) = zU_t(0,\vec{x}). \tag{3.19}$$

The Polyakov loop inherits the boundary condition

$$P(\vec{x}+L\hat{i}) = zP(\vec{x}). \tag{3.20}$$

This means that we must cross a spacelike center vortex when we traverse the volume in the $\hat{i}$ direction. The stack of plaquettes in the (t,i)-plane that contain the non-trivial links in Eq. (3.19) are modified by $\square_{it} \to z\square_{it}$ compared to the untwisted system. They are closed by lattice periodicity and mark the insertion of center flux (Fig. 3.4).

In the language of holonomies, parallel transport of a color charge around a (t,i) cross section of the lattice measures the enclosed flux quantized by,

$$\pi_1(\mathrm{SU}(N)/Z_N) \simeq Z_N. \tag{3.21}$$

These boundary conditions correspond to a gauge transformation that is singular about this loop, in the same way that global center transformations are singular in the compact time direction.

Twists in temporal planes are the relevant ones for confinement, since they enforce interfaces between Polyakov loop center sectors. The partition functions for an ensemble with a given temporal twist are labeled by $Z_k(\vec{k})$, where $k_i = n_{0i},\ i = 1,\ldots,d-1$.

Twists in spatial planes introduce magnetic center flux $\vec{m}$ defined by $n_{ij} = \epsilon_{ijk}m_k$ in $3+1$ d or simply $n_{ij} = \epsilon_{ij}m$ in $2+1$ d. Magnetic twist is related to the worldlines of static center monopoles, which condense on both sides of the deconfinement transition [48, 49].[2] These are timelike objects with no analog in an effective spin description of the gauge theory. We will not take advantage of these twists in what follows and will suppress the index $\vec{m}$. We will come back to magnetic twist in Chapter 4, where it is used to enforce magnetic charge in grand unified $\mathrm{SU}(N)$ theories with an adjoint Higgs field.

2 Combinations of magnetic with electric twists can be used, however, to force fractional topological charge and to measure the topological susceptibility without cooling [49].

When center flux is enforced with non-trivial center flux $\vec{k}$, it is not restricted to thin vortices. This would correspond to a sharp seam between Z_N sectors with a huge cost in action. The transition can instead be gradual. The interface can dynamically thicken and fluctuate so as to lower its free energy. Lattice studies suggest that the size of center vortices stabilizes at about 1 fm [13].[3]

The excess free energy of an ensemble with twist is given by the ratio over the strictly periodic ensemble,

$$\frac{Z_k(\vec{k})}{Z_k(\vec{0})} \equiv e^{-F_k(\vec{k};T,L)}. \tag{3.22}$$

If this approaches unity, center vortex interfaces have negligible free energy and may freely disorder the system. That is, Z_N center symmetry is manifest. In this case, entropy promotes pair creation of vortices and center flux is only conserved modulo N. The free energy $F_k(\hat{\imath};T,L)$ should be thought of as the cost an *additional* vortex.

3.2.2 *Electric fluxes*

Ensembles with fixed color electric flux may be constructed from those with fixed (spacelike) center flux $\{Z_k(\vec{k})\}$, and therefore give the free energy F_e of static color charges in an elegant, gauge invariant manner. 't Hooft's original construction [47] relied on projection operators in the Hamiltonian formulation. Here we will follow the more intuitive picture in terms of Polyakov loops that was put forward in Ref. [50] and refined in Ref. [15].

The free energy of color-electric fluxes is usually measured via Wilson loops or Polyakov loop correlators on strictly periodic ensembles. Gauss' law then forbids a net source of color-electric flux, which causes several headaches. Correlators for Polyakov loops separated by the system length L must be trivial in every direction. The correlators for charge pairs must then be constructed within the confines of the finite periodic volume, and one is stuck with ultraviolet self-energy contributions along the measured loops that require renormalization. Moreover, the gauge variant singlet and adjoint contributions to the naive expectation value $\langle P(\vec{x})\, P(\vec{y})^\dagger \rangle$ are difficult to disentangle [51].

The enlarged set of ensembles $\{Z_k(\vec{k})\}$ provide a remedy. Non-trivial correlators between Polyakov loops in neighboring volume cells are possible because they may belong to different Z_N sectors, i.e., these loops are sensitive to the phase $e^{i2\pi k_i/N}$ from crossing a twist-induced spacelike center vortex. This means that non-zero expectation values are possible for correlators between charges in neighboring cells, which can be used to define the free energy of the color flux that runs between them.

Some care must be taken when constructing a gauge invariant Polyakov loop correlator for a static quark at $\vec{x}$ and its antiparticle at $\vec{x} + L\hat{\imath}$, because the world lines may belong to different center sectors if there is non-zero twist. The correlator should be constructed from a closed loop to properly take into account the transition functions $\Omega_\mu(x)$ when we wind around the torus. For a single untraced

3 This thickening is essential to generate an intermediate string tension for different N-ality (e.g. center blind) representations [13].

Polyakov loop this amounts to undoing the effect of the transition function $\Omega_t(0,\vec{x})$ in the time direction,

$$\mathfrak{P}(\vec{x}) = \Omega_t(0,\vec{x})U_t(\vec{x},1)U(\vec{x},2)\dots U_t(\vec{x},1/T-1) \in \mathrm{SU}(N), \tag{3.23}$$

where Gothic notation is used to distinguish this from the usual lattice definition. It is then gauge invariant under possibly non-periodic gauge transformations that may change the transition functions but not the physical twist sector.

When forming a correlator with separation $L\hat{i}$, the trace in color space must be taken *after* forming a product of untraced Polyakov loops (3.23), so that the spatial transition functions may be taken into account. Carefully applying the cocycle condition (3.17) and the boundary conditions for the gauge fields (3.16), one finds that the phases $e^{2\pi i k_i/N}$ are picked up in the product $\mathfrak{P}(\vec{x})\mathfrak{P}^\dagger(\vec{x}+\hat{i}L)$. Parallel transport picks up the center flux, as expected. Taking the trace and forming an average over the twisted ensembles $\{Z_k(\vec{k})\}$ gives,

$$\frac{1}{N}\left\langle \mathrm{tr}\Big(\mathfrak{P}(\vec{x})\mathfrak{P}^\dagger(\vec{x}+\hat{i}L)\Big)\right\rangle_{\text{no-flux}} = \sum_{\vec{k}\in Z_N^d} e^{2\pi i k_i/N}\, Z_k(\vec{k}) \Big/ \sum_{\vec{k}\in Z_N^d} Z_k(\vec{k}). \tag{3.24}$$

When performing successive translations to create a diagonal separation $L\vec{e} \in LZ_N^d$, one picks up the twists along the way and obtains a discrete Fourier transform over the twist vector $\vec{k}$,

$$\frac{1}{N}\left\langle \mathrm{tr}\Big(\mathfrak{P}(\vec{x})\mathfrak{P}^\dagger(\vec{x}+\vec{e}L)\Big)\right\rangle_{\text{no-flux}} = \sum_{\vec{k}\in Z_N^d} e^{2\pi i\, \vec{e}\cdot\vec{k}/N}\, Z_k(\vec{k}) \Big/ \sum_{\vec{k}\in Z_N^d} Z_k(\vec{k}). \tag{3.25}$$

The correlator in Eq. (3.25) creates the color electric flux corresponding to a color charge in the direction of a mirror charge displaced by $\vec{e}L$. If $e_i > 1$, then the electric flux wraps several times around the lattice to give multiple units of flux in the same direction. Ratios of the electric flux partition functions $Z_e(\vec{e}) \propto \sum_{\vec{k}} e^{2\pi i\, \vec{e}\cdot\vec{k}/N} Z_k(\vec{k})$ subsequently define the excess free energy of electric fluxes via

$$\frac{Z_e(\vec{e})}{Z_e(\vec{0})} \equiv e^{-F_e(\vec{e};T,L)}. \tag{3.26}$$

The subscript 'no-flux' is a reminder that the expectation value is normalized with respect to the sum $\sum_{\vec{k}\in Z_N^d} Z_k(\vec{k})$ with $\vec{e} = \vec{0}$.

Note that there is no explicit computation of loop operators, so the self-energy of static color charges does not contribute to the free energy. The dynamic spreading of center flux in the twisted ensembles $Z_k(\vec{k})$ prevents any singular behavior.

The spreading of center flux in Euclidean space also provides a intuitive picture for the deconfinement transition. At low temperatures the compact temporal direction is large and does not prevent spacelike center vortices from spreading their flux over a large area. As temperature is increased, however, they are gradually squeezed by the finite extent $1/T$. The system, must more abruptly rotate between center sectors. At some critical temperature T_c, the increased cost of interfaces overwhelms the entropic contribution to their free energy and spacelike center vortices are completely suppressed. One is stuck with systems in a given center sector and only the strictly periodic ensemble $Z_k(\vec{0})$ contributes to the electric flux partition

functions. This breaks center symmetry and signals deconfinement through vanishing electric flux free energies $F_e(\vec{e})$. As the deconfinement temperature is crossed from below, center and electric flux free energies reflect this via the dual relationship,

$$\begin{aligned} \frac{Z_k(\vec{k})}{Z_k(\vec{0})} &\to 0, \quad F_k(\vec{k}; T, L) \to \infty, \\ \frac{Z_e(\vec{e})}{Z_e(\vec{0})} &\to 1, \quad F_e(\vec{e}; T, L) \to 0. \end{aligned} \tag{3.27}$$

3.3 UNIVERSALITY

If the Z_N breaking deconfinement transition of an SU(N) gauge theory is first order, a dimensionally reduced spin system can only provide an effective description. The correlation length ξ is finite, so the effect of microscopic physics shows up at some scale. If both systems have a second order transition, however, then the correlation length ξ diverges at criticality. Svetitsky and Yaffe conjectured that the phase transitions should then have the same universal properties [38].

This is explained by the renormalization group (RG).[4] As the correlation length diverges, the system becomes self-similar at all scales. The microscopic features of the system are encoded in irrelevant operators that vanish at criticality, leaving behind the few relevant operators that are responsible for macroscopic physics. These are the operators that are shared by theories in the same *universality* class. As scale invariance emerges at criticality, models in the same universality class may be thought of as different realizations of the same theory, with a dictionary relating their operators.

In the vicinity of criticality, thermodynamic quantities exhibit scaling laws. For a finite temperature transition, the correlation diverges like,

$$\xi = \xi^0_{\pm}|t|^{-\nu} + \cdots , \quad t = \frac{T}{T_c} - 1 \to 0^{\pm} . \tag{3.28}$$

Other thermodynamic quantities follow suit and diverge with their own critical exponents. For instance, the specific heat C and susceptibility χ scale with exponents,

$$C \sim |t|^{-\alpha}, \; \chi \sim |t|^{-\gamma}, \tag{3.29}$$

while the order parameter, which is the magnetization $|M|$ in a spin system, scales above T_c like,

$$|M| \sim (-t)^{\beta}, \quad t = \frac{T}{T_c} - 1 \to 0^{+}. \tag{3.30}$$

The renormalization group predicts that these exponents should be the same for all models in the same universality class, and, moreover, not all independent. Several scaling, and for $d < 4$, 'hyperscaling' relations reduce the number of critical exponents needed to specify a universality class. The amplitudes, on the other hand, depend on microscopic physics. Nevertheless, they are not all independent. RG predicts the universality of several amplitude ratios [52].

Universality is an extremely powerful tool, as it allows one to use the simplest model in a universality class to make quantitative statements about all of its universal partners.

Unfortunately, the finite temperature transition of SU(3) in $3+1$ d falls just short of universality. It is first order, but only weakly so. Reducing the number of colors or dimensions leads theories with second order transitions. SU(2) in $3+1$ d is in the universality class of the $3d$ Ising model, while SU(2) and SU(3) in $2+1$ d are in the universality classes of the corresponding $2d$ N-state Potts models.

Each of these spin systems possess an exact dual. The $3d$ Ising model is dual to Z_2 gauge theory in $2+1$ d, while the $2d$ N-state Potts models are all self-dual.

4 See [52] for a thorough review.

These dualities are tied to the global symmetries and topology of the theories and emerge at criticality for all models in the same universality class.

In what follows we focus on gauge theories in $2+1$ d, which allows us to explore universality for $N = 2,\ 3$ and the borderline case $N = 4$.

3.3.1 *Universality of interface free energies*

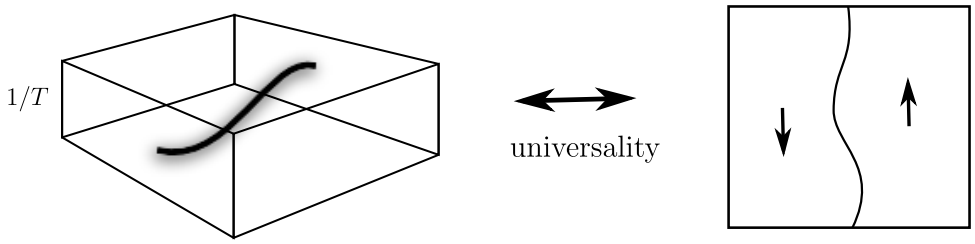

Figure 3.5: Center vortices between Z_N center sectors in SU(N) gauge theories (left) correspond to spin interfaces (right).

The analogy of spins and Polyakov loops becomes exact for systems in the same universality class in the sense that their correlators map to those of same scale invariant theory at criticality. There is then an equivalence between Z_N interfaces. Spin ensembles with cyclically shifted boundary conditions,

$$s(\vec{x} + L\hat{i}) = e^{i2\pi n/N} s(\vec{x}), \tag{3.31}$$

map to gauge ensembles with temporal twist,

$$P(\vec{x} + L\hat{i}) = e^{i2\pi n/N} P(\vec{x}), \tag{3.32}$$

and we can relate the respective free energies F_I of spin interfaces and center vortices F_k,

$$F_I(\vec{k}) = -\ln \frac{Z^{(\vec{k})}}{Z^{(0)}}, \text{ and,} \tag{3.33}$$

$$F_k(\vec{k}) = -\ln \frac{Z_k(\vec{k})}{Z_k(0)}, \tag{3.34}$$

where the partition functions with cyclically shifted spins are denoted by $Z^{(\vec{k})}$. At criticality, these free energies converge to the same universal value, which depends on the aspect ratio of the lattice but not on the specific model.[5]

Real systems are necessarily finite, so the divergence of the correlation length ξ is tempered. In the vicinity of a phase transition the relevant scale is set by the ratio of the box size and the correlation length, assuming that the correlation length is already much larger than the lattice spacing. Generalized couplings with fixed points such as the interface free energies become functions of $L/\xi \sim L^{1/\nu} t$ [52]. This means that the behavior of vortices in the gauge theory is universal with spin interfaces not only at T_c, but also in a window around criticality. Once the physical

5 A argument for the universality of such partition function ratios is given in Ref. [53].

units for the correlation length in each model have been matched, interface free energies share the same universal function of the scaling variable $x = L^{1/\nu}t$,

$$F_I(\vec{k}, L, T) = f_I(\vec{k}, L^{1/\nu}t)\ , t = T/T_c - 1, \tag{3.35}$$

up to some finite volume correction to scaling of order $L^{-\omega}$. Results for spin interfaces can then be exploited in the gauge theory via the universal functions $f_I(\vec{k}, L^{1/\nu}t)$. In what follows we will use f_I as shorthand for the universal function for an interface with $\vec{k} = (1, 0)$.

3.4 EXPLOITING UNIVERSALITY

We begin with SU(2) in $2+1$ d, where universality is especially powerful. In this case, *exact* partition function solutions are available for the $2d$ Ising model for all combinations of periodic and antiperiodic boundary conditions on finite rectangular lattices [54]. So the universal functions $f_I(\vec{k}, L^{1/\nu}t)$ may be computed with arbitrary accuracy.

First we use the exact universal value at criticality, $f_I(0)$, for $\vec{k} = (1, 0)$, to locate the SU(2) deconfinement transition on the lattice with high precision. We will then perform a finite size scaling analysis of vortex and electric flux free energies. The self-duality of the $2d$ Ising model surfaces in their behavior about T_c, which uncovers a link between the Z_N-Fourier transform for color electric fluxes and the embodiment of self-duality for N-state Potts models on the torus.

3.4.1 *Locating the* SU(2) *deconfinement transition*

In Ref. [53], Hasenbusch exploited the fixed point of the interface free energy to locate the phase transition in the $3d$ Ising model via the pairwise intersections of partition function ratios on finite volumes. He found that these estimates provide much more rapid convergence than those obtained from another phenomenological coupling, the Binder cumulant [55, 56].

For SU(2) in $2+1$ d, pairwise intersections are not required, because the universal critical value for the interface free energy is exactly known. For a straight interface in the square $2d$ Ising model [57],

$$\lim_{N\to\infty} -\ln(Z^{(1,0)}/Z^{(0,0)}) = f_I(0) = \ln(1 + 2^{3/4}). \tag{3.36}$$

Since the SU(2) lattice spacing $a \equiv a(\beta)$ sets the relationship between temperature and lattice coupling β via $1/T = N_t a$, where N_t is the number of sites in the time direction, the critical temperature T_c corresponds to an N_t dependent coupling $\beta_c(N_t)$. Provided that the length $L = N_s a$ in the spacelike directions is large enough, the intersection of the vortex free energy F_k with the universal value provides an accurate determination of $\beta_c(N_t)$.

The temperature is linear in the lattice coupling to leading order at T_c, so we assume a finite size scaling (FSS) ansatz of the form

$$\begin{aligned} F_k &= -\ln(Z_k(1,0)/Z_k(0,0)) \\ &= (1 + 2^{3/4}) + b(\beta - \beta_c)N_s^{1/\nu} + cN_s^{-\omega} + \dots \end{aligned} \tag{3.37}$$

where the correction to scaling exponent ω should be approximately independent of N_t, and $\nu = 1$ is exactly known from the $2d$ Ising model. The requirement that the corrections to the universal value in (3.37) vanish defines a pseudo-critical coupling,

$$\beta_c(N_t, N_s) \quad = \quad \beta_c(N_t) - \frac{c}{b} N_s^{-(\omega+1/\nu)} + \dots \tag{3.38}$$

that can be calculated for several finite lattices and extrapolated to infinite volumes.

3.4.2 *Numerical recipe*

Twist is implemented in the usual way [58]. The center phases for the non-periodic links in (3.19) may be incorporated into the action by observing that they multiply a stack of plaquettes perpendicular to the twisted plane. For SU(2) we can therefore use periodic boundary conditions but flip the coupling $\beta \to -\beta$ for these plaquettes. This inserts a thin Z_2 vortex into the action in an analogous way to inserting an interface in the Ising model via a seam of anti-ferromagnetic couplings.

In practice, the overlap of $Z_k(1,0)$ and $Z_k(0,0)$ is poor and a direct measurement of their ratio leads to a noisy signal. The problem is overcome by interpolating in the number of flipped plaquettes [59]. The cost of flipping 'one more' plaquette is calculated for $N_\Box$ intermediate ratios of partition functions, where $N_\Box$ is the total number of plaquettes to be flipped. For general SU(N) one calculates the ratios

$$\frac{Z_k^{(n)}}{Z_k^{(n-1)}} = \langle \exp(\frac{\beta}{N} \mathrm{Re}(1 - z^{(n)}) \mathrm{tr}\, \Box^{(n)}) \rangle_{n-1}, \quad z^{(n)} \in Z_N, \tag{3.39}$$

where the n^{th} flipped plaquette $\Box^{(n)}$ acquires the phase $z^{(n)}$ and

$$Z_k^{(0)} = Z_k(\vec{0}), \; Z_k^{(n)} = Z_k(\vec{k}). \tag{3.40}$$

Center flux is thus inserted one plaquette at a time. Translational invariance is restored at the final step by multiplying together the $N_\Box$ ratios from independent Monte Carlo simulations to obtain $Z_k(\vec{k})/Z_k(\vec{0})$.

For each combination of N_t and N_s we performed simulations for ~ 10 values of β around the intersection of the vortex free energy F_k with the exact Ising value (3.36). The standard recipe of one heatbath update to four overrelaxation steps was employed, together with additional variance reduction tricks described in [59]. Statistical errors were estimated via the bootstrap method. Since $2+1$ d SU(2) lattice gauge theory is less computationally expensive than for $3+1$ d, we were able to perform a large number of measurements. $1-30$ million configurations were used for each β, depending on the lattice size.

For each $N_t \times N_s^2$ lattice we then performed linear fits to $F_k(\beta)$ according to the FSS ansatz (3.37) to obtain estimates $\beta_c = \beta_c(N_t, N_s)$ of the critical lattice coupling. See Fig. 3.6 for some representative fits. The finite N_s scaling of the slopes provides a simple crosscheck of the exponent ν. Fitting the slopes of $F_k(\beta)$ to the expected $N_s^{1/\nu}$ dependence gives $\nu = 0.99(3)$ for our $N_t = 4$ lattices, fully consistent with $\nu = 1$ for the $2d$ Ising universality class.

Note that a small reduced χ^2 per degree of freedom for these linear fits does not exclude a systematic error from the curvature near β_c. Fitting windows must be carefully chosen. For each N_t, we measured F_k in a quadratic fitting window for one or more of our smallest lattices. We then translated the data to larger N_s using the finite size scaling variable $x \propto Nt$. This made it possible to estimate the systematic error for a given fitting window without performing unnecessary simulations, and thereby ensure that they are negligible.

3.4.3 *Determinations of $\beta_c(N_t)$*

Our infinite volume estimates for $\beta_c(N_t)$, obtained from the extrapolations of pseudo-critical couplings $\beta_c(N_t, N_s)$, are summarized in Table 3.1 for each N_t between 2 and 9.

See Fig. 3.7 for typical $N_s \to \infty$ extrapolations of $\beta_c(N_t, N_s)$. The data was fitted according to the FSS ansatz (3.38) with all three parameters free. This method typically surpasses the precision of literature values for the critical couplings by two orders of magnitude, where they exist.

Estimates of the correction to scaling exponent ω are obtained as a byproduct. Ignoring any N_t dependence we obtain a naive error weighted average of $\omega = 1.48(4)$, roughly in agreement with the value of 1.64 obtained by Engels et al. [60] from the scaling of Polyakov loops.

For the sake of comparison, we obtained estimates of $\beta_c(N_t = 4)$ from the peak in the Polyakov loop susceptibility,

$$\chi \propto \langle |\sum_{\vec{x}} P(\vec{x})|^2 \rangle - \langle |\sum_{\vec{x}} P(\vec{x})| \rangle^2, \tag{3.41}$$

which is commonly used to locate phase transitions. The results are plotted in Fig. 3.8. They set a benchmark to highlight the rapid convergence of our estimates using vortex free energies.

To see how much was gained from using the exact universal value (3.36) we have also extracted critical couplings using the pairwise intersection of vortex free energies on $N_t = 4$ lattices using N_s ratios of $2 : 1$. The results are summarized in Table 3.2. Exploiting the universal value $F_k(\beta_c) = \ln(1 + 2^{3/4})$ provides a boost equivalent to increasing the statistics by one order of magnitude.

3.4.3.1 *Universality of the correction to scaling exponent*

The exact solutions for $Z^{(1,0)}$ and $Z^{(0,0)}$ partition functions on $N \times N$ Ising lattices from Ref. [54] allow one to numerically determine the correction to scaling exponent ω for direct comparison with SU(2) in $2 + 1$ d. Mathematica was used to find $K = T/J$ at the intersection of $Z^{(1,0)}/Z^{(0,0)}$ with the universal value (3.36) and define pseudo-critical couplings with a FSS ansatz of the form,

$$K_c(N) = K_{c,\infty} - cN^{-(\omega+1)}. \tag{3.42}$$

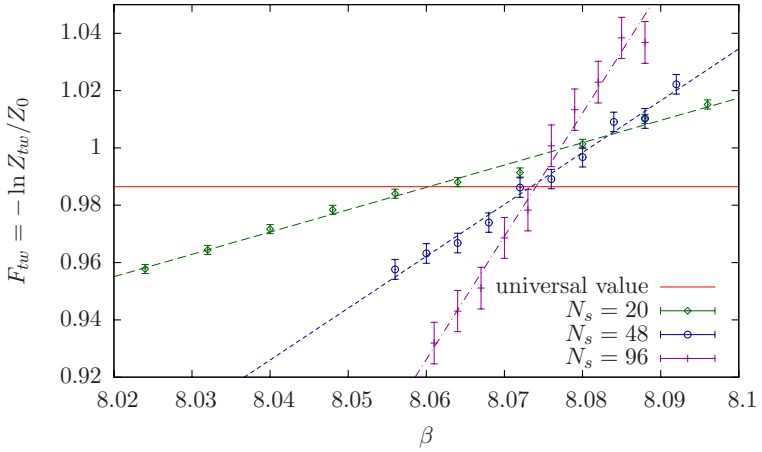

Figure 3.6: Linear fits to the vortex free energy for $N_t = 5$, selected for clarity.

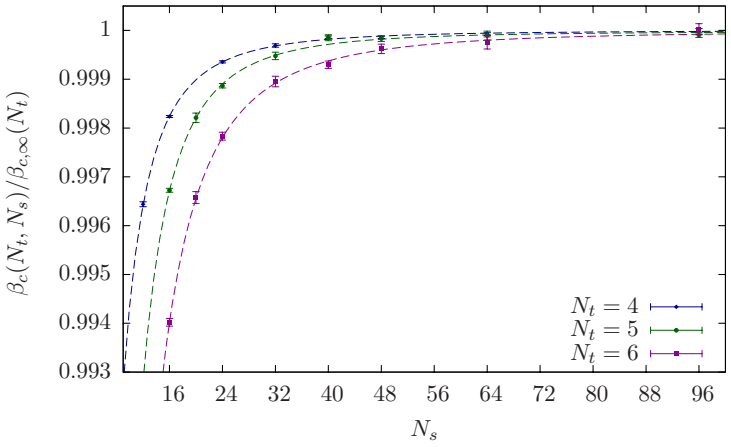

Figure 3.7: $\beta_c(N_t, N_s)$ critical coupling estimates versus N_s relative to their infinite volume limits for $N_t = 4$, 5 and 6, and the corresponding fits to (3.38).

N_t	$\beta_{c,\infty}(N_t)$	N_s	ω fit	χ^2/dof.	Lit. values
2	3.45171(3)	$8-64$	1.37(9)	0.59	$3.4475(36)^\dagger$, $3.469(6)^\S$
3	4.98492(35)	$16-48$	1.16(50)	0.21	$4.943(13)^\dagger$, $5.013(15)^\S$
4	6.53658(16)	$12-96$	1.51(8)	1.53	$6.483(26)^\dagger$, $6.588(25)^\S$, $6.52(3)^\ddagger$
5	8.07463(38)	$16-96$	1.74(15)	1.35	$8.143(57)^\dagger$
6	9.6002(12)	$16-96$	1.48(7)	0.37	$9.55(4)^\ddagger$
7	11.1164(15)	$20-96$	1.38(43)	1.75	
8	12.6301(32)	$24-96$	1.66(52)	0.89	
9	14.1453(10)	$24-96$	1.48(83)	0.98	

Table 3.1: Summary of results from the $N_s^2 \times N_t$ lattices specified in columns 1 and 2 with the the infinite volume extrapolations from fits to Eq. (3.38) in column 3 with the resulting exponents ω and χ^2/dof. in columns 5 and 6. Literature values are quoted for comparison from Refs. † [39], ‡ [61] and § [62].

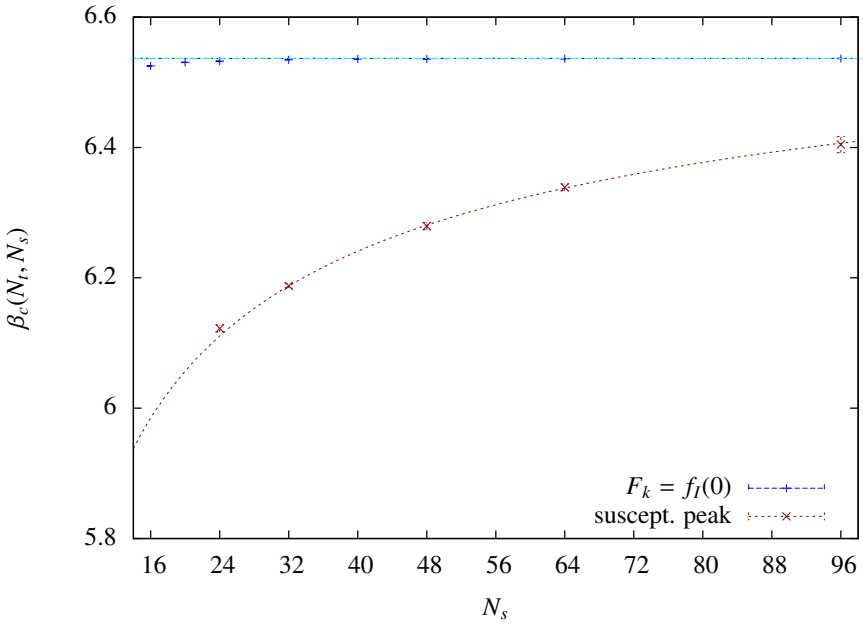

Figure 3.8: $\beta_c(N_t, N_s)$ critical coupling estimates obtained from the peak in the Polyakov loop susceptibility (red) and from the intersection of vortex free energies with their universal value $F_k = f_I(0)$ (blue). The horizontal line indicates our best estimate of the infinite volume result.

$N_s' - N_s$	intersection coupling	N_s	$\beta_c(4, N_s)$ from (3.37)
$12 - 24$	6.5539(19)	24	6.53240(14)
$16 - 32$	6.5451(12)	32	6.53459(23)
$24 - 48$	6.53816(37)	48	6.53569(16)
$32 - 64$	6.53706(45)	64	6.53611(19)
$48 - 96$	6.53756(94)	96	6.53648(37)
Extrap.	6.5358(45)		6.53658(16)∗

Table 3.2: Comparison of critical couplings obtained for $N_t = 4$ via pairwise intersection (left) and via intersection with the universal reference line (right). *This is the extrapolation using all 8 available $N_s \in (12, 96)$ spatial lattices in Table 3.1, restriction to the 5 values shown here results in an unnaturally small error.

In this case, $K_{c,\infty}$ was fixed at the known value of $2/\ln(1+\sqrt{2})$. The correction to scaling exponent tends towards 2 from above, $\omega = 2+\delta$ with $\delta \to 0^+$ as we increase the lower bound $N_{\min}$ used in the fit (δ starts at around $2 \cdot 10^{-4}$ for the full range of N shown in Fig. 3.9, and it falls below 10^{-5} at $N_{\min}$ around 400). Since the exponent of the leading irrelevant operator that breaks rotational invariance is predicted to be exactly 2 [63], our result is consistent with the conjecture of Ref. [64] that the only irrelevant operators that appear in the $2d$ nearest neighbor Ising model are those due to the lattice breaking of rotational symmetry. This may be tested on a triangular $2d$ lattice where the leading irrelevant operator to break rotational invariance leads to $\omega = 4$ instead, while the leading rotationally invariant operator would give an isotropic correction to scaling with $\omega = 2$ in either case [64].

On the other hand, our correction exponent for SU(2) is clearly at odds with $\omega = 2$. In this case, it is possible that there exists an irrelevant operator that is not present in the $2d$ Ising model or the corresponding conformal theory. It is more likely, however, that our exponent is really an effective exponent. When there are several nearby competing exponents it is extremely difficult to extract the smallest one from simulations.[6]

3.4.4 *From coupling to temperature*

In $2+1$ dimensions the coupling g_3^2 has the dimension of mass and sets the scale. The bare lattice coupling is then given by [61],

$$\beta = \frac{2N_c}{a g_{3B}^2}, \quad g_{3B}^2 = g_3^2 + c_1 a g_3^4 + c_2 a^2 g_3^6 + \dots \tag{3.43}$$

Substituting the expansion into β and using $T = 1/(N_t a)$ gives the lattice coupling in terms of temperature, which at criticality reads,

$$\frac{\beta_c(N_t)}{2N_c} \simeq \frac{T_c}{g_3^2} N_t - c_1 - c_2 \frac{g_3^2}{T_c} \frac{1}{N_t} + \dots \tag{3.44}$$

The theory is super-renormalizable with a rapid approach to the continuum limit, which is reflected here in the leading order linearity of the critical coupling in N_t.

Our high precision estimates for $\beta_c(N_t)$ allow us to determine the subleading corrections to linearity.

It is not clear to the naked eye, but the results in Fig. 3.10 are *not* well fitted by a straight line. Indeed, fitting all data points with an acceptable reduced χ^2 requires three subleading coefficients that are not all well constrained. Restricting to $N_t \geq 3$ yields a more sensible fit

$$\beta_c(N_t) = 1.4927(26) N_t + 0.868(34) - 1.58(14) \frac{1}{N_t} + 1.48(19) \frac{1}{N_t^2} + \cdots, \tag{3.45}$$

6 It was noted in [60] that the observed correction to scaling exponent of $2+1$-dimensional SU(2), $\omega = 1.64$ in their case or $\omega = 1.48(4)$ in ours, agreed well with some predictions for the universality class of the $2d$ Ising model that included 1.6 [65]. At the time it was discussed whether such non-integral correction exponents could arise in other ferromagnetic models in this class, and whether the corresponding correction amplitudes happened to vanish identically in the Ising model, see [66]. This appears to be ruled out by a conformal field theory analysis: there is no irrelevant operator with $\omega < 2$ in any unitary model of the $2d$ Ising class [67, 64].

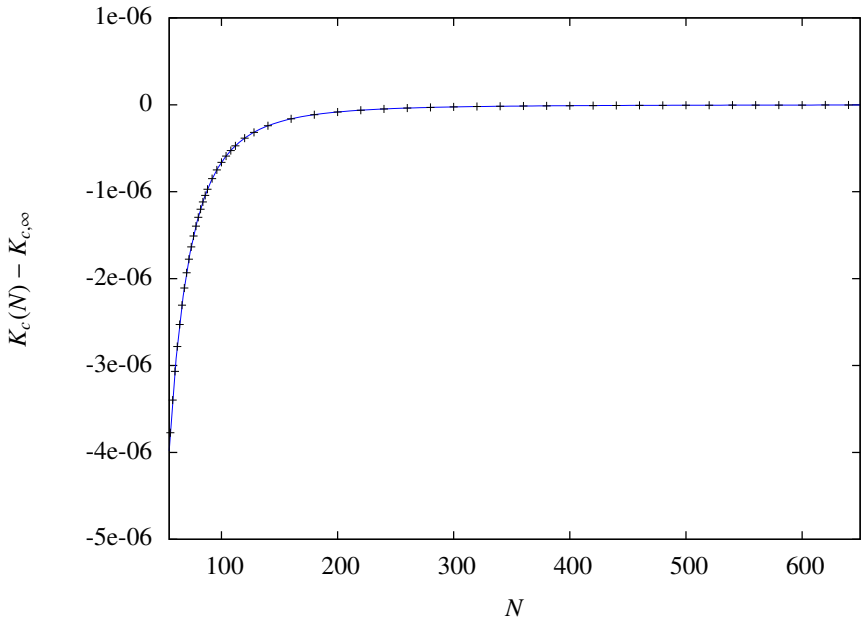

Figure 3.9: Critical coupling estimate vs N for the $2d$ Ising model together with a fit by (3.42) yielding $\omega = 2.0002$ for $N_{\text{min}} = 100$, or $\omega = 2.00001$ for $N_{\text{min}} = 400$.

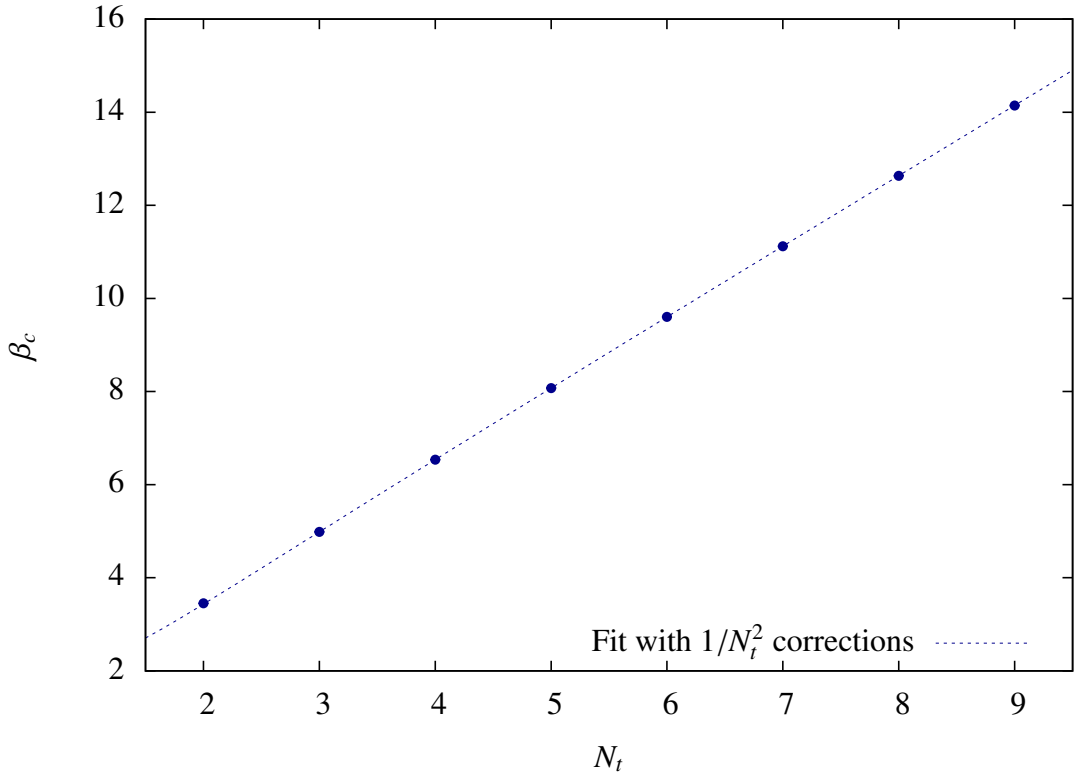

Figure 3.10: Infinite volume extrapolations $\beta_c(N_t)$ of pseudo-critical couplings $\beta_c(N_s, N_t)$, together with a fit for $N_t \geq 3$ with $\mathcal{O}(1/N_t^2)$ corrections.

with a reduced $\chi^2/\mathrm{dof.} \sim 0.64$.

Of particular interest is the leading coefficient, which determines the critical temperature T_c in units of the dimensionful continuum coupling g_3^2. A further restriction to $N_t \geq 5$ allows one to dispense with the $\mathcal{O}(1/N_t^2)$ correction, obtaining,

$$\beta_c(N_t) = 1.4950(17)N_t + 0.797(19) - 0.985(53)\frac{1}{N_t} + \cdots\,,\ N_t \geq 5, \tag{3.46}$$

where the errors are somewhat underestimated owing to a low reduced $\chi^2/\mathrm{dof.} \sim 0.19$. The important point is the consistency of the leading term within the quoted errors.

Using the fit (3.45) and Eq. (3.44) with $N_c = 2$ gives,

$$T_c/g_3^2 = 0.3732(6), \tag{3.47}$$

without including any additional uncertainty owing to the choice of fit. This is compatible with the estimate $T_c/g_3^2 \simeq 0.385(10)$ quoted in Ref. [62]. Note that $1/N_t$ corrections lead systematically to a lower value.

To convert T_c into units of the zero-temperature string tension σ, one can use the four $N = 2$ values for $\sqrt{\sigma}/g_3^2$ listed in [68]. Taking their mean value and standard error to construct pairs of upper and lower bounds gives,

$$\sqrt{\sigma}/g_3^2 = 0.3347(5), \tag{3.48}$$

including some systematic uncertainty. With uncorrelated error propagation, this together with our estimate of T_c/g_3^2 (3.49) yields,

$$T_c/\sqrt{\sigma} \;=\; 1.1150(24)\,, \tag{3.49}$$

in agreement with the corresponding result of [39],

$$T_c/\sqrt{\sigma} = 1.1224(90). \tag{3.50}$$

Since $T = 1/N_t a$, a change in N_t at a fixed lattice spacing is equivalent to a change of temperature. In particular, a simulation at criticality on an N_t' lattice, with fixed $a_c(N_t') = a(N_t)$, then corresponds to a simulation at $T = (N_t'/N_t)T_c$ on the N_t lattice, i.e., with $\beta \equiv \beta(a)$, we have

$$\beta_c(N_t') = \beta(1/(N_t' T_c)) = \beta(1/(N_t T))\,. \tag{3.51}$$

Our precise determination of $\beta_c(N_t)$ therefore yields an equation for the temperature dependence of the lattice coupling near criticality at a fixed N_t,

$$\frac{\beta(T,N_t)}{4} - \frac{\beta_c(N_t)}{4} = \frac{N_t}{g_3^2}\,(T - T_c) - c_2\frac{g_3^2}{N_t}\Big(\frac{1}{T} - \frac{1}{T_c}\Big) + \ldots\,. \tag{3.52}$$

Or in terms of the reduced temperature $t = T/T_c - 1$,

$$\frac{\beta(t,N_t)}{4} - \frac{\beta_c(N_t)}{4} = N_t\frac{T_c}{g_3^2}\,t + c_2\frac{g_3^2}{T_c}\frac{1}{N_t}\frac{t}{1+t} + \mathcal{O}(1/N_t^2)\,. \tag{3.53}$$

The physical length of the spatial volume follows from,

$$L = aN_s = \frac{N_s}{N_t T} = \frac{N_s}{N_t T_c}\,\frac{1}{1+t(\beta)}\,. \tag{3.54}$$

These equations allow us to perform a finite size scaling (FSS) analysis of vortex and electric flux free energies on $N_t \times N_s^2$ lattices in suitable windows of lattice couplings β around β_c. Our precise numerical analysis may thereby be used to gain conceptual insight into the deconfinement transition.

3.5 FINITE SIZE SCALING AND SELF-DUALITY

As explained in Sec. 3.3.1, the center vortex free energy is determined about criticality by the universal scaling function $f_I(L^{1/\nu}t)$ for interfaces in the $2d$ Ising universality class. Different lattice realizations simply require a rescaling of the correlation length in order to match their FSS variables, $x = L^{1/\nu}t \propto L/\xi$.

We may determine f_I in terms of the FSS variable on a square $N \times N$ $2d$ Ising model,

$$x_I = N^{1/\nu}t, \text{ with } t = K/K_c - 1, \ \nu = 1. \tag{3.55}$$

Then, in SU(2), T_c may be used as a length scale to form a dimensionless FSS variable that differs by a non-universal coefficient λ from x_I in the $2d$ Ising model,

$$x_{SU(2)} = T_c L^{1/\nu}t, \text{ with } t = T/T_c - 1, \ L = aN_s, \tag{3.56}$$

$$x_I = -\lambda x_{SU(2)}. \tag{3.57}$$

The minus sign is required because the disordered, Z_2 center symmetric phase is at low temperature for SU(2) whilst it is at high temperature for the Ising model. We will suppress the subscript where it is not likely to cause confusion.

A full determination of the vortex free energies $F_k(\vec{k})$ at criticality follows after fitting for λ,

$$F_k(x_{SU(2)}) = f_I(-\lambda x_{SU(2)}), \tag{3.58}$$

where we can obtain the scaling function f_I to arbitrary accuracy using the exact solutions for interface free energies on finite $2d$ Ising lattices from Ref. [54].

In Fig. 3.11 we plot $N_t = 4$ results for $Z_k(1,0)/Z_k(0,0) = e^{-F_k}$ for one unit of center flux as a function of the FSS variable $x_{SU(2)}$, fitted by λ to the universal scaling function f_I computed in the $2d$ Ising model. Included also is the partition function ratio $Z_e(1,0)/Z_e(0,0) = e^{-F_e}$ for one unit of electric flux.

The colored data represents various $4 \times N_s^2$ lattices with up to $N_s = 96$ spatial points. This impressive collapse of the data onto the universal curve is typical of each of our fixed N_t data sets. Even more striking is the way in which the vortex and electric flux ensembles collapse onto *each other* as perfect mirror images under $x \to -x$. SU(2) in $2+1$ dimensions exhibits a self-duality at criticality.

This remarkable fact stems from self-duality in the $2d$ Ising model. It is well known that the $2d$ Ising model and, indeed, all $2d$ N-state Potts models are self-dual for infinite volumes via Kramers-Wannier duality [69]. Dualities are less well studied in finite volumes, however, where the boundary conditions become a nuisance.

The behavior of SU(2) fluxes at criticality indicates that Kramers-Wannier duality for the $2d$ Ising model on a torus takes the form of 't Hooft's discrete Fourier transform over twists. Indeed, the $2d$ Ising model is self-dual on a rectangular lattice with N_{sites} sites under a $2d$ Z_2- Fourier transform

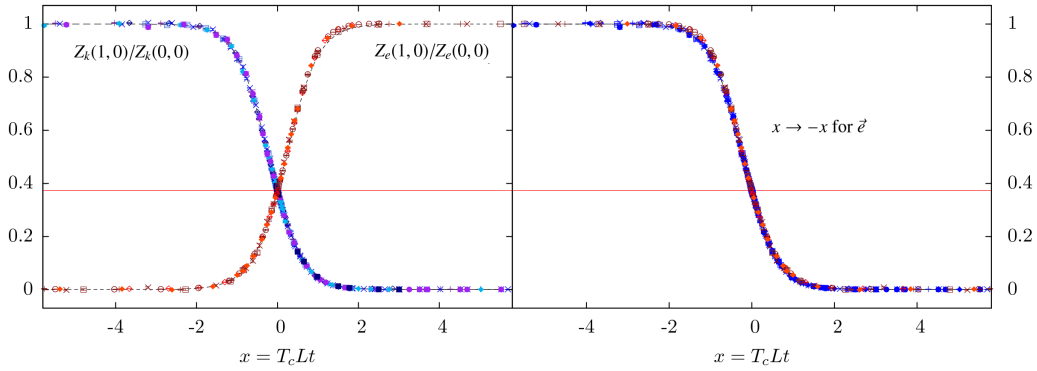

Figure 3.11: The ratio $Z_k(1,0)/Z_k(0,0)$ of the partition function with twist $\vec{k} = (1,0)$ over the periodic ensemble in the $2+1$ dimensional SU(2) gauge theory compared to $Z_e(1,0)/Z_e(0,0)$ for one unit of electric flux $\vec{e} = (1,0)$ relative to the no-flux ensemble (left), and to its mirror image (right). The data here is obtained for $N_t = 4$ and spatial volumes with up to $N_s = 96$ [17]. The dashed lines represent the universal scaling function from the $2d$ Ising model, $\exp\{-f_I(-\lambda x)\}$ for Z_k and its mirror $\exp\{-f_I(\lambda x)\}$ for Z_e from self-duality.

$$\begin{pmatrix} Z^{(0,0)}(\tilde{K}) \\ Z^{(1,0)}(\tilde{K}) \\ Z^{(0,1)}(\tilde{K}) \\ Z^{(1,1)}(\tilde{K}) \end{pmatrix} = \frac{1}{2}\sinh(2K)^{-N_{sites}} \begin{pmatrix} 1 & 1 & 1 & 1 \\ 1 & 1 & -1 & -1 \\ 1 & -1 & 1 & -1 \\ 1 & -1 & -1 & 1 \end{pmatrix} \begin{pmatrix} Z^{(0,0)}(K) \\ Z^{(1,0)}(K) \\ Z^{(0,1)}(K) \\ Z^{(1,1)}(K) \end{pmatrix} \tag{3.59}$$

with dual coupling

$$\tilde{K} = -\frac{1}{2}\ln\tanh K, \quad K = J/T. \tag{3.60}$$

This is easy to verify using the analytic solutions in Ref. [54] for partition functions with mixtures of periodic and antiperiodic boundary conditions. A proof of the result is also given in Ref. [70].

The couplings $\tilde{K}$ and K have a linear relationship at criticality,

$$\tilde{K} - \tilde{K}_c = -(K - K_c) + \mathcal{O}(K^2), \; K_c = \tilde{K}_c = \frac{1}{2}\ln(1+\sqrt{2}), \tag{3.61}$$

which ensures that the dual partition functions are mirror images of the originals when plotted as functions of the reduced temperature t or FSS variable x.

The duality relation generalizes to the N-state Potts model. For partition functions $Z^{(m,n)}$ with cyclically shifted spins, $s(\vec{x} + L\hat{i}) = e^{i2\pi n/N} s(\vec{x})$, in orthogonal directions on a torus, the duality transformation (3.59) becomes [17],

$$Z^{(-s,r)}(\widetilde{K}) = \left(\frac{e^{\widetilde{K}} - 1}{e^K - 1}\right)^{N_{\rm sites}} \frac{1}{N} \sum_{m,n} e^{2\pi i\,(rm+sn)/N}\; Z^{(m,n)}(K)\;, \qquad m,n,r,s = 0,1,\ldots N-1, \tag{3.62}$$

with the dual coupling $\widetilde{K}$ obtained from

$$\left(e^{\widetilde{K}} - 1\right)\left(e^K - 1\right) \;=\; N\;. \tag{3.63}$$

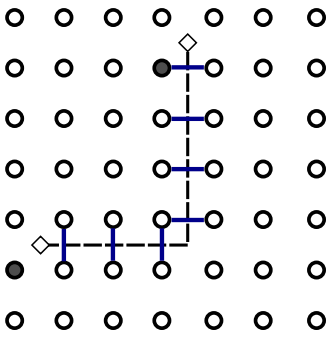

Figure 3.12: Kramers-Wannier duality maps the correlators of $2d$ Ising spins (order variables) to correlators on a dual lattice. These 'disorder' variables correspond to the insertion of an interface.

At criticality,

$$K = \widetilde{K} = K_c = \ln(1 + \sqrt{N}) \; . \tag{3.64}$$

Note the conventional shift $K \to K/2$ here compared to the $2d$ Ising model. For the 3-state Potts model, this finite volume Kramers-Wannier duality agrees with a result in Ref. [71] obtained under the guise of the vector Potts model, which is equivalent to the N-state Potts for $N \leq 3$.

The finite volume Kramers-Wannier duality Eq. (3.62) permits a proof using the random cluster methods developed in [57]. These maps the formulation of the model in terms of spins, to a formulation in terms of the interfaces (bonds) between spins. A detailed sketch of the proof is presented in [15].

The form of Kramers-Wannier duality on finite volumes clearly highlights its origin in the non-trivial topology inherited from global Z_N symmetry. In terms of the original theory, the spins of the dual theory are disorder variables that mark the beginning and endpoints of Z_N interfaces. The dual lattice is again 2 dimensional, with the disorder variables living 'between' the sites of the original spins, which are order variables (see Fig. 3.12). There is a one-to-one map between the correlators of the order and disorder variables, which is what allows for the exact duality at all temperatures. Kramers-Wannier duality gives more than just an equivalence of partition functions, there is an equivalence between the configurations of the degrees of freedom in the high and low temperature phases.

For SU(N) in $2+1$ d, 'disorder' variables are the would-be endpoints of line-like center vortices. They are the source terms for center flux. Note, however, that just as interfaces appear as closed loops for a given spin configuration, center vortices are closed loops on a gauge field configuration. They obey a Bianchi identity. This is also true of the color electric flux lines created by Wilson loop holonomies. Sources of fundamental color flux don't appear as dynamical variables in the pure Yang-Mills theory, only as test charges.

Since Wilson loops and center vortices are both line-like objects in $2+1$ d,, their topological link via 't Hooft's Z_N-Fourier transform is able to morph into an exact duality at criticality. This can be framed in terms of the dimensionally reduced system at a second order phase transition. At criticality, only the dynamics of the Z_N center sectors (spins) and the center vortices (interfaces) between them survive. Viewed along the short $1/T$ direction, the squeezed color-electric flux between

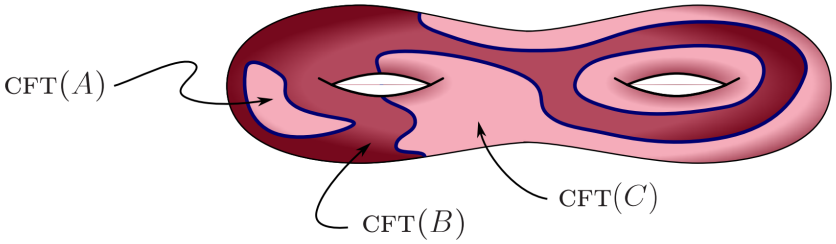

Figure 3.13: A 2*d* worldsheet with conformal defects separating different CFT phases. From Ref. [72].

Polyakov loops, and the percolating center flux that disorders it, acquire the same dimensionality as temperature increases. They may then inherit the mapping from the Kramers-Wannier duality of the spin model such that the physics of confined electric fluxes just below T_c has the same content as that of confined center fluxes just above T_c.

This drives home the correctness of the center vortex confinement mechanism. In $3+1$ d, center vortices become surface like, and their dimensionality no longer matches that of color-electric flux at criticality. Nevertheless, a topological linking remains between the operators that create these fluxes: non-singular gauge transformations for center vortices ('t Hooft loops), and Wilson loops for color-electric fluxes.

3.5.0.1 *Duality and conformal theories*

Self-duality on a 2*d* torus is a general feature of the N-state Potts models, valid at all temperatures. At the second order phase transitions of Potts models with $N \leq 4$, it extends to the 2*d* conformal field theories (CFT) that describe the universality class.

This establishes a link with the keenly studied dualities in conformal and supersymmetric theories. The discovery of dualities between various string theories led to a revolution in the 1990s that spread to gauge theories via Maldacena's conjectured AdS/CFT correspondence [73].

2*d* conformal field theories have a special theoretical significance. For starters, the infinitesimal conformal transformations form an infinite-dimensional algebra in two dimensions. This large symmetry makes 2*d* CFTs much more tractable than conformal theories in higher dimensions, which have finite dimensional algebras. It allows them to be solved by symmetry considerations alone [74]. In particular, 2*d* CFTs are classified by the central charge c of their Virasoro algebras, which is specified by a coefficient $c = 1/2$ for the 2*d* Ising universality class and $c = 4/5$ for the 2*d* 3-state Potts universality class.

The peculiarities of 2*d* CFTs are a blessing not only for condensed matter physicists, but also for string theorists. They emerge naturally from perturbation theory on the 2*d* worldsheet of strings and bestow string theory with much of its rich mathematical structure [75]. Dualities in 2*d* CFTs then become important as dualities of the string worldsheet.

In the context of 2*d* CFTs, the defects responsible for Kramers-Wannier duality are a subclass of what have been coined *conformal defects* [72]. They are obtained by

cutting a $2d$ surface along a $1d$ defect line and re-gluing it with boundary conditions for the CFTs on each side. If the boundary conditions conserve the stress-energy tensor, then they are totally transmissive for momentum and the defect is termed *topological*. This corresponds to translationally invariant boundary conditions (the torus). In the case of the $2d$ Ising model, periodic and antiperiodic boundary conditions yield a trivial defect ($\uparrow\uparrow$) and a spin interface ($\uparrow\downarrow$) respectively. These enact the symmetry group of the conformal theory at criticality, i.e., they flip between Z_2 sectors of the CFT. At criticality, translationally invariant boundary conditions on the torus become boundary states of the conformal field theory.

Kramers-Wannier duality is a consequence of the fact that these defects are *grouplike.* They can be undone by the insertion of another defect [72].

There is a third type of conformal defect in the CFT that has a less straight forward interpretation in the spin model. It can be thought of as enacting Kramers-Wannier duality itself. That is, exchanging the order and disorder fields between the low and high temperature phases. It is associated with free boundary conditions. This conformal defect underlies the duality relation between free and fixed boundary conditions in the $2d$ Ising model [76, 77].

Note that the framework of conformal defects also allows one to study dualities between different critical theories. For instance, the tetra-critical Ising model and 3-state Potts model both have central charge $c = 4/5$. One can construct a Kramers-Wannier duality via conformal defects between their in-equivalent CFT phases [72].

3.6 EXPLOITING SELF-DUALITY

Self-duality implies that center vortices and electric flux free energies in SU(2) are determined around criticality by the *same* universal scaling functions for spin interfaces in the $2d$ Ising model. For single units of flux,

$$F_k(x) \simeq F_e(-x) \simeq f_I(-\lambda x). \tag{3.65}$$

We will first exploit this to infer the asymptotic dual (vortex) and electric string tensions at T_c. Then we will see that the self-dual point provides an even more efficient method of locating the phase transition than does the universality of F_k alone.

3.6.1 *String tensions*

Tensions are naturally extracted by dividing the free energy by the minimal length of the surface. For the square $N \times N$ $2d$ Ising model in the low temperature ordered phase, the interface tension is defined by

$$\sigma_I = \lim_{N\to\infty} F_I(N,T)/N,\ T < T_c. \tag{3.66}$$

In higher dimensions one divides by N^{d-1}.

Onsager [78] obtained the tension for a straight interface in the thermodynamic limit $N \to \infty$,

$$\sigma_I = 2K + \ln\tanh K\ ,\ 0 \le T \le T_c \text{ with } K = J/T. \tag{3.67}$$

which determines the scaling of the interface tension with reduced temperature as one approaches criticality [52],

$$\sigma_I = \sigma_0(-t)^\mu + \cdots\ ,\ \text{with}\ \ \mu = (d-1)\nu\ ,\ \ t \to 0^-. \tag{3.68}$$

μ is set by a hyperscaling relation as the product of the dimension of the interface $d-1$ and the correlation length exponent ν. This ensures that the amplitude σ_0 determines also the asymptotic behavior of the universal scaling function $f_I(x)$ with the FSS variable $x = N^{1/\nu}t$,

$$f_I(x) = \sigma_0\,(-x)^\mu + \cdots\ ,\ \ x \to -\infty\,. \tag{3.69}$$

For the $2d$ Ising model with $\nu = 1$ the relationship is simple.

$$\sigma_I = -\sigma_0 t,\ f_I(x) = -\sigma_0\,x + \cdots\ ,\ \ x = Nt \to -\infty, \tag{3.70}$$

$$\sigma_0 = 2\ln(1+\sqrt{2}), \tag{3.71}$$

with σ_0 obtained by expanding Onsager's formula in t at criticality $K_c = \ln(1+\sqrt{2})/2$.

Knowledge of the exact amplitude σ_0 is helpful, since the the direct extraction of the asymptotic slope σ_0 from finite volume data is inevitably hampered by deviations from the universal function $f_I(x)$ in the limit $x = Nt \to -\infty$. This is demonstrated for the $2d$ Ising model in Fig. 3.14, which shows the asymptotic approach

to linearity in x for the interface free energy at T_c calculated from the finite volume solutions in Ref. [54]. The deviations between even these rather large $N = 100$ and $N = 1000$ lattices are significant for $x < -5$.

The situation is much worse for SU(2) in $2+1$ d, where we are limited to Monte Carlo data on much smaller volumes. Fig. 3.15 shows how difficult it is to extract the analogous center vortex dual tension directly from lattice data. Asymptotically large x requires ever larger lattice sizes $L = N_s a$ in order to keep t small enough that we remain in the universal scaling window. The computational cost of calculating vortex free energies grows like $N_s^{d+d(d-1)}$. Beating the scaling violations by brute force would be a joyless task in the $2+1$ d theory and is even less feasible in higher dimensions.

Fortunately, brute force is not required. We can match our SU(2) data to f_I obtained from the Ising model at small values of x. Here it remains in the universal scaling window for moderate, low cost values of N_s. This allows for a cheap rescaling of the correlation length ξ and the asymptotic $x \to \infty$ critical behavior of center vortices and electric fluxes is obtained as a byproduct.

The electric string tension σ and dual string tension $\tilde{\sigma}$ are then given by,

$$F_e = \sigma L/T = f_I(\lambda x), \quad \text{and,} \tag{3.72}$$

$$F_k = \tilde{\sigma} L = f_I(-\lambda x), \text{ as } L \to \infty. \tag{3.73}$$

The electric string tension is obtained by dividing the $2d$ worldsheet of the electric flux string between static color charges, while a center vortex is a line like object. This explains the factor of $1/T$ difference from the compact temporal extent.

From the asymptotic behavior of the scaling function (3.70), the leading behavior for the string tensions below and above T_c is then,

$$\begin{aligned} \sigma &= \lambda_\infty T_c^2 2\ln(1+\sqrt{2})\,|t| + \cdots\,, \quad t \to 0^-\,, \text{ and} \\ \tilde{\sigma} &= \lambda_\infty T_c 2\ln(1+\sqrt{2})\,t + \cdots\,, \quad t \to 0^+\,. \end{aligned} \tag{3.74}$$

We have inserted the amplitude $\sigma_0 = 2\ln(1+\sqrt{2})$ and also used $T \simeq T_c$ to remove a factor of T in the equation for the string tension σ. Note that λ_∞ applies to the *continuum* theory. SU(2) lattice models with different numbers of time slices are really different theories in the same universality class. Their correlation lengths require different rescaling factors $\lambda(N_t)$ to match the $2d$ Ising model, which must be extrapolated with $N_t \to \infty$ to yield the continuum result.

3.6.1.1 *Matching the correlation lengths*

To convert lattice data into the physical units in the finite size scaling variable $x = T_c L t$, we solve for the reduced temperature $t(\beta)$ in terms of the lattice coupling β,

$$\frac{\beta(t,N_t)}{4} - \frac{\beta_c(N_t)}{4} = N_t \frac{T_c}{g_3^2}\, t + c_2 \frac{g_3^2}{T_c}\frac{1}{N_t}\frac{t}{1+t} + \mathcal{O}(1/N_t^2), \tag{3.75}$$

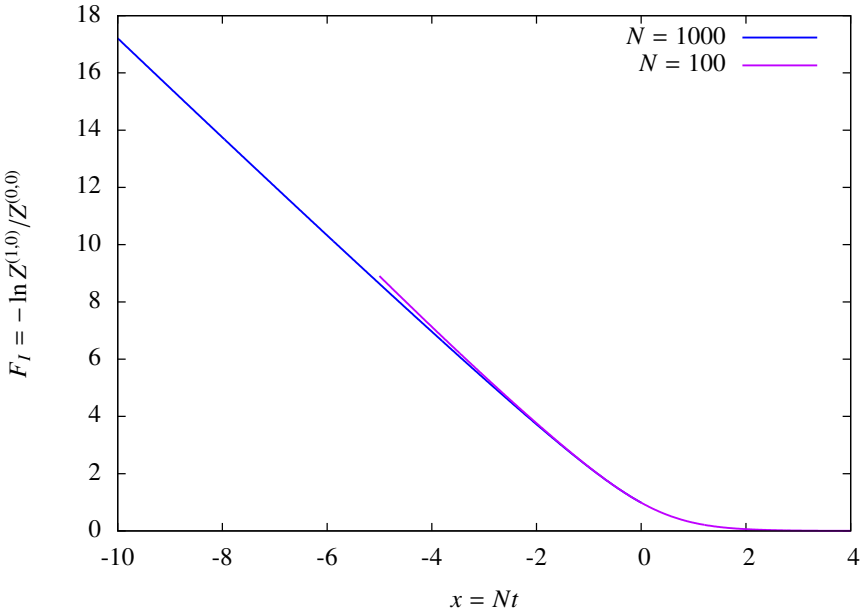

Figure 3.14: The universal scaling function $f_I(x)$ calculated for a $(1,0)$ interface corresponding to one anti-periodic direction from the ratio of exact finite volume partition functions $Z^{(1,0)}/Z^{(0,0)} = e^{-F_I}$ for the $N \times N$ square Ising model in [54].

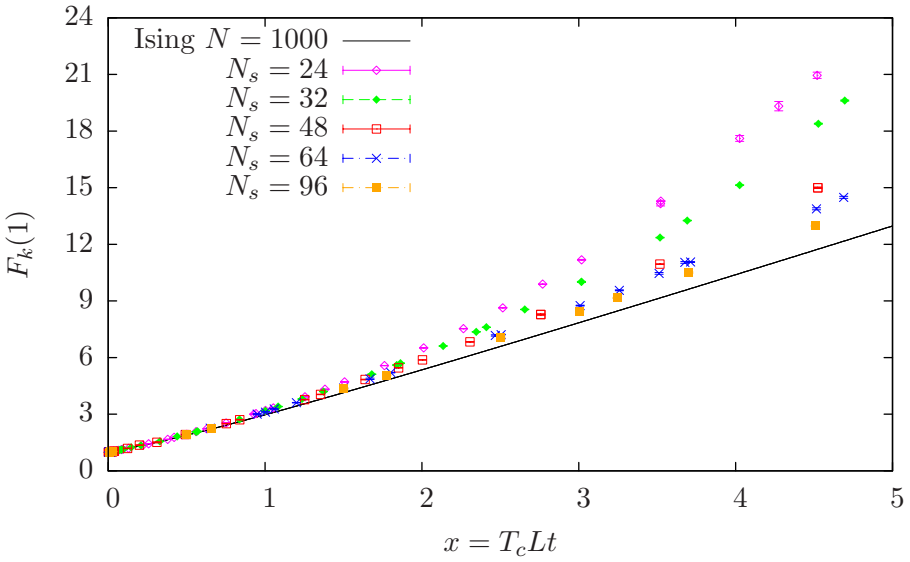

Figure 3.15: Vortex free energies $F_k(1,0)$ in SU(2) above T_c for $N_t = 4$. Here $x = -4$ equates to $x_I \simeq -6$ in the $2d$ Ising model where scaling violations are also significant for $N \times N$ lattices as large as $N = 100$ (c.f. Fig. 3.14)

where the coefficients were numerically determined in Section 3.4.4 by fitting the N_t dependence of the critical lattice couplings $\beta_c(N_t)$. With the formula for the system length (3.54),

$$L = \frac{N_s}{N_t T_c} \frac{1}{1+t(\beta)} , \tag{3.76}$$

we have for each $N_t \times N_s^2$ lattice,

$$x = \frac{N_s}{N_t} \frac{t(\beta)}{1+t(\beta)}. \tag{3.77}$$

Vortex partition function ratios $Z_k(1,0)/Z_k(1,0) = e^{-F_k}$ are plotted against x for various N_t in Fig. (3.17). The N_t dependence of the correlation length is reflected in the smearing of the slope at $x = 0$.

While matching the correlation lengths via fits for $\lambda(N_t)$, we can also deal with the scaling violations from the finite size N_s. Criticality in a finite volume is a fuzzy concept, so there is some leeway. If we define criticality from the pseudo-critical couplings $\beta_c(N_s, N_t)$, obtained from the intersection of vortex free energies with their universal value, then this amounts to a horizontal correction of the FSS variable x. Self-duality implies, however, that we should respect the symmetry in F_k and F_e around β_c. This favors a correction to account for the $\propto N_s^{-\omega}$ offsets of the flux free energies on finite volumes from the universal value $f_I(0)$ at β_c. The choice between these approaches amounts to a small systematic uncertainty in our extraction of each $\lambda(N_t)$.

We determine $\lambda(N_t)$ by fitting the SU(2) vortex data to the analytic $N = 1000$ solution for interfaces in the $2d$ Ising model, which differs from f_I with only negligible FSS corrections $\mathcal{O}(N^{-\omega})$ near $x = 0$. It is best to fit the partition function ratios,

$$Z_k(1,0)/Z_k(0,0) \sim \exp(-f_I(-\lambda x)), \tag{3.78}$$

instead of the interface free energy, since then the tails converge to the fixed values 1 and 0 at $x = \pm\infty$. This allows us to benefit from asymmetric fitting windows between $x \sim -1$ below and $x \sim 0.1$ above criticality while maintaining an excellent fit between the Ising model and SU(2) data. The systematic uncertainty from the fit window was checked by varying the cutoffs.

Results for $\lambda(N_t)$ are presented in Fig. 3.16. The removal of finite N_s corrections via horizontal or vertical shifts of the partition function curves yield consistent values. The $1/N_t$ corrections to the continuum result for $N_t \in (4, 10)$ are well-described by a polynomial fit,

$$\lambda(N_t) = \lambda_\infty + b/N_t + c/N_t^2 . \tag{3.79}$$

The extrapolated values obtained by horizontal or vertical shifts of the curves to correct for finite N_s offsets at $x = 0$ are, respectively,

$$\lambda_\infty = 1.354(25), \text{ and } 1.380(35), \tag{3.80}$$

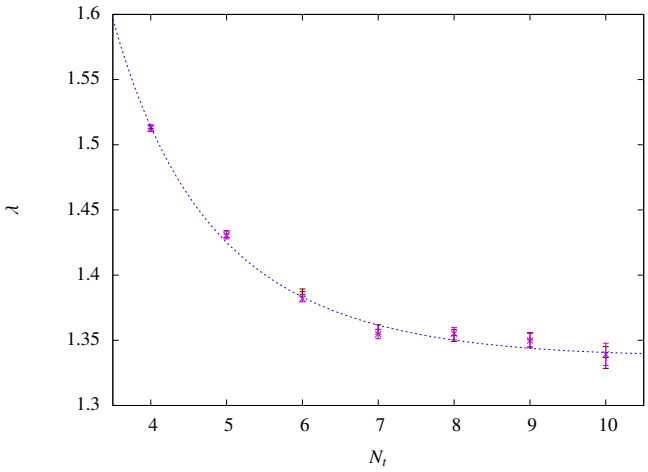

Figure 3.16: Rescaling factor $\lambda(N_t)$ obtained by fitting center vortex partition function ratios $Z_k(1,0)/Z_k(0,0)$ as a function of the FSS variable $x = T_c L t$ to the universal function $\exp(-f_I)$ known exactly from the $2d$ Ising model. Data for removing finite N_s corrections at $x = 0$ via both horizontal (red) and vertical (magenta) offsets are included. A polynomial fit in $1/N_t$ yields the continuum value for λ, here for the red data points.

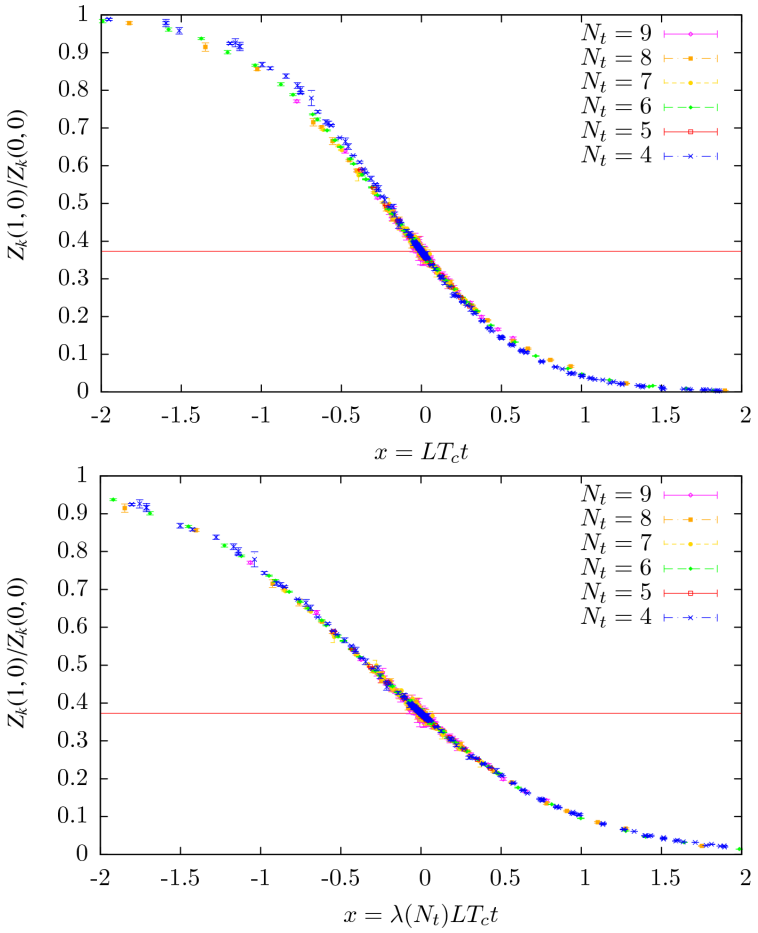

Figure 3.17: Center vortex partition function ensembles against the renormalized FSS variable x for various N_t, before and after renormalization by a factor $\lambda(N_t)$.

with reduced χ^2/dof.'s of 1.5 and 2.5. They are consistent within the rather generous fitting errors. Our $\lambda(N_t)$ points actually agree within ± 0.01 for $N_t \geq 7$.[7]

After rescaling the FSS variable x by $\lambda(N_t)$, our data for vortex ensembles on various $N_t \times N_s^2$ lattices collapses beautifully onto the universal Ising curve in a large window around $x = 0$. Compare the data in Fig. 3.17 before and after renormalization of the FSS variable $x = \lambda T_c L t$. The electric flux partition function ratios obtained from vortex ensembles by a discrete Fourier transform scale equally well (not shown).

With our determination of the non-universal constant λ_∞, the scaling of the *continuum* string tension σ and dual string tension $\tilde{\sigma}$ at criticality is now completely specified in units of T_c. Repeating Eq. (3.74) for convenience,

$$\begin{aligned} \sigma(t) &= \lambda_\infty T_c^2 2\ln(1+\sqrt{2})\,|t| + \cdots\,, \quad t \to 0^-\,, \quad \text{and} \\ \tilde{\sigma}(t) &= \lambda_\infty T_c 2\ln(1+\sqrt{2})\,t + \cdots\,, \quad t \to 0^+\,, \; \lambda_\infty = 1.354(35). \end{aligned} \tag{3.81}$$

One may convert the length scale T_c to units of the continuum coupling g_3 or, if preferred, the zero temperature string tension using our earlier determinations,

$$T_c/g_3^2 = 0.3732(6),\; T_c/\sqrt{\sigma(T=0)} \;=\; 1.1150(24)\,. \tag{3.82}$$

3.6.1.2 *Diagonal string formation*

Our determination of the string tensions Eq. (3.74) is also valid for pairs of orthogonal fluxes under the assumption that they minimize the total length by forming a diagonal string. A string tension implies that the free energy for a pair of perpendicular fluxes on a symmetric volume should be $\sqrt{2}$ that of a single flux.

This can also be coaxed out of the $2d$ Ising model. The free energy per N for a diagonal interface (anti-periodic boundary conditions in both directions) is provided by Baxter in Ref. [79],

$$\frac{F_I^{(1,1)}}{N} = \sigma_I^{(1,1)} = 2\ln\sinh(2K),\; N \to \infty. \tag{3.83}$$

Multiplying by $K = T/J$ gives the tension per coupling J, which we plot in Fig. 3.18 together with the the result for a straight interface $\sigma_I^{(1,0)}$.

On a rectangular lattice, discretization breaks rotational invariance such that straight and diagonal fluxes are not on an equal footing. For the Ising model at zero temperature, the system is in a state of maximum order. In that case a diagonal spin interface is forced to take a step-like path through the lattice and is *twice* the length of a straight interface. Isotropy only emerges when thermal fluctuations become large and the correlation length dwarfs the finite lattice spacing. At criticality, the underlying lattice geometry becomes irrelevant and a $\sqrt{2}$ factor between straight and diagonal interfaces emerges,

$$\sigma_I^{(1,1)} = 2\sqrt{2}\ln(1+\sqrt{2})|t| = \sqrt{2}\,\sigma_I^{(1,0)},\; K = K_c\,. \tag{3.84}$$

7 The data is better described by a power law fit with extrapolated values $\lambda_\infty = 1.337(5)$ and $1.338(5)$ for the horizontal and vertical N_s offset corrections, with reduced χ^2/dof. of 1 and 1.9 respectively. Without a justification for the fitting function we prefer to quote the less constrained results that better accommodate any remaining systematic uncertainties.

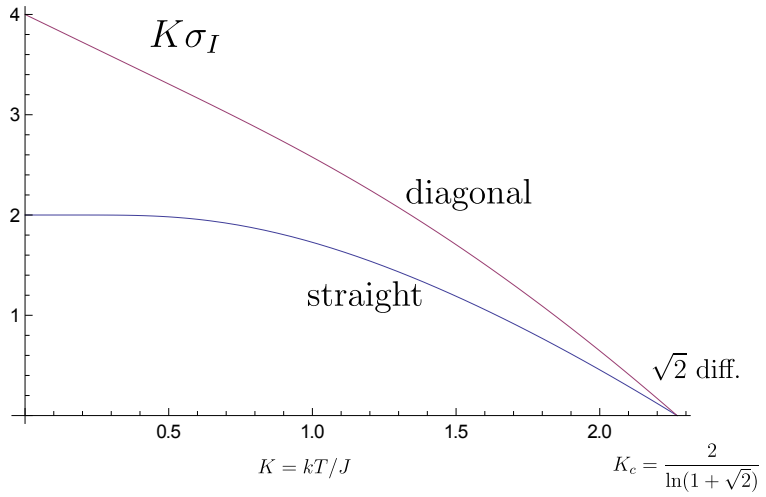

Figure 3.18: The exact interface tensions per coupling, $K\sigma_I$ over temperature $K = T/J$, for straight $(1,0)$ and diagonal $(1,1)$ interfaces. They differ by factor $\sqrt{2}$ at criticality. This implies string formation at criticality for all models in the $2d$ Ising universality class.

It is here that the interface tension amplitude $\sigma_0 = 2\ln(1+\sqrt{2})$ is relevant to all models in the $2d$ Ising universality class, irrespective of the microscopic physics.

String formation in $2+1$ d SU(2) gauge theory for electric fluxes in the scaling window below T_c, and for spacelike center vortices above T_c, then follows from universality and this square root signature for diagonal interfaces at criticality in the $2d$ Ising model.

In the continuum limit of the gauge theory, we also expect isotropy and hence square root scaling for center and electric fluxes *away* from criticality. This is verified in Appendix A.

3.6.1.3 *A note for* $3+1$ d

We have used self-duality to fix the relationship between the electric string and dual center vortex tension in $2+1$ d. More generally, this is fixed by the universal amplitude ratio that relates the relevant scales on each side of criticality. For Ising models, this is the interface tension σ_I in the ordered phase and the exponential correlation length, i.e., inverse mass gap $\xi^+_{\rm gap}$, in the disordered phase. The hyperscaling relation $\mu = (d-1)\nu$ gives the universal amplitude ratio [52]

$$\sigma_I(\xi^+_{\rm gap})^{d-1} = R^+_{\sigma\ {\rm gap}}\ , \quad \text{where} \tag{3.85}$$

$$R^+_{\sigma\ {\rm gap}} = \begin{cases} 1\ , \text{ for } \ q = 2,\, 3,\, 4\ , \text{ in } \ d = 2\ , \\ 0.40(1)\ , \text{ for } \ q = 2\ , \text{ in } \ d = 3\ . \end{cases}$$

For the 2, 3 and 4-state Potts models with second order phase transitions, self-duality gives unity for the amplitude ratio. The value for the $3d$ Ising model is determined numerically. It can be applied to SU(2) gauge theory in $3+1$ d, where the mass gap in the disordered phase comes from the electric string tension $\sigma/T =$

ξ_-^{-1}. After correcting for the non-universal constant in $\sigma \propto |t|^\mu$ from the scaling of the correlation length, the dual string tension is then determined at criticality by,

$$\tilde{\sigma} \;=\; R^+_{\sigma\,\mathrm{gap}}\,(\sigma/T)^{d-1}. \tag{3.86}$$

3.6.2 *Critical couplings from self-duality and universality*

The intersection of interface free energies with their universal value at criticality, when known, is an exceptionally precise method of locating a second order phase transition. Our estimates for $\beta_c(N_t)$ for SU(2) in $2+1$ d from center vortex ensembles are testaments to this. At the time of their publication in [14] we believed that this was the best available method.

The self-duality relation at criticality suggests an alternative pseudo-critical coupling $\beta_c(N_t, N_s)$. We can employ the intersection of vortex and electric flux free energies to locate the transition,[8]

$$F_k(\beta_c(N_t, N_s)) \simeq F_e(\beta_c(N_t, N_s)). \tag{3.87}$$

The symmetry of this definition ensures extremely rapid convergence as $N_s \to \infty$. The leading finite volume corrections to scaling are universal and thus cancel around β_c in the intersection of F_k and F_e . Writing once more our FSS ansatz for vortex free energies,

$$F_k = \ln(1+2^{3/4}) + b(\beta-\beta_c)N_s^{1/\nu} + cN_s^{-\omega} + \dots\,, \tag{3.88}$$

self-duality dictates the same ansatz for electric fluxes,

$$F_e = \ln(1+2^{3/4}) + b(\beta-\beta_c)N_s^{1/\nu} + cN_s^{-\omega} + \dots\,, \tag{3.89}$$

with identical coefficients b and c. The leading FSS corrections shift the free energies equally,

$$F_k(\beta_c) = F_e(\beta_c) = \ln(1+2^{3/4}) + cN_s^{-\omega} + \dots\,, \tag{3.90}$$

so they are absent in the estimates $\beta_c(N_t, N_s)$.

A comparison of critical coupling estimates obtained via self-duality and those obtained from the universal value for the vortex free energy is shown for $N_t = 4$ in Fig. 3.19 and summarized in Table 3.3. The results from self-duality on lattices as small as $N_s = 16$ are already within the error bars of our previous best infinite volume extrapolation. The intersection $F_k = F_e$ requires the simulation of an additional set of vortex ensembles ($\vec{k} = (1,1)$ for symmetric SU(2) lattices) so that we can perform the discrete Fourier transform used to obtain F_e. But this cost is insignificant compared to the computational savings from eliminating FSS corrections.

The offset of the intersection $F_k = F_e$ from their universal value at criticality gives the leading correction to scaling term, $cN_s^{-\omega}$. Fitting the N_s dependence then gives the correction to scaling exponent ω for a given N_t data set. See Table 3.4 for a

8 One could, of course, use any pair $F_k(\vec{k})$ and $F_e(\vec{e})$ with $\vec{k} = \vec{e}$. A single unit of flux is the simplest choice.

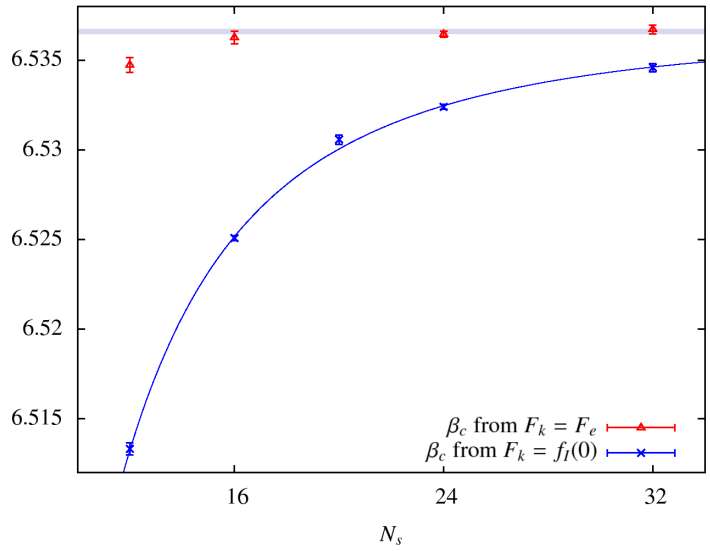

Figure 3.19: Critical couplings for $2+1$ d SU(2) ($N_t = 4$) from self-duality compared to those of Table 3.1, with N_s up to 96 and the infinite-volume extrapolated result $\beta_c = 6.53658(16)$ shown as the narrow gray band here.

N_s	$\beta_c(F_k = F_e)$	$\beta_c(F_k = f_I(0))$
12	6.53474(42)	6.51333(33)
16	6.53627(36)	6.52508(13)
24	6.53645(17)	6.5324(14)
32	6.53672(24)	6.5346(23)
	w. av. $N_S = 24, 32$	exp. (full set $N_s \leq 96$)
	6.53654(14)	6.53658(16)

Table 3.3: Comparison of $N_t = 4$ pseudo-critical critical couplings $\beta_c(N_t, N_s)$ for SU(2) in $2+1$ d obtained using self-duality (with weighted mean) versus the intersection of F_k with its known universal value (with infinite volume extrapolation from the full set of N_s lattices). The intersections $F_k = F_e$ were obtained using a simultaneous linear fit.

N_t	ω from $F_k = F_e$ offset	red. χ^2	ω from $\beta_c(N_t, N_s)$ extrap.	red. χ^2
2	1.61(9)	0.78	1.34(12)	0.83
3	1.53(25)	0.36	1.16(50)	0.21
4	1.54(7)	1.52	1.47(6)	0.98

Table 3.4: SU(2) correction to scaling exponents obtained from the offset of $F_k = F_e$ from the universal value $f_I(0)$ (left) and from the extrapolations of pseudo-critical couplings in Section 3.4.3, together with the reduced χ^2 of the fits that they were extracted from.

comparison with the values for ω obtained as a fit parameter in our extrapolations of pseudo-critical couplings $\beta_c(N_t, N_s)$ in Section 3.4.3 from universality alone. Exploitation of self-duality to single out the scaling correction yields a more consistent estimate for ω between various values of N_t, and is therefore the preferred method.

3.7 SU(3) IN 2 + 1 d

The deconfinement transition of pure SU(3) gauge theory in $2+1$ d is also known to be second order. Its critical exponents are consistent with the self-dual $2d$ 3-state Potts model [61, 80], as predicted by the Svetitsky-Yaffe conjecture [81].

Unlike for the $2d$ Ising model universality class, the universal functions $f_I(\vec{k}, x)$ for interface free energies are not available from analytic solutions. The universal values at criticality have, however, been computed for all sets of spin interfaces induced on a torus with cyclically shifted boundary conditions $\vec{k}$, and for all of the 2, 3 and 4-state Potts models with continuous phase transitions [57]. For the 3-state Potts model on a symmetric lattice, there are two relevant universal values,

$$\frac{Z^{(1,0)}}{Z^{(0,0)}}|_{T_c} = \frac{Z^{(2,0)}}{Z^{(0,0)}}|_{T_c} = 0.30499982\ldots, \tag{3.91}$$

and

$$\frac{Z^{(1,1)}}{Z^{(0,0)}}|_{T_c} = \frac{Z^{(2,2)}}{Z^{(0,0)}}|_{T_c} = \frac{Z^{(2,1)}}{Z^{(0,0)}}|_{T_c} = 0.19500018, \tag{3.92}$$

which determine the interface free energies via

$$\frac{Z^{(\vec{k})}}{Z^{(0,0)}}|_{T_c} = e^{-f_I(\vec{k},0)}. \tag{3.93}$$

The elementary center vortex in SU(3) is not its own anti-vortex as it is in SU(2), but symmetry under reflection of the lattice and the quantization of center flux modulo 3 ensures that partition function ratios with one or two units of flux in a given direction are equivalent.

We have carried out lattice simulations of twisted ensembles as before, employing the usual Cabibbo-Marinari method to update SU(2) subgroups of SU(3) via heatbath and overrelaxation steps [82]. Once more, self-duality (3.62) of the Potts model manifests itself in the free energies of center vortex ensembles and their electric flux counterparts. Matching pairs of free energies with $\vec{k} = \vec{e}$ are again mirror images around criticality, i.e., identical under $x \leftrightarrow -x$ as functions of the finite size scaling variable,

$$x = \pm L T_c |t|^{\nu} \propto L/\xi_{\pm}, \tag{3.94}$$

where $\nu = 5/6$ for the 3-state Potts universality class.

The intersection of the $\vec{k} = (1,0)$ center vortex partition function ratio with the universal $3-$state Potts value (3.91) at criticality, together with the $\vec{e} = (1,0)$ electric flux partition function ratio, is evident in Fig. 3.20. Even on this small 2×24^2 lattice, the intersection $F_k(1,0) = F_e(1,0)$ is almost exactly at the universal value.

From universality and self-duality, we have again a FSS ansatz for vortex and electric flux free energies,

$$F_k(1,0) = F_e(1,0) = -f_I(0) + b(\beta - \beta_c) N_s^{1/\nu} + c N_s^{-\omega} + \ldots, \tag{3.95}$$

where $f_I(x)$ is shorthand for the universal scaling function for interface free energies with one unit of flux $\vec{e} = \vec{k} = (1,0)$.

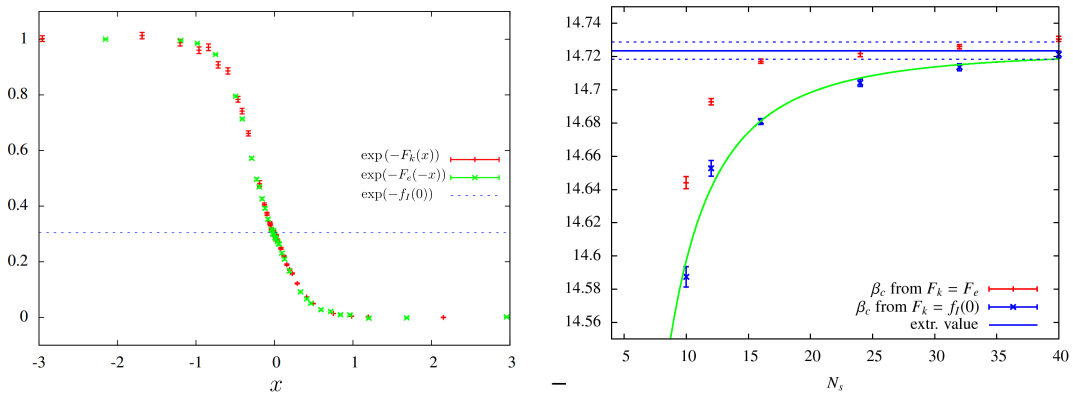

Figure 3.20: (left) Numerical evidence of self-duality for $2+1$ d SU(3), for single units of flux $\vec{k} = \vec{e} = (1,0)$ on 2×24^2 lattices. (right) Pseudo-critical couplings obtained via self-duality $F_e = F_k$ and universality $F_k = f_I(0)$ for one unit of flux, for $N_t = 4$.

3.7.1 *Critical couplings and correction to scaling exponent*

Fig. 3.20 compares the $N_t = 4$ pseudo-critical couplings on finite volumes obtained from self-duality, $F_k(1,0) = F_e(1,0)$, to those obtained by intersecting F_k with its universal value at T_c. The $\mathcal{O}(N_s^{-(\omega+1/\nu)})$ finite volume corrections that afflict the pseudo-critical couplings obtained from universality alone is again notably absent from the critical couplings obtained using self-duality, which exhibit much more rapid convergence.

Results from the intersection of flux free energies $F_k(1,0) = F_e(1,0)$ are summarized in Table 3.5 for several values of N_t. For lattices with aspect ratios $N_s : N_t$ of at least $6:1$, the residual finite size corrections to $\beta_c(N_s, N_t)$ extracted from self-duality are within the statistical errors. This provides a heuristic criterion for the weighted means in Table 3.5. Note, however, that a residual systematic underestimation remains from not extrapolating the data.

We also present estimates for the correction to scaling exponent ω. It is evaluated by fitting the N_s dependent offset of $F_k(1,0) = F_e(1,0)$ with the universal 3−state Potts value at criticality with the expected $N_s^{-\omega}$ behavior from our FSS ansatz.

N_t	$\beta_c(F_k = F_e)$	$\beta_c(F_k = f_I(0))$	Lit.	ω
2	8.15309(11)	8.15297(57)	8.1489(31)†	0.73(25)
4	14.7262(9)	14.7194(45)	14.717(17)†	0.98(14)
6	21.357(25)	-	21.34(4)‡	-
8	27.84(12)	-		-

Table 3.5: SU(3) critical couplings from self-duality (weighted means), and intersection with the universal value (extrapolated) from [16], previous literature values from †[39], ‡[61].

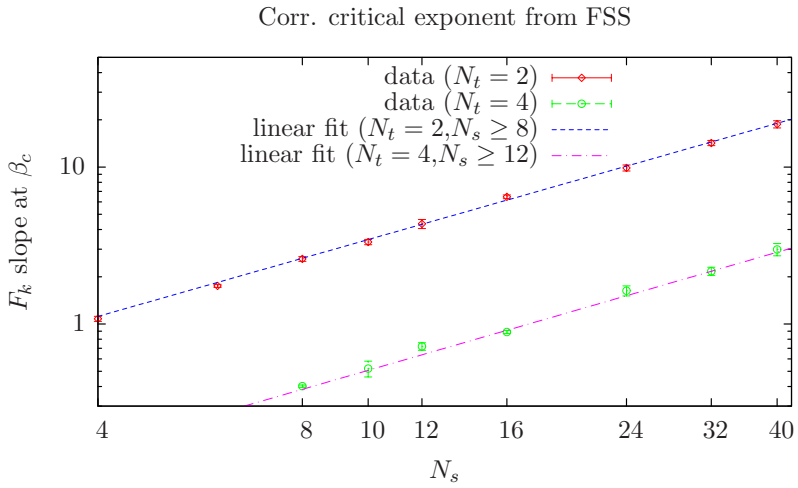

Figure 3.21: Slope of F_k at criticality versus N_s for $N_t = 2,\ 4$, with linear fits.

3.7.1.1 *Crosscheck of the correlation length exponent*

So far we have assumed that that the correlation length critical exponent $\nu = 5/6 \sim 0.8\bar{3}.$ for the $2d$ 3-state Potts model holds for SU(3) in $2+1$ d. This may be cross-checked by calculating the slope of vortex free energies F_k in terms of the reduced temperature $t \propto (\beta - \beta_c)$ at criticality, and fitting it to expected $N_s^{1/\nu}$ scaling behavior. For our $N_t = 2$ lattices we obtain $\nu = 0.812(17)$, while $N_t = 4$ volumes give $\nu = 0.80(6)$ (Fig. 3.21). A weighted average of these fits yields the exponent, $\nu = 0.818(24)$, fully consistent with universality.

3.7.1.2 *Critical couplings versus temperature*

The linear dependence of the critical lattice coupling on N_t at leading order follows as for SU(2) from the definition of the bare lattice coupling, $\beta = 2N_c/ag_3^2$, in terms of the dimensional continuum coupling, cf. (3.43). The slope

$$\frac{\beta_c(N_t)}{2N_c} = \frac{T_c}{g_3^2} N_t + \dots \tag{3.96}$$

obtained from a fit to $\beta_c(N_t = 4, 6, 8)$ in Table 3.5 without $1/N_t$ corrections is

$$\frac{T_c}{g_3^2} = 0.5475(3), \text{ or } \frac{T_c}{\sqrt{\sigma}} = 0.9938(9), \tag{3.97}$$

where the weighted mean $\sqrt{\sigma}/(g_3^2) = 0.5509(4)$ of the four values for $N_c = 3$ in [68] is used for the the conversion into units of the zero temperature string tension. This is consistent with the estimate $T_c/\sqrt{\sigma} = 0.9994(40)$ obtained in [39].

3.8 SU(4) IN 2 + 1 d

The deconfinement transition for SU(4) in $2+1$ d is especially interesting. Z_4 center symmetry is not enough to specify the simplest effective spin model. There may be different tensions for the interfaces that separate 'orthogonal' center sectors with center flux $e^{i\pi/2} \in Z_4$, and those that separate 'anti-parallel' sectors, with flux $-1 \in Z_4$. If one performs a strong coupling expansion of the effective action in terms of Z_4 invariant operators as in Ref. [83], the two fundamental representations 4, $\bar{4}$, as well as the double-fundamental representation $6 = 6^*$ that is obtained from the antisymmetric product, $(4 \otimes 4)_{asym}$, must be taken into account. The relative weight of the couplings between loops in the $4/\bar{4}$ representations and loops in the 6 representation is required to pin down the corresponding spin system. It could be any one from a wide class of symmetric Ashkin-Teller models.

It is conventional to formulate states of the symmetric[9] Ashkin-Teller model in terms of a pair of Ising models spins $(s_i, \sigma_i) = (\pm 1, \pm 1)$ coupled via the Hamiltonian [79],

$$\mathcal{H} = -\sum_{<i,j>} (J s_i s_j + J \sigma_i \sigma_j + J' s_i s_j \sigma_i \sigma_j). \tag{3.98}$$

There is a critical line of second order transitions between the limiting cases of the 4-state Potts model, with $J = J'$, and the vector Potts model, with $J' = 0$. In the 4-state Potts model, it doesn't cost additional energy to flip an orthogonal pair of neighboring spin states,

$$(1,1), (-1,1), \tag{3.99}$$

to an antiparallel pair, e.g.,

$$(1,1), (-1,-1). \tag{3.100}$$

In the vector model, on the other hand, antiparallel pairs cost twice as much energy, and the system corresponds to decoupled Ising systems. Along the line of second order transitions the critical exponents vary continuously with the relative weight $J : J'$ between those for the $4-$state Potts model, $\nu = 2/3$, $\beta = 1/12$,[10] and those for the 4-state vector Potts model, $\nu = 1$, $\beta = 1/8$.

Not only does the Svetitsky-Yaffe conjecture not predict a universality class for SU(4) in $2+1$ d, but its finite temperature transition and that of the 4-state Potts model lie right on the separation line between first and second order transitions (see Fig. 3.2). Increases in the size of the Z_N center or number of dimensions result in systems with first order transitions.

Numerical determination of the order of the SU(4) transition has proven to be surprisingly challenging. Simulations are hampered by logarithmic finite size corrections, present also for the $2d$ 4-state Potts model, and the existence of a bulk crossover centered at lattice coupling $\beta \sim 13.5$ [41]. This necessitates large spatial volumes as well as N_t values large enough to ensure that the bulk transition does not influence the order of the deconfinement transition.

9 *Symmetric* means that the couplings for the pair Ising spin systems are identical. They may differ in a generic Ashkin-Teller model.

10 β is the critical exponent for the magnetization, $\langle s_i \rangle \sim \langle \sigma_i \rangle \sim -t^\beta$. On the critical line away from the limiting cases $J = \{J', 0\}$ this 'magnetic' order parameter is distinguished from an additional 'electric' one $\langle s_i \sigma_i \rangle$ [79].

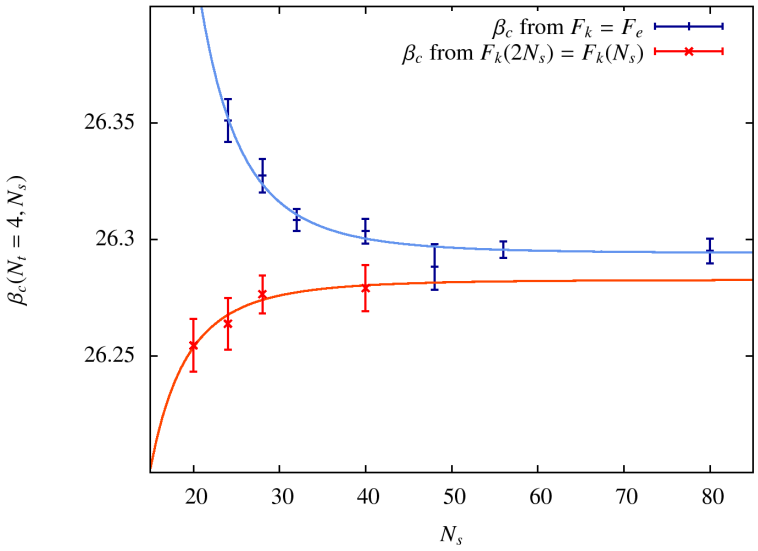

Figure 3.22: $N_t = 4$ pseudo-critical couplings obtained from the pairwise intersection of vortex free energies (red), and intersection with the universal value for interface free energies in the 4-state Potts universality class (blue).

Clear first order transitions were reported in Ref. [41] for $N_t = 1,\ 2$, for which the couplings are still near to the bulk crossover. Finite size scaling consistent with second order Potts model was found on their available $N_t = 3,\ 4$ volumes, however. More recent evidence [39, 40] suggests that the transition is in fact weakly first order. We will check for evidence of this in center vortex ensembles.

3.8.1 *Scaling of vortex free energies at criticality*

To obtain an estimate of the critical lattice coupling β_c that assumes a second order transition, but is independent from 4-state Potts model scaling, we have extracted it from pairwise intersections of center vortex free energies $F_k(1,0)$ on lattices with N_s ratios of $2:1$. We obtain the estimate $\beta_c = 26.283(9)$ for $N_t = 4$. It may be compared with the result obtained from intersecting vortex free energies with the exact universal value for interfaces in the 4-state Potts model given in [57]. This yields the consistent value $\beta_c = 26.294(2)$. Both extrapolations are plotted in Fig. 3.22. They are likewise consistent with $\beta_c = 26.228(75)$ from [39], but deviate with significance from $\beta_c = 26.251(16)$ in [40], in which first order scaling was assumed.

Under the assumption of second order scaling, the critical exponent ν may be extracted from the slopes of $F_k(\beta)$ at β_c, exactly as for SU(2) and SU(3). Fitting to an assumed $N_s^{1/\nu}$ dependence in a one-sigma interval around β_c yields $\nu = 0.59(5)$ for our $N_t = 4$ volumes. This favors the lower bound $\nu = 2/3$ for the 4-state Potts model along the critical line of symmetric Ashkin-Teller models, which is consistent with the slight underestimations of ν for SU(2) and SU(3). Indeed, center vortex free energies on finite $4 \times N_s^2$ lattices with up to $N_s = 80$ scale well around criticality under the assumption of 4-state Potts scaling, $\nu = 2/3$ (Fig. 3.23).

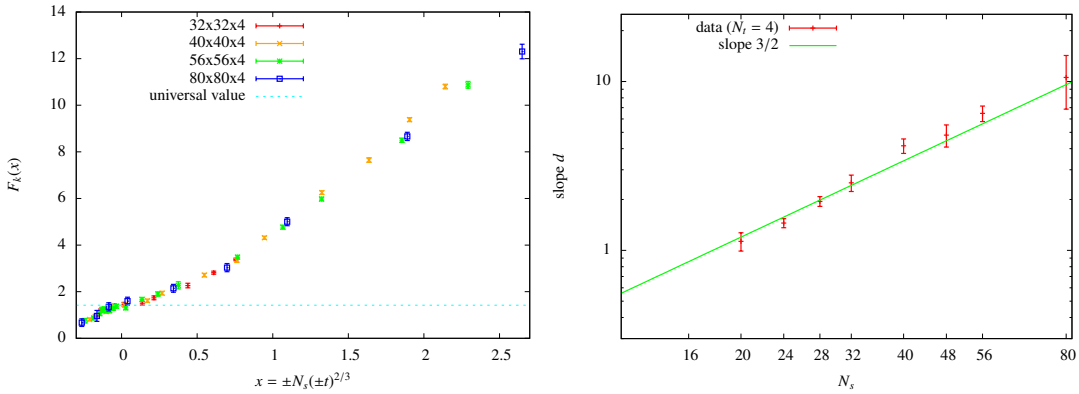

Figure 3.23: (left) Scaling of vortex free energies under the assumption of Potts model exponents.

(right) Slopes of vortex free energies at β_c compared to Potts model scaling $\nu = 2/3$.

3.8.2 *Distinguishing first from second order scaling*

Finite size scaling laws for a second order transition follow from the idea that, as the correlation length ξ diverges at criticality, it is eventually limited by the finite size L of the system and the ratio ξ/L determines the behavior of thermodynamic quantities. If ξ is large but finite at criticality, as for a weakly first order transition, then this ratio becomes effectively infinite for small and intermediate volumes. From this point of view, it is not surprising that we observe second order scaling in intermediate volumes for SU(4) in $2+1$ d, if the transition is weakly first order.

The evidence in Refs. [39, 40] that best supports a first order transition stems from the behavior of the Polyakov loop near criticality. If the SU(4) phase transition is first order, then the system may tunnel between the disordered, confined phase and the four deconfined, ordered center secters that all coexist at T_c. This is revealed by peaks in the probability distribution for the Polyakov loop P for each sector. A probability density plot of

$$|\frac{1}{V}\sum_{\vec{x}} P(\vec{x})| \tag{3.101}$$

exhibits tell-tale peaks near zero for the disordered phase and at $1/4$ for the Z_4 centor sectors, since the trace for the Polyakov loop is normalized by the number of colors $N_c = 4$. This was observed for various volumes in [39, 40].

There is a slight subtlety. A double peak structure may also be observed on finite volumes near a second order transition, since the volume average of the Polyakov may pass through zero when the system tunnels between deconfined center sectors. We demonstrate this for SU(3) in $2+1$ d on a 4×40^2 lattice in Fig. 3.24 (left). In this case, examination of the Monte Carlo history in Fig. 3.24 (right) indicates that the deconfined sectors do not coexist with a confined phase in which the the volume averaged Polyakov loop is disordered.

SU(4) Monte Carlo histories were presented in Ref. [40] for $N_t = 3$, which revealed evidence for phase coexistence near T_c and strengthened the case for a first order transition.

To see if this is maintained closer to the continuum limit, we have measured the Polyakov loop on large $N_t = 5$ volumes near T_c. Probability densities of its volume averaged magnitude for $N_s = 100,\ 160$ are shown in Fig. 3.26 and Fig. 3.25. The double peaked structures, together with an examination of the Monte Carlo histories as in Fig. 3.27, are indicative of phase coexistence and hence a first order transition.

This is not quite enough, though. The smoking gun for a first order transition is a non-zero latent heat L_h. On the lattice this is the difference of the action densities of the confined and deconfined phases,

$$L_h = (S_d - S_o)/N_p,\ N_p = (d+1)N_s^d N_t, \tag{3.102}$$

where N_p is the number of plaquettes. To be sure of a first order transition in the continuum limit, a non-zero latent heat must be measured and proven to persist in the limit $N_t \to \infty$.

The latent heat shows up as a double peak in a histogram plot of the average action at criticality, as a result of phase coexistence. When the latent heat is small, however, it is difficult or impossible to resolve the closely spaced peaks. This is the case for SU(4) in $2+1$ d, which is evident in our simulations (see Fig. 3.27) and was also noted in Refs. [39, 40].

A scaling analysis of the specific heat,

$$C = \frac{1}{N_p}(\langle S^2\rangle - \langle S\rangle^2), \tag{3.103}$$

provides an alternative route. On the lattice, the specific heat is the variance of the action S normalized by the number of plaquettes. Exactly at a first order phase transition, fluctuations in the action are maximized, since the disordered and ordered phases have equal probability, and the maximum of the specific heat gives the latent heat via,

$$C^{\max} = \frac{N_p}{4}L_h^2. \tag{3.104}$$

A scaling analysis of the specific heat was performed for $N_t \in \{3,4,5\}$ in Ref. [40]. The authors concluded that the finite $L = aN_s$ corrections to the specific heat were consistent with first order (i.e., extensive) scaling,

$$\frac{C^{\max}}{N_p} = \frac{1}{4}L_h^2 + c_1 L^{-d} + \ldots, \tag{3.105}$$

on their available volumes, with non-zero latent heats $L_h(N_t)$ that extrapolate to a non-zero value in the continuum limit $N_t \to \infty$.

A comparison with second order scaling was not presented, however, and the regular contribution to the specific heat was not taken into account. Due to the unphysical bulk crossover of the lattice model at $\beta \sim 13.5$, the volume independent part dominates the singular N_s dependence of the specific heat, as noted in Ref. [41]. On our 5×100^2 lattice, for example, the regular contribution is 95% of $C^{\max}$ (see Fig. 3.28). The large regular part of the specific heat, calculated on symmetric

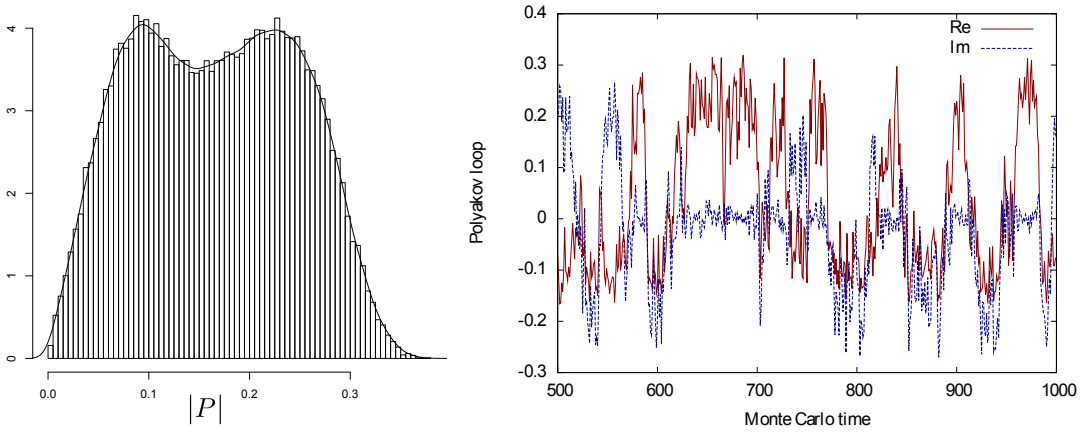

Figure 3.24: (left) A double peak structure in a density distribution of the absolute value for the Polyakov loop near the second order transition of $2+1$ d SU(3), here at $\beta_{col} = 14.4$ on a 4×40^2 lattice.

(right) Monte Carlo history of the real and imaginary parts of the Polyakov loop, with tunneling between center sectors.

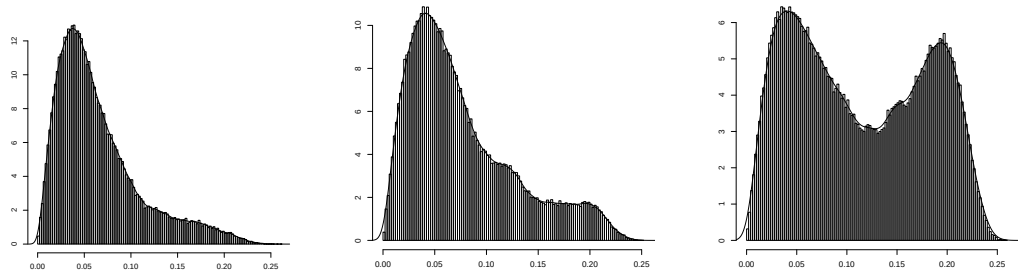

Figure 3.25: Density plots of the volume averaged absolute value of the Polyakov loop on 5×160^2 lattices, with $\beta = 31.97,\ 32.,\ 32.05$ from left to right. A clear double peak structure emerges at the transition.

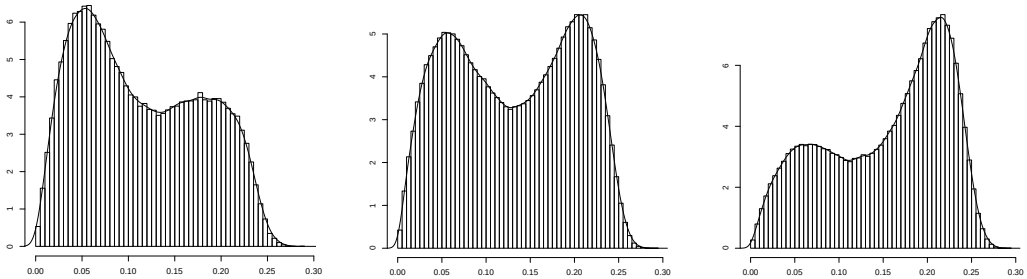

Figure 3.26: Density plots of the volume averaged absolute value of the Polyakov loop on 5×100^2 lattices, with $\beta = 31.95,\ 32.,\ 32.05$ from left to right.

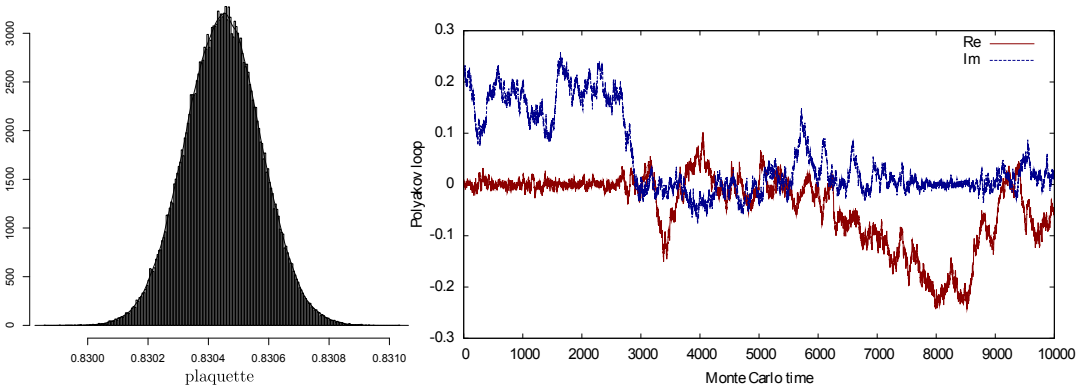

Figure 3.27: (left) Density distribution of the SU(4) plaquette near the transition at $\beta = 32.05$ on a 5×160^2 lattice. Only the hint of closely separated peaks is visible, via a slight deformity.

(right) Monte Carlo history of the real and imaginary parts of the corresponding Polyakov loop, which indicates tunneling from a deconfined center sector to the confined disordered phase.

lattices, must be subtracted from $C^{\max}$ before a consistent scaling analysis may be performed.

After calculating and subtracting the regular part of $C(\beta)$ from the tabulated data for $C^{\max}$ in Ref. [40], first order scaling may not be distinguished with statistical significance from second order scaling of the form [52],

$$\frac{C^{\max}}{N_p} = c_0 L^{\alpha/\nu - d} + c_2 L^{-d} + \ldots, \tag{3.106}$$

where α is the exponent that governs the divergence of the specific heat at a second order transition,

$$C \sim |t|^{-\alpha}, \tag{3.107}$$

and we use $\alpha = \nu = 2/3$ for the 4-state Potts model. That is, the data is consistent with zero latent heat. We illustrate this for $N_t = 5$ in Fig. 3.30, where we have included estimates for $C^{\max}$ from our own simulations in the fits. The goodness of fits via the reduced χ^2/dof. are, in this case, 0.85 for the assumption of first order scaling, and 1.17 for second order Potts model scaling.

Our results are therefore in agreement with Refs. [39, 40], that deconfinement is consistent with a first order transition for $N_t \leq 5$. The continuum limit $N_t \to \infty$ must be taken with care, however. The lingering effects of the bulk crossover make it difficult to draw definitive conclusions from finite volume lattice data. Larger N_t may be required in order to determine whether the deconfinement transition of SU(4) in $2+1$ d remains first order or weakens to second order on the approach to continuum physics.

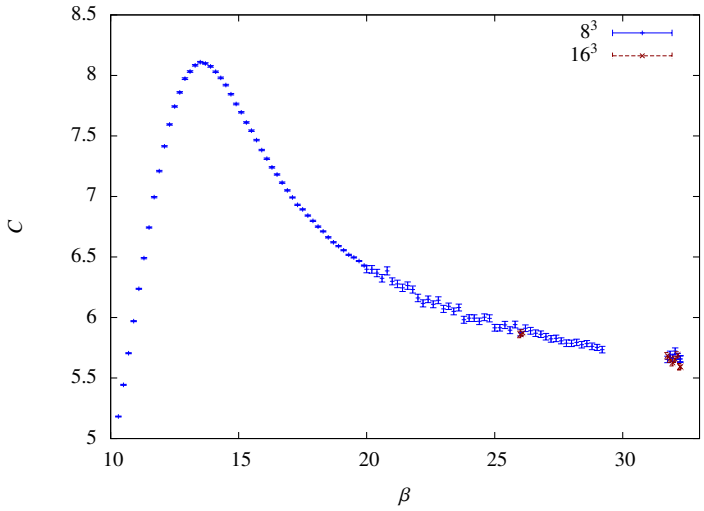

Figure 3.28: The specific heat C on symmetric volumes, which reveals the lingering tail of the bulk transition at $\beta \sim 13.5$.

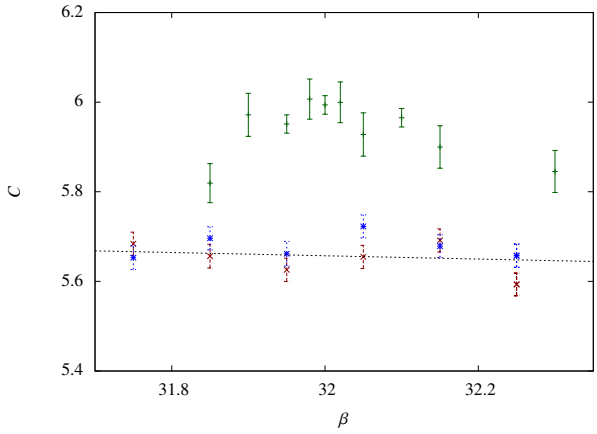

Figure 3.29: Specific heat C across the deconfinement transition on 5×100^2 lattices (green). The large regular contribution to the specific heat, here measured on 8^3 and 16^3 lattices, must be subtracted in order to obtain the singular N_s dependence.

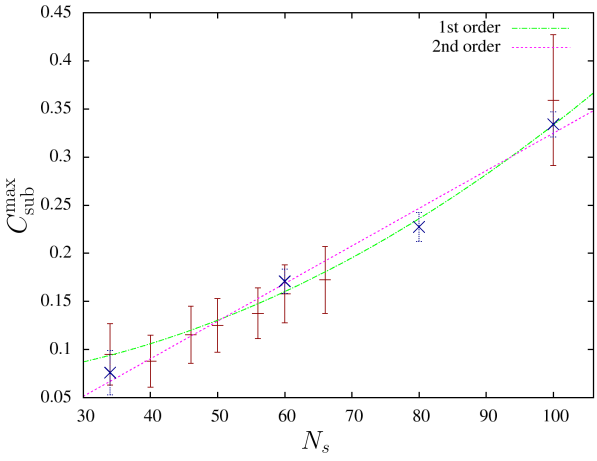

Figure 3.30: The maximum of the specific heat versus N_s for $N_t = 5$, after subtraction of the large contribution from the smooth background. Both first order Eq. (3.105) and second order Eq. (3.106) scaling is consistent with the data. The fits combine data from Ref. [40] (maroon), and our own simulations (blue).

3.8.3 *Directions*

The deconfinement transition of SU(4) Yang-Mills theory in $2+1$ d deserves further study. Even if it remains weakly first order in the continuum limit, the question remains: how is an effective critical model singled out from an infinite class of symmetric Ashkin-Teller models? Why is one of the limiting cases, the 4-state Potts model, favored by our data on intermediate volumes?

SU(4) is unique in that it's the smallest SU(N) gauge group in which the interfaces between center sectors must be distinguished. A better understanding of how this is dynamically realized would provide insight into the effective degrees of freedom near criticality.

For this purpose, a detailed analytic study of the effective Polyakov loop model in the framework of Ref. [83] could be enlightening.

In addition, Monte Carlo simulations with non-trivial boundary conditions could be of further use. Several possibilities present themselves.

Dual string tension ratios

A computation of the dual string tension ratio $\tilde{\sigma}_k(2,0)/\tilde{\sigma}_k(1,0)$ for two units $\vec{k} = (2,0)$ versus one unit $\vec{k} = (1,0)$ of center flux using 't Hoofts's twisted ensembles is one way forward. This ratio tells us the relative cost of separating center sectors that differ by a phase $-1 \in Z_4$ compared to a phase $e^{i\pi/2} \in Z_4$. That is, the analog of 'anti-parallel' and 'orthogonal' spins in a Z_4-symmetric statistical system.

The corresponding ratios of color-electric string tensions are studied under the guise of *k-strings* [13]. Asymptotic tensions only depend on the N-ality k_r of the representation, which labels the phase picked up by a source in that representation under a Z_N center transformation.[11] This is due to screening by the adjoint gluons, which transform any color-electric string into the lightest, stable string with the same N-ality.

Various theoretical predictions are available with different physical implications. If bound states do not form, then one expects for a generic string tension σ with N-ality k_r,

$$\sigma(k_r) = \min(k_r, N-k_r) \cdot \sigma(k_r = 1). \tag{3.108}$$

That is, the tension is proportional to the number of elementary fluxes. We take the smaller of k_r and $(N-k_r)$ since these are just fluxes with opposite directions in color space, i.e., anti-strings. For the SU(4) dual string tension such a prediction gives simply,

$$\frac{\tilde{\sigma}_k(2,0)}{\tilde{\sigma}_k(1,0)} = 2, \tag{3.109}$$

This is analogous to the *vector* Potts model.

Additional theoretical predictions include the sine law ratio

$$\frac{\sin(\pi k_r/N)}{\sin(\pi/N)} \simeq 1.414... \text{ for } k_r = 2,\ N = 4, \tag{3.110}$$

11 There is room for confusion with our notation $\vec{k}$ for temporal twists. The N-ality of our interfaces may just be set by the number of units of center flux.

which is inspired from supersymmetric models, and Casimir scaling

$$\frac{k_r(N-k_r)}{N-1} \simeq 1.333 \text{ for } k_r = 2,\ N = 4. \tag{3.111}$$

SU(N) $2+1$ d electric string tensions have been studied extensively in Refs. [84, 68, 85, 86, 87]. The scaling of electric k_r-string ratios is close to Casimir scaling, which occurs naturally if the flux tube has a cross-section that is nearly independent of the flux carried [84]. For SU(4) the zero temperature ratio is about 1.35 [84], which implies that two fundamental electric flux tubes are quite tightly bound.[12]

The approximate Potts scaling that we observe implies that elementary center fluxes are also tightly bound, with a similarly low *dual* string tension ratio $\tilde{\sigma}_k(2,0)/\tilde{\sigma}_k(1,0)$. A systematic study that reveals difference at T_c from the corresponding electric string tension ratio would indicate a violation of the self-duality of the 4−state Potts universality class.

Restriction of ensembles via C-periodic boundary conditions

Even on a symmetric spatial volume, the calculation of electric flux $Z_e(\vec{e})$ partition functions for $2+1$ d SU(4) requires simulations for five distinct temporal twists $\vec{k}$.[13] And a system in the deconfined phase may tunnel between any of the four center sectors on a periodic volume. It would be helpful to reduce the degeneracy, both for computational ease, and to disentangle the interactions of the various sectors, i.e, the $4/\bar{4}$ and 6 loop representations.

If charge conjugation is included via the C-periodic boundary conditions [89] discussed in Chapter 4, then the number of allowed flux sectors is reduced. They eliminate twist for SU(N), N odd, and reduce them to Z_2^3 for N even. They were used in Ref. [90], for instance, to restrict the SU(3) Polyakov loop to the $1 \in Z_3$ center sector in the deconfined phase.

The analogous use of C-periodic boundary conditions in SU(4) restricts the simulations to a Z_2 subgroup of the center, which may enhance the signal for a first order transition by reducing the number of degenerate deconfined sectors.

One can furthermore study C-periodic center flux partition function ratios and their corresponding Z_2 Fourier transforms. A thorough discussion of C-periodic twists is presented in the next chapter. For now we mention that the C-periodic twists single out the center fluxes quantized by $-1 \in Z_4$. A comparison with the Z_2 center fluxes of SU(2) in $2+1$ d, corresponding to the $2d$ Ising model, would give an indication of how tightly bound the SU(4) interfaces are.

We will now close this lengthy chapter and change the pace by turning to another type of topological object, the magnetic monopole. See the final summary of the thesis for a reminder of what we have learned here.

12 Interestingly, a linear, as opposed to logarithmic, broadening of the flux tube with the source separation has been observed in finite temperature lattice simulations, which is consistent with analytic predictions [88, 87].

13 Every combination of one and two units of flux through the two spatial planes must be accounted for (symmetry provides the rest).

4

'T HOOFT MONOPOLES IN LATTICE GUTS

The experimental search for magnetic monopole has been fruitless [91]. Still, they retain theoretical interest as a general prediction of grand unified theories (GUTs) and as a tool for studying the non-perturbative properties of quantum field theories via dualities [92]. The absence of magnetic sources in Maxwell's equations is conspicuous. Their existence would at once restore electric-magnetic symmetry and justify the quantization of electric charge [93]. This is relevant to the puzzling link between the fractional electric charge of quarks and their confinement that is explored in the next chapter.

Most of the existing studies of monopoles in non-supersymmetric theories have been restricted to the level of classical solutions. Little is known about quantum mechanical effects. Even the leading order corrections are usually only calculable in simple one-dimensional models [94].

Lattice field theory offers us a fully non-perturbative tool for studying monopoles. There are two available approaches. One can either define suitable creation and annihilation operators and measure their correlators [95, 96, 97], or else impose boundary conditions that restrict the path integral to a non-trivial topological sector [98]. The former approach gives, in principle, access to a wide range of observables including, e.g., the vacuum expectation value of the monopole field. However, because monopoles are surrounded by a spherical infinite-range magnetic Coulomb field, it is difficult to find a suitable operator and separate the true ground state from excited states.

Instead, while non-trivial boundary conditions provide access to a more limited set of observables, they ensure that the monopole is always in its ground state. Early attempts to simulate monopoles were based on fixed boundary conditions [99], which introduce large finite-size effects. Translationally invariant boundary conditions are preferred. They were introduced for the SU(2) Georgi-Glashow model in [100] and were used to calculate the mass of 't Hooft-Polyakov monopoles in [101, 102].

The relevant boundary conditions are a version of twisted boundary conditions for the gauge-Higgs system that include charge conjugation. In [18] we generalized the result for SU(N) with an adjoint Higgs field for $N > 2$. The boundary conditions treat all monopole species in the same way, so one cannot fix the magnetic charge absolutely. One chooses between odd and even charges for each species. This is only possible for even N, so it rules out the prototypical SU(5) GUT. Nevertheless, the generalization is relevant as many analytical results are valid only in the large-N limit. Moreover, a richer theoretical structure with new questions arises when one goes beyond the special case of SU(2). For instance, there can be several different monopole species and also unbroken non-abelian gauge groups.

The presentation here differs from Ref. [18]. After reviewing the continuum and lattices definitions of the magnetic field in SU(N) -Higgs theories, we introduce twisted C-periodic twisted boundary conditions. Before presenting a formal proof

for the magnetic charges, however, we explore the connection between abelian monopoles and center vortices. This allows for a more intuitive understanding of the allowed magnetic charges in terms of center fluxes.

4.1 MAGNETIC CHARGES IN THE CONTINUUM

The most general renormalizable Lagrangian for SU(N) gauge field theory A_μ with an adjoint Higgs field Φ is

$$\begin{aligned}\mathcal{L} &= -\mathrm{tr}G^{\mu\nu}G_{\mu\nu} + \mathrm{tr}[D_\mu,\Phi][D^\mu,\Phi] \\ &\quad -m^2\mathrm{tr}\Phi^2 - \kappa\mathrm{tr}\Phi^3 - \lambda_1(\mathrm{tr}\Phi^2)^2 - \lambda_2\mathrm{tr}\Phi^4,\end{aligned} \tag{4.1}$$

with the covariant derivative and field strength tensor defined by

$$D_\mu = \partial_\mu + igA_\mu, \quad G_{\mu\nu} = -\frac{i}{g}[D_\mu, D_\nu], \tag{4.2}$$

respectively. Both Φ and A_μ are Hermitian and traceless $N \times N$ matrices. They can be expanded in terms of the (N^2-1) group generators T^A,[1]

$$\Phi(x) = \phi^A(x)T^A, \quad A_\mu(x) = A^A_\mu(x)T^A, \tag{4.3}$$

with real coefficients ϕ^A and A^A_μ.

For SU(2), the Pauli matrices are a convenient choice for the generators,

$$T^A = \frac{\sigma^A}{2}. \tag{4.4}$$

Their properties imply that $\mathrm{tr}\Phi = \mathrm{tr}\Phi^3 = 0$ and $(\mathrm{tr}\Phi^2)^2 = 2\mathrm{tr}\Phi^4$. So the Lagrangian (4.1) can be simplified via $\kappa = \lambda_2 = 0$ without any loss of generality.

In the broken phase, where $m^2 < 0$, the Higgs field acquires a vacuum expectation value

$$\langle \mathrm{tr}\Phi^2\rangle = \frac{1}{2}\langle\phi^A\phi^A\rangle = \frac{v^2}{2} \equiv \frac{m^2}{\lambda}. \tag{4.5}$$

that spontaneously breaks the SU(2) symmetry to U(1). The normalized field

$$\hat{\Phi}(x) = \frac{\Phi(x)}{\sqrt{2\mathrm{tr}\Phi(x)^2}}, \tag{4.6}$$

represents the direction of symmetry breaking in color space. The residual U(1) gauge freedom consists of rotations about this direction, which is well defined whenever $\Phi \neq 0$. Following 't Hooft [103], the field strength for the residual U(1) symmetry is defined by,

$$\begin{aligned}F_{\mu\nu} &= 2\mathrm{tr}\hat{\Phi}G_{\mu\nu} - \frac{4i}{g}\mathrm{tr}\hat{\Phi}[D_\mu,\hat{\Phi}][D_\nu,\hat{\Phi}] \\ &= \partial_\mu(\hat{\phi}^A A^A_\nu) - \partial_\nu(\hat{\phi}^A A^A_\mu) + \frac{\epsilon_{ABC}}{g}\hat{\phi}^A(\partial_\mu\hat{\phi}^B)\partial_\mu\hat{\phi}^C.\end{aligned} \tag{4.7}$$

$$\tag{4.8}$$

1 We use lower case Latin letters for $a = 1,\ldots,N$ and upper case Latin letters for $A = 1,\ldots,(N^2-1)$. Greek letters represent Lorentz indices.

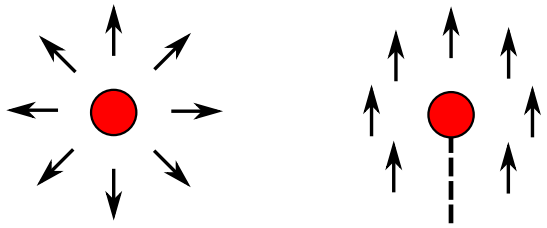

Figure 4.1: Diagonalization of the Higgs field Φ uncovers monopoles as gauge fixing singularities. The unphysical Dirac string is gauge dependent, but the location of degenerate eigenvalues for Φ is not.

This definition is more transparent in the unitary gauge, where the Higgs field has been diagonalized using a gauge transform $R(x)$,

$$\tilde{\Phi}(x) \equiv R^\dagger(x)\Phi(x)R(x) = \sqrt{2\mathrm{tr}\Phi^2}\frac{\sigma^3}{2}. \tag{4.9}$$

In terms of the transformed gauge field

$$\tilde{A}_\mu = R^\dagger A_\mu R - \frac{i}{g}R^\dagger\partial_\mu R, \tag{4.10}$$

the field strength tensor has the familiar form,

$$F_{\mu\nu} = \partial_\mu \tilde{A}^3_\nu - \partial_\nu \tilde{A}^3_\mu. \tag{4.11}$$

This defines a two-component vector of field strength tensors for the diagonal elements of the gauge field,

$$F^a_{\mu\nu} = \partial_\mu \tilde{A}^{aa}_\nu - \partial_\nu \tilde{A}^{aa}_\mu. \tag{4.12}$$

But tracelessness of A_μ implies $F^2_{\mu\nu} = -F^1_{\mu\nu}$. The conventional field strength $F_{\mu\nu}$ is the sum $F_{\mu\nu} = F^1_{\mu\nu} - F^2_{\mu\nu}$.

The conserved magnetic current corresponding to the residual U(1) group is defined as

$$j^a_\mu = \partial^\nu {}^\star F^a_{\mu\nu}, \tag{4.13}$$

where ${}^\star F^a_{\mu\nu}$ is the dual tensor,

$${}^\star F^a_{\mu\nu} = \frac{1}{2}\epsilon_{\mu\nu\rho\sigma}F^{a\,\rho\sigma}. \tag{4.14}$$

Like the field strength, the magnetic currents satisfy $j^2_{\mu\nu} = -j^1_{\mu\nu}$, so there is only one monopole species. The current is obtained by substituting Eq. (4.7),

$$j^1_\mu = \frac{1}{4g}\epsilon_{\mu\nu\rho\sigma}\epsilon_{ABC}(\partial^\nu\hat{\phi}^A)(\partial^\rho\hat{\phi}^B)(\partial^\sigma\hat{\phi}^C) = -j^2_\mu., \tag{4.15}$$

which is only non-zero when Φ vanishes. Monopoles arise from singularities in the gauge fixing procedure. The magnetic charge within a volume V whose boundary encloses a zero is

$$Q = \int_V d^3x j_0 = \pm\frac{2\pi}{g}(1,-1). \tag{4.16}$$

The generalization to SU(N) is more or less straightforward [104]. The matrices $\{T^A\}$ in Eq. (4.3) are now the generators of SU(N) in the fundamental representation with the usual normalization

$$\mathrm{tr} T^A T^B = \frac{1}{2}\delta^{AB}. \tag{4.17}$$

As in Eq. (4.9), consider a gauge transformation $R(x)$ that diagonalizes $\Phi(x)$ and places the eigenvalues in descending order,

$$\tilde{\Phi}(x) = R^\dagger(x)\Phi(x)R(x) = \mathrm{diag}(\lambda_1, ..., \lambda_N), \tag{4.18}$$

where $\lambda_1 \geq \lambda_2 \geq ... \geq \lambda_N$.

Classically, it is common to choose a potential that is minimized when the Higgs points in the direction of a single diagonal generator, so that there is only one residual U(1) group. For instance, the minimal symmetry breaking pattern,

$$\mathrm{SU}(3) \to \mathrm{SU}(2) \times \mathrm{U}(1)/Z_2, \tag{4.19}$$

that follows from $\tilde{\Phi} \sim \mathrm{diag}(1, 1, -2)$ yields a unique electromagnetic U(1) in the low energy theory.

In lattice Monte Carlo simulations the eigenvalues are generally distinct. Then $\tilde{\Phi}(x)$ is only invariant under gauge transformations generated by the $N-1$ diagonal generators of SU(N) . We are left with a residual $\mathrm{U}(1)^{N-1}$ gauge invariance corresponding to the Cartan subgroup of SU(N) . Following 't Hooft [104] the residual U(1) field strengths are defined by Eq. (4.12), with $a \in \{1, \ldots, N\}$. The corresponding magnetic currents j^a_μ are given by Eq. (4.13). The tracelessness condition

$$\sum_{a=1}^{N} F^a_{\mu\nu} = \sum_{a=1}^{N} j^a_{\mu\nu} = 0, \tag{4.20}$$

means that there are only $N-1$ independent U(1) fields and magnetic charges, one for each diagonal generator.

In three dimensions any two eigenvalues coincide, $\lambda_b = \lambda_{b+1}$, in a discrete set of points, which behave like magnetic charges with respect to the components $F^b_{\mu\nu}$ and $F^{b+1}_{\mu\nu}$ of the field strength tensor (4.12) [104]. That is, like magnetic monopoles with charge $Q = \pm\hat{q}_b$, where the elementary magnetic charges are

$$\hat{q}^a_b = \frac{2\pi}{g}\left(\delta_{a,b} - \delta_{a,(b+1)}\right), \tag{4.21}$$

or in vector notation

$$\hat{q}_b = \frac{2\pi}{g}\left(\overbrace{0, ..., 0}^{b-1}, 1, -1, \overbrace{0, ..., 0}^{N-b-1}\right). \tag{4.22}$$

The elementary charges are embeddings of the SU(2) monopole. In the core of the monopole, the SU(2) subgroup involving the bth and $(b+1)$th components of the fundamental representation is restored.

4.2 MAGNETIC CHARGE ON THE LATTICE

On the lattice, the Higgs field is defined on sites x and parallel transported by SU(N) link variables $U_\mu(x)$. For the Lagrangian we use the Wilson gauge action with additional terms for the Higgs field

$$\begin{aligned}\mathcal{L} &= \frac{\beta}{N}\sum_{\nu>\mu}\mathrm{Re}\,[\mathrm{tr}\,\Box_{\mu\nu}] \\ &\quad +2\sum_\mu\left[\mathrm{tr}\Phi(x)^2-\mathrm{tr}\Phi(x)U_\mu(x)\Phi(x+\hat{\mu})U_\mu^\dagger(x)\right] \qquad (4.23)\\ &\quad +m^2\mathrm{tr}\Phi^2+\kappa\mathrm{tr}\Phi^3+\lambda_1(\mathrm{tr}\Phi^2)^2+\lambda_2\mathrm{tr}\Phi^4. \qquad (4.24)\end{aligned}$$

Again, we diagonalize Φ by a gauge transformation $R(x)$,

$$\tilde{\Phi}(x)=R^\dagger(x)\Phi(x)R(x). \qquad (4.25)$$

which transforms the link variables to

$$\tilde{U}_\mu(x)=R^\dagger(x)U_\mu(x)R(x+\hat{\mu}). \qquad (4.26)$$

The diagonalized field $\tilde{\Phi}$ is still invariant under diagonal gauge transformations,

$$\begin{aligned}D(x) &= \mathrm{diag}\,(e^{i\Delta_1(x)},\ldots,e^{i\Delta_N(x)}),\\ &\quad \sum_{a=1}^N\Delta_a=0 \mod 2\pi, \qquad (4.27)\end{aligned}$$

which form the residual U$(1)^{N-1}$ symmetry group and contain the elements of the center Z_N of SU(N). To identify the corresponding U(1) field strength tensors, we must decompose $\tilde{U}_\mu$ [105],

$$\tilde{U}_\mu(x)=C_\mu(x)u_\mu(x), \qquad (4.28)$$

where $u_\mu(x)$ represents the residual U(1) gauge fields and transforms as

$$u_\mu(x)\to D^\dagger(x)u_\mu(x)D(x+\hat{\mu}), \qquad (4.29)$$

and $C_\mu(x)$ represents fields charged under the U(1) groups. This decomposition is not unique [105]. A simple choice is to define abelian link variables as the diagonal elements of $\tilde{U}_\mu$ in direct analogy with Eq. (4.12),

$$u_\mu(x)=\mathrm{diag}\,\tilde{U}_\mu(x). \qquad (4.30)$$

It is more convenient to work with link angles and define an N-component vector

$$\alpha_\mu^a(x)=\arg u_\mu^{aa}. \qquad (4.31)$$

As angles, these are only defined modulo 2π, and we choose them to be in the range $-\pi<\alpha_\mu^a\le\pi$. As in the continuum we have a tracelessness condition

$$\sum_a\alpha_\mu^a(x)=0 \mod 2\pi. \qquad (4.32)$$

So $\alpha^a_\mu(x)$ has only $N-1$ independent components, one for each residual U(1) gauge group.

The lattice analogs of the abelian field strength are the plaquette angles,

$$\alpha^a_{\mu\nu}(x) = \alpha^a_\mu(x) + \alpha^a_\nu(x+\hat{\mu}) - \alpha^a_\mu(x+\hat{\nu}) - \alpha^a_\nu(x), \tag{4.33}$$

which are related in the continuum limit by

$$F^a_{\mu\nu} = \frac{1}{g}\alpha^a_{\mu\nu}. \tag{4.34}$$

Since the links α^a_μ are defined modulo 2π, so too are the plaquettes. We again choose $-\pi < \alpha^a_{\mu\nu} \leq \pi$.

Using Eq. (4.33), the corresponding lattice magnetic currents are

$$j^a_\mu = \frac{1}{g}\Delta^f_\nu \, {}^\star\alpha^a_{\mu\nu}, \tag{4.35}$$

where Δ^f_ν is the forward derivative in direction ν on the lattice and

$${}^\star\alpha^a_{\mu\nu} = \frac{1}{2}\epsilon_{\mu\nu\rho\sigma}\alpha^a_{\rho\sigma}. \tag{4.36}$$

These are integer multiples of 2π, because each contribution of $\alpha^a_\mu(x)$ is canceled by a $-\alpha^a_\mu(x)$ modulo 2π.

In particular, the abelian magnetic charge inside a single lattice cell is given by

$$q^a(x) = j^a_0 = \frac{1}{2g}\sum_{ijk}\epsilon_{ijk}\left(\alpha^a_{ij}(x+\hat{k}) - \alpha^a_{ij}(x)\right). \tag{4.37}$$

Each component of this vector is an integer multiple of $(2\pi/g)$, and they all add up to zero. The elementary charges, corresponding to individual monopoles, are the same as in the continuum (4.22). Other values of the charge vector q correspond to composite states made of elementary monopoles.

The diagonalization procedure in Eq. (4.18) is ill defined when the Higgs field has degenerate eigenvalues, but such lattice configurations are a set of zero measure. Physically, the core of the monopole never lies exactly at a lattice site. So these configurations do not contribute to physical observables and do not have to be considered separately.

4.3 MONOPOLE MASS

The abelian magnetic charge Q of any lattice field configuration is defined by adding up the contributions (4.37) from each lattice cell,

$$Q = \sum_x q(x). \tag{4.38}$$

As it is discrete, the partition function decomposes to a product of partition functions Z_Q for each magnetic charge sector.

$$Z = \prod_Q Z_Q. \tag{4.39}$$

The free energy per temperature of a given charge sector is defined as for center vortices

$$F_Q = -\ln \frac{Z_Q}{Z_0}, \tag{4.40}$$

where Z_0 is the partition function of the charge zero sector. The mass M_j of a single monopole $\hat{q}_j$ is given by the ground state energy of the corresponding charge sector.

A lattice calculation requires boundary conditions that enforce non-trivial abelian magnetic charge. Moreover, they should preserve translational invariance. Boundary effects would otherwise swamp the contribution from a point-like monopole.

Gauss' law rules out periodic boundary conditions. They fix the charge to zero. However, translational invariance only requires periodicity up to the symmetries of the Lagrangian (4.23). And since the magnetic current is conserved, only spatial boundary conditions need to be considered.

For SU(2), it was found in [100] that the boundary conditions

$$\begin{aligned} \Phi(x + L\hat{\jmath}) &= -\sigma_j \Phi(x) \sigma_j = (\sigma_2\sigma_j)^\dagger \Phi^*(x) (\sigma_2\sigma_j), \\ U_\mu(x + L\hat{\jmath}) &= \sigma_j U_\mu(x) \sigma_j = (\sigma_2\sigma_j)^\dagger U_\mu^*(x) (\sigma_2\sigma_j), \end{aligned} \tag{4.41}$$

force an odd value for the magnetic charge, whilst

$$\begin{aligned} \Phi(x + L\hat{\jmath}) &= -\sigma_2 \Phi(x) \sigma_2 = \Phi^*(x) \\ U_\mu(x + L\hat{\jmath}) &= \sigma_2 U_\mu(x) \sigma_2 = U_\mu^*(x), \end{aligned} \tag{4.42}$$

are compatible with any even value.

These are an example of C-periodic boundary conditions, as introduced by Kronfeld and Wiese [89]. Note that twisted C-periodic and twisted periodic boundary conditions are equivalent for the gauge links. The Higgs field is anti-periodic when we convert from one form to the other. Physically, this means that charge conjugation is carried only by the Higgs field in SU(2).

Assuming that monopoles do not form bound states, the weight of the multi-monopole configurations in the path integral is exponentially suppressed. So the partition function Z_{odd} for twisted C-periodic boundary conditions is dominated by configurations with a single monopole, while the partition function Z_{even} is dominated by configurations with no monopoles. The non-perturbative mass

$$M = -\lim_{T \to 0} T \ln Z_{\text{odd}} / Z_{\text{even}} \tag{4.43}$$

of the 't Hooft-Polyakov monopole was calculated in [101, 102], with good agreement with classical expectations.

4.4 TWISTED C-PERIODIC BOUNDARY CONDITIONS

Translational invariance requires periodicity up to the symmetries of the theory. In the case of the gauge-Higgs Lagrangian (4.23), the available symmetries are complex conjugation of the fields and gauge invariance. When $\kappa = 0$, reflection of the Higgs field $\Phi \to -\Phi$ is also a symmetry, but this is not general so we do not consider it. The appropriate extension of (4.41) for SU(N) is then

$$\begin{aligned}\Phi(x+L\hat{\jmath}) &= \Omega_j^\dagger(x)\Phi^*(x)\Omega_j(x),\\ U_\mu(x+L\hat{\jmath}) &= \Omega_j^\dagger(x)U_\mu^*(x)\Omega_j(x+\hat{\mu}),\end{aligned} \tag{4.44}$$

with SU(N) gauge transformations $\Omega_j(x)$. We have started with the natural choice of complex conjugation in each spatial direction. We will call these C-periodic boundary conditions [89].[2]

As for 't Hooft's twisted boundary conditions, successive applications in different directions should not depend on their order. This implies the equalities [89]

$$\begin{aligned}&\Omega_j^\dagger(x+L\hat{k})\Omega_k^T(x)\Phi(x)\Omega_k^*(x)\Omega_j(x+L\hat{k})\\ &\quad=\Phi(x+L\hat{\jmath}+L\hat{k})\\ &\quad=\Omega_k^\dagger(x+L\hat{\jmath})\Omega_j^T(x)\Phi(x)\Omega_j^*(x)\Omega_k(x+L\hat{\jmath}),\end{aligned} \tag{4.45}$$

and

$$\begin{aligned}&\Omega_j^\dagger(x+L\hat{k})\Omega_k^T(x)U_\mu(x)\Omega_k^*(x+\hat{\mu})\Omega_j(x+L\hat{k}+\hat{\mu})\\ &\quad=U_\mu(x+L\hat{\jmath}+L\hat{k})\\ &\quad=\Omega_k^\dagger(x+L\hat{\jmath})\Omega_j^T(x)U_\mu(x)\Omega_j^*(x+\hat{\mu})\Omega_k(x+L\hat{\jmath}+\hat{\mu}).\end{aligned} \tag{4.46}$$

Since both fields are blind to center elements, Eq. (4.45) implies the cocycle condition

$$\begin{aligned}\Omega_i^*(x)\Omega_j(x+L\hat{\imath}) &= z_{ij}\,\Omega_j^*(x)\Omega_i(x+L\hat{\jmath}),\\ z_{ij} &= e^{in_{ij}},\end{aligned} \tag{4.47}$$

where the Nth roots of unity $z_{ij}=z_{ji}^*$ formed by the antisymmetric 'twist tensor' $n_{ij}=-n_{ji}$ have the usual parametrization in terms of three Z_N-valued numbers m_i,

$$n_{ij}=\frac{2\pi}{N}\,\epsilon_{ijk}m_k,\quad m_i\in Z_N. \tag{4.48}$$

Furthermore, Eq. (4.46) implies that the z_{ij} have to be independent of position.

All choices of $\Omega_i(x)$, $\Omega_j(x)$ with the same twist z_{ij} are gauge equivalent [47, 89], and we therefore assume that we can choose the matrices Ω_j to be independent of position analogous to the standard 'twist eaters' in the case of 't Hooft's twisted boundary conditions without charge conjugation [106].

Non-trivial twists are only possible for even N, which is revealed by applying the cocycle condition (4.47) to the product $\Omega_i\Omega_j^*\Omega_k$ [89]. On the one hand,

$$\begin{aligned}\Omega_i\Omega_j^*\Omega_k &= z_{jk}\Omega_i\Omega_k^*\Omega_j\\ &= z_{jk}z_{ki}\Omega_k\Omega_i^*\Omega_j\\ &= z_{jk}z_{ki}z_{ij}\Omega_k\Omega_j^*\Omega_i,\end{aligned} \tag{4.49}$$

but applying the condition in the opposite order yields

$$\begin{aligned}\Omega_i\Omega_j^*\Omega_k &= z_{ji}\Omega_j\Omega_i^*\Omega_k\\ &= z_{ji}z_{ik}\Omega_j\Omega_k^*\Omega_i\\ &= z_{ji}z_{ik}z_{kj}\Omega_k\Omega_j^*\Omega_i.\end{aligned} \tag{4.50}$$

2 In fact, in the terminology of Ref. [89], these correspond to C-periodic boundary conditions with $C=-1$, and $C=1$ would correspond to boundary conditions without complex conjugation.

Therefore the twist tensors satisfy the constraint

$$z_{ji}^2 z_{jk}^2 z_{ki}^2 = 1. \tag{4.51}$$

This implies a constraint for the sum of Z_N-valued magnetic twists m_i,

$$(m_1 + m_2 + m_3) \in \{0, N/2\} \in \{0, 1, \ldots, N-1\}. \tag{4.52}$$

Hence, for non-trivial C-periodic twist, $N/2$ must be in Z_N, i.e., N must be even [89].

Moreover, not all combinations of allowed C-periodic twists are physically distinguishable. Transition functions that differ by a constant center element ζ are equivalent, i.e., Ω_i is equivalent to $\zeta_i \Omega_i$. This redefines the twists by

$$z'_{ij} = z_{ij} \zeta_i^2 \zeta_j^{*2}. \tag{4.53}$$

For even, N the freedom allows one to fix $m_2 \in \{0, 1\}$ and $m_3 \in \{0, 1\}$, with the constraint (4.52) satisfied by $m_1 \in \{0, N/2\}$, i.e., 2^3 distinct possibilities (in 3 dimensions). A summary of the proof from [89] is given in Appendix B.2.

4.5 INTUITIVE PICTURE

Prior to the technical proof of the allowed magnetic charges in Section 4.6, we will develop some intuition. First we will relate C-periodic boundary conditions to the continuum magnetic charge. Then we will see how this relates to the center flux familiar from 't Hooft's center vortex ensembles in pure SU(N) gauge theory. As a by-product we will be able to interpret the restrictions of C-periodic twist in terms of allowed vortex fluctuations.

4.5.1 *The continuum and zeroes of the Higgs field for SU(2)*

It's instructive to see how the boundary conditions (4.41) for SU(2) fix the magnetic charge in the continuum theory. Since abelian monopoles are located at zeroes of the Higgs field, an odd number of monopoles implies an odd number of zeroes of Φ. The vector components of the Higgs field $\Phi = \phi^A \sigma^A / 2$ inherit from

$$\Phi(x + L\hat{\jmath}) = -\sigma_j \Phi(x) \sigma_j \tag{4.54}$$

the boundary conditions

$$\begin{aligned} \phi^1(x + L\hat{x}) &= -\phi^1(x), \\ \phi^2(x + L\hat{y}) &= -\phi^2(x), \\ \phi^3(x + L\hat{z}) &= -\phi^3(x), \end{aligned} \tag{4.55}$$

with all other components periodic. This respects the well-known 'hedgehog' configuration for the classical 't Hooft-Polyakov monopole.

Note, for example, that ϕ^1 must have an odd number of zeroes on every line through the box in the x direction. By continuity, these combine to form surfaces pinned to the boundary of the othogonal plane. Similarly, there must be an odd

number of surfaces through the y and z directions where ϕ^2 and ϕ^3 are respectively zero. Because of their relative orthogonality, these surfaces intersect in an odd number of points where all three components are zero. To help picture this, consider the surfaces where ϕ^1 and ϕ^2 are zero. These intersect to form an odd number of lines in the z direction on which ϕ^1 and ϕ^2 are both zero. Since ϕ^3 is antiperiodic in the z direction, there must be an odd number of points on these lines (and in total) where ϕ^A vanishes.

All of the (partial or mixed) C-periodic boundary conditions that force an odd magnetic charge have this property. Conversely, those with trivial magnetic charge modulo 4π to permit only an even number points where the Higgs field is zero.

4.5.2 *Center vortices and monopoles*

Understanding the relationship between abelian monopoles and center vortices is not only helpful for the interpretation of C-periodic boundary conditions, it is also interesting from the perspective of confinement in pure SU(N) gauge theory. For many years, the dual Meissner picture of confinement from a monopole condensate was an antagonist to the center vortex scenario. It turns out that these descriptions are complementary, at least in certain gauges. Evidence has accumulated that monopole world lines are embedded on the surface of center vortices [107, 108, 109, 110, 111, 112, 113]. Percolation of one implies percolation of the other. From this perspective, we can regard center vortices as abelian vortices, sourced by the monopoles. For SU(2) gauge theory, the monopoles are like beads on a necklace. For general SU(N) , several center vortices may meet at point, forming monopole-vortex nets. Similar objects have been found in various supersymmetric gauge theories containing Higgs fields [114].

Start again with SU(2), where there is no distinction between twisted C-periodic and twisted periodic boundary conditions for the gauge fields [89]. The gauge content of our configurations can then be interpreted in terms of the center vortex ensembles in Chapter 3, with charge conjugation carried entirely by the Higgs field.

We need a way of locating center vortices, which are generally thick objects. This proceeds via gauge fixing and center projection. A common choice in pure SU(N) gauge theory is Maximal Center Gauge followed by a projection of the link variables onto the nearest center element [115]. The resultant excitations are thin Z_N vortices dubbed P-vortices. They are expected to reveal the location of center vortices in the unprojected configurations.

Since there is a Higgs field at our disposal it is more sensible to use a modified version of Laplacian Center Gauge to define the location of vortices [116, 117, 109, 118]. After diagonalizing the Higgs field Φ we're left with a residual $\mathrm{U}(1)^{N-1}$ gauge symmetry. The idea of Laplacian Center Gauge is to use the lowest-lying eigenvector of the adjoint Laplacian operator as a faux Higgs field for gauge fixing. We can reduce the gauge symmetry to Z_N by fixing $N-1$ phases of this auxiliary field. Thin vortices then arise a la Nielsen-Olesen.

The construction follows de Forcrand and Pepe [109]. It starts from the adjoint lattice Laplacian,

$$\begin{aligned} &-\Delta^{AB}_{xy}(U) \\ &= \sum_{\mu}(2\delta_{x,y}\delta^{AB} - U^{AB}_{\mu}(x)\delta_{y,x+\hat{\mu}} - U^{BA}_{\mu}(x-\hat{\mu})\delta_{y,x-\hat{\mu}}), \end{aligned} \tag{4.56}$$

where A, B are the color indices and U^{AB}_{μ} are the link variables in the adjoint representation,

$$U^{AB}_{\mu}(x) = 2\mathrm{Tr}(T^A U_{\mu}(x) T^B U^{\dagger}_{\mu}(x)). \tag{4.57}$$

Since the Laplacian Δ is a real symmetric matrix, its eigenvalues are real. If we take λ_1 to be the smallest eigenvalue, the corresponding eigenvector allows us to associate a real 3-dimensional vector $\phi^A_{(1)}(x)$ with each lattice site. The eigenvalues of Δ are invariant under gauge transformations $R(x)$, and $\phi^A_{(1)}$ transforms like an adjoint scalar field [109], with $\Phi_{(1)}(x) = \phi^A_{(1)}(x)T^A$,

$$\Phi_{(1)}(x) \to \tilde{\Phi}_{(1)}(x) = R^{\dagger}(x)\Phi_{(1)}(x)R(x). \tag{4.58}$$

After diagonalizing the physical Higgs field, the transformed field $\tilde{\Phi}_{(1)}(x)$ will not in general be invariant under remnant $\mathrm{U}(1)^{N-1}$ transformations. The gauge freedom may then be reduced to Z_N by eliminating the phases of all $(N-1)$ sub-diagonal elements. Gauge ambiguities arise when any of the sub-diagonal elements of $\tilde{\Phi}_{(1)}(x)$ are zero. This involves two conditions, so gauge ambiguities form lines in three dimensions. Since they carry quantized center flux, these defects are identified as Z_N vortices [109].

For SU(2), note that we have a Z_2 vortex whenever $\phi^A_{(1)}(x)$ is parallel or antiparallel to the physical Higgs field in color space. The relative sign of $\phi^A_{(1)}(x)$ and the Higgs defines its local orientation. In the neighborhood of a monopole, the Higgs field has a hedgehog shape in color space. So there is necessarily some direction along which $\phi^A_{(1)}(x)$ and the Higgs field are collinear. What's more, their relative orientation changes sign at the location of the abelian charge. It follows that every monopole lies on a thin Z_2 vortex, which appears as two oppositely directed strings. Monopoles and anti-monopoles form an alternating bead-like structure on the vortices. See [109] for the generalization to $\mathrm{SU}(N)$.

How does this relate to C-periodic boundary conditions (4.44)? Twist in a plane forces an odd number of Z_2 vortices through that plane. For each of these to contribute an odd number of monopoles/anti-monopoles, the orientation of Z_2 flux must change an odd number of times. Therefore $\phi^A\phi^A_{(1)} = 2\mathrm{Tr}\Phi\Phi_{(1)}$ must be antiperiodic. The boundary conditions

$$\begin{aligned} \Phi(x+L\hat{\jmath}) &= \pm\Omega^{\dagger}_j(x)\Phi(x)\Omega_j(x), \\ U_{\mu}(x+L\hat{\jmath}) &= \Omega^{\dagger}_j(x)U_{\mu}(x)\Omega_j(x+\hat{\mu}), \end{aligned} \tag{4.59}$$

give

$$\begin{aligned} &2\mathrm{Tr}\Phi(x+N\hat{\jmath})\Phi^{(1)}(x+N\hat{\jmath}) \\ &\quad = \pm 2\mathrm{Tr}\Omega^{\dagger}_j\Phi(x)\Omega_j\Omega^{\dagger}_j\Phi^{(1)}(x)\Omega_j \\ &\quad = \pm 2\mathrm{Tr}\Phi(x)\Phi^{(1)}(x). \end{aligned} \tag{4.60}$$

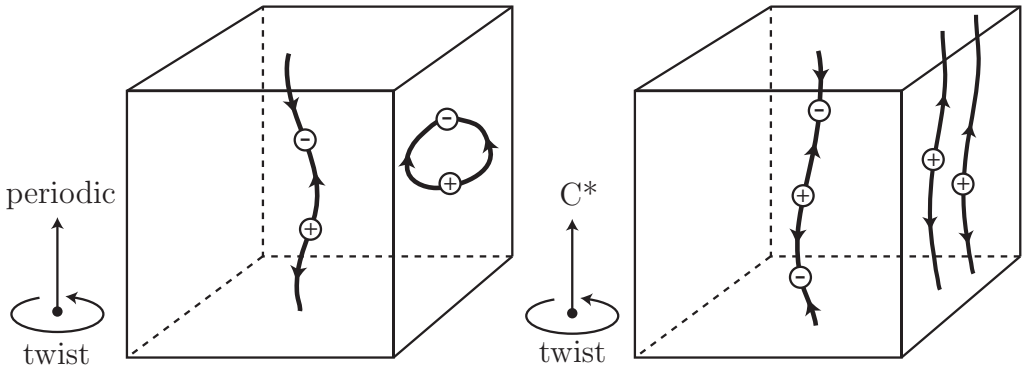

Figure 4.2: For SU(2), abelian monopoles form a bead-like structure on center vortices. To have odd net charge we need an odd number of vortices that contain an odd number of monopoles. i.e. both twist and charge conjugation.

So if the Higgs field is antiperiodic/C-periodic, $2\mathrm{Tr}\Phi\Phi_{(1)}$ is also antiperiodic, and there will be an odd number of monopoles on every vortex in that direction (Fig. 4.2).

The net magnetic charge is then obtained from counting arguments. Closed vortices and vortices through periodic directions do not contribute, since they contain an equal number of monopoles and anti-monopoles. And without twist we can only have an even number of monopoles, since there will be an even number of vortices. For the net charge to be odd, there must be an odd number of directions that are both conjugated and twisted in the orthogonal plane. We then have an odd number of vortices that contain an odd number of monopoles. This interpretation is in perfect agreement with the results of Sec. 4.6.2 and the Appendix.

Consider the decomposition (4.30) of the gauge fields in unitary gauge. Since it commutes with complex conjugation, C-periodic boundary conditions (4.44) imply antiperiodicity of the abelian projected fields (4.31) and their fluxes.[3]. This means that the abelian (center) flux of the vortices must be equal and opposite at the boundary in each C-periodic direction.

This fixes the allowed twists when combined with Gauss' law for center flux. For general $\mathrm{SU}(N)$, several Z_N vortices are permitted to meet at a point provided that center flux is conserved modulo N. We may have more complicated monopole-vortex nets than the necklaces of SU(2). These source any abelian flux leaving the volume in units of N. With a single C-periodic direction, the abelian flux must be split evenly between opposite faces, which implies that the flux from twist in the plane is restricted to $m_{\parallel} \in \{0, N/2\}$.

With an even number of colors $N \geq 4$ and multiple C-periodic directions, the flux has more freedom when leaving the volume. To see this, decompose the equal and opposite fluxes exiting a C-periodic direction into elementary units quantized by the minimal center phase $e^{i2\pi/N} \in Z_N$. They can be arranged in matching pairs and dragged to the corners of the volume while still preserving the equal and opposite condition for abelian projected fluxes. This is depicted in Fig. 4.3. If the orthogonal direction is also C-periodic, they can be traded *across* the boundary.

3 Subtleties from the twist are addressed in the formal proof.

This illustrates why there are only 2^3 inequivalent combinations of twists for $d = 3$ C-periodic spatial dimensions, N even. The trading of two units of center flux between C-periodic directions means that it can only be fixed to be even or odd in each direction. The total abelian flux $2(m_1 + m_2 + m_3)$ leaving the volume through the C-periodic directions must be sourced in units of N by Gauss's law. But it may be split between the various faces of the box. This is the physical interpretation of the constraint on the twists [4]

$$(m_1 + m_2 + m_3) \in \{0, N/2\}. \tag{4.61}$$

The constituent charges for abelian flux will generally be scattered around the box, connected by vortices that conserve center flux at each monopole. The N-vector for abelian magnetic charge is then obtained in units of $2\pi/g$ by adding up the flux measured by parallel transport around each face of the box,

$$\exp i\pi \frac{2(m_1 + m_2 + m_3)}{N} = \exp \frac{igQ}{2}. \tag{4.62}$$

This relationship is more precisely formulated in Section 4.6.2. Since the flux sums to a center phase, the monopoles species are treated equally. The formation of monopole-vortex nets is reflected in the various solutions for Q.

If $2(m_1 + m_2 + m_3) = N$, then

$$Q = \frac{2\pi}{g}(1, 1, \ldots, 1 - N) + \frac{2\pi}{g} 2(n_1, n_2, \ldots, -\sum_{i=1}^{N-1} n_i). \tag{4.63}$$

That is, the net always contains an *odd* number of each monopole species. If $2(m_1 + m_2 + m_3) = 0$ we're left with the second term and hence an *even* number of each monopole species.

The problem with N odd colors is apparent within this vortex picture. We need an even number of elementary units of flux leaving the volume in order to satisfy antiperiodicity, so we're stuck with even multiples of N and hence an even number of each monopole species. Moreover, the trading of pairs of elementary fluxes between directions means that the boundary conditions are always equivalent to those with zero units of center flux modulo N in each direction, i.e., no twist at all.

4 Vortices may also be traded between C-periodic and periodic direction which leads to an analogous constraint.

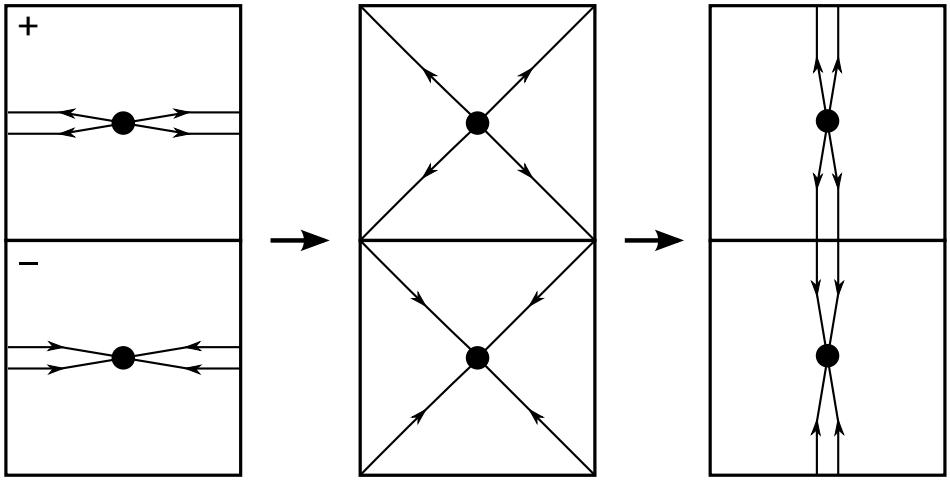

Figure 4.3: Pairs of elementary vortices may be traded between pairs of C-periodic direction by dragging their flux to the corners of the volume, as is illustrated here for SU(4). Together with Gauss's law for center flux modulo N, this fixes the inequivalent twist sectors.

4.6 ALGEBRAIC FORMULATION

Let us now consider in detail the effect of the boundary conditions (4.44) on the residual U(1) fields. Because the eigenvalues of the Higgs field Φ don't change under the twists in (4.44), i.e. $\Phi(x)$ and $\Phi(x+L\hat{\jmath})$ have the same set of eigenvalues, which are all real, we can choose the diagonalized field $\tilde{\Phi}$ defined in Eq. (4.25) to be periodic,

$$\tilde{\Phi}(x+L\hat{\jmath}) = \tilde{\Phi}(x). \tag{4.64}$$

Then, on one hand we have

$$\begin{aligned} \Phi(x+L\hat{\jmath}) &= \Omega_j^\dagger \Phi^*(x)\Omega_j \\ &= \Omega_j^\dagger \left(R(x)\tilde{\Phi}(x)R^\dagger(x)\right)^* \Omega_j \\ &= \Omega_j^\dagger R^*(x)\tilde{\Phi}(x+L\hat{\jmath})R^T(x)\Omega_j, \end{aligned} \tag{4.65}$$

while on the other,

$$\Phi(x+L\hat{\jmath}) = R(x+L\hat{\jmath})\tilde{\Phi}(x+L\hat{\jmath})R^\dagger(x+L\hat{\jmath}). \tag{4.66}$$

To ensure the compatibility of the two, we impose spatial boundary conditions for $R(x)$ as follows,

$$R(x+L\hat{\jmath}) = \Omega_j^\dagger R^*(x). \tag{4.67}$$

When we apply multiple translations by L, however, we observe Z_N jumps in the definition of gauge transforms $R(x)$ in SU(N). For example, successive translations by L, first along the $\hat{k}$ direction, and then along $\hat{\jmath}$, is defined by,

$$R^{jk}(x+L\hat{\jmath}+L\hat{k}) \equiv \Omega_j^\dagger \Omega_k^T R(x), \tag{4.68}$$

while the reverse order gives,

$$R^{kj}(x+L\hat{\jmath}+L\hat{k}) \equiv \Omega_k^\dagger \Omega_j^T R(x), \tag{4.69}$$

It follows immediately from (4.47) that

$$R^{jk}(x + L\hat{j} + L\hat{k}) = z_{kj} R^{kj}(x + L\hat{j} + L\hat{k}). \tag{4.70}$$

From their effect in (4.25), or generally in $\mathrm{SU}(N)\ /Z_N$, these two would be equivalent. In $\mathrm{SU}(N)$ they are not, however. There, transformations where the $R's$ applied at a corner site to links in different directions attached to that corner differ, by center elements as in (4.70), can be used to change the twist sector. If we allowed such multi-valued, and hence singular gauge transformations, we could then arrange matters such that the transformed link variables $\tilde{U}$ would all be C-periodic,

$$\begin{aligned} \tilde{U}_\mu(x + L\hat{\jmath}) &= R^\dagger(x + L\hat{\jmath}) U_\mu(x + L\hat{\jmath}) R(x + \hat{\mu} + L\hat{\jmath}) \\ &= R^T(x) U_\mu^*(x) R^*(x + \hat{\mu}) \\ &= \tilde{U}_\mu^*(x). \end{aligned} \tag{4.71}$$

The twist would then be completely removed by the singular gauge transformation, however. Conversely, when comparing a fundamental Wilson loop that winds around a plane with non-trivial twist to the corresponding loop formed by the $\tilde{U}$'s, one would observe that the original loop obtained its center flux entirely from the Z_N jump of the multi-valued gauge transformation, while the $\tilde{U}$ loop, with purely C-periodic b.c.'s (4.71), would be trivial.

In order to preserve the Z_N center flux in $\mathrm{SU}(N)$, we must apply single-valued and hence proper $\mathrm{SU}(N)$ gauge transformations, without such a jump. Those will of course not change the Wilson loop at all, when transforming the U's to the gauge-fixed links $\tilde{U}$. Then however, we have to decide how we define the gauge transformation at those corner sites where Z_N ambiguities as in (4.70) arise. Consequently, the boundary conditions (4.71) for the gauge-fixed $\tilde{U}$'s attached to such a corner will have to be amended. This is best exemplified in two dimensions (with two integer coordinates x and y both ranging from 0 to $(L-1)$: At the site with coordinates (L, L) we define the gauge transformation R as, say

$$R(L, L) \equiv \Omega_y^\dagger \Omega_x^T R(0, 0) = \Omega_y^\dagger R^*(L, 0). \tag{4.72}$$

If we consider the x link attached to this corner site, we obtain the boundary condition

$$\begin{aligned} \tilde{U}_x(L-1, L) &= R^\dagger(L-1, L) U_x(L-1, L) R(L, L) \\ &= R^T(L-1, 0) U_x^*(L-1, 0) R^*(L, 0) \\ &= \tilde{U}_x^*(L-1, 0), \end{aligned} \tag{4.73}$$

as in (4.71) and as for every other link that is not connected to this corner. For the corresponding y link at this corner on the other hand,

$$\begin{aligned} \tilde{U}_y(L, L-1) &= R^\dagger(L, L-1) U_y(L, L-1) R(L, L) \\ &= R^T(0, L-1) U_y^*(0, L-1) \Omega_x \Omega_y^\dagger \Omega_x^T R^*(0, 0) \\ &= z_{21}\, R^T(0, L-1) U_y^*(0, L-1) R^*(0, L) \\ &= z_{21}\, \tilde{U}_y^*(0, L-1), \end{aligned} \tag{4.74}$$

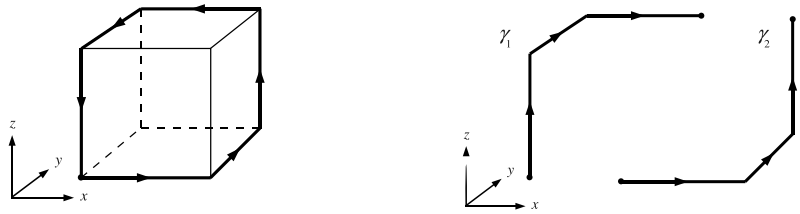

Figure 4.4: The integration curve used to calculate the flux through half of the box (left) may be decomposed into line segments γ_1 and γ_2 (right).

because $\Omega_y^\dagger \Omega_x^T = z_{21} \Omega_x^\dagger \Omega_y^T$ and $R^*(0,L) = \Omega_y^T R(0,0)$. This shows that all but one of the gauge-fixed links in the plane are C-periodic (4.71) and that the center flux comes about by the boundary condition of the one link remaining. Compare this to the lattice implementation of twist in Chapter .

In the following we will only consider proper transformations R, single-valued in $\mathrm{SU}(N)$, so that the center flux is preserved in the gauge-fixed links, $\tilde{U}$. In higher dimensions we therefore introduce the convention that for gauge transformations R involving multiple translations by L these translations are always applied in lexicographic order. In three dimensions, this leads to the following definitions for the far edges of our L^3 box with one corner in the origin at $(0,0,0)$,

$$\begin{aligned} R(L,L,z) &\equiv \Omega_y^\dagger \Omega_x^T R(0,0,z), \\ R(L,y,L) &\equiv \Omega_z^\dagger \Omega_x^T R(0,y,0), \\ R(x,L,L) &\equiv \Omega_z^\dagger \Omega_y^T R(x,0,0), \end{aligned} \tag{4.75}$$

where x, y and z run from 0 to $L-1$; and for the corner diagonally opposite to the origin, we use

$$R(L,L,L) \equiv \Omega_z^\dagger \Omega_y^T \Omega_x^\dagger R^*(0,0,0). \tag{4.76}$$

In particular, we then have

$$R(L,L,L) = z_{12} z_{23} z_{31} \Omega_x^\dagger \Omega_y^T \Omega_z^\dagger R^*(0,0,0), \tag{4.77}$$

and the factor

$$z_{12} z_{23} z_{31} = \exp\left\{ \frac{2\pi i}{N} (m_1 + m_2 + m_3) \right\} \tag{4.78}$$

represents the total center flux as measured by a maximal-size Wilson loop $W(C)$ along the corners of the three-dimensional cube that cuts its surface into two equal halfs as in Fig. 4.4. To see this, let the loop C in Fig. 4.4 be composed of two line segments $-\gamma_1$ and γ_2, and consider gauge transforming the two Wilson lines $W(\gamma_1)$ and $W(\gamma_2)$. To make them equal, so that $W(C) = W(\gamma_2) W^\dagger(\gamma_1) = 1$, we would need to apply a gauge transform

$$R^{(1)}(L,L,L) = \Omega_z^\dagger \Omega_y^T \Omega_x^\dagger R^*(0,0,0) \tag{4.79}$$

at the end of line $W(\gamma_1)$, but

$$R^{(2)}(L,L,L) = \Omega_x^\dagger \Omega_y^T \Omega_z^\dagger R^*(0,0,0) \tag{4.80}$$

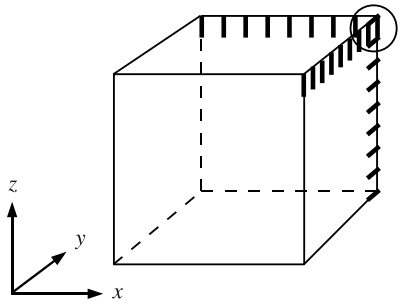

Figure 4.5: Illustration of links with special boundary conditions in three dimensions. When center flux is moved to the upper right plaquettes of all two dimensional planes, it piles up near the corner at (L, L, L) as highlighted by the circle.

at the end of $W(\gamma_2)$. This would be a multi-valued gauge transform with a jump at the far corner at (L, L, L). If we apply the same $R(L, L, L) \equiv R^{(1)}(L, L, L)$ at the end of both lines, $W(\gamma_1)$ and $W(\gamma_2)$, the loop $W(C)$ remains unchanged, and we have,

$$W(C) = W(\gamma_2)W^\dagger(\gamma_1) = z_{12}z_{23}z_{31} \ . \tag{4.81}$$

In terms of the gauge-fixed links $\tilde{U}$, we still have C-periodic boundary conditions (4.71) for most of the links, with the following exceptions:

$$\begin{aligned} \tilde{U}_y(L, L-1, z) &= z_{21}\, \tilde{U}_y^*(0, L-1, z), \\ \tilde{U}_z(L, y, L-1) &= z_{31}\, \tilde{U}_z^*(0, y, L-1), \\ \tilde{U}_z(x, L, L-1) &= z_{32}\, \tilde{U}_z^*(x, 0, L-1), \end{aligned} \tag{4.82}$$

where the third variable runs from 0 to $L-1$ again; and, from the corner at (L, L, L),

$$\begin{aligned} \tilde{U}_y(L, L-1, L) &= z_{12}\, \tilde{U}_y(0, L-1, 0), \\ \tilde{U}_z(L, L, L-1) &= z_{32}z_{13}\, \tilde{U}_z(0, 0, L-1). \end{aligned} \tag{4.83}$$

The set of special links whose boundary conditions are modified by center elements is sketched in Fig. 4.5.

Along the loop of Fig. 4.4 this means that almost every link in the first half of the loop has a partner in the opposite direction in the second half that is related by two successive C-periodic translations (4.71), and hence periodic. There are only two exceptions from the set of twisted links that the loop picks up. These are

$$\begin{aligned} \tilde{U}_y(L, L-1, 0) &= z_{21}\tilde{U}_y^*(0, L-1, 0) \\ &= z_{21}\tilde{U}_y(0, L-1, L), \end{aligned} \tag{4.84}$$

and the last link of the first half of the loop which ends at the corner at (L, L, L), as given in (4.83),

$$\tilde{U}_z(L, L, L-1) = z_{32}z_{13}\tilde{U}_z(0, 0, L-1). \tag{4.85}$$

The combined center elements are again responsible for the same total center flux through the loop, now in terms of the gauge-fixed links, $\tilde{U}$.

4.6.1 *Magnetic flux*

Since the decomposition of the gauge fixed links (4.30) commutes with charge conjugation, C-periodic boundary conditions imply anti-periodicity of the $\alpha^a_\mu(x)$ in (4.31). The abelian projected fields inherit anti-periodic boundary conditions

$$\alpha^a_\mu(x + L\hat{\jmath}) = -\alpha^a_\mu(x), \tag{4.86}$$

except for the special cases, in three dimensions corresponding to the links in Eqs. (4.82), where

$$\begin{aligned} \alpha^a_y(L, L-1, z) &= -\alpha^a_y(0, L-1, z) - \frac{2\pi}{N} m_3, \\ \alpha^a_z(L, y, L-1) &= -\alpha^a_z(0, y, L-1) + \frac{2\pi}{N} m_2, \\ \alpha^a_z(x, L, L-1) &= -\alpha^a_z(x, 0, L-1) - \frac{2\pi}{N} m_1, \end{aligned} \tag{4.87}$$

and in Eqs. (4.83), where

$$\begin{aligned} \alpha^a_y(L, L-1, L) &= \alpha^a_y(0, L-1, 0) + \frac{2\pi}{N} m_3, \\ \alpha^a_z(L, L, L-1) &= \alpha^a_z(0, 0, L-1) - \frac{2\pi}{N} (m_1 + m_2). \end{aligned} \tag{4.88}$$

The fluxes in three dimensions,

$$\alpha^a_{ij}(\vec{x}) = \alpha^a_i(\vec{x}) + \alpha^a_j(\vec{x} + \hat{\imath}) - \alpha^a_i(\vec{x} + \hat{\jmath}) - \alpha^a_j(\vec{x}) \tag{4.89}$$

are essentially anti-periodic, because the twist angles $(2\pi/N)m_i$ cancel when we compare fluxes on opposite sides of the lattice. There is a single exception,

$$\begin{aligned} \alpha_{23}(L, L-1, L-1) &= \\ &-\alpha_{23}(0, L-1, L-1) - \frac{2\pi}{N} 2(m_1 + m_2 + m_3). \end{aligned} \tag{4.90}$$

Because of the constraint on the possible twists in Eq. (4.52), and because flux is only defined modulo 2π, the additional contribution has no effect, and this is equivalent to anti-periodic boundary conditions also. We therefore have fully anti-periodic abelian field strengths. This means that when we cross the boundary we enter a charge conjugated copy of the same lattice from the opposite side.

To determine the magnetic charge we repeat the trick of [100]. The curve shown in Fig. 4.4 divides the boundary into two halves. We denote the magnetic flux through them by Φ_+ and Φ_- choosing the positive direction to be pointing outwards. The two halves are related by the boundary conditions, and in particular, antiperiodicity (4.89) of the field strength implies that they are equal $\Phi_- = \Phi_+$. The magnetic charge inside the lattice is given by the total flux, which is the sum of the two contributions,

$$Q = \Phi_+ + \Phi_- = 2\Phi_+. \tag{4.91}$$

Applying Stokes's theorem, we can write

$$\begin{aligned}\Phi^a_+ &= -\frac{1}{g}\left(\sum_{x=0}^{L-1}\alpha^a_x(x,0,0)+\sum_{y=0}^{L-1}\alpha^a_y(L,y,0)\right.\\ &\quad+\sum_{z=0}^{L-1}\alpha^a_z(L,L,z)-\sum_{x=0}^{L-1}\alpha^a_1(x,L,L)\\ &\quad\left.-\sum_{y=0}^{L-1}\alpha^a_y(0,y,L)-\sum_{z=0}^{L-1}\alpha^a_3(0,0,z)\right).\end{aligned} \tag{4.92}$$

When we apply the boundary conditions, all terms cancel except those involving the cases,

$$\begin{aligned}\Phi^a_+ &= -\frac{1}{g}\left(\alpha^a_y(L,L-1,0)+\alpha^a_z(L,L,L-1)\right.\\ &\quad\left.-\alpha^a_y(0,L-1,L)-\alpha^a_z(0,0,L-1)\right)\\ &= \frac{1}{g}\frac{2\pi}{N}\left(m_1+m_2+m_3\right).\end{aligned} \tag{4.93}$$

Where we have used the first equation in (4.87) with $z=0$ and $\alpha^a_y(0,L-1,0) = -\alpha^a_y(0,L-1,L)$, and the second equation in (4.88). As the link angles α^a_μ are defined modulo 2π, the fluxes $\Phi_\pm$ are only defined modulo $(2\pi/g)$. Therefore we find

$$Q^a = \frac{4\pi}{gN}(m_1+m_2+m_3) \mod \frac{4\pi}{g}. \tag{4.94}$$

4.6.2 *Allowed magnetic charges*

Substituting the constraint on the twists for even N in Eq. (4.52) into Eq. (4.94) gives the charge quantisation condition

$$Q^a = \frac{2\pi}{g}\mathbb{Z}_2, \tag{4.95}$$

up to integer multiples of $(4\pi/g)$. Because all components of the charge vector Q^a are the same, modulo $(4\pi/g)$, the constraint,

$$\sum_a Q^a = NQ_a = 0 \mod \frac{4\pi}{g} \tag{4.96}$$

is automatically satisfied.

This means that we can use twised C-periodic boundary conditions in SU(N) , when N is even, to restrict the ensemble to either of two distinct classes of monopole configurations. If the allowed twists satisfy $m_1+m_2+m_3 = 0$ (modulo N), then their total charges are integer multiples of $(4\pi/g)$,

$$Q^a = 0 \mod \frac{4\pi}{g} \text{ for all } a. \tag{4.97}$$

If the twists are such that $m_1+m_2+m_3 = N/2$, then every component of the total charge vector is a half-odd integer multiple of $(4\pi/g)$,

$$Q^a = \frac{2\pi}{g} \mod \frac{4\pi}{g} \text{ for all } a. \tag{4.98}$$

These two sectors differ by at least one unit of abelian magnetic charge $(2\pi/g)$ (modulo $(4\pi/g)$) in each of the $N-1$ U(1)'s. This may be due to a single monopole in a diagonally embedded U(1) or due to several monopoles in different U(1)'s depending on the symmetry breaking pattern. If the symmetry breaking is maximal, these could be $N-1$ individual monopoles, one in every U(1) factor of the maximal abelian subgroup of SU(N). Since N must be even, the total number of monopoles in the twisted sector will be odd in either case. The ratio of partition functions of the two sectors in the infinite volume limit determines the free energy of such monopole configurations or, at zero temperature, their total mass as discussed in Section 4.3.

To force an odd number of monopoles, a convenient position independent choice for the gauge transformations Ω_i is

$$\begin{aligned} \Omega_1 &= \mathrm{diag}(i\sigma_3, ..., i\sigma_3) \\ \Omega_2 &= \mathrm{diag}(I, ..., I) \\ \Omega_3 &= \mathrm{diag}(i\sigma_1, ..., i\sigma_1). \end{aligned} \tag{4.99}$$

These are simply the SU(2) matrices from Eq. (4.41) repeated in block diagonal form. They satisfy

$$\Omega_i^* \Omega_j = -\Omega_j^* \Omega_i, \; i \neq j, \tag{4.100}$$

corresponding to a π twist angle in each plane, i.e. $m_1 = m_2 = m_3 = N/2$. We could equally well use a a single twisted plane by replacing Ω_1 or Ω_3 by the unit matrix 1. An even number of monopoles, corresponding to Eq. (4.97) is obtained from

$$\Omega_1 = \Omega_2 = \Omega_3 = 1. \tag{4.101}$$

Imposing complex conjugation in all three directions has the advantage of preserving the invariance of the theory under 90-degree rotations. However, for a non-zero magnetic charge, it is enough to have complex conjugation in one direction, so that the flux can escape through at least one face. As is suggested by our vortex picture in Section 4.5, this does not lead to fewer restrictions on the magnetic charges. We leave the proof to the appendix.

4.7 THE PUNCHLINE

C-boundary conditions (4.44) allow one to impose a non-zero magnetic charge in SU(N) gauge theories with an adjoint Higgs field, but with several restrictions. It only works for SU(N) with even N, the charges can only be constrained to be odd or even, and every residual U(1) group has the same magnetic charge.

It is rather natural that we cannot specify the exact charge but only whether it is odd or even with boundary conditions that preserve translational invariance [119]. If a monopole is transported through one face of the torus, its antiparticle emerges from the other side. The net magnetic charge changes by two units.

The other restriction, that all charges must have the same value, arises because our boundary conditions are linear operations on the fields. The transformation matrices Ω_j are therefore independent of the direction of symmetry breaking Φ, which defines the different residual U(1) groups. The boundary conditions cannot treat any U(1) group differently from the others. It may be possible to avoid

this restriction by considering non-linear transformations. In principle, one could specify the boundary conditions in the unitary gauge in which the different U(1) groups can be treated separately. It might then be impossible, however, to respect translational invariance.

The absence of a non-trivial charge sector for odd N is also natural in this light. Since we cannot single out an abelian subgroup, the abelian flux is quantized by Z_N center flux. A monopole requires an odd number of elementary Z_N fluxes for N odd, which cannot be closed on the torus.

In summary, the boundary conditions (4.44) allow one to define the partition functions Z_{odd} and Z_{even} in Eq. (4.43) using the gauge transformation (4.99) and (4.101), respectively. Using Eq. (4.43), one may calculate the energy difference between these two sectors.

If there is only one residual U(1) group, then only the monopole species that corresponds to it is massive. Eq. (4.43) gives that monopole's mass, just as in SU(2). If there are several residual U(1) groups, there is a magnetic charge corresponding to each U(1) group, and Z_{odd} represents a multi-monopole state. Depending on which configuration has the lowest energy, the monopoles may either be separate free particles, in which case Eq. (4.43) gives the sum of their masses, or else it may give the energy of a bound state of magnetic charges. We leave the exploration of this dynamical issue to a future project.

5

FRACTIONAL ELECTRIC CHARGE AND QUARK CONFINEMENT

The relevance of center symmetry to the finite temperature deconfinement transition of QCD is obscured by the inclusion of dynamical color charges. Quarks fields faithfully represent the center subgroup $Z_3 \in \mathrm{SU}(3)$. Their fluctuations explicitly break center symmetry, which throws a wet blanket on the classification of deconfinement as a spontaneous symmetry breaking transition. With dynamical quarks in the picture, neither the Polyakov loop nor the center vortex free energy are true order parameters. Center vortices are dynamically suppressed by quarks such that the center sector $1 \in Z_3$ is favored. So the Polyakov loop and center vortex free energy always have non-zero expectation values.

Consequently, the second order transitions of SU(2) gauge theory in $3+1$ d, and of SU(2) and SU(3) in $2+1$ d, become smooth crossovers when quarks with an arbitrarily large mass are added. For the physically relevant model, SU(3) in $3+1$ d, the first order temperature transition of the pure gauge theory may persist for very heavy quarks, but contemporary lattice studies have concluded that it also weakens to a crossover at zero chemical potential for the physical quark masses [120, 121, 122].

It is usual to treat QCD in isolation and expect that the electroweak sector contributes only small perturbative corrections. It is suspicious, however, that quarks are both confined and carry a fractional electric charge with respect to the electron. They are the only known matter fields with either of these properties. Is it their fundamental color charge that is confined, or their fractional electric charge?

The fact that isolated fractional electric charges have never been found [123] is puzzling if deconfinement is indeed a crossover. Neglecting confinement, the abundance of free quarks predicted in the standard cosmological model differs from the experimental bound by a factor of $\mathcal{O}(10^{15})$ [124]. Such a large suppression is a considerable burden for an analytic crossover. It would be more natural if confinement were protected by a symmetry at low temperatures, as in the pure gauge theory.

Owing to the quarks' fractional electric charges, there is in fact a hidden Z_6-like symmetry that combines the centers of the color and electroweak gauge groups. The phase acquired by quark fields under a color center transformation may be compensated by an appropriate electromagnetic phase. The existence of this global symmetry offers the possibility of a spontaneous symmetry breaking transition, driven by disorder that combines color center vortices with additional topological structure from the electroweak sector.

In this chapter, we consider implications for the phase structure of the Standard Model. To start things off, we will detail how a finite quarks mass breaks center symmetry in lattice models, which will guide our intuition when we turn later to lattice simulations. We then discuss the hidden symmetry that is present when the quarks' fractional electric charges are included, the historical connection with grand

unified theories, and the new topological possibilities. Prototypical unified theories provide instructive, motivating examples of how a topological link between the Standard Model gauge groups may emerge in practice. Their details are not, however, essential to our investigation of whether the inclusion of fractional electric charge allows for the resurrection of a center symmetry breaking deconfinement transition in the presence of dynamical quarks. For this, the vital assumption is that the Standard Model gauge groups which are inherited from higher energy physics are compact, irrespective of their origin. For a preliminary study, we implement 2-color lattice models with fractional electric charge with respect to a compact U(1) gauge group as conceptual playgrounds.

5.1 CENTER SYMMETRY BREAKING BY QUARKS

The explicit breaking of the center symmetry by quark fields in an SU(N) gauge theory is best understood in analogy with the ordering of spins by an external magnetic field. Consider the lattice action for Wilson quarks in the fundamental representation of SU(N), Eq. (2.31). Integrating over the quark fields gives their contribution to the weight of a given gauge configuration in the partition function,

$$\int \prod_x d\psi(x) d\bar{\psi}(x) \exp(-a^4 \sum_{x,y} \bar{\psi}(x)(1-\kappa D(x|y))\psi(y)) = \det(1-\kappa D), \tag{5.1}$$

where the hopping matrix $D(x|y)$ contains the parallel transporters connecting neighboring sites. This fermion determinant may be re-expressed as an effective action in terms of a power series. The formal result is [31],

$$\det(1-\kappa D) = \exp(\mathrm{tr}\,[\ln(1-\kappa D)]) = \exp(-\sum_{j=1}^{\infty} \frac{1}{j} \kappa^j \mathrm{tr}[D^j]), \tag{5.2}$$

which converges when the hopping parameter is small,

$$\kappa = \frac{1}{2(am+4)} < \frac{1}{8}, \tag{5.3}$$

i.e., for large bare quark masses m.

Each term in the exponential in Eq. (5.2) is the product of parallel transporters U_μ along a closed quark loop. Large loops are exponentially suppressed in powers of the hopping parameter κ, which plays the role of the inverse quark mass in lattice units. The loops which close within the lattice volume merely renormalize the lattice gauge coupling β. They are plaquettes and higher dimensional analogs that are likewise invariant under global center transformations that multiply every link in a timeslice by a Z_N phase (cf. Eq. (3.8)).

Loops that wind around the lattice are another story. In the thermodynamic limit, $L \to \infty$, the relevant loops are those wrapping around the compact temporal $1/T$ direction. The shortest possible winding gives a Polyakov loop corresponding to a static quark worldline. Since loops in opposite temporal directions are treated equally, the hopping expansion in Eq. (5.2) contributes terms of the form,

$$\propto -\kappa^{N_t}(P(\vec{x}) + P(\vec{x})^\dagger) = -2\kappa^{N_t} \mathrm{Re}\, P(\vec{x}), \tag{5.4}$$

to the effective action, which are minimized for $P = 1$. That is, they order the Polyakov loop towards the center element $1 \in Z_N$ in the same manner as turning on a constant external magnetic field H orders spins in the Potts model with Hamiltonian,

$$\mathcal{H} = -J \sum_{<s_x, s_y>} \delta(s_x, s_y) - H \sum_x \delta(s_x, 1), \; s_x =\in Z_N. \tag{5.5}$$

Regions of spacetime in which $P(\vec{x}) \neq 1$ are dynamically suppressed. Physically, quarks pick up an Aharonov-Bohm phase from the total enclosed color flux when they propagate in a loop. In a quantum mechanical picture, a non-trivial phase from parallel transportation about a loop leads to a multivalued wavefunction. Fluctuating quark fields suppress this in the functional integral by penalizing disorder in the gauge configurations, and, in particular, vortex interfaces between sectors with $P(\vec{x}) \neq 1$. The center flux piercing large quark loops must then be correlated such that it tends to cancel in total. An asymptotic string tension for the color flux between static quarks may no longer be generated by Z_N center vortices that percolate at all scales. This is one perspective of how screening by dynamic quarks leads to string breaking.

The vortex picture of confinement should not require a complete overhaul when quark fluctuations are added, however. It would be unnatural if the mechanism of color confinement in the presence of arbitrarily heavy quarks were fundamentally different from that in the pure gauge theory. Chiral symmetry presents a similar situation in the limit of massless quarks. The spontaneous breakdown of chiral symmetry is able to explain why the pions are so much lighter than the vector rho mesons by characterizing them as Goldstone modes. Chiral symmetry is explicitly broken by the small but finite mass of the up and down quarks, and pions are not massless, but this does not invalidate the correctness of the spontaneous symmetry breaking argument as an approximation.

Likewise, one may still attribute the formation of a linear potential for dynamical quark-antiquark pairs at intermediate scales to magnetic disorder in the gauge fields that stems from a vortex structure. That is, configurations with disorder in the spacelike gauge degrees of freedom which link with timelike Wilson loops. The way in which this structure differs from the pure gauge theory remains unclear, however [13]. A compelling scenario has been suggested in Ref. [125], which reframes vortices in terms of overlapping domains of the center sectors that they separate. For QCD with explicitly broken center symmetry, each of these domains must carry a trivial total center flux. One is stuck with the trivial homotopy group,

$$\pi_1(\mathrm{SU}(3)) = 1, \tag{5.6}$$

so the center flux must be correlated asymptotically. This weak constraint on the fluctuations within a domain does not prevent spacelike disorder at intermediate scales, however. The domain picture has been applied to centerless groups such as G(2), which also exhibit the formation of a linear potential at intermediate scales [125, 126, 127].

Still, it remains difficult to make rigorous quantitative statements about large scale field fluctuations when they are not topologically stable objects. The neat classification of color center vortex and electric flux ensembles into superselection

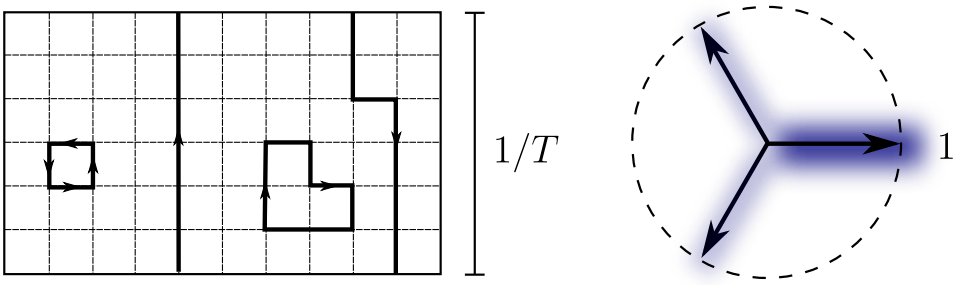

Figure 5.1: Dynamical quarks explicit break center symmetry. Quark loops that wrap around the compact temporal direction (left) order the Polyakov loop towards the trivial center sector (right).

sectors, with a quantitative implementation via twisted boundary conditions, is no longer possible when quark fluctuations are included. And, at the same time, there is no obvious way to pinpoint the difference between confined and deconfined phases and understand the origin of the colorless hadronic spectrum.

Within the framework of local quantum field theory, one may hope to apply the Kugo-Ojima confinement criterion to identify colorless asymptotic states as BRST singlets [128]. This hinges on a mass gap and unbroken global gauge charges to distinguish the confinement of color flux with a Gauss law from screening via the Higgs mechanism. Here the existence of a global, spacetime independent symmetry is crucial. In Landau gauge, this may be identified as a subgroup of local gauge invariance that preserves the gauge-fixing condition, $\partial_\mu A^\mu = 0$. Such a remnant symmetry from gauge fixing is not subject to Elitzur's theorem, which forbids the spontaneous breakdown of a local gauge symmetry [129]. The breaking of a remnant gauge symmetry is a possible criterion to distinguish between confined and Higgs phases. It is not clear that this is sensible, however. The breaking of remnant symmetry in Landau gauge, as well as the analogous symmetries in Coulomb gauge and the abelian monopole confinement, have been found to predict transitions in lattice theories where no physical transitions exist [130, 131], i.e., where the supposed phases are not distinguished by a non-analyticity in the spectrum or other thermodynamic quantity.

5.2 A HIDDEN GLOBAL SYMMETRY

A striking coincidence emerges when electric charge is included. Since quarks carry fractional electric charges $Q = \frac{2}{3}e$ or $-\frac{1}{3}e$ in units of the proton's charge, the combined color and electromagnetic phases,

$$(e^{i2\pi/3}, e^{i2\pi Q/e}),\ (e^{-i2\pi/3}, e^{-i2\pi Q/e}) \in \mathrm{SU}(3) \times \mathrm{U}(1)_{em}, \tag{5.7}$$

precisely cancel when they are applied to a quark field or wavefunction. That is, the color phase $e^{\pm i2\pi/3} \in Z_3$ that quarks pick up from a non-trivial global center

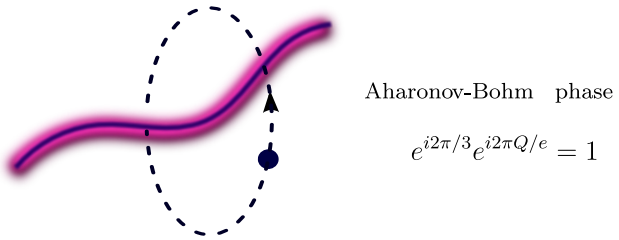

Figure 5.2: Quarks are blind to a combination of the electromagnetic vortex with minimal quantized flux with respect to the electron, and a matching color center vortex.

transformation, or from encircling a center vortex, may be undone by an additional $\mathrm{U}(1)_{em}$ phase (Fig. 5.2).[1]

What's more, these transformations act trivially on all other Standard Model particles, each of which carry integer electric charges and are blind to the the Z_3 center of SU(3). The phase $e^{\pm i2\pi Q/e}$ is the Aharonov-Bohm phase picked up by a particle with electric charge Q when it encircles a topologically stable $\mathrm{U}(1)_{em}$ defect quantized minimally with respect to e. An example of such a defect is the time-like worldsheet traced out by the $\mathrm{U}(1)_{em}$ Dirac string of a magnetic monopole. A singular string supplying the flux of the monopole is unobservable for a particle with electric charge e if the magnetic flux is quantized in units of $2\pi/e$. Parallel transport around the string yields a trivial 2π phase change. This is Dirac's quantization condition [93]. The phase picked up by a quark encircling the Dirac string is non-trivial, however, since the quarks' electric charge is only a fraction of e.

Since this Aharonov-Bohm phase is equal to a factor $e^{\pm i2\pi/3} \in Z_3$ from an SU(3) center transformation, it may exactly cancel the contribution from a matching color center vortex. The wavefunctions of all particles remain single valued when they are parallel transported around such a combined $\mathrm{U}(1)_{em}$ and SU(3) defect. That is, this combination is a topologically stable object, which stems from the fact that no known particles represent the Z_3 subgroup of $\mathrm{SU}(3) \times \mathrm{U}(1)_{em}$ comprised of the elements in (5.7) and the identity.

We may formulate this center symmetry in terms of the electroweak gauge group by first writing down the relationship between electric charge Q, hypercharge Y and the third component of weak isospin t_3,

$$Q/e = t_3 + Y/2. \tag{5.8}$$

Since $e^{i2\pi t_3} = -1 \in \mathrm{SU}(2)$, and hypercharge is normalized in units of $1/3$, the symmetry is generated by the element

$$(e^{i2\pi/3}, -1, e^{i\pi Y}) \in \mathrm{SU}(3) \times \mathrm{SU}(2) \times \mathrm{U}(1)_Y. \tag{5.9}$$

1 This has long been known, see e.g. Ref. [132]. A reminder of the cancellation by Creutz [133] sparked the renewed interest here.

Including the identity, this gives a discrete group of six elements, isomorphic to Z_6. It is straightforward to verify that the transformations generated by (5.9) act identically on the Standard Model matter representations,[2]

$$\begin{aligned}
\begin{pmatrix} \nu_e \\ e \end{pmatrix}_L, \begin{pmatrix} \nu_\mu \\ \mu \end{pmatrix}_L, \begin{pmatrix} \nu_\tau \\ \tau \end{pmatrix}_L &: \quad (1,2,-1) \\
e_R, \mu_R, \tau_R &: \quad (1,1,-2) \\
\begin{pmatrix} u \\ d \end{pmatrix}_L, \begin{pmatrix} c \\ s \end{pmatrix}_L, \begin{pmatrix} t \\ b \end{pmatrix}_L &: \quad (3,2,\tfrac{1}{3}) \\
u_R, c_R, t_R &: \quad (3,1,\tfrac{4}{3}) \\
d_R, s_R, b_R &: \quad (3,1,-\tfrac{2}{3}) \\
\phi = \begin{pmatrix} \phi^+ \\ \phi^0 \end{pmatrix} &: \quad (1,2,1),
\end{aligned} \tag{5.10}$$

where ϕ is the Higgs doublet and the fundamental SU(3) and SU(2) representations are labeled by their dimension. In this form the fractional charge of quarks is expressed as fractional hypercharge relative to the leptons and the Higgs.

5.2.1 *Historical notes*

The discrete Z_6 symmetry is often overlooked when the Standard Model gauge group is written down, but it has played an important historical role. For one thing, the matter representations in Eq. (5.10) are almost completely fixed by demanding the cancellation of anomalies that otherwise spoil the consistent formulation of a quantum field theory [134, 135]. There are three sources of anomalies that must be taken care of. First of all, the perturbative triangular chiral anomaly must be avoided, which destroys gauge invariance and renormalizability. Then there is Witten's SU(2) chiral gauge anomaly [136], which is a global anomaly that forces the path integral to vanish for an SU(2) gauge theory with an odd number of chiral fermion doublets. Finally there is the chiral gauge-gravity anomaly, which, like the triangle anomaly, is perturbative. It breaks general covariance. Canceling all three of these anomalies fixes the relative $\mathrm{U}(1)_Y$ charges uniquely for $N = 3$ colors [135].[3]

Anomaly cancellation tightly constrains the charge assignments in the Standard Model. Grand unification is often invoked as a possible origin story. Placing the various matter fields in the same representation of a larger gauge group fixes their assignments after symmetry breaking. In fact, the Standard Model representations (5.10) would not easily fit in grand unified theories based on the prototypical gauge groups $\mathrm{SU}(5) \subset \mathrm{SO}(10)$ without the Z_6 symmetry. A product of the color and electroweak gauge groups may only be accommodated after dividing out the Z_6 redundancy,

$$\mathrm{SU}(3) \times \mathrm{SU}(2) \times \mathrm{U}(1)_Y / Z_6 \simeq \mathrm{S}(\mathrm{U}(3) \times \mathrm{U}(2)) \subset \mathrm{SU}(5). \tag{5.11}$$

2 We've left out right-handed neutrinos, which are present if a Dirac mass is at least partly responsible for neutrino oscillations.

3 It is more accurate to say that anomaly cancellation *almost fixes* the relative charge assignments. There is a so-called *bizarre* solution with zero-hypercharge for the leptons [134, 135].

The product $SU(3)\times SU(2)\times U(1)_Y$ is a cover of the 'true' minimal gauge symmetry in the same sense that $SU(N)$ is a cover of the minimal gauge symmetry $SU(N)/Z_N$ in pure Yang-Mills theory.

In SU(5) GUT [137], the Standard Model gauge symmetry is reproduced when an adjoint scalar field Φ acquires an expectation value at some energy scale above the electroweak transition, which leads to an effective reduction of the gauge theory,

$$\begin{aligned} SU(5) &\xrightarrow{M_{\rm GUT}} SU(3)\times SU(2)\times U(1)_Y/Z_6 \\ &\xrightarrow{\mathcal{O}(200)\,\rm GeV} SU(3)\times U(1)_{em}/Z_3. \end{aligned} \tag{5.12}$$

A potential for the GUT Higgs Φ is chosen such that it is minimized in the unitary gauge by,

$$\langle\Phi\rangle \propto Y = \text{diag}\,(-2/3,-2/3,-2/3,1,1), \tag{5.13}$$

which generates a compact hypercharge $U(1)_Y$ and commutes with $\mathfrak{su}(3)$ and $\mathfrak{su}(2)$ generators that are arranged in blocks along the diagonal. Tracelessness of Y then quantizes the hypercharge of, for instance, matter in the fundamental 5 representation of SU(5) that decomposes into $SU(3)\times SU(2)\times U(1)_Y$ representations like,

$$5 \xrightarrow{M_{\rm GUT}} (3,1,-\frac{2}{3})\oplus(1,2,1). \tag{5.14}$$

Placing the down quark SU(3) triplet and an SU(2) doublet $(e^+,\bar{\nu}_e)$ in this representation fixes their quantum numbers. See Ref. [138] for a detailed treatment of the algebra of several GUTs, how they accomodate the Standard Model, and how they relate to one another. Note that it is usual to describe the electroweak and GUT transition via the Higgs mechanism as spontaneous symmetry breaking transitions, in spite of Elitzur's theorem which states that local gauge symmetry cannot break spontaneously. This is rather misleading, and the subtleties require a careful treatment when one goes from a semi-classical to fully quantum description of a theory with the Higgs mechanism. Ref. [139] provides an up to date discussion.

5.2.1.1 *Topological inspiration from GUTs*

This is where we make contact with the GUT monopoles considered in Chapter 4. Toplogical defects are a generic consequence of breaking a unified gauge group via the Higgs mechanism, provided that it that has a simply connected cover [132]. The latter point ensures that the effective low energy gauge theories inherits non-trivial topology.

If the unifying gauge group is $SU(N)$, then magnetic charge is quantized with respect to the residual $U(1)^{N-1}$ gauge invariance that is generated by the diagonal Lie algebra elements that commute with the Higgs field in unitary gauge (cf. Section 4.1).

For SU(5) GUT, the U(1) subgroups are embedded in the hypercharge $U(1)_Y$ and the enlarged residual SU(3) color and electroweak SU(2) gauge symmetries that follow from the submaximal symmetry breaking pattern in (5.12).

Consider the residual U(1) subgroup generated by exponentiating the Lie algebra element,

$$\text{diag}(0,0,-1,1,0)\in\mathfrak{su}(5), \tag{5.15}$$

for instance. This is a sum of color, weak, and hypercharge generators,

$$\hat{q}_{col} + t_3 + Y/2, \text{ where,} \tag{5.16}$$

$$\hat{q}_{col} = \text{diag}(1/3, 1/3, -2/3, 0, 0), \tag{5.17}$$

$$t_3 = \text{diag}(0, 0, 0, 1, -1), \text{ and} \tag{5.18}$$

$$\frac{Y}{2} = \text{diag}(-2/3, -2/3, -2/3, 1, 1). \tag{5.19}$$

So the corresponding 't Hooft-Polyakov monopoles carry both color and electroweak magnetic charges. The latter are electromagnetic in nature, since $(t_3 + Y/2)$ generates the compact $\text{U}(1)_{em}$ gauge group after the electroweak transition.

These magnetic defects are associated with the hidden Z_6 symmetry. In unitary gauge, the flux of the monopole is formally supplied by a Dirac string that traces out a $2d$ worldsheet. This is a singularity from diagonalizing the GUT Higgs field. When a quark or other Standard Model particle is dragged around the Dirac string, the phase that it picks up winds around this residual $\text{U}(1)$ subgroup back to the identity element

$$e^{i2\pi(\hat{q}_{col} + t_3 + Y/2)} = 1 \in \text{SU}(3) \times \text{SU}(2) \times \text{U}(1)_Y / Z_6 \subset \text{SU}(5). \tag{5.20}$$

In the cover, $\text{SU}(3) \times \text{SU}(2) \times \text{U}(1)_Y$, on the other hand, parallel transport takes us to the center element (5.7) that generates the global Z_6 symmetry.

In any case, the homotopy group that classifies the topologically stable (timelike or spacelike) defects is,

$$\pi_1(\text{SU}(3) \times \text{SU}(2) \times \text{U}(1)_Y / Z_6) \simeq \mathbb{Z}, \tag{5.21}$$

or after electroweak breaking,

$$\pi_1(\text{SU}(3) \times \text{U}(1)_{em} / Z_3) \simeq \mathbb{Z}. \tag{5.22}$$

Note that the singular gauge transformation that corresponds to a defect may contain an arbitrary number of windings around the compact U(1), so the homotopy groups here are isomorphic to the integers, $\mathbb{Z}$. The SU(3) charge is quantized by Z_3 but the electroweak charge is unbounded.

Monopoles are timelike. The vortices that are responsible for confinement in pure SU(N) gauge theories are spacelike objects. The spacelike equivalent of a GUT monopole worldsheet is, then, a spacelike color center vortex that is laced with an additional U(1) vortex. And this combinaton is topologically stable, even in the presence of dynamical quark fields.

There is an obvious problem with identifying the confining disorder in QCD with spacelike vortices from a garden variety unified theory, however. In such models, the unification scale is extremely high, typically $\mathcal{O}(10^{16})$ GeV if one assumes a desert scenario with an absence of new physics between the electroweak and GUT transitions. This presents a decoupling conundrum. Topological defects are interfaces between different perturbative sectors, which means a rotation of the GUT Higgs field that defines the residual Standard Model gauge symmetry at low energies. This is an expensive proposition. Magnetic monopoles then have a mass on

the order of the GUT scale. The related spacelike vortices are similarly costly and therefore not expected to condense at the $\mathcal{O}(200)$ MeV confinement scale of QCD.

Keep in mind, however, that naive GUTs such as the Georgi-Glashow SU(5) model are not the whole story. They have been ruled out by the null result for proton decay [140] and have several theoretical shortcomings, including the failure to explain the origin of identical fermion generations, the absence of gravity, as well as large separation of scales between the electroweak and GUT scale.

Nevertheless, they are a source for inspiration. They provide concrete examples of how a topological link may emerge between the color and electroweak gauge groups, which is a generic possibility due to Z_6 symmetry in the Standard Model matter representations. It is natural to assume that this is a feature of whatever the true unifying theory is.

As an aside, we should make a distinction that is pedantic, but is conceptually relevant. After the Z_6 kernel has been divided out of $\mathrm{SU}(3) \times \mathrm{SU}(2) \times \mathrm{U}(1)_Y$, there is no longer an explicit global center symmetry, just as $\mathrm{SO}(3) \simeq \mathrm{SU}(2)/Z_2$ has no center. The vortex content is identical, however. For SO(3) and SU(2) gauge theory, vortices are classified by the homotopy group,

$$\pi_1(\mathrm{SU}(2)/Z_2) \simeq Z_2, \tag{5.23}$$

and the vortex free energy remains a good order parameter for a disorder-order transition [141]. For the product of color and elecroweak gauge groups, the vital ingredient is not the hidden Z_6 symmetry, but rather the non-triviality of,

$$\pi_1(\mathrm{SU}(3)\times\mathrm{SU}(2)\times\mathrm{U}(1)_Y/Z_6) \simeq \mathbb{Z}. \tag{5.24}$$

Explicit center symmetry is not required by the vortex confinement mechanism. Without it, though, one cannot fix center vortex superselection sectors using twisted boundary conditions. For, e.g., SO(3) gauge theory, the periodic ensemble is a sum over topological sectors. And while pure SO(3) and SU(2) gauge theories are expected to have the same non-perturbative continuum limit, it is has been an ongoing struggle to establish this from their various lattice formulations [142, 143, 144].

5.2.1.2 *Perturbative sectors versus topology*

In a perturbative Lagrangian, the quarks' electric charges appear as couplings to the photon field via the covariant derivative, where they are quantized in units of $e/3$. Rescaling the photon field $A_\mu \to A_\mu/3$ changes the coupling of the quadratic $F_{\mu\nu}F^{\mu\nu}$ term in the Lagrangian. But one could start over with electric charge (equivalently hypercharge) normalized by quarks. 'Fractional' charge is, in this sense, a historical artifact from the fact that electrons were discovered before quarks.

Things are different when the $\mathrm{U}(1)$ gauge group is compact. In that case, the particle with minimal electric charge is the one that represents the whole gauge group and determines its 'volume'. Consider the $\mathrm{U}(1)_Y$ generated by the direction of the GUT scalar field (5.13) in SU(5) GUT, for instance. Parallel transport that amounts to a complete 2π phase rotation for the lepton doublet only takes the quarks part of the way around $\mathrm{U}(1)_Y$. In terms of the compact electromagnetic $\mathrm{U}(1)_{em}$ generated by $Q/e = t_3 + Y/2$, a complete revolution for the electron is only one third of a

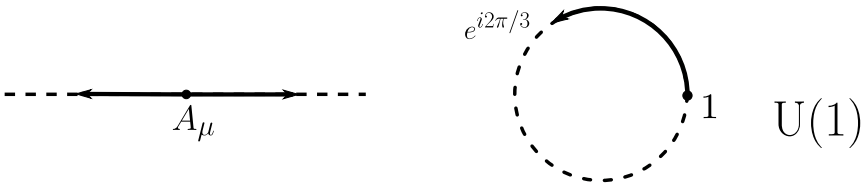

Figure 5.3: (left) Perturbatively, one may choose the normalization for the electric charge. (right) A compact U(1) gives meaning to 'fractional' electric charge. A trivial 2π phase rotation of the wavefunction or quantum field for an electron only takes that for quarks a fraction of the way around the U(1).

revolution for the quarks (Fig. 5.3), corresponding to the electromagnetic phase in (5.9).

This will serve as our definition of fractional electric charge. It means that a quark picks up a phase when it encircles a U(1) vortex with the minimal flux that gives a trivial 2π rotation for an electron. U(1) vortices are interfaces between different perturbative sectors, just as color center vortices interface between Z_N center sectors in SU(N) gauge theories. From the quantum mechanical viewpoint, the hidden symmetry of the Standard Model means that the quark wavefunction remains single valued if the SU(3) and U(1) topological disorder sits on top of one another. This is not possible in QCD alone.

5.2.2 *The proposal*

Like Gell-Mann, we borrow the words of T.H. White:

> 'Everything not forbidden is compulsory.'

A topological link between the color and electroweak gauge groups via a compact U(1) is a possible, well-motivated consequence of beyond Standard Model physics. Assuming that it is present, we may explore a connection with the familiar order-disorder transition in pure SU(N) gauge theory.

We have, once more, the possibility of a spontaneous symmetry breaking transition, associated with the hidden Z_6 symmetry that relates the quarks' color and electroweak quantum numbers and the corresponding combined defects. A modified version of the center vortex confinement mechanism may be able to explain why fractionally charged quarks are confined, but electrons are not.[4]

If the U(1) interfaces associated with the electroweak gauge group are sufficiently thin, then they will not generate a confining string tension for integer charged particles. The seams will behave as invisible Dirac strings and not disrupt perturbative electroweak physics. Note that this argument also applies to the effect of combined SU(3)×U(1) vortices on quarks. Assuming that there is some dynamic spreading of color center flux, however, Wilson loops for quarks may pick up a non-trivial phase from a partial intersection with the combined defects. This is analogous to the need for thick center vortices to generate the correct N-ality dependence for the intermediate string tension of, e.g., adjoint sources in pure SU(N) theories [13]. In a scenario with dynamic spreading of color flux, SU(3) center vortices and thin U(1)

4 The first steps in this direction were made for coupled U(1)×U(1) groups in Ref. [145, 146].

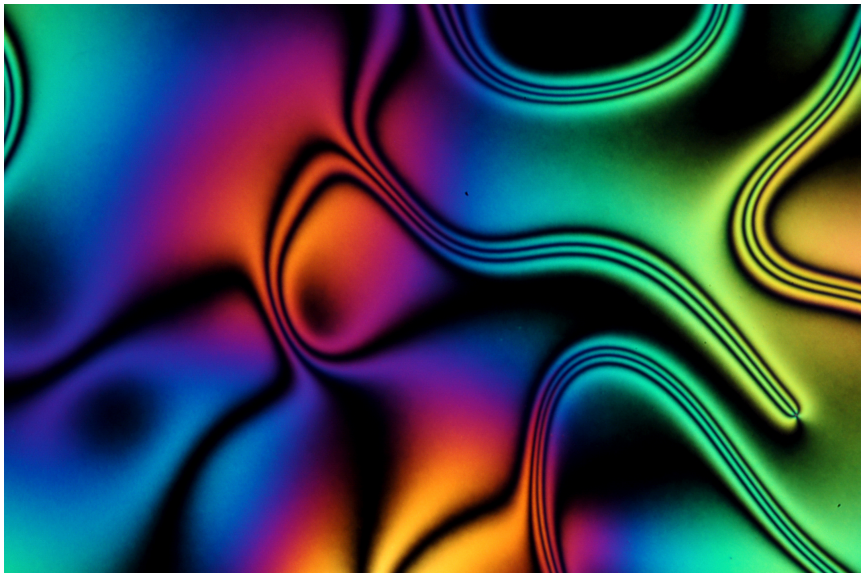

Figure 5.4: View of a nematic crystal through a polarizing microscope [147]. One may imagine that the seams here are analogous to interfaces between perturbative U(1) sectors, correlated with thickened color center vortices. Colorless particles, with integer electric charge, are blind to U(1) interfaces if these are sufficiently thin.

interfaces are correlated, but not perfectly, and the disorder could generate a linear potential for quarks.

This suggests the enticing possibility to smoothly connect deconfinement with dynamical quarks to the spontaneous symmetry breaking transition of the pure gauge theory, by extending the center vortex picture to these combined defects.

This hinges on new physics. Topological disorder in the U(1) sector must be inherited from a unifying theory and included in the phenomenology. Ultimately, contact needs to be made with measured hadron masses and a suitable string tension.

In what follows we take a bottom up approach, and explore the conceptual implications in toy lattice models. We put aside the question of the UV completion of the Standard Model, and take a first look at what happens when topological disorder is coupled between color and U(1) sectors in the presence of dynamical quarks. The nematic liquid crystal in Fig. 5.4 provides a compelling cartoon to keep in mind.

5.3 EXPLORATIONS IN A 2-COLOR WORLD

Lattice simulations of the full Standard Model are both beyond reach, and superfluous for this preliminary study. Our starting point is, instead, a simplified 2-color model of QCD plus electromagnetism in $3+1$ d. By including 'up' and 'down' quarks with fractional charge $\pm\frac{1}{2}e$ relative to a compact $\mathrm{U}(1)_{em}$ gauge action, we can construct a toy model with a global Z_2 symmetry that is the analog of the hidden symmetry in the Standard Model. Weak interactions are neglected, but we retain a discrete symmetry that relates compact color and electromagnetic gauge groups. The restriction to two colors is sufficient for a conceptual study. SU(2) gauge theory shares many the non-perturbative features of SU(3) that are most relevant to us, including a spontaneous symmetry breaking deconfinement transition for static quarks (cf. Chapter 3).

5.3.1 *Model setup*

We choose a simple lattice action

$$S = -\sum_{\text{plaq.}} \left(\frac{\beta_{col}}{2} \text{Re tr } \square_{col} + \beta_{em} \cos 2\alpha_{\mu\nu} \right) + S_{f,W}, \tag{5.25}$$

where $S_{f,W}$ is the usual Wilson fermion action (2.31) with the distinction that parallel transporters for quarks are now products of an SU(2) color matrix and a U(1) phase, of the form

$$U_\mu(x) e^{i\alpha_\mu(x)}, \;\; U_\mu(x) \in \mathrm{SU}(2), \; \alpha_\mu(x) \in (-\pi, \pi]. \tag{5.26}$$

The SU(2) plaquettes $\square_{col}$ are formed from links U_μ in the usual way. In this model 'fractional electric charge' means that the U(1) angles α_μ that appear in the parallel transporters for quarks are half of those in the U(1) gauge action. That is, the gauge action is formed from U(1) plaquette angles,

$$2\alpha_{\mu\nu}(x) = 2[\alpha(x) + \alpha_\nu(x+\hat{\mu}) - \alpha_\mu(x+\hat{\nu}) - \alpha_\nu(x)], \; \beta_{em} = 1/e^2. \tag{5.27}$$

These U(1) angles correspond to the parallel transport of 'integer' charged particles, such as a charged meson or the the analog of an electron in this model. This means, for instance, that an $e^{i\alpha_\mu} = -1$ electromagnetic link for quarks appears as an $e^{i2\alpha_\mu} = +1$ link in the gauge action. The volume of the U(1), i.e. the range of $\alpha_\mu(x)$, is chosen such that we integrate over all possible electromagnetic transporters for the quarks. This amounts to a double counting of the U(1) from the perspective of integer charged particles.

It is evident from Eq. (5.26) that a combination of the center element $-1 \in \mathrm{SU}(2)$ and the U(1) phase $e^{i\alpha_\mu} = -1$ acts identically on the quarks. So the model has an explicit Z_2 center symmetry that combines the color and U(1) gauge groups.

Comments on the action

1. As the U(1) coupling β_{em} is increased, the gauge action orders the links towards $e^{i2\alpha_\mu} \simeq +1$, up to gauge transformations. Compact QED in $3+1$ d has

a transition from a strongly coupled, disordered phase, to a weakly coupling, ordered phase at $\beta_{em} \simeq 1.01$. Above this transition, the theory is in a deconfined, Coulomb phase for integer charged particles. The dynamic inclusion of integer charges singles out the $e^{i2\alpha_\mu} \simeq +1$ sector, which can be understood from those terms of the hopping expansion that have the effect of an external magnetic field (cf. Sec. 5.3.4). As far as integer charges are concerned, the only fluctuations that remain are small electromagnetic perturbations. For fractionally charged quarks, however, this does not constrain a additional $e^{i\alpha_\mu} = \pm 1 \in Z_2 \subset \mathrm{U}(1)_{em}$ degree of freedom that couples to the SU(2) sector via the fermion determinant. This is a simple way of introducing additional topological structure. Quarks 'see' SU(2) and $Z_2 \subset \mathrm{U}(1)_{em}$ vortices unless they sit on top of one another, and act to correlate them.

2. The model has an *explicit* center symmetry, since the action is invariant under a simultaneous global center transformation with the center element $(-1,-1) \in \mathrm{SU}(2) \times \mathrm{U}(1)$, but the Polyakov loops for each gauge group pick up the individual phases,

$$P_{col}(\vec{x}) \to -P_{col}(\vec{x}), \qquad P_{col}(\vec{x}) = \frac{1}{2}\sum_{t=0}^{N_t-1} \mathrm{tr}\; U_t(t,\vec{x}) \tag{5.28}$$

$$P_{em}(\vec{x}) \to -P_{em}(\vec{x}), \qquad P_{em}(\vec{x}) = \sum_{t=0}^{N_t-1} \alpha_t(t,\vec{x}). \tag{5.29}$$

So they can be used as order parameters for the spontaneous breaking of the global combined Z_2 symmetry. This is a consequence of choosing an SU(2) gauge action that is in the fundamental representation.[5]

3. Since quarks couple the SU(2) and U(1) gauge groups, only the combined center symmetry may break spontaneously at a phase transition. If the SU(2) Polyakov loop P_{col} orders, for instance, then the quarks generate a symmetry breaking term for the U(1) loop P_{em} via the fermion determinant, and vice versa.

5.3.1.1 *Algorithmic notes*

We carried out simulations using the Hybrid Monte Carlo (HMC) algorithm using a pair of degenerate (i.e. equal charge $+\frac{1}{2}e$) quark flavors [148, 31]. Since charge conjugation in SU(2) is equivalent to a gauge transformation, $i\sigma_2 \in \mathrm{SU}(2)$, we can interpret the degenerate flavors as an 'up' and 'anti-down' quark. With a a change of color basis, this is physically equivalent to simulations with $\pm\frac{1}{2}e$ 'up' and 'down' quarks.

5 It would be more natural, in some sense, to construct color plaquettes from the parallel transporters for quarks, since there are no known dynamical fundamental color charges that are electrically neutral. The theory would then be centerblind, however, since no operator would represent the change of variables

$$(U_\mu, e^{i\alpha_\mu}) \to (-U_\mu, -e^{i\alpha_\mu}). \tag{5.30}$$

Such an action would correspond, in fact, to a $\mathrm{U}(2) \simeq \mathrm{SU}(2) \times \mathrm{U}(1)/Z_2$ gauge theory with dynamical fermions. This is what emerges in unitary gauge if one considers a lattice version of a simple GUT (cf. Appendix C.). Given the difficulties of probing confinement in the centerblind lattice formulations of $\mathrm{SU}(2)/Z_2 \simeq \mathrm{SO}(3)$, we will avoid the subtleties in the choice of action for now.

Ergodicity becomes a tricky business, owing to the additional topology that has been introduced via the U(1). HMC trajectories only propose small changes to the link variables and have difficulty changing the sign of the U(1) links,

$$e^{i\alpha_\mu} \to -e^{i\alpha_\mu} \in \mathrm{U}(1) \tag{5.31}$$

For large β_{em}, the U(1) gauge action strongly suppresses fluctuations away from links that are gauge equivalent to $\pm 1 \in \mathrm{U}(1)$, i.e. $e^{i2\alpha_\mu} = 1$. Additional local updates are necessary to ensure ergodicity.

The first of these is a simultaneous flip of SU(2) and U(1) links,

$$U_\mu(x) \to -U_\mu(x); \;\; e^{i\alpha_\mu(x)} \to -e^{i\alpha_\mu(x)}. \tag{5.32}$$

Only the SU(2) Wilson gauge action is affected by this combined update. The U(1) gauge action is blind to such phases by default, and the quark determinant is also blind because this transformation belongs to the Z_2 symmetry of the $\mathrm{SU}(2) \times \mathrm{U}(1)$ model. It introduces a thin combined color-electromagnetic vortex that pierces the plaquettes belonging to the affected link, which allows for tunneling between topological sectors. The color-flux is subsequently free to spread. Between HMC trajectories we propose such an update on a random link and accept/reject using a Metropolis check [149] for the SU(2) gauge action, repeating many times.

This is efficient when β_{col} is small, but the acceptance rate is exponentially suppressed by the Boltzmann weight e^{-S} as the cost of flipping SU(2) plaquettes increases with β_{col}. Thin color vortices become expensive. It is necessary to also include local updates that flip only U(1) links,

$$e^{i\alpha_\mu(x)} \to -e^{i\alpha_\mu(x)}. \tag{5.33}$$

Here the fermion action requires a costly recalculation for each Metropolis check, but the acceptance rate is much improved when β_{col} is large. In what follows, we have tuned the the number of sweeps of each type of local update to obtain an acceptable compromise for different parameter regions, and carried out simulations from both ordered starts (i.e., all links are unity), and disordered starts (i.e., all links are random) for confirmation of ergodicity.

5.3.2 *Dynamical restoration of symmetry*

So what are the consequences of coupling quarks with fractional charge to a U(1) gauge group in this model? The usual ordering of color links by dynamical quarks is negated, which is best understood via the hopping expansion. To leading order in the hopping parameter with $N_t = 4$ time slices, our Wilson quarks contribute the $\mathcal{O}(\kappa^4)$ effective action,

$$S_{f,\mathrm{eff}} = -16\kappa^4 \left(\sum_{\mathrm{plaq.}} \cos\alpha_{\mu\nu} \cdot \; \mathrm{tr}\, \square_{col} + 8 \sum_{\vec{x}} \mathrm{Re} P_{em} \cdot \; P_{col} \right) + \ldots, \tag{5.34}$$

These minimal quark loops generate plaquette-plaquette and Polyakov loop-Polyakov loop couplings between the gauge groups. The trivial $P_{col} = 1$ sector is no longer favored, provided that there is disorder in the U(1) Polyakov loop P_{em}. From the

perspective of the SU(2) gauge degrees of freedom, center symmetry is *dynamically* restored by U(1) disorder.

The effect is analogous to subjecting a spin system to a fluctuating magnetic field rather than a homogeneous one. In that case, spins are not forced to align in any particular direction. Novel phase structures may emerge even with static, spatial fluctuations, with the existence and type of order-disorder transitions depending on the magnitude of the applied field [150].

In our model the fluctuations are dynamic. The spin equivalent is obtained by replacing the magnetic field by U(1) variables at each site to construct, for instance, the XY-Ising model [151]. This is reminiscent of the Peccei-Quinn mechanism [152], in which the CP violating θ-term in QCD is coupled to an axion field. In each example the symmetry breaking term is suppressed by coupling it to a source of disorder.

If one considers more complicated lattice structures, such as hexagonal cells, more exotic inspirations for frustrated topological disorder are available. In a quantum spin liquid, for instance, the magnetic moments are strongly correlated but do not order or freeze out, even at zero temperature. The spin correlations may be short ranged, but the quantum coherence is long ranged. There is exciting new evidence that this state of matter is realized in nature [153, 154].

Turning our attention to the results in our 2-color $\mathrm{SU}(2)\times\mathrm{U}(1)$ model with dynamical quarks, we see in Fig. 5.5 that the SU(2) Polyakov loop is indistinguishable from the pure gauge result at values of the hopping parameter that cause a significant amount of ordering in standard 2-color QCD. This is true in both the disordered, strongly coupled U(1) phase $\beta_{em} \lesssim 1.01$, *and* in Coulomb phase $\beta_{em} \gtrsim 1.01$ for integer charges. Note that the inclusion of electrically charged Wilson fermions shifts the location of the compact QED transition to lower values of β_{em} [155, 156]. Here we are not concerned with its precise location, but merely that it is present in our toy model, as is indicated in Fig. 5.6.

In the disordered phase of compact QED, the links $e^{i\alpha_\mu(x)}$ are distributed over the unit circle. The disorder generates a confining potential for all electric charges, which can be attributed to a condensate of magnetic monopoles with flux quantized with respect to the unit of electric charge e in the gauge action [13].[6] In this phase the U(1) parallel transporters corresponding to an 'electron' in this theory are disordered. Above $\beta_{em} \simeq 1.01$ the gauge action orders the U(1) links such these magnetic defects are suppressed and integer electric charges enter a deconfined Coulomb phase. But since the U(1) gauge action is unable to distinguish $e^{i\alpha_\mu} = \pm 1$ links, it is unable to remove $\mathrm{Z}_2 \subset \mathrm{U}(1)$ topological disorder as seen by fractionally charged quarks. In this lattice model, such Z_2 defects separate different perturbative U(1) sectors, which, via the coupling to quarks, are correlated with the SU(2) gauge degrees of freedom.

The finite temperature transition of pure SU(2) in $3+1$ d is a center symmetry breaking transition in the $3d$ Ising/Z_2 gauge universality class. This is embodied up to finite size corrections in the quenched result for the SU(2) Polyakov loop in Fig. 5.5. It has clearly turned into a crossover in unquenched 2-color QCD at this value for the hopping parameter, $\kappa = 0.15$, with quark loops acting as a symmetry breaking external field. In the $\mathrm{SU}(2)\times\mathrm{U}(1)$ model with fractional electric charge,

6 Since U(1) is abelian, the magnetic flux is not quantized by discrete center elements into vortices.

the curve falls back to the pure gauge result. A global $Z_2 \in \mathrm{SU}(2) \times \mathrm{U}(1)$ center symmetry is manifest, which is free to break spontaneously at an order-disorder transition, with the SU(2) Polyakov loop serving as an order parameter.

5.3.3 *Physical scales*

It is important to check what has happened to the mass scale before proceeding further.

We have performed zero temperature measurements of meson masses in the U(1) Coulomb phase, $\beta_{em} > 1.01$. ρ and π masses were extracted from all-to-all 2-point correlation functions with pointlike sources that were diluted in the spin and time indices. The use of diluted sources provides a tremendous boost to the precision of propagators calculated via stochastic estimation. To avoid a lengthy technical detour, the reader is directed to Ref. [157] for an outline of this method. Note that the masses quoted below are for electrically neutral mesons, constructed from the propagators for a quark and anti-quark.

The comparison between our toy model and standard 2-color QCD in Fig. 5.7a reveals that the mass scale has changed dramatically. With the inclusion of fractional charge with respect to a compact U(1), much larger values of the hopping parameter κ are required to achieve an equivalent mass ratio m_ρ/m_π for a given SU(2) coupling β_{col}. For example, a mass ratio of $m_\rho/m_\pi \simeq 1.28$, which is obtained with $\kappa = 0.178$ at $\beta_{col} = 1.7$ in standard 2-color QCD, requires $\kappa \simeq 0.223$ in the SU(2)×U(1) model at $\beta_{em} = 2$. The chiral limit, obtained by a linear extrapolation of $(am_\pi)^2$ to zero as a function of $1/\kappa$, is correspondingly pushed from $\kappa_c \simeq 0.185$ to $\kappa_c \simeq 0.241$. This is rather close to the critical hopping parameter $\kappa_c = 1/4$ in a quenched theory, i.e., without dynamic 'sea' quarks [31].

We can understand the increase in masses in the SU(2)×U(1) model compared to standard 2-color QCD via an increase in disorder in the gauge configurations. The more disorder along paths between sources and sinks in the 2-point correlator, the larger the effective mass of the propagating particle. In particular, disorder in the quarks' U(1) links adds to their confining potential. In addition to the usual color flux string, they possess a string from $Z_2 \in$U(1) disorder. This is separate from a Coulombic contribution from the perturbative fluctuations allowed by the finiteness of β_{em}. We should think of it as a *topological* contribution to the confining potential.

Note that the strength of the purely color string is also enhanced compared to 2-color QCD at the same parameters, because the dynamical ordering of SU(2) links by the sea quarks is suppressed. One can disentangle the color and Z_2 contributions by calculating meson masses using only the SU(2) links from dynamically generated SU(2)×U(1) configurations. These masses correspond to 'quarks' that have been stripped of their U(1) charge. At parameters such as as $\kappa = 0.178$ and $\beta_{col} = 1.7$ in Fig. 5.7b, these masses are extremely close to those calculated on *quenched* SU(2) configurations. The jump in meson masses when the U(1) parallel transporters are once again included indicates the contribution from the topological $Z_2 \subset \mathrm{U}(1)$ disorder that is not suppressed by the gauge action.

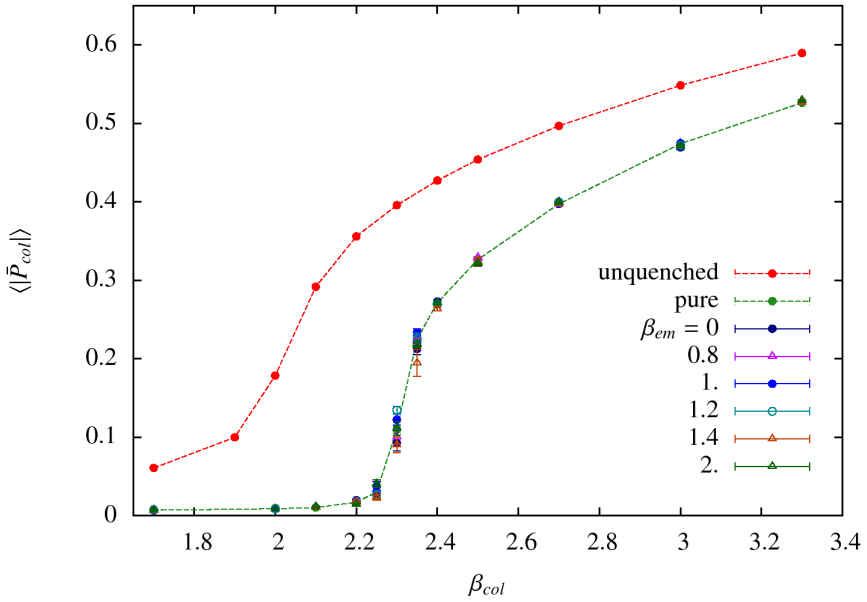

Figure 5.5: Volume averaged SU(2) Polyakov loop on 4×16^3 lattices, in the pure gauge theory (green), 2-color QCD with $\kappa = 0.15$ Wilson quarks (red), and the SU(2)×U(1) toy model with fractionally charged quarks. The electromagnetic coupling β_{em} here is varied from total U(1) disorder, $\beta_{em} = 0$, to deep in the Coulomb phases, $\beta_{em} = 2$.

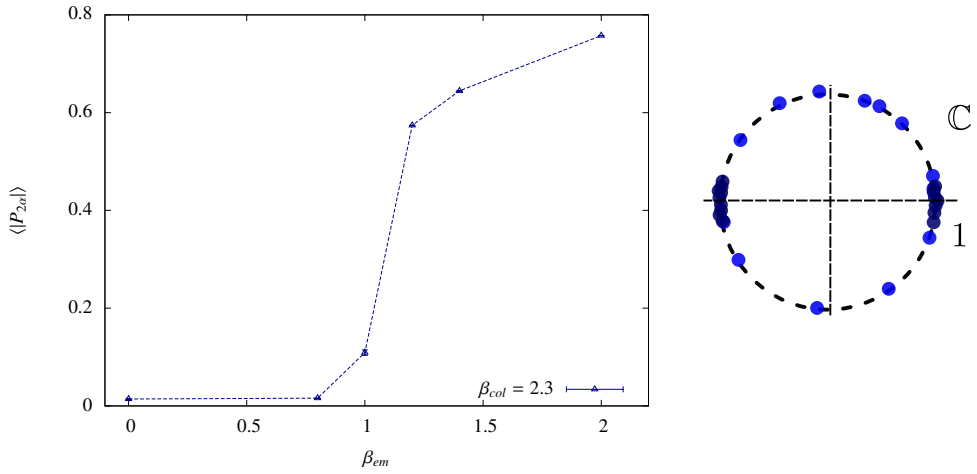

Figure 5.6: (left) Volume averaged U(1) Polyakov loop corresponding to integer charged particles, on the 4×16^3 ensembles as in Fig. 5.5 for $\beta_{col} = 2.3$, in the presence of fractionally charged Wilson quarks with $\kappa = 0.15$. Here we see the ordering of the U(1) links $e^{i2\alpha_\mu(x)}$ for integer charges as ones crosses into the Coulomb phase $\beta_{em} \geq 1$. (right) Depiction of the qualitative difference across the transition for the U(1) angles that appear in the parallel transporters for quarks. The U(1) gauge coupling β_{em} is unable to remove a Z_2 phase.

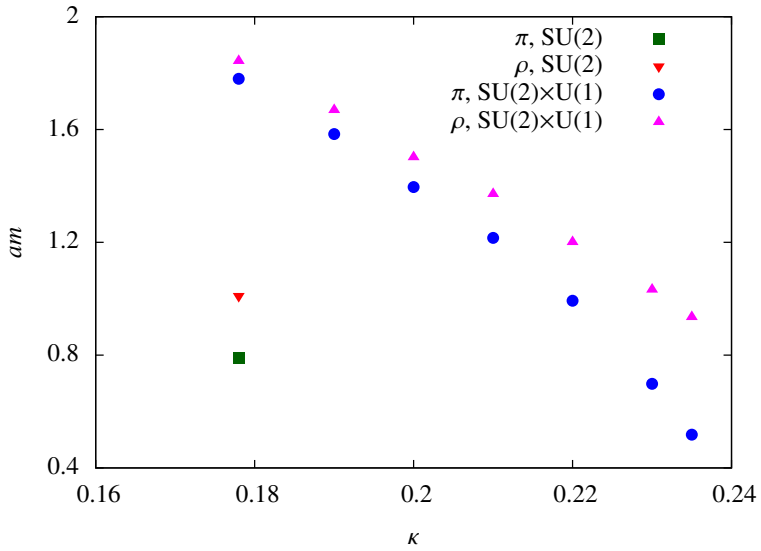

(a) Meson masses in lattice units on a 16×8^3 lattice in the Coulomb phase, $\beta_{\text{em}} = 2$, with $\beta_{col} = 1.7$. The chosen values of β_{col} and κ allow for a crosscheck with Ref. [158]. 'SU(2)' results are from standard 2-color QCD. Masses in the 'SU(2)×U(1)' model exhibit a radical shift of scale. Much larger values of κ are required in order to obtain an equivalent ratio of ρ and π masses at a given β_{col}.

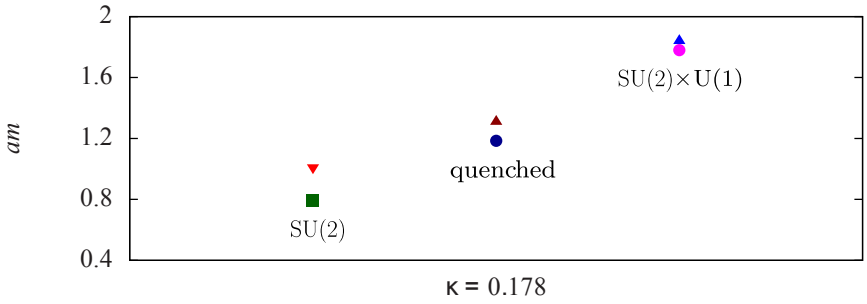

(b) Meson masses in lattice units on a 16×8^3 lattice at $\beta_{em} = 2$, with $\beta_{col} = 1.7$, as in Fig. 5.7a above, here for fixed $\kappa = 0.178$. 'SU(2)' results are from standard 2-color QCD with dynamical quarks, and 'quenched' with static quarks. The additional jump to the 'SU(2)×U(1)' results indicate the topological contribution of a $Z_2 \subset \mathrm{U}(1)$ string to the confining potential.

5.3.3.1 *Correlation of SU(2) and U(1) sectors*

One might wonder if dynamical quarks have effectively been removed from the functional integral via their U(1) coupling, as far as the SU(2) sector is concerned. This would be true if the $Z_2 \subset \mathrm{U}(1)$ phases were in fact random. Then for each SU(2) gauge configuration, every quark loop would cancel against another that differs only by a phase factor $-1 \in$U(1) when the integration over U(1) configurations is performed.

Remember, however, that quarks loops induce a coupling that favors a correlation between SU(2) and U(1) links. This back-reaction is evident in the hopping expansion effective action Eq. (5.34), which is minimized when the product of SU(2) and U(1) degrees of freedom is unity.

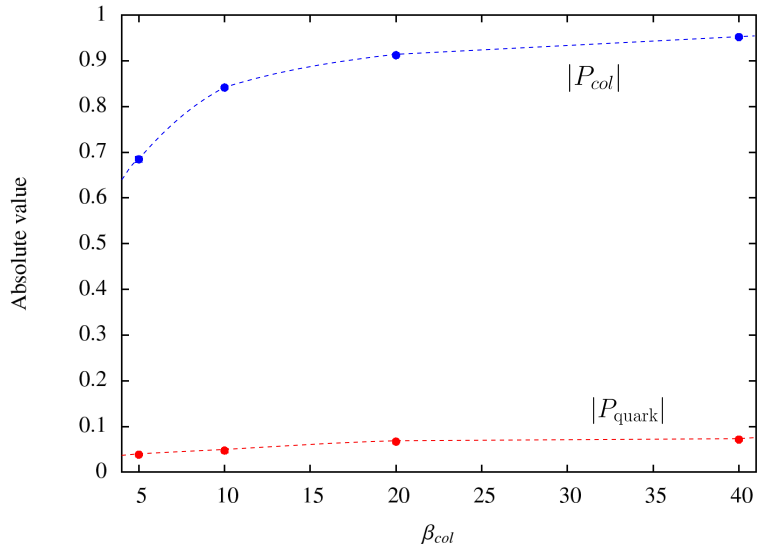

Figure 5.7: Volume averaged SU(2)×U(1) Polyakov loop corresponding to a static quark, $P_{quark}(\vec{x}) = P_{em}(\vec{x}) \cdot P_{col}(\vec{x})$, on an 4×8^3 lattice with $\beta_{em} = 2$ and $\kappa = 0.15$, compared with $P_{col}(\vec{x})$. Quark loops do not significantly correlate the SU(2) and U(1) links at this value of the hopping parameter.

The extent of the correlation is measured by the combined SU(2)×U(1) Polyakov loop that corresponds to a static quark worldline,

$$P_{quark}(\vec{x}) = P_{em}(\vec{x}) \cdot P_{col}(\vec{x}). \tag{5.35}$$

Its volume averaged absolute value increases as κ is increased, i.e., as the bare quark mass is reduced. See Fig. 5.8.

For moderate values of κ, the effect is weak. The volume averaged absolute value of the combined SU(2)×U(1) Polyakov loop rises only slowly as β_{col} orders the SU(2) links, which is clear in Fig. 5.7. For these ensembles, quarks loops have difficulty correlating the disorder belonging to the two gauge sectors such that combined Aharonov-Bohm phases are reduced and P_{quark} is ordered, i.e., forcing $Z_2 \subset$ U(1) vortices to pair with SU(2) center vortices. Quark masses much closer to the chiral limit are necessary to reveal such a correlation (cf. Fig. 5.8).

This is a consequence of the fact that the $Z_2 \subset$U(1) degree of freedom in this model was introduced without a coupling, and hence a scale, of its own. A large gauge coupling β_{em} prevents $Z_2 \subset$U(1) interfaces from spreading much larger than the lattice spacing, but does not otherwise suppress or relate them to the color sector. Quark fluctuations are burdened with this sole responsibility. They must be given a smaller and smaller bare mass to dynamically correlate U(1) and SU(2) disorder and thereby balance their contribution to the confining potential.

Unfortunately, ergodicity is difficult to maintain as κ increases towards the chiral limit. The condition number of the fermion determinant grows dramatically, so its approximation requires many more matrix inversions. Eventually, the frequent calculation of the fermion action S_f in the Metropolis check of the topology-changing local updates in Sec. 5.3.1.1 becomes prohibitively expensive. Moreover, Wilson quarks suffer from unphysical flavor-parity breaking Aoki phases in the vicinity of

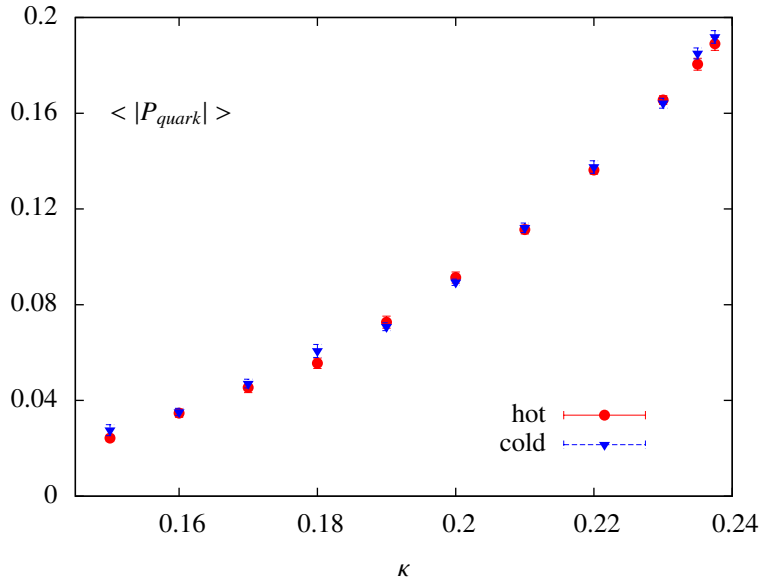

Figure 5.8: Volume averaged SU(2)×U(1) Polyakov loop corresponding to a static quark, $P_{quark}(\vec{x}) = P_{em}(\vec{x}) \cdot P_{col}(\vec{x})$, on an 4×8^3 lattice with $\beta_{col} = \beta_{em} = 2$. SU(2) and U(1) links order with respect to one another as the quark mass is decreased. Agreement between 'hot' and 'cold' starts confirms ergodicity.

the (gauge coupling dependent) chiral limit κ_c [159].[7] These difficulties make an attempt to fine tune the lattice couplings and search for scaling of masses along 'lines of constant physics' an expensive and unpleasant proposition. It is sensible to instead turn back to the hopping expansion to see what more may be learnt.

5.3.4 *Back to the hopping expansion*

We have explored the (β_{col}, κ) phase diagram using the $\mathcal{O}(\kappa^4)$ effective quark action Eq. (5.34) on asymmetric (i.e. finite temperature) lattices. This allows us to check our intuition about the coupling of SU(2) and U(1) links without worrying about the chiral limit. For this purpose the $\mathcal{O}(\kappa^4)$ action is taken at face value, beyond its range of applicability as an effective theory at small κ.

The action consists of the pure gauge and $\mathcal{O}(\kappa^4)$ hopping terms,

$$\begin{aligned} S_{eff} \quad = \quad & -\sum_{\text{plaq.}} \left(\tfrac{\beta_{col}}{2} \text{ tr } \square_{col} + \beta_{em} \cos 2\alpha_{\mu\nu} \right) \\ & -16\kappa^4 \left(\sum_{\text{plaq.}} \cos \alpha_{\mu\nu} \cdot \text{ tr } \square_{col} + 8 \sum_{\vec{x}} \text{Re } P_{em} \cdot P_{col} \right) . \end{aligned} \tag{5.36}$$

7 In fact, for an 'ordered' start for values of κ near 0.25, the simulation starts in an Aoki phase of standard 2-color QCD in terms of the SU(2) links, which then sit on a background of 'cold' links $e^{i\alpha_\mu(x)} = 1 \in \text{U}(1)$. Passing over to a flavor-parity unbroken phase requires the HMC algorithm to overcome a dramatic rise in the condition number of the fermion determinant and associated low acceptance rates for HMC trajectories of reasonable length. It becomes troublesome to make contact with a 'hot' start on the other side, even when the step size and length of HMC trajectories are dynamically adjusted.

Let us simplify matters by taking the limit $\beta_{em} \to \infty$, which amounts to the restriction of U(1) links to $e^{i\alpha_\mu(\vec{x})} = \pm 1 \in Z_2$. We plot the results for the SU(2) and $Z_2 \subset$U(1) Polyakov loops in Fig. 5.9 and Fig. 5.10 respectively. These results are typical of finite β_{em} simulations in the Coulomb phase for integer electric charges, $\beta_{em} > 1.01$.

As κ is gradually increased from zero, the behavior of the SU(2) Polyakov loop indicates that the disorder-order transition shifts to slightly smaller values of β_{col} without an evident qualitative change. As κ increases further, the transition then sharpens dramatically and clearly becomes first order in nature with a large discontinuity in both the SU(2) and U(1) order parameters.

Keep in mind that when either P_{col} or P_{em} become non-zero, the term in Eq. (5.36) that corresponds to the Polyakov loop for a static quark becomes an explicit symmetry breaking term for the other gauge sector. It is the global symmetry of the combined center,

$$Z_2 = \{(1,1),(-1,-1)\} \subset \mathrm{SU}(2) \times Z_2, \tag{5.37}$$

that breaks spontaneously at this transition with β_{col}. This fact is not obvious from inspection of the U(1) order parameter P_{em} in Fig. 5.10 for small values of the hopping parameter κ, but is apparent as κ becomes larger.

For our curves in β_{col} with $\kappa = 0.375$ in Figs. 5.9 and 5.10, there is a signal for a continuous transition in the respective SU(2) and $Z_2 \subset$U(1) Polyakov loops, centered at $\beta_{col} \sim 1.97$, which is followed by a jump at ~ 2.05 at for the 'ordered' start data presented here.[8]

The abrupt β_{col} transitions can be understood by inspecting the action (5.36). In the combined limit $\kappa,\ \beta_{em} \to \infty$, the plaquette-plaquette coupling forces the SU(2) plaquettes to take values ± 1 according to the value of $Z_2 \subset \mathrm{U}(1)$ links. For very large κ the transition line must therefore terminate with the first order bulk transition of Z_2 gauge theory at $\beta_{col} = \ln(1+\sqrt{2})/2 \sim 0.44$ [160].

Note that when $\beta_{col} > 2.3$, center symmetry is broken for all κ in the finite temporal direction, as indicated by the finite values for the $\mathrm{SU}(2)$ and $Z_2 \subset \mathrm{U}(1)$ Polyakov loops serving as order parameters. Yet they exhibit an additional jump with κ near $\kappa \sim 0.35$. Measurements of the spacelike versions of Polyakov loops, spacelike Wilson lines, help to characterize this transition.[9] We observe abrupt jumps as κ increases, as shown in Fig. 5.11, where the $Z_2 \subset \mathrm{U}(1)$ spacelike Wilson line is plotted together with the timelike Polyakov loop for $\beta_{col} = 2.4$. Here we also plot the average SU(2) and $Z_2 \subset \mathrm{U}(1)$ plaquettes, which both indicate a discontinuous transition.

The bulk first order transition of Z_2 gauge theory in $3+1$ d may also be understood to be at the the root of these transitions with κ. To make this clear, it helps

8 'Hot' starts exhibit a slightly later transition at ~ 2.1, which is indicative of hysteresis and is further evidence that this jump is a first order transition.

9 We also measured SU(2) Creutz ratios with smeared links, in order to to observe a transition in the string tension of spacelike Wilson loops, but this does not add to the discussion.

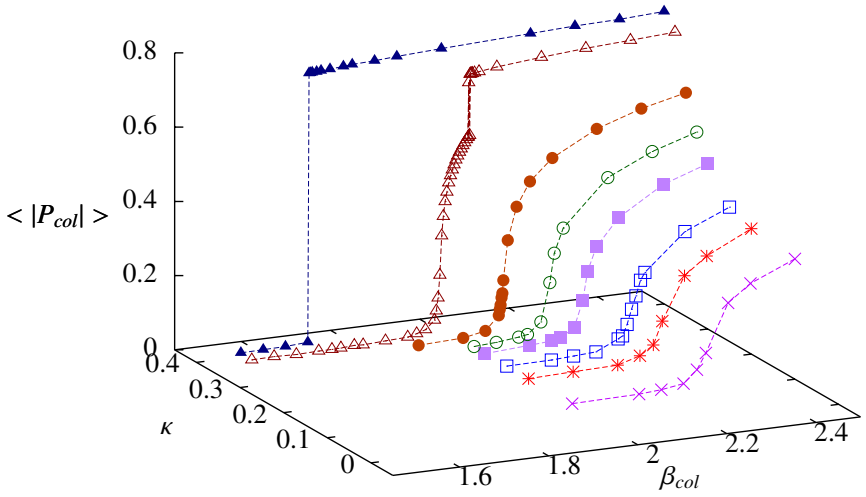

Figure 5.9: Volume averaged SU(2) Polyakov loop on 4×16^3 lattices, using an $\mathcal{O}(\kappa^4)$ hopping effective fermion action, at $\beta_{em} \to \infty$. The location of the transition is shifted with increasing κ. For $\kappa = 0.375$ we see the indication of a continuous transition, followed by a first order transition with an abrupt discontinuity.

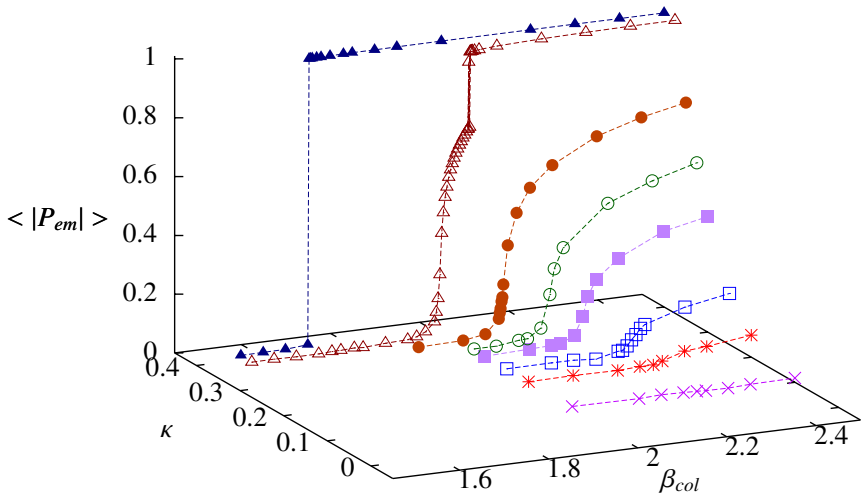

Figure 5.10: $Z_2 \subset$ U(1) Polyakov loop, on the same 4×16^3 ensembles as in Fig. 5.9.

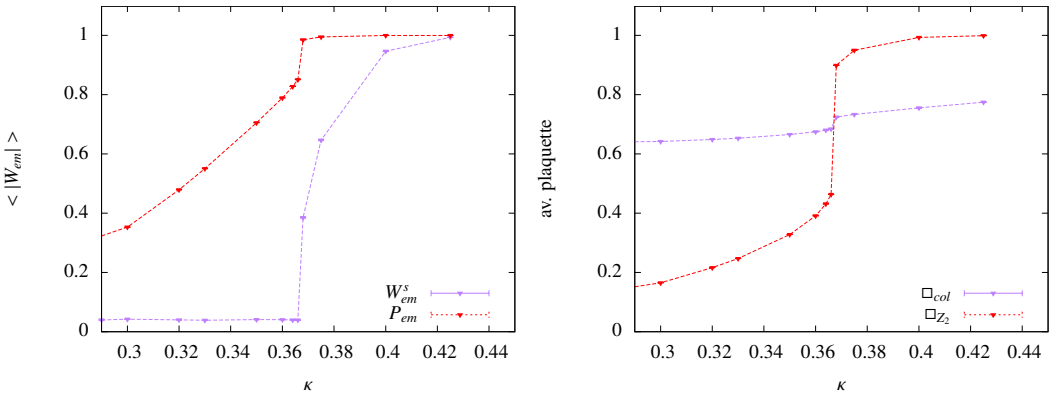

Figure 5.11: (left) Volume averaged spacelike Wilson line W^s_{em} and the usual timelike Polyakov loop P_{em} versus κ, and (right) average plaquettes constructed from SU(2) and $Z_2 \subset$ U(1) links, here for $\beta_{col} = 2.4$ on a 4×24^2 lattice. Temporal center symmetry has already been broken for all κ at this value of β_{col}, but there remains a strong first order transition bulk transition with κ that breaks spatial center symmetry and totally removes $Z_2 \subset$ U(1) disorder.

to alter the notation of the action in our $\beta_{em} \to \infty$, SU(2)$\times Z_2$ effective model to the suggestive form,

$$S_{eff} = -\sum_{\text{plaq.}} \left(\frac{\beta_{col}}{2} \text{ tr } \square_{col} + \frac{\beta_v}{2} \square_{Z_2} \text{tr } \square_{col} \right) - H \sum_{\vec{x}} P_{Z_2} \cdot \; P_{col} \; , \tag{5.38}$$

where we have absorbed the coefficients from Eq. (5.36) into couplings $(\beta_{col}, \beta_v, H)$ and relabeled the plaquette $\square_{Z_2}$ and Polyakov loop P_{Z_2} for the $Z_2 \subset$ U(1) links. The symbol β_v has been chosen for the plaquette-plaquette term because this is precisely the Villain action for pure SO(3) gauge theory [161]. The effective action (5.38) is, in fact, a mixed fundamental-adjoint SU(2) action. Furthermore, since $\square_{Z_2}$ is constructed from $Z_2 \subset$ U(1) link variables, it is an exact 2-form. A Bianchi identity then ensures that the flux piercing $\square_{Z_2} = -1$ plaquettes is conserved. That is, $Z_2 \subset$ U(1) interfaces may not terminate, which means that dynamic Z_2 monopoles are forbidden.

Note also that the couplings $\beta_{col} \leftrightarrow \beta_v$ are interchanged under a change of variables that multiplies every SU(2) link by its $Z_2 \subset$ U(1) counterpart,

$$U_\mu(x) \in \text{SU}(2) \to Z_\mu(x) U_\mu(x), \text{ where } Z_\mu(x) \in Z_2. \tag{5.39}$$

This removes the Z_2 dependence of the Polyakov loop term in (5.38),

$$P_{Z_2} \cdot \; P_{col} \to P_{col}. \tag{5.40}$$

In the absence of this term, which comes from the compact temporal direction, the action (5.38), is symmetric in (β_{col}, β_v).

It turns out that the (β_{col}, β_v) phase diagram of the symmetric action (5.38) with $H = 0$ and monopole suppression has been mapped out at finite temperature, $N_t = 4$, by Datta and Gavai in Ref. [161]. We present their result in Fig. 5.12. They too observed that that the deconfinement transition becomes first order for large adjoint coupling, $\beta_v = 16\kappa^4$. Moreover, the symmetry in $\beta_{col} \leftrightarrow \beta_v$ means that a line of first order transitions in β_v must end with the $3+1$ d bulk transition of

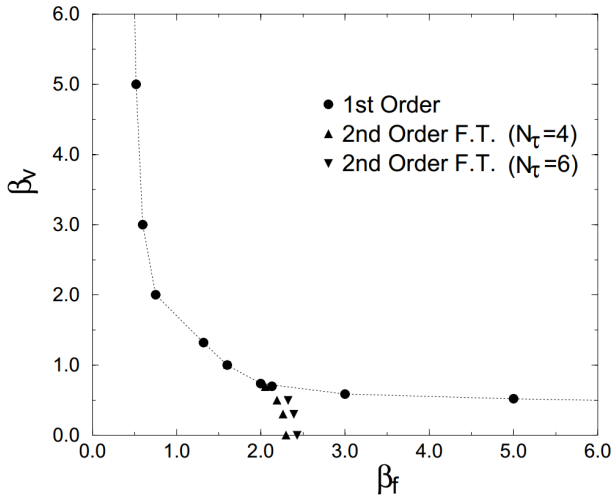

Figure 5.12: Phase structure for a mixed fundamental-adjoint SU(2) action with monopole suppression obtained in Ref. [161], corresponding to Eq. 5.38 with $H = 0$.

Z_2 gauge theory in the limit $\beta_{col} \to \infty$, just as for the β_{col} transition in the limit $\beta_v \to \infty$. In the intermediate region of the (β_{col}, β_v) plane, the SU(2) plaquette, tr $\square_{col}$, sets the effective coupling for the Z_2 degrees of freedom together with β_v and determines the position of the first order transition. This was found to run uninterrupted and separate the (β_{col}, β_v) plane in two. The deconfining transition with the SU(2) gauge coupling β_{col} was found to remain second order with $2d$ Ising exponents as β_v increased from zero, until joining the first order line of bulk transitions [161]. It was furthermore verified that the second order deconfinement transition shifts with β_{col} when the number of time slices increases to $N_t = 6$, unlike the first order bulk transition.

Our $\mathcal{O}(\kappa^4)$ hopping expansion effective model in the limit $\beta_{em} \to \infty$ differs from the mixed action model in Ref. [161] by the additional term for the quark Polyakov loop. When (temporal) center symmetry is spontaneously broken by the ordering of the SU(2) Polyakov loop at the β_{col} transition, this term has the effect of an external magnetic field for the Polyakov loop constructed from $Z_2 \subset \mathrm{U}(1)$ links and forces it to acquire a non-zero expectation value. However, spacelike center symmetry, corresponding to the equivalent of global center transformations for spacelike Wilson lines, remains free to break at a first order bulk transition when κ is increased. The result is a fully ordered 'Higgs' state without a string tension for timelike *or* spacelike Wilson loops. This ordering of $Z_2 \subset \mathrm{U}(1)$ links is clearly indicated for $\beta_{col} = 2.4$ in Fig. 5.11.

Assimilating our results with those of Ref. [161], we arrive at the phase structure sketched in Fig. 5.13. The β_{col} transitions from Fig. 5.9 are indicated on the plot, as well as additional first order points for which we have observed clear discontinuities in spacelike Wilson lines, as in Fig. 5.11. The diagram contains three regions. The first is an unbroken center symmetric phase at small (β_{col}, κ) with both spacelike and timelike disorder. It is separated from the ordered phase for Polyakov loops by a line of continuous β_{col} transitions for small κ that break temporal center symmetry and join with the second order transition of pure SU(2)

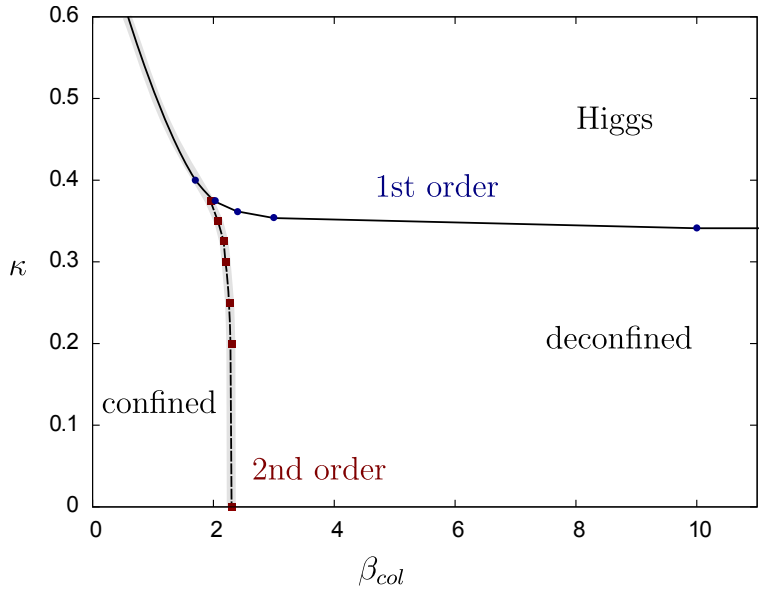

Figure 5.13: Phase diagram of our $\mathcal{O}(\kappa^4)$ effective action for $N_f = 2$ fractionally charged Wilson quarks, for $N_t = 4$. The center symmetry breaking β_{col} transition meets a first order bulk transition that separates the the phases in the low κ region from a totally ordered 'Higgs' phase. The gray band highlights where (temporal) center symmetry is broken. 'Confined' and 'deconfined' refer to the analogous color disordered and ordered phases of the pure gauge theory.

gauge theory at $\kappa = 0$. Finally, a first order bulk line separates these two phases from a totally ordered phase that meets the line of continuous transitions in the vicinity of $\kappa = 0.375$.

5.3.5 *Tuning the Z_2 disorder*

As one follows the line of β_{col} disorder-order transitions with increasing hopping parameter κ, quarks become lighter and the $\mathcal{O}(\kappa^4)$ loops more effectively suppress $Z_2 \subset \mathrm{U}(1)$ disorder that is not correlated with SU(2) color disorder. The breaking of center symmetry at the transition is then more evenly reflected in the order parameters for the corresponding Polyakov loops. This necessitates parameters very close to the bulk transition, however, as is indicated by the $\kappa = 0.375$ curve in Fig. 5.9.

We can suppress the disorder directly by adding a $Z_2 \subset \mathrm{U}(1)_{em}$ plaquette term to the action,

$$-\beta_{Z_2} \sum_{\text{plaq.}} \cos \alpha_{\mu\nu} \simeq -\beta_{Z_2} \sum_{\text{plaq.}} \square_{Z_2}. \tag{5.41}$$

The coupling β_{Z_2} may be thought of as the scale for $Z_2 \subset \mathrm{U}(1)$ disorder handed down from whatever unifying theory explains the origin of the gauge groups. The burden of suppressing Z_2 disorder is then lifted from the $\mathcal{O}(\kappa^4)$ quark loops.

In Fig. 5.14 we plot the SU(2) and $Z_2 \subset \mathrm{U}(1)$ Polyakov loops in the vicinity of the β_{col} transition for $\kappa = 0.15$. With the addition of the β_{Z_2} plaquette coupling, we observe a rapid transition to an ordered $Z_2 \subset \mathrm{U}(1)$ phase at a critical β_{Z_2}, which is somewhat less than $\beta_{Z_2} \sim 0.44$ for Z_2 gauge theory as the ordering effect of

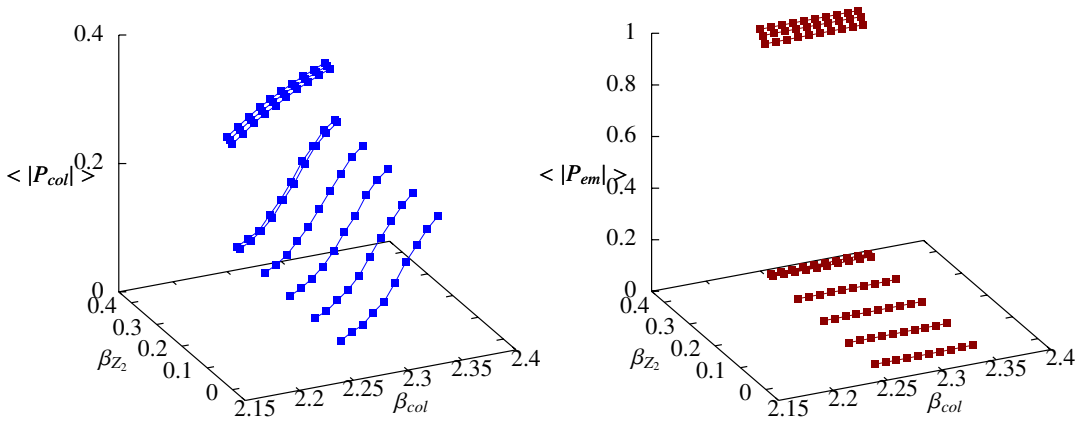

Figure 5.14: (left) Volume averaged SU(2) Polyakov loop across the β_{col} transition on 4×12^3 lattices with $\kappa = 0.15$ and a suppressing coupling β_{Z_2} for the the $Z_2 \subset \mathrm{U}(1)$ disorder. The usual $\mathcal{O}(\kappa^4)$ SU(2) behavior with explicitly broken center symmetry is recovered at the Z_2 bulk transition. A spontaneous symmetry breaking transition with β_{col}, with a balanced contribution of $\mathrm{SU}(2)$ and Z_2 disorder in the parallel transporters for quarks, would require fine tuning in the vicinity of the abrupt bulk transition. This transition is most apparent in the U(1) Polyakov loop P_{em} (right).

$\mathcal{O}(\kappa^4)$ quark loops is also present. That is, the Z_2 disorder is suddenly removed and we obtain a standard $\mathcal{O}(\kappa^4)$ unquenched result for the SU(2) Polyakov loop with broken center symmetry, and a crossover in β_{col}. Because Z_2 gauge theory has such a strong first order bulk transition, fine tuning within a small window would be required to retain a spontaneous center symmetry breaking transition with β_{col} and yet balance the topological SU(2) and $Z_2 \subset \mathrm{U}(1)$ contributions to the confining potential.

5.4 FUNDAMENTAL HIGGS WITH FRACTIONAL ELECTRIC CHARGE

In collaboration with J. Greensite and K. Langfeld, we have also studied fundamental SU(2)-Higgs models with fractional electric charge with respect to a compact U(1) gauge group.

SU(2) gauge theory with a scalar matter field in the fundamental representation, $\phi = (\phi_1, \phi_2) \in \mathbb{C}^2$, is a typical example of a theory with explicitly broken center symmetry. The lattice action takes the form,

$$S = -\sum_{\text{plaq.}} \frac{\beta_{col}}{2} \operatorname{tr} \Box_{col} - \frac{\kappa}{2} \sum_{\mu,x} (\phi^\dagger(x) U_\mu(x) \phi(x+\hat{\mu}) + \text{c.c.}) \tag{5.42}$$

$$- \sum_x (\frac{1}{2} \phi^\dagger(x)\phi(x) + \lambda([\phi^\dagger(x)\phi(x)]^2), \tag{5.43}$$

where we have reused the symbol κ to denote the coupling of matter to the gauge fields.

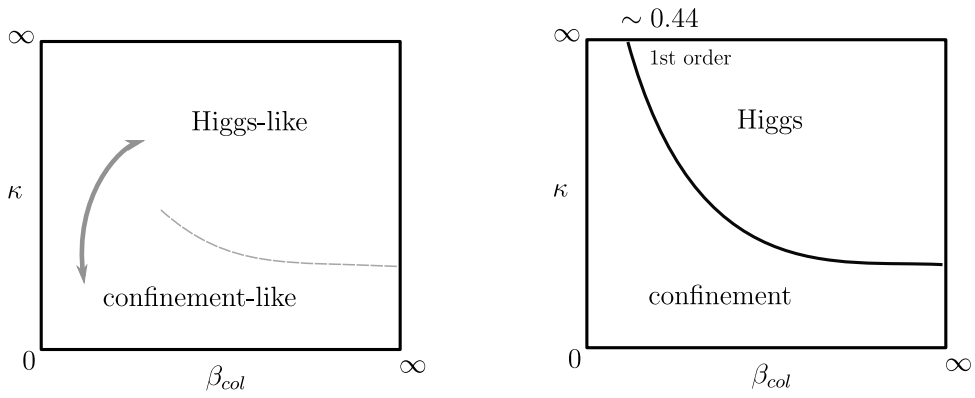

Figure 5.15: (left) The confinement-like and Higgs-like phases are analytically connected in a SU(2) gauge theory with a Higgs field in the fundamental representation.
(right) Coupling fractional electric charge with respect to a compact U(1) restores center symmetry and allows for a spontaneous symmetry breaking transition, which, however, is strongly first order [162].

It is convenient to freeze the length of the Higgs via the unimodular limit $\lambda \to \infty$, $\phi^\dagger \phi \to 1$, dispensing with the Higgs potential. The complex doublet can then be expressed as an SU(2) matrix,

$$\Phi = \begin{pmatrix} \phi_1 & -\phi_2^* \\ \phi_2 & \phi_1^* \end{pmatrix}, \tag{5.44}$$

such that the gauge-Higgs coupling simplifies to,

$$-\frac{\kappa}{2}\sum_{\mu,x}\frac{1}{2}\mathrm{tr}\,(\Phi^\dagger(x)U_\mu(x)\Phi(x+\hat{\mu})). \tag{5.45}$$

The ensuing theory is referred to as the Fradkin-Shenker model. At zero temperature its (β_{col}, κ) phase diagram contains a confinement-like region for small κ. Here the potential between fundamental charges rises linearly at intermediate distances, but flattens asymptotically due to dynamical color charge screening just as in standard QCD with fundamental quarks.

For large κ, on the other hand, the potential is Yukawa-like. There is no electric flux tube formation. Instead, color charges are screened by short range gauge interactions. In both regions the asymptotic states are colorless, but the mechanisms that explain this are superficially different.

The important point is that these regions are not separated by the spontaneous breaking of a global gauge symmetry. The Fradkin-Shenker theorem ensures the existence of a path in parameter space between the confinement-like and Higgs-like regions in which all local observables are analytic [163, 164]. So there is no thermodynamic phase boundary, and the the 'flux-tube' and 'Yukawa-screening' pictures must transform smoothly into one another.

We set out to circumvent the Fradkin-Shenker theorem by coupling the scalar Higgs with fractional electric charge to a compact U(1), thereby resurrecting center symmetry as in our Wilson quark model. We considered the SU(2) × U(1) model,

$$\begin{aligned} S = &- \sum_{\text{plaq.}} \left(\frac{\beta_{col}}{2} \text{ tr } \square_{col} + \beta_{em} \cos 2\alpha_{\mu\nu} \right) \\ &- \kappa \sum_{\mu,x} (\phi^\dagger(x) U_\mu(x) e^{i\alpha_\mu(x)} \phi(x+\hat{\mu}) + \text{c.c.}) \end{aligned} , \tag{5.46}$$

where the fractional charge is encoded in the same way as our toy quark model in Sec. 5.3.1. The U(1) gauge action is constructed from links with *twice* the angle used in the parallel transporters for the Higgs field, $e^{i\alpha_\mu(x)} \in \text{U}(1)$.

The explicit global symmetry from the combined center subgroup,

$$Z_2 = \{(1,1),(-1,-1)\} \subset \text{SU}(2) \times \text{U}(1), \tag{5.47}$$

once again allows for a well defined separation of phases via spontaneous symmetry breaking.

In the combined limit $\beta_{em} \to \infty$, $\kappa \to \infty$, the gauge-Higgs coupling forces the SU(2) and U(1) links to take values from the values in (5.47), just as in the $\mathcal{O}(\kappa^4)$ hopping expansion model in Section 5.3.4. This is most obvious in unitary gauge, in which the unimodular Higgs field is rotated to the identity matrix, $\Phi = \text{diag}\,(1,1)$. Subsequently, the model also reduces to Z_2 gauge theory in this limit, with a first order bulk transition at $\beta_{col} \sim 0.44$. As in the $\mathcal{O}(\kappa^4)$ hopping expansion model, preliminary investigations indicated that this first order line extends between the (β_{col}, κ) axes and forms a true phase boundary between the confined and Higgs phases [162], characterized by the spontaneous breakdown of the combined SU(2) × U(1) center symmetry. A sketch of the phase diagram obtained by unpublished simulations by Greensite and Langfeld is shown in Fig. 5.15.

The scale is once again dominated, however, by the $Z_2 \subset \text{U}(1)$ degrees of freedom that are only suppressed by fluctuations of the scalar matter field. As for the hopping expansion model, a plaquette term (5.41) with coupling β_{Z_2} was added to the action to directly suppress $Z_2 \subset \text{U}(1)$. To see whether a continuum limit might then be possible, a second order phase transition was searched for in $(\beta_{col}, \beta_{Z_2}, \kappa)$ parameter space, including negative couplings β_{Z_2}. The divergence of the correlation length at a second order point is needed to take the lattice spacing to zero while holding mass ratios fixed. No second order points were found, however [162].

5.5 DISCUSSION

Let us summarize our motivation, and what we have learned from toy lattice models.

When a simple product of the color and electroweak gauge groups is formed, there is a global Z_6 center symmetry generated by the element,

$$(e^{i2\pi/3}, -1, e^{i\pi Y}) \in \mathrm{SU}(3) \times \mathrm{SU}(2) \times \mathrm{U}(1)_Y, \tag{5.48}$$

which is a consequence of the quarks' fractional electric charges with respect to the electron. The symmetry relates color and electromagnetic phases,

$$(e^{i2\pi/3}, e^{i2\pi Q/e}) \in \mathrm{SU}(3) \times \mathrm{U}(1)_{em}. \tag{5.49}$$

As a result, a true phase transition corresponding to the breakdown of this global symmetry is possible in the presence of dynamical quarks, driven by topological disorder that combines SU(3) center vortices with an additional U(1) vortex.

The results

We set out to observe such a symmetry breaking transition in a lattice model with 2-color quarks that carry also fractional electric charge with respect to a compact U(1) gauge group. And, indeed, that is what we found. The explicit symmetry breaking effect of dynamical quarks in ordinary 2-color QCD was undone by their coupling to an additional source of $Z_2 \subset$U(1) topological disorder. We saw a clear disorder-order transition using the SU(2) Polyakov loop as an order parameter. There was, however, a large shift in the meson masses calculated with these fractionally charged quarks, owing to a large topological contribution from $Z_2 \subset$U(1) disorder, which added to the confining potential from the color sector.

A separation of scales was inevitable, because the extra $Z_2 \subset$U(1) structure was introduced without reference to its origin in some unifying UV completion. Although dynamical quark loops coupled this U(1) degree of freedom back to the SU(2) color sector, their bare mass had to be tuned via the hopping parameter to make the effect significant.

Turning to an $\mathcal{O}(\kappa^4)$ effective hopping expansion model, the fine tuning required to balance gauge disorder between the $Z_2 \subset$U(1) and SU(2) degrees of freedom, and hence their relative contribution to mass scales, became more clear. Here we found that the disorder-order transition strengthened with κ and merged with a very stout first order bulk transition stemming from that of $3+1$ d Z_2 gauge theory.

The theme was similar for the SU(2)×U(1) fundamental gauge-Higgs model mentioned in Sec. 5.4. The Fradkin-Shenker theorem may be circumvented by the existence of a global center symmetry, but at the expense of strong first order deconfining transitions. One can expect the same behavior in analogous $\mathrm{SU}(3) \times \mathrm{U}(1)$ formulations, since Z_3 gauge theory in $3+1$ d also has a bulk first order transition [165].

Note that these lattice models are not expected to possess continuum limits. This may be disconcerting, but familiarity with SU(N) gauge theories is partly to blame for such a feeling. SU(N) gauge theories are unreasonably well-behaved. Their continuum limits are protected by asymptotic freedom, even though we may not expect

a non-abelian gauge theory such as QCD to describe Nature at all energy scales. The electroweak sector is less fortunate in this regard. It is likely that UV triviality prevents the construction of a continuum limit from a QED lattice construction [166, 167], and the implementation of chiral theories on the lattice is an ongoing problem. This does not mean that we should discard half of the Standard Model, however. Since we expect new physics to provide a UV cutoff, we may always regard lattice models as effective theories valid below this scale.

The message for Standard Model physics and beyond

The Z_6 center symmetry in the Standard Model matter representations opens the door for a spontaneous symmetry breaking transition. But, if this is relevant to phenomenology at the $\mathcal{O}(200)$ MeV QCD confinement scale, we are met with a tuning problem. In our proposal, unbroken global gauge symmetry relies on additional topological disorder corresponding to interfaces between perturbative $\mathrm{U}(1)_{em}$ sectors, which adds to the confining potential for quarks and must be balanced against the SU(3) degrees of freedom.

Where could such structure come from? This is not addressed in our lattice models, which do not define the gauge fields or the UV physics between lattice sites.

If the gauge forces are unified by some GUT based on the Higgs mechanism, similar to $\mathrm{SU}(5)$ GUT, then topological disorder may be identified as defects of the GUT. Between the sites of a low energy lattice theory, one imagines that the GUT Higgs field that defines a residual Standard Model gauge symmetry has rotated (Fig. 5.16). But, as we mentioned, such a fluctuation costs an enormous amount of energy if the unification scale is as high as $\mathcal{O}(10^{16})$ GeV. Disorder should be suppressed, such that the fields in the low energy theory belong to the same topological GUT sector.[10]

Such a decoupling argument suggests that the Z_6 symmetry of the Standard Model should be broken at much higher energies than the deconfinement and electroweak transitions. In terms of our toy models, it suggests that the suppressing coupling for the topological $\mathrm{U}(1)$ disorder should be taken beyond an ordering transition, where we can expect the usual corrections to color dynamics from a perturbative U(1) sector.

If this viewpoint is correct, then Nature does not make use of the symmetry between the quarks' SU(3) color charge and their electric charges at the modest energy scales of hadron physics. It is a remnant of higher energy physics.

We need not wholeheartedly embrace this pessimistic attitude, however. For one thing, subtleties are sometimes missed by decoupling arguments. An example is low energy fermion-monopole scattering, for which the outcome is strongly dependent on the structure of the monopole core but largely independent of its size [132]. Moreover, new physics can impact length scales much lower than the GUT scale via vacuum polarization effects. For instance, the 'true' core of a magnetic defect is sur-

10 This is also clear if we start from a lattice version of a unified SU(N) theory and identity the low energy degrees of freedom when we send the GUT scale to infinity. The top down perspective is outlined in Appendix C.

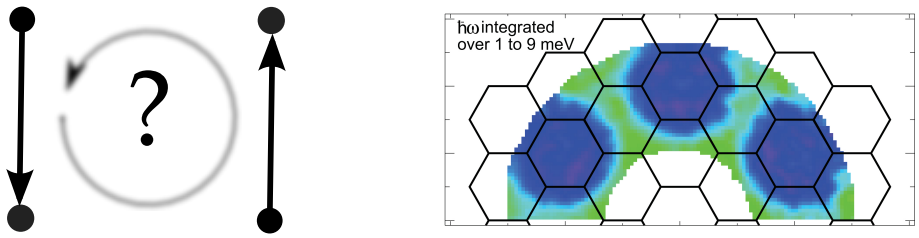

Figure 5.16: (left) New physics lies between lattice sites where the usual color and electroweak gauge fields are not defined. (right) Neutron scattering from a Herbertsmithite crystal. Disordered magnetic materials show uniform color. The data suggests 'order within disorder', which may herald the first realization of a spin liquid [173]. There are many inspirations for topological disorder in Nature.

rounded by an electroweak cloud whose extension is set by the electoweak scale.[11] And vacuum polarization sets the electric charge radius of the dyonic excitations of a monopole to the Compton wavelength of the electron [132].

These considerations are separate from general criticisms of GUTs, and the incredible hubris of assuming that we have already determined physics across a $\mathcal{O}(10^3)$ GeV to $\mathcal{O}(10^{16})$ GeV desert.

Note that the typical lattice spacing in modern QCD calculations is about 0.1 fm$\simeq$ 2 GeV, which is not so widely separated from a hypothetical scale of new physics in the TeV region. In that case, non-trivial topology that relates the color and electroweak gauge groups may still to made to play role in the non-perturbative physics of confinement and mass generation. Without experimental guidance, however, we have little idea of which theoretical road leads beyond the Standard Model.

So far, the take home message from the LHC is that we should reconsider our devotion to naturalness as a guiding principle. Nature may not be flustered about fine-tuning the quantum corrections to the electroweak Higgs mass, for example, if the absence of a signal for supersymmetry is any indication [171]. Meanwhile, string theory is stricken by a landscape of vacua and a loss of predictivity [172]. And we should not forget QCD's strong CP problem, and the puzzles of the tiny cosmological constant and neutrino masses. Large separations of scale and hierachies are a recurrent theme in modern physics.

Perhaps there is a lesson to be learned from condensed matter physics, where the emphasis is on *novelty*, rather than theoretical simplicity and tractability. Fine-tuning is often essential in the experimental setup of the most interesting condensed matter systems. Careful preparation rewards experimentalists with states of matter that have remarkable, unintuitive properties (cf. Fig. 5.16, right). We should be mindful of dismissing coincidences, such as the confinement of color and fractional electric charge, without an exhaustive understanding of their possible implications, even when these involve fine-tuning or hierachies.

11 We have neglected the weak interactions in this work. For more on the hidden Z_6 symmetry in the context of electroweak physics, see Refs. [168, 169, 170].

6

CONCLUDING REMARKS

As this thesis draws to an end, we are confronted with the elusive nature of strong interactions. In spite of the great experimental successes of the Standard Model, a complete theoretical understanding follows only in baby steps. In particular, the non-linear, complex nature of the QCD sector hinders its analytical study. We have searched for an intuitive grasp of the underlying mechanisms, and their connections with symmetries that emerge under various deformations of the theory.

We have been motivated in particular by the global center symmetry of SU(N) gauge theories in the limit of infinitely heavy, i.e., static quarks. It allows deconfinement at finite temperature to be classified as a spontaneous symmetry transition in close analogy with magnetization in an N-state spin system. As we reviewed in Chapter 3, global center symmetry allows one to prepare superselection sectors for the color electric flux of static charges via a combination of boundary conditions with center vortex interfaces. This places topology at the heart of color confinement in the pure gauge theory, which results at low temperature from the disorder generated by vortices and is lost when these interfaces are suppressed at high temperature.

We performed a further deformation, a reduction of spacetime dimensions to $2+1$ d, to fully exploit the correspondence with spin systems and glean insight into the universal aspects of the confinement mechanism. This provided us full access to the powerful tools of universality. The second order transitions of SU(2) and SU(3) in $2+1$ d fall into the universality classes of the $2d$ Ising and 3-state Potts models, respectively, in which a wealth of exact analytical results are available. By making use of the universality of interfaces in the gauge and spin systems, we were able to locate the deconfinement transition on the lattice with extreme precision. Our subsequent scaling studies unveiled a self-dual relationship between center vortices and color electric fluxes at criticality, stemming from Kramers-Wannier self-duality of the $2d$ N-state Potts models, and led us to precisely determine the continuum vortex and electric SU(2) string tensions at criticality.

The manifestation of self-duality on finite volumes via 't Hooft's Fourier transform over center sectors emphasizes the relevance of global center symmetry to deconfinement, at least for static charges. A self-dual relation between center vortices and electric fluxes in $2+1$ d is only possible because the center vortex confinement mechanism pinpoints the pertinent degrees of freedom. As our analysis of SU(4) revealed, still more may be learnt from these $2+1$ d models. The effective spin system and order of the deconfining transition is, in this case, not trivially determined. A better understanding of the interplay of the larger set of Z_4 center sectors, via a combination of analytic and numerical methods, would shed further light on confining gluonic dynamics.

This is a lesson for $3+1$ d, where the dynamics are similar but universality is not applicable for $N \geq 3$ colors. Our results highlight the benefits of studying simpler

QCD-like theories that allow one to catch a glimpse of the essential character of strong interactions.

At the same time, we are reminded that the symmetries treasured by theorists are, all too often, only approximate. The explicit breaking of center symmetry by dynamical quarks prevents a tidy classification of QCD states into superselection sectors, and we must reconcile ourselves with the possibility that the confined and deconfined phases are analytically connected, with a mass gap that varies smoothly across the transition. How can we arrive at the true meaning of 'confinement', when we are unable pinpoint a difference between the physical asymptotic states on either side of the transition?

In the proceeding chapter, we looked beyond QCD for possibilities. The fact that quarks are both confined and have fractional electric charge hints at a deeper underlying connection. We have, after all, never isolated a quark or any other fractionally charged particle.

We saw that this is related to a global center symmetry of the Standard Model matter representations. A possible topological link emerges in the form of defects that carry flux with respect to both the quarks' color and electroweak quantum numbers. This prompted a proposal that the percolation of these objects might explain why quarks with fractional electric charge are confined, but not colorless integer charged particles. The suppression of combined topological disorder at a spontaneous symmetry breaking transition could then provide a thermodynamic distinction between 'confined' and 'deconfined' phases.

This spurred our interest in grand unified theories, not as realistic physical theories, but as an important historical framework for exploring the origin and topology of the Standard Model gauge groups. The search for a better understanding of these connections was an underlying motivation for the side project in Chapter 4, in which we studied monopole inducing boundary conditions for grand unified theories on the lattice.

In our lattice studies of 2-color models in Chapter 5, we set aside the unknown origin of the gauge groups and simply studied the consequences of a hidden global symmetry in the presence of quarks that carry fractional electric charge with respect to a compact U(1). We found, however, that if topology related to fractional electric charge plays a role in confinement, its scale from beyond Standard Model physics must be addressed. Confinement remains a *hard* problem.

A

TWIST AWAY FROM CRITICALITY

A.0.1 *Magnetic twist and spatial string screening*

Twist in purely spatial planes inserts timelike center flux perpendicular to the twisted planes. In $3+1$ d, this is the center flux of a propagating pair of static center monopoles in adjacent volumes. In $2+1$ d spatial twist introduces one extra pointlike magnetic defect whose worldline is closed by the temporal extent of the lattice. An increase in temperature shortens this worldline but does not prevent the magnetic flux from lowering its free energy by spreading in the plane of the twist. These magnetic defects may condense at all temperatures and do not play a role in the deconfinement transition.

They do, however, have importance for the spatial Wilson loop. Just as spacelike center vortices disorder temporal Wilson loops, the world lines of magnetic defects disorder spatial Wilson loops. In [47], 't Hooft discussed the behavior of electric and magnetic fluxes in the confined phase for $3+1$ dimensions. Using Euclidean rotation symmetry and the assumption that electric and magnetic flux free energies should factorize at low temperature, he showed that the free energy of an additional magnetic flux should vanish like $\exp(-\sigma L^2)$, where σ is the zero temperature electric string tension and L^2 is the area perpendicular to the magnetic flux. Since the area law for the spatial Wilson loop persists in the deconfined phase, one expects a similar behavior but with σ replaced by the spatial string tension $\sigma_s(T)$.

We can check this numerically. Letting $Z_m(L,T)$ denote the partition function with magnetic twist for SU(2) in $2+1$ d, the free energy of one extra magnetic defect is defined in the same way as for spacelike center vortices,

$$Z_m(L,T)/Z_0(L,T) = e^{-F_m(L,T)}, \tag{A.1}$$

where $Z_0(L,T)$ is the untwisted partition function. We then expect the screening

$$F_m(L,T) \propto e^{-\sigma_s(T)L^2}, \tag{A.2}$$

where σ_s is the spatial string tension. In order to test this prediction we've calculated the magnetic flux free energy at $\beta = 9$ for various spatial sizes $L = aN_s$ and varied the temperature by varying the number of time slices N_t between 2 and 8. The parameters were chosen for easy comparison with the values for the spatial string tension in [174]. F_m is screened rapidly with the lattice size L, which restricts us to rather small spatial extents N_s. Nevertheless, we obtain excellent agreement with the expectation (A.2) using the string tension and a constant of proportionality as fit parameters, even far from the thermodynamic limit $N_s \gg N_t$. See Fig. A.1 for an example.

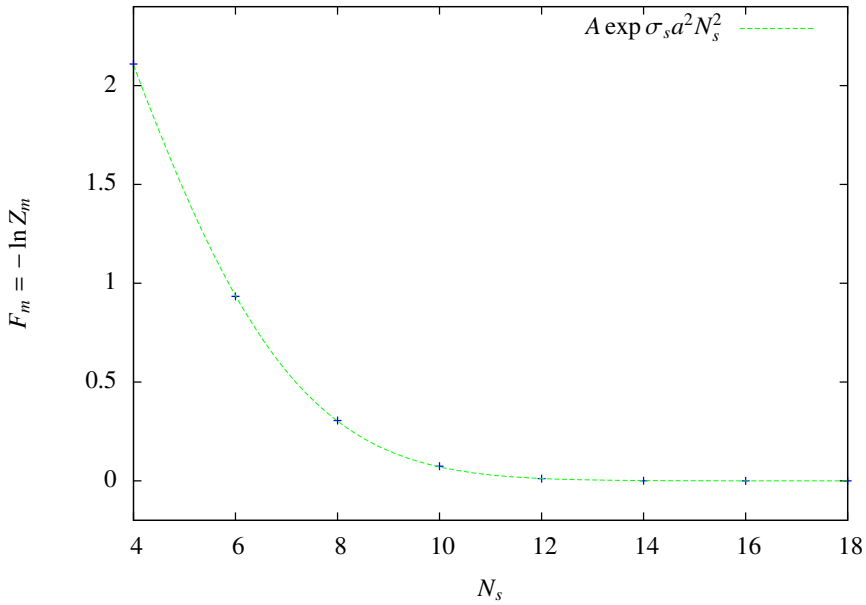

Figure A.1: Screening of magnetic center flux for $N_t = 4$ in the deconfined phase $\beta = 9 > \beta_c$. The spreading of center flux is impeded by the spatial extent of the lattice.

In Fig. A.2 we plot our extracted values for the spatial string tension versus temperature. This should be compared with Fig 2. of [174], where the spatial string tension was extracted from Wilson line correlators. Our results agree within a $5-10$ percent systematic difference. Note that the spatial string tension grows linearly with temperature in the deconfined phase, as is expected from dimensional reduction [175, 176]. As temperature increases a spacelike Wilson loop has less transverse volume for fluctuations, so it is more rigid. Our fit for the slope is,

$$\sigma_s(T) \approx 0.42(3) g_3^2 T, \; T > T_c, \tag{A.3}$$

which agrees well with the coefficient of 0.40 obtained in [174].

Our results can be compared to the predictions of a gas of thin vortices. If the magnetic defects are uncorrelated then the probability of n magnetic vortices piercing an area A is given by

$$P(n; A) \propto \frac{(\mu A)^n}{n!} \tag{A.4}$$

where μ is the probability of a vortex piercing a unit area. The difference between twisted and untwisted partition functions is that they enforce an odd or even number of defects respectively. The partition functions for our $L \times L$ lattices should then be given by

$$Z_m(L,T) = \sum_{n \text{ odd}} \frac{(\mu(T) L^2)^n}{n!} = \sinh(\mu L^2) \tag{A.5}$$

$$Z_0(L,T) = \sum_{n \text{ even}} \frac{(\mu(T) L^2)^n}{n!} = \cosh(\mu L^2). \tag{A.6}$$

The magnetic flux free energy is then predicted to behave like

$$F_m(L,T) = -\ln \tanh(\mu L^2) \tag{A.7}$$

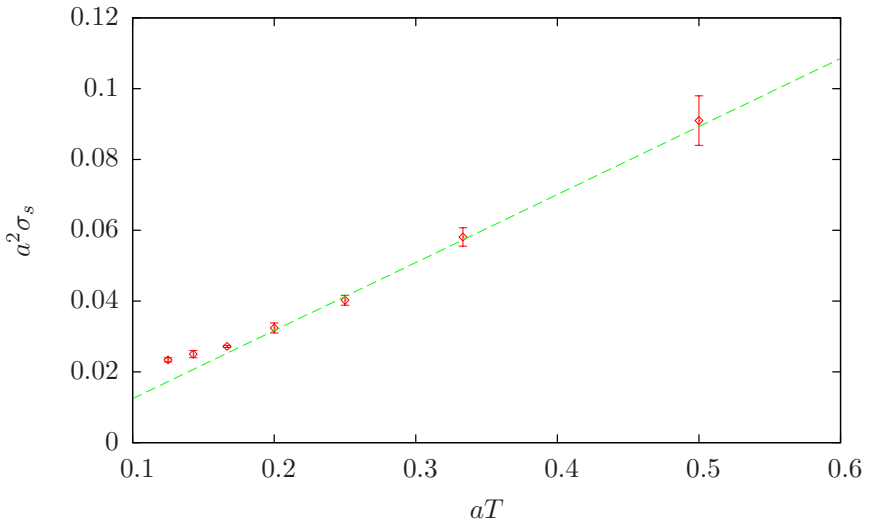

Figure A.2: Spatial string tension versus temperature, calculated from the screening of magnetic flux free energies $F_m \sim e^{-\sigma_s(T)L^2}$.

In a gas of thin vortices, the expectation value of a spatial Wilson loop with minimal area A is given by

$$\langle W \rangle = e^{-2\mu A}. \tag{A.8}$$

The probability μ is therefore related to the spatial string tension via $\sigma_s = 2\mu$. However, we find that Eq. (A.7) gives a very poor fit to the data, especially for small $L = aN_s$. This is in contrast to the results of Ref. [174], where the difference of the *action* ΔS between twisted and untwisted systems was calculated, rather than the free energy. In that case the thin vortex model provided a rather good description of the data. We also tried a modified version of a vortex gas in which the vortices have some fixed thickness but are otherwise uncorrelated. Their probability is then given by a binomial distribution. This did not offer much improvement. This suggests that the entropic contribution to the free energy from the nontrivial spreading, overlapping, and other interactions of magnetic center flux may not be neglected.

A.0.2 *Center vortex string formation at high temperature*

The confinement of spacelike center vortices via string formation just above T_c was inferred from universality with the $2d$ Ising model in Chapter 3. Away from criticality, the smoking gun signature for string formation on a symmetric volume, $F_k(1,1) = \sqrt{2}F_k(1,0)$, can be checked numerically for pairs of orthogonal center fluxes. These quantities are plotted in Fig. A.3 for selected $N_t = 4$ volumes in the high temperature phase. The free energy for center flux in both directions $F_k(1,1)$ is an excellent match to the prediction $\sqrt{2}F_k(1,0)$.

The dual string tension $\tilde{\sigma}(T)$ could be extracted by calculating $F_k(1,0)$ for successively larger volumes and performing a linear fit. However, de Forcrand, Lucini and Vettorazzo have provided a more elegant method [177]. Recall that the twisted

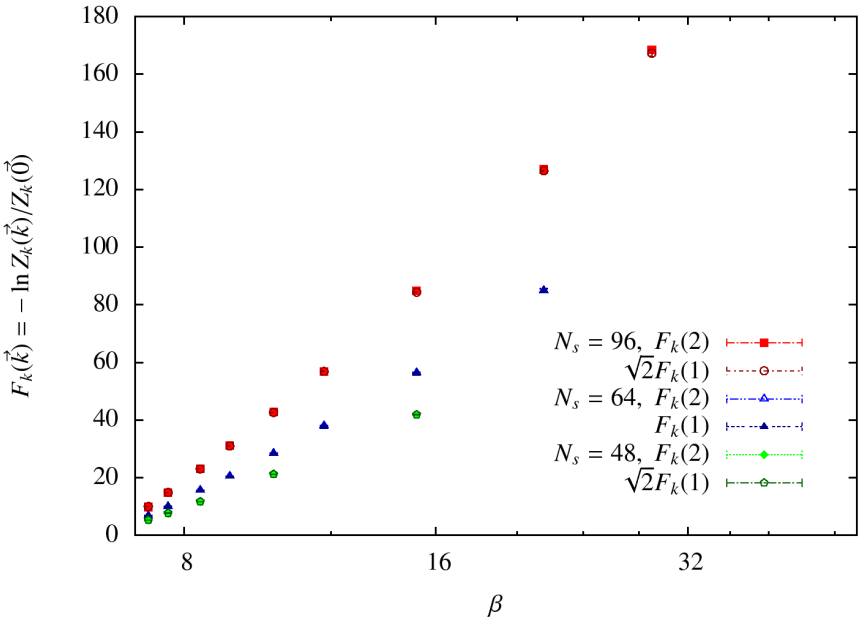

Figure A.3: Center vortex free energies for one and two units of flux.

partition function $Z_k(L,T)$ is calculated by successively flipping the coupling of a line of plaquettes and performing a simulation at each step of the ratio,

$$\frac{Z_k^{(n)}}{Z_k^{(n-1)}} = \langle \exp(\frac{\beta}{N}\mathrm{Re}(1-z^{(n)})\mathrm{tr}\,\square^{(n)})\rangle_{n-1}\ z^{(n)} \in Z_N, \tag{A.9}$$

where the *nth* flipped plaquette $\square^{(n)}$ acquires the phase $z^{(n)}$ and

$$Z_k^{(0)} = Z_k(\vec{0}),\ Z_k^{(0)} = Z_k(\vec{k}). \tag{A.10}$$

The intermediate partition functions $Z_k^{(n)}$ contain a vortex with fixed end points separated by $a \times n$. These intermediate ratios measure the cost of lengthening the vortex by one lattice spacing a. In the regime of string formation,

$$\frac{Z_k^{(n)}}{Z_k^{(n-1)}} = e^{-\tilde{\sigma}(T)a + \text{F.S. effects}}. \tag{A.11}$$

So, only one simulation is required to measure the dual string tension at a given temperature.

Finite size effects are reduced by making the partial vortex as large as possible, i.e., half of the spatial extent length $n \approx N_s/2$. If the center flux almost winds through the lattice, $n \approx N_s$, the system may reduce its free energy by trading the long partial vortex for a vortex closed by the lattice plus a smaller one of length $(N_s - n)$. The translational invariance of the closed vortex contributes entropy, which leads to the free energy reduction.

For small n, on the other hand, one expects a large initial cost associated with the creation of a short vortex with fixed end points. This should reduce with increasing length n into a broad plateau where (A.11) is a good approximation. The cost of

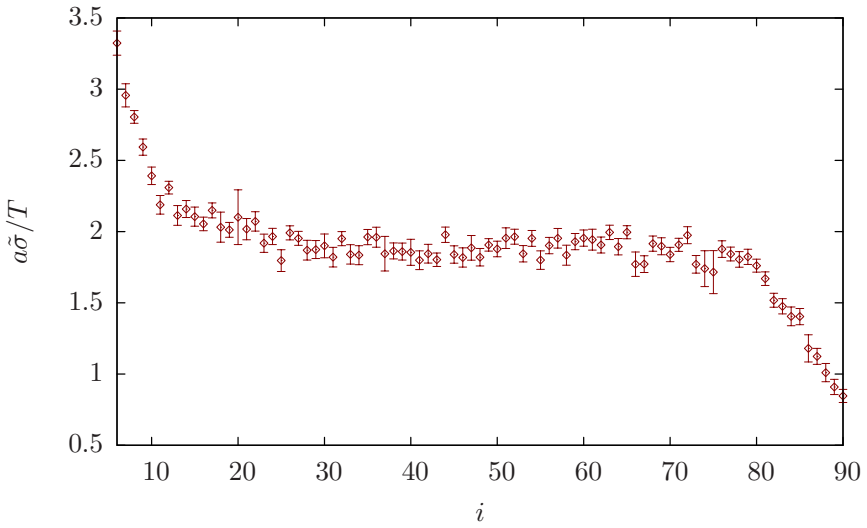

Figure A.4: Cost of flipping one additional plaquette on a 4×96^2 lattice for $\beta = 50$.

lengthening the vortex is then expected to decrease more rapidly for $n \approx N_s$, where the production of a closed vortex becomes viable. This prediction is borne out for SU(2) in $2+1$ d in Fig. A.4.

In the region of the plateau, the leading finite size corrections originate from Gaussian fluctuations of the vortex. These may be estimated by considering the vortex as the worldline of a Euclidean particle propagator [178]. The effective string tension is, then,

$$a\tilde{\sigma}_{eff}(T) = -\ln Z_k^{(n+1)}/Z_k^n = a\tilde{\sigma}(T) + \ln\left((n+1)/n\right). \tag{A.12}$$

The second term is the $1+1$ d string worldsheet analog of the Lüscher term. We extracted $a\tilde{\sigma}(T)$ after the removal of this correction for $N_t = 4$ and $N_s = 96$. The results are plotted against β in Fig. A.5.

The high temperature perturbative result for the dual string tension was determined in Ref. [179],

$$\tilde{\sigma} = \frac{\alpha}{g_3} T^{1.5}, \tag{A.13}$$

where the factor α is an N_t dependent coefficient. Since $aN_t = 1/T$, we have $a\tilde{\sigma} = \tilde{\sigma}/(N_t T)$. So our plot of $a\tilde{\sigma}$ versus T should go like $T^{0.5}$ for large T. Our results match this perturbative prediction quite well.

A.0.3 *Electric string formation at zero temperature*

We have also studied string formation for electric flux free energies at zero temperature for SU(2) in $2+1$ d.

As $L_t = aN_t \to \infty$, the free energy $F_e(\vec{e})$ becomes the zero temperature energy or mass $E(\vec{e})$ of a system with electric flux $\vec{e}$,

$$\lim_{L_t \to \infty} \frac{Z_e(\vec{e})}{Z_e(\vec{0})} \equiv e^{-L_t E(\vec{e}; L_i)}. \tag{A.14}$$

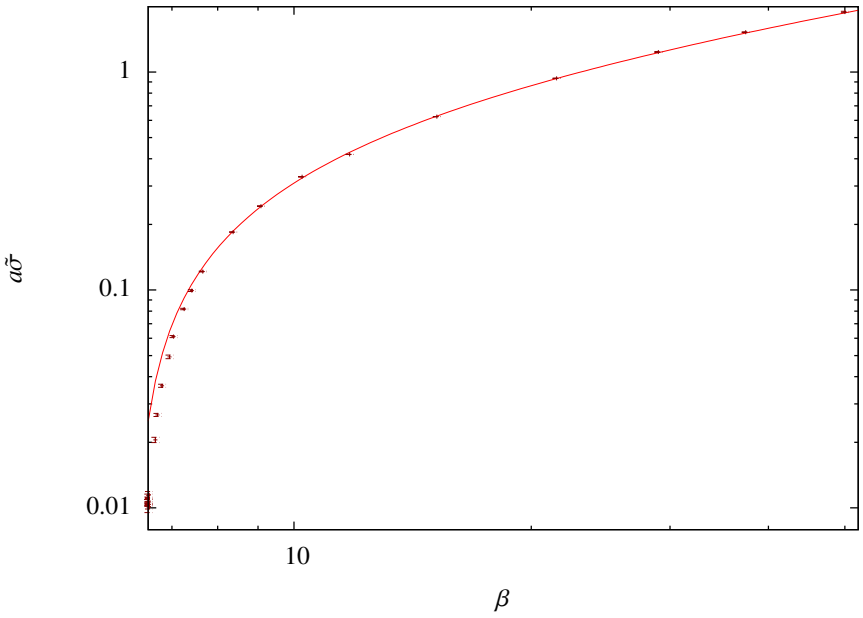

Figure A.5: Dual string tension versus $\beta \sim T$. The asymptotic slope tends toward the perturbative $T^{0.5}$ prediction.

We can convert our lattice data into physical units using the determination of the zero temperature string tension in Ref. [174],

$$a\sqrt{\sigma} = \frac{1}{\beta}(1.337 + \frac{0.945}{\beta} + \frac{1.10}{\beta^2}). \tag{A.15}$$

Results for two units of orthogonal flux $\vec{e} = (1,1)$, and one unit of flux $\vec{e} = (1,0)$, obtained on symmetric lattices for $\beta = 10,\ 12,\ 14$, are plotted in Fig. A.6. The results agree well with the smoking gun $\sqrt{2}$ signature for the formation of a diagonal string.

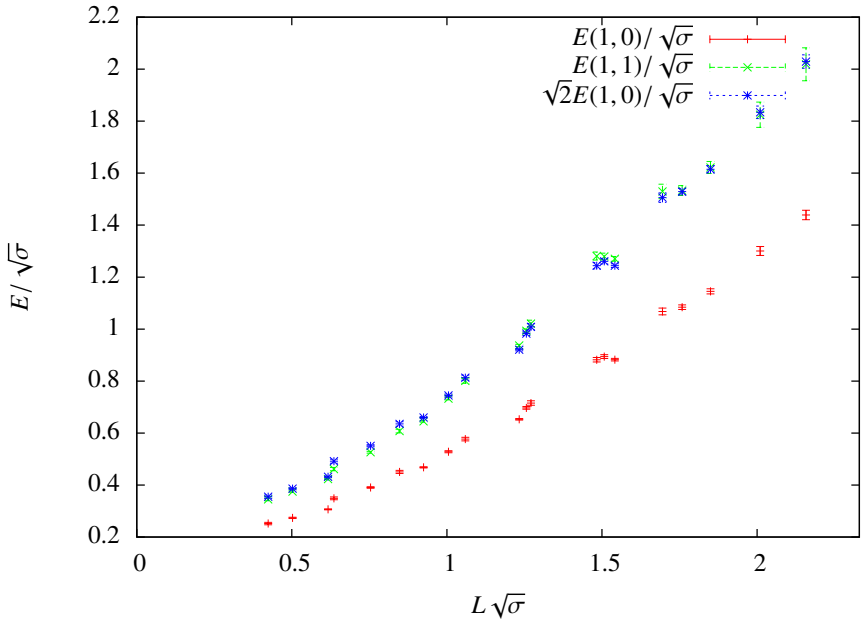

Figure A.6: Electric flux energies in units of the zero temperature string tension.

B

MORE ON C-PERIODIC BOUNDARY CONDITIONS

B.1 CLASSIFICATION OF C-PERIODIC TWISTS

For $N > 2$ not all combinations of C-periodic twists that are allowed by Eq. (B.3) are physically distinguishable. The complete classification of inequivalent C-periodic twists

$$\begin{aligned} \Omega_i^*(x)\Omega_j(x+L\hat{\imath}) &= z_{ij}\,\Omega_j^*(x)\Omega_i(x+L\hat{\jmath}), \\ z_{ij} &= e^{i\frac{2\pi}{N}\epsilon_{ijk}m_k}, \quad m_i \in Z_N \end{aligned} \tag{B.1}$$

was given in Ref. [89]. Here we summarize the main argument for completeness. First, one observes that transition functions which differ themselves only by a constant center element ζ are equivalent, i.e. Ω_i is equivalent to $\zeta_i\Omega_i$. This allows one to redefine the twists as

$$z'_{ij} = z_{ij}\zeta_i^2\zeta_j^{*2}. \tag{B.2}$$

The constraint

$$(m_1 + m_2 + m_3) \in \{0, N/2\} \in \{0, 1, \ldots, N-1\}. \tag{B.3}$$

is unaffected. One has

$$z'_{ij}z'_{jk}z'_{ki} = z_{ij}z_{jk}z_{ki} = \pm 1, \tag{B.4}$$

but we can use this freedom to restrict the inequivalent choices for two of the three twists z_{ij}. To be specific, let $\zeta_1 = 1$, so that

$$z'_{12} = z_{12}\zeta_2^{*2}, \text{ and } z'_{13} = z_{13}\zeta_3^{*2}\,. \tag{B.5}$$

If N is odd, every Nth root of unity has a square root in the set of Nth roots of unity and we can therefore choose ζ_2 and ζ_3 such that $z'_{12} = z'_{13} = 1$, or $m_2 = m_3 = 0$, without loss of generality. Then, from (B.3), which reads $m_1 + m_2 + m_3 = 0$ for odd N, we also have $m_1 = 0$ and there is thus no non-trivial C-periodic twist in this case.

If N is even, either z_{ij} or $z_{ij}\exp(2\pi i/N)$ have a square root in the set of Nth roots of unity. The same freedom from (B.5) allows one to restrict m_2 and m_3 to $m_2 \in \{0,1\}$ and $m_3 \in \{0,1\}$ (which is no restriction for $N = 2$). These four possibilities can always be completed with (B.3), by choosing m_1 such that the sum is either 0 or $N/2$. This means that for even N there are altogether $8 = 2^3$ distinct possibilities (in 3 dimensions) of having C-periodic twist,[1] 4 with $m_1 + m_2 + m_3 = 0$ and 4 with $m_1 + m_2 + m_3 = N/2$.

1 In the pure SU(2) gauge theory these are equivalent to the 2^3 choices for 't Hooft's original twisted b.c.'s. For $N = 4, 6, \ldots$, however, there are still only 8 C-periodic twists while the number of standard twists increases as N^3 in 3 dimensions.

B.2 MIXED C-PERIODIC BOUNDARY CONDITIONS

B.2.1 *x direction C-periodic, y, z directions periodic*

Suppose that we employ boundary conditions with a single C-periodic direction, chosen to be the x direction. These boundary conditions may be written as

$$\begin{aligned}
\Phi(x+L\hat{x}) &= \Omega_x^\dagger \Phi^*(x)\Omega_x, \qquad & U_\mu(x+L\hat{x}) &= \Omega_x^\dagger U_\mu^*(x)\Omega_x,\\
\Phi(x+L\hat{y}) &= \Omega_y^\dagger \Phi(x)\Omega_y, \qquad & U_\mu(x+L\hat{y}) &= \Omega_y^\dagger U_\mu(x)\Omega_y,\\
\Phi(x+L\hat{z}) &= \Omega_z^\dagger \Phi(x)\Omega_z, \qquad & U_\mu(x+L\hat{z}) &= \Omega_z^\dagger U_\mu(x)\Omega_z.
\end{aligned}$$

Again assuming constant transition funcitons, consistency of the boundary conditions now requires

$$\begin{aligned}
\Omega_x\Omega_y &= z_{12}\Omega_y^*\Omega_x,\\
\Omega_x\Omega_z &= z_{13}\Omega_z^*\Omega_x,\\
\Omega_y\Omega_z &= z_{23}\Omega_z\Omega_y,
\end{aligned} \tag{B.6}$$

where $z_{ij} = e^{in_{ij}}$, $n_{ij} = (2\pi/N)\,\epsilon_{ijk}m_k$ with $m_k \in Z_N$, are center elements as before. Note that charge conjugation only ever happens on one side of the equation.

The gauge transformations to diagonalise the Higgs field have the following genuine boundary conditions,

$$\begin{aligned}
R(x+L\hat{x}) &= \Omega_x^\dagger R^*(x),\\
R(x+L\hat{y}) &= \Omega_y^\dagger R(x),\\
R(x+L\hat{z}) &= \Omega_z^\dagger R(x),
\end{aligned} \tag{B.7}$$

and we define the following doubly translated R's at the far edges and corner by lexicographic order,

$$\begin{aligned}
R(L,L,r) &\equiv \Omega_y^\dagger\Omega_x^\dagger R^*(0,0,r),\\
R(L,r,L) &\equiv \Omega_z^\dagger\Omega_x^\dagger R^*(0,r,0),\\
R(r,L,L) &\equiv \Omega_z^\dagger\Omega_y^\dagger R(r,0,0),
\end{aligned} \tag{B.8}$$

for $r = 0,\dots L-1$, and

$$R(L,L,L) \equiv \Omega_z^\dagger\Omega_y^\dagger\Omega_x^\dagger R^*(0,0,0). \tag{B.9}$$

It is straightforward to derive the corresponding boundary conditions for the Abelian projected fields (4.31),

$$\begin{aligned}
\alpha_i^a(x+L\hat{x}) &= -\alpha_i^a(x),\\
\alpha_i^a(x+L\hat{y}) &= \alpha_i^a(x),\\
\alpha_i^a(x+L\hat{z}) &= \alpha_i^a(x),
\end{aligned} \tag{B.10}$$

with the following exceptions,

$$\begin{aligned}
\alpha_y^a(L,L-1,r) &= -\alpha_y^a(0,L-1,r) - \frac{2\pi}{N}\,m_3,\\
\alpha_z^a(L,r,L-1) &= -\alpha_z^a(0,r,L-1) + \frac{2\pi}{N}\,m_2,\\
\alpha_z^a(r,L,L-1) &= \alpha_z^a(r,0,L-1) - \frac{2\pi}{N}\,m_1,
\end{aligned} \tag{B.11}$$

$r = 0, \ldots L-1$, and

$$\begin{aligned} \alpha_y^a(L, L-1, L) &= -\alpha_y^a(0, L-1, 0) - \frac{2\pi}{N} m_3 \\ &= -\alpha_y^a(0, L-1, L) - \frac{2\pi}{N} m_3 \\ &= \alpha_y^a(L, L-1, 0), \end{aligned} \tag{B.12}$$

as well as

$$\begin{aligned} \alpha_z^a(L, L, L-1) &= -\alpha_z^a(0, 0, L-1) - \frac{2\pi}{N} (m_1 - m_2) \\ &= -\alpha_z^a(0, L, L-1) - \frac{2\pi}{N} (2m_1 - m_2) \\ &= \alpha_z^a(L, 0, L-1) - \frac{2\pi}{N} m_1. \end{aligned} \tag{B.13}$$

As expected, it follows that the Abelian field strengths $\alpha_{ij}^a(x)$ (4.33) are periodic in the y and z directions, but anti-periodic in the x direction, again with one exception. And that exception is

$$\alpha_{23}(L, L-1, L-1) = -\alpha_{23}(0, L-1, L-1) - \frac{2\pi}{N} 2m_1. \tag{B.14}$$

It is this single plaquette where our single-valued gauge transformation $R(x)$ has moved the net magnetic flux to. It leads to opposite fluxes each of strength $(2\pi/gN)m_1$ through the faces at $x = 0$ and L as illustrated in Figure B.1. For the total flux along the positive x direction, for example, we obtain

$$\begin{aligned} \Phi_+^{(1)} &= -\frac{1}{g} \sum_{r=0}^{L-1} \big(\alpha_y(L, r, 0) + \alpha_z(L, L, r) \\ &\qquad\qquad -\alpha_y(L, r, L) - \alpha_z(L, 0, r)\big) \\ &= \frac{1}{g} \frac{2\pi}{N} m_1. \end{aligned} \tag{B.15}$$

Analogously, we obtain for the total flux in the negative x direction at $x = 0$,

$$\begin{aligned} \Phi_-^{(1)} &= -\frac{1}{g} \big(\alpha_z(0, 0, L-1) - \alpha_z(0, L, L-1)\big) \\ &= \frac{1}{g} \frac{2\pi}{N} m_1 = \Phi_+^{(1)}. \end{aligned} \tag{B.16}$$

The analogous Abelian projected fluxes in the y and z directions are not quantised, because they each involve anti-periodic line segments, but they are both conserved. We have

$$\begin{aligned} \Phi_+^{(2)} &= -\frac{1}{g} \left(2 \sum_{r=0}^{L-1} \alpha_z(0, 0, r) - \frac{2\pi}{N} m_2 \right), \\ &= -\Phi_-^{(2)} \end{aligned} \tag{B.17}$$

and

$$\begin{aligned} \Phi_+^{(3)} &= \frac{1}{g} \left(2 \sum_{r=0}^{L-1} \alpha_y(0, r, 0) + \frac{2\pi}{N} m_3 \right), \\ &= -\Phi_-^{(3)} \end{aligned} \tag{B.18}$$

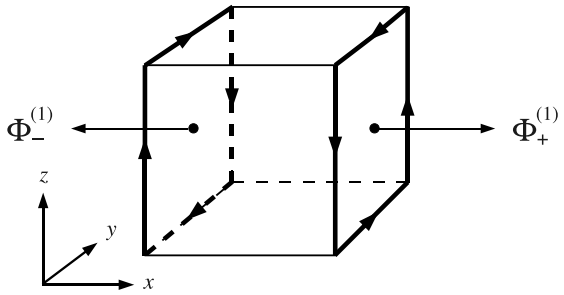

Figure B.1: Quantised Abelian fluxes of equal strength in opposite directions, $\Phi_+^{(1)} = \Phi_-^{(1)}$, with C-periodic x direction.

Therefore, the Abelian projected fluxes in the y and z directions are not quantised but they are conserved, i.e.

$$\Phi_+^{(2)} + \Phi_-^{(2)} = \Phi_+^{(3)} + \Phi_-^{(3)} = 0. \tag{B.19}$$

There is one extra source of strength $2m_1/N$ in units of magnetic charge $(2\pi/g)$ whose entire flux goes along the x direction through the α_{23} plaquettes in the opposite $y = z = L-1$ corners at $x = 0$ and L,

$$Q = \Phi_+^{(1)} + \Phi_-^{(1)} = \frac{2\pi}{g}\,\frac{2m_1}{N}\,, \tag{B.20}$$

again modulo $(4\pi/g)$ and the same for all $a = 1, \ldots N-1$.

It would be interesting if the twist angle in the plane perpendicular to the C-periodic direction were permitted to be a phase other than 0 or π. Unfortunately this is not the case. The proof involves permutations of the twist matrices as before. With C-periodic b.c.'s in the x direction, comparison of

$$\begin{aligned} \Omega_x\Omega_y\Omega_z &= z_{23}\Omega_x\Omega_z\Omega_y \\ &= z_{23}z_{13}\Omega_z^*\Omega_x\Omega_y \\ &= z_{23}z_{13}z_{12}\Omega_z^*\Omega_y^*\Omega_x \end{aligned} \tag{B.21}$$

with

$$\begin{aligned} \Omega_x\Omega_y\Omega_z &= z_{12}\Omega_y^*\Omega_x\Omega_z \\ &= z_{12}z_{13}\Omega_y^*\Omega_z^*\Omega_x \\ &= z_{12}z_{13}z_{32}\Omega_z^*\Omega_y^*\Omega_x \end{aligned} \tag{B.22}$$

yields

$$z_{23} = z_{32} = z_{23}^*. \tag{B.23}$$

Therefore

$$m_1 = \begin{cases} 0 & \text{for odd } N \\ 0 \text{ or } N/2 & \text{for even } N. \end{cases} \tag{B.24}$$

It follows that the allowed charges are exactly those found for fully C-periodic boundary conditions.

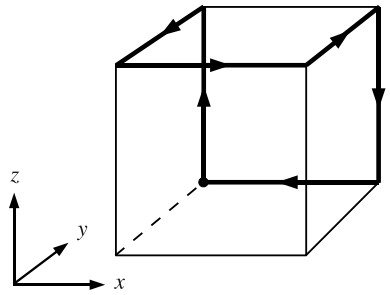

Figure B.2: Integration curve for C-periodic y and z directions.

B.2.2 *y, z directions C-periodic, x direction periodic*

We can also consider boundary conditions with two C-periodic directions, chosen to be the y and z directions. Then the consistency conditions are modified to

$$\begin{aligned} \Omega_x^* \Omega_y &= z_{12} \Omega_y \Omega_x, \\ \Omega_x^* \Omega_z &= z_{13} \Omega_z \Omega_x, \\ \Omega_y^* \Omega_z &= z_{23} \Omega_z^* \Omega_y \end{aligned} \tag{B.25}$$

with $z_{ij} = e^{i\theta_{ij}} \in \mathbb{Z}_N$, $\theta_{ij} = (2\pi/N)\,\epsilon_{ijk} m_k$. The Abelian projected fields inherit boundary conditions with anti-periodicity in both C-periodic directions,

$$\begin{aligned} \alpha_i(x + L\hat{x}) &= \alpha_i(x), \\ \alpha_i(x + L\hat{y}) &= -\alpha_i(x), \\ \alpha_i(x + L\hat{z}) &= -\alpha_i(x), \end{aligned} \tag{B.26}$$

except for the special cases, which in this case are,

$$\begin{aligned} \alpha_y^a(L, L-1, r) &= \alpha_y^a(0, L-1, r) - \frac{2\pi}{N} m_3, \\ \alpha_z^a(L, r, L-1) &= \alpha_z^a(0, r, L-1) + \frac{2\pi}{N} m_2, \\ \alpha_z^a(r, L, L-1) &= -\alpha_z^a(r, 0, L-1) - \frac{2\pi}{N} m_1, \end{aligned} \tag{B.27}$$

for $r = 0, \ldots L-1$, and

$$\begin{aligned} \alpha_y^a(L, L-1, L) &= -\alpha_y^a(0, L-1, 0) + \frac{2\pi}{N} m_3 \\ &= \alpha_y^a(0, L-1, L) + \frac{2\pi}{N} m_3 \\ &= -\alpha_y^a(L, L-1, 0), \end{aligned} \tag{B.28}$$

as well as

$$\begin{aligned} \alpha_z^a(L, L, L-1) &= -\alpha_z^a(0, 0, L-1) - \frac{2\pi}{N} (m_1 + m_2) \\ &= \alpha_z^a(0, L, L-1) - \frac{2\pi}{N} m_2 \\ &= -\alpha_z^a(L, 0, L-1) - \frac{2\pi}{N} m_1. \end{aligned} \tag{B.29}$$

To find the total flux we integrate $\alpha_i^a(x)$ around the curve shown on the right of Figure B.2, and double the result,

$$\begin{aligned} Q &= -\frac{2}{g}\sum_{r=0}^{L-1}\Big(\alpha_z(0,L,r)-\alpha_y(0,r,L)+\alpha_x(r,0,L) \\ &\qquad -\alpha_z(L,L,r)+\alpha_y(L,r,L)-\alpha_x(r,L,0)\Big). \end{aligned}$$

The x links here are translated in two anti-periodic directions relative to one another and hence cancel. The y and z links are related to one another by a single periodic translation along the x direction and therefore also cancel except for contributions from the special links above, which yield

$$\begin{aligned} Q &= -\frac{2}{g}\Big(\alpha_y(L,L-1,L)-\alpha_y(0,L-1,L) \qquad\qquad (B.30) \\ &\qquad -\alpha_z(L,L,L-1)+\alpha_z(0,L,L-1)\Big) \\ &= \frac{2\pi}{g}\frac{2}{N}\big(m_2+m_3\big), \qquad\qquad (B.31) \end{aligned}$$

modulo $(4\pi/g)$ and the same for all $a = 1,\dots N-1$, as before. And as before, we find that the center fluxes in the C-periodic directions are restricted. Comparison of

$$\begin{aligned} \Omega_x^*\Omega_y\Omega_z^* &= z_{32}\Omega_x^*\Omega_z\Omega_y^* \\ &= z_{32}z_{13}\Omega_z\Omega_x\Omega_y^* \\ &= z_{32}z_{13}z_{21}\Omega_z\Omega_y^*\Omega_x^* \end{aligned} \qquad (B.32)$$

with

$$\begin{aligned} \Omega_x^*\Omega_y\Omega_z^* &= z_{12}\Omega_y\Omega_x\Omega_z^* \\ &= z_{12}z_{31}\Omega_y\Omega_z^*\Omega_x^* \\ &= z_{12}z_{31}z_{32}\Omega_z\Omega_y^*\Omega_x^* \end{aligned} \qquad (B.33)$$

now yields

$$z_{21}^2 z_{13}^2 = 1. \qquad (B.34)$$

So,

$$m_2+m_3 = \begin{cases} 0 & \text{for odd } N \\ 0 \text{ or } N/2 & \text{for even } N. \end{cases} \qquad (B.35)$$

Once more, we are left with the same possibilities for the Abelian magnetic charges. We conclude that the allowed charges are identical whether we have one, two, or all three directions charge conjugated.

It is instructive to compare this to the case of standard twisted boundary conditions, without any C-periodic direction, where the analogously defined Abelian projected fluxes are all quantised *and* conserved, i.e. where

$$\Phi_+^{(i)} = -\Phi_-^{(i)} = \frac{1}{g}\frac{2\pi}{N}\,m_i\,, \quad \text{for all } i = 1,2,3. \qquad (B.36)$$

The introduction of one C-periodic direction thus led to non-quantised contributions of Abelian projected flux in the orthogonal directions in addition to the center flux (B.36) of the corresponding sectors with standard twists a la 't Hooft, cf. Eqs. (B.17) and (B.18). These non-quantised contributions are due to the Abelian projection and may not have any physical significance at all. So unlike standard center flux, the flux in the orthogonal directions is no-longer quantised, but like standard center flux it is still conserved.

In contrast, the flux along the C-periodic direction is still quantised in units of center elements, see Eqs. (B.15) and (B.16), but it is no-longer conserved. The introduction of the C-periodic direction has led to a reversal of the center flux when passing through the volume along this direction, by introducing a source of a strength of twice that magnetic flux into the volume.

But this only works for center fluxes with $-m = m$, which can be non-trivial only when -1 is among the roots of unity and N is even. Then however, these particular fluxes are Z_2 valued and do not have a direction. In the pure gauge theory we cannot even distinguish positive from negative flux in this case, which is why we can reverse it without harm in the first place. So for the pure gauge theory we have gained nothing new here. Moreover, 't Hooft's magnetic fluxes as employed here play no role in the deconfinement transition of the pure gauge theory, the free energy of the corresponding center vortices always vanishes in the thermodynamic limit [48].

But together with our adjoint Higgs fields, which have anti-periodic abelian components in such a C-periodic direction, we can distinguish the relative orientations of center vortex and Higgs field as described in Sec. 4.5.2 below. And together with the adjoint Higgs field, the different magnetic sectors have now become relevant – not for confinement in the pure gauge theory, but for the masses of 't Hooft-Polyakov monopoles and the Higgs mechanism.

C

LOW-ENERGY REPRESENTATIONS FROM A LATTICE GUT

The simplest motivation for a compact U(1) is a grand unified theory with Higgs mechanism. Take a toy model with a minimal symmetry breaking breaking,

$$\mathrm{SU}(3) \to \mathrm{SU}(2) \times \mathrm{U}(1)/Z_2, \tag{C.1}$$

for example where the potential for an adjoint SU(3) Higgs field is minimized by an 8-like expectation value

$$\langle \Phi \rangle \propto \mathrm{diag}(1, 1, -2). \tag{C.2}$$

In a lattice formulation (cf. Chapter 4), we can decompose the SU(3) gauge links in unitary gauge to isolate the residual $\mathrm{SU}(2) \times \mathrm{U}(1)/Z_2$ gauge degrees of freedom. Taking the symmetry breaking scale to infinity freezes the Higgs field to the ground state and decouples the off-diagonal massive vector bosons. One ends up with an $\mathrm{SU}(2) \times \mathrm{U}(1)/Z_2$ model that is parametrized by SU(3) matrices.

A general $\mathrm{SU}(2) \times \mathrm{U}(1)/Z_2 \subset \mathrm{SU}(3)$ element is obtained by exponentiating the generators that commute with Φ, which in unitary gauge are

$$\begin{pmatrix} \frac{1}{2}\sigma_i & & \\ & 0 & \\ & & \end{pmatrix}, \quad \begin{pmatrix} 1 & & \\ & 1 & \\ & & -2 \end{pmatrix}. \tag{C.3}$$

The parallel transporters inherited from links in the fundamental representation of SU(3) are

$$\begin{pmatrix} U_\mu e^{i\alpha_\mu} & & \\ & e^{-i2\alpha_\mu} & \end{pmatrix} \in \mathrm{SU}(3),\ U_\mu \in \mathrm{SU}(2),\ \alpha_\mu = [-\pi, \pi) \tag{C.4}$$

The range of angles α_μ was chosen to match our toy models. This is how a 2-color quark field Ψ_q and an 'electron' ψ_e with twice the U(1) charge transform if they are placed in a fundamental triplet representation of SU(3),

$$\begin{pmatrix} \Psi_q \\ \psi_e \end{pmatrix},\ \Psi_q = \begin{pmatrix} \Psi_q^1 \\ \Psi_q^2 \end{pmatrix}. \tag{C.5}$$

Note that nothing represents SU(2) independently. Only parallel transporters corresponding to the matter content inherited from SU(3) representations can be constructed from (C.4). For example, a traced plaquette constructed from (C.4) is of the form

$$\cos \alpha_{\mu\nu} \cdot \mathrm{Re\ tr}\ \square_{col} + \cos\ \alpha_{\mu\nu},\ \square_{col} \in \mathrm{SU}(2), \tag{C.6}$$

where $\alpha_{\mu\nu}$ are the U(1) plaquette angles constructed from α_μ. The first term corresponds to a loop for the fractionally charged quarks, the second is a loop for the

integer charged electron. These are, in fact, possible terms in a U(2) gauge theory that is formulated redundantly using SU(2) and U(1) degrees of freedom. We have the isomorphism,

$$\mathrm{SU}(2) \times \mathrm{U}(1)/Z_2 \simeq \mathrm{U}(2) \subset \mathrm{SU}(3). \tag{C.7}$$

A transformation $(U_\mu, e^{i\alpha_\mu}) \to (-U_\mu, -e^{i\alpha_\mu})$ is not so much a symmetry as it is a change of variables. Nothing represents it, so it may be removed using the invariance of the Haar measure [180].

There is great similarity with the Villain lattice action for $\mathrm{SO}(3) \simeq \mathrm{SU}(2)/Z_2$ gauge theory [161], which is formulated redundantly in terms of $\mathrm{SU}(2)$ and Z_2 variables. Pure SU(2) gauge theory is modified by coupling a Z_2 variable to each fundamental SU(2) plaquette,

$$\square_{Z_2} \cdot \ \mathrm{Re\ tr}\, \square_{col}, \quad \square_{Z_2} = \pm 1 \tag{C.8}$$

such that a center transformation can also becomes a simple change of variables. Both models have the some vortex content, however, which is classified by the homotopy group $\pi_1(\mathrm{SU}(2)/Z_2)$.

As we run to the continuum limit, the coupling constants of the terms (C.6) may separate as they renormalize. Pure U(2) gauge theory has been simulated on the lattice with these two terms in Ref. [181], with the conclusion being that it has the same physical content as the simple product SU(2)×U(1) in the continuum limit. This is to be expected from the decoupling of the 'electromagnetic' term as we run to the continuum limit, see Ref. [180] for details.

The same essential arguments hold for SU(5) GUT. We can only end up with center blind terms in representations of,

$$\mathrm{SU}(3) \times \mathrm{SU}(2) \times \mathrm{U}(1)_Y/Z_6 \subset \mathrm{SU}(5), \tag{C.9}$$

after we freeze out the Higgs field to unitary gauge.

Note that in this 'top down' approach, we have assumed that we are in a given perturbative GUT sector by fixing the Higgs to its expectation value. Topological disorder from the unified theory is not inherited, in this case.

BIBLIOGRAPHY

[1] S. Glashow, Partial Symmetries of Weak Interactions, Nucl. Phys. 22 (1961) 579–588. (Cited on page 1.)

[2] S. Weinberg, A Model of Leptons, Phys. Rev. Lett. 19 (1967) 1264–1266. (Cited on page 1.)

[3] A. Salam, Weak and Electromagnetic Interactions, Conf. Proc. C680519 (1968) 367–377. (Cited on page 1.)

[4] M. Gonzalez-Garcia, Y. Nir, Neutrino masses and mixing: Evidence and implications, Rev. Mod. Phys. 75 (2003) 345–402. arXiv:hep-ph/0202058. (Cited on page 1.)

[5] R. Mohapatra, A. Smirnov, Neutrino Mass and New Physics, Ann. Rev. Nucl. Part. Sci. 56 (2006) 569–628. arXiv:hep-ph/0603118. (Cited on page 1.)

[6] S. Chatrchyan, et al., Observation of a new boson at a mass of 125 GeV with the CMS experiment at the LHC, Phys. Lett. B716 (2012) 30–61. arXiv:1207.7235. (Cited on page 1.)

[7] G. Aad, et al., Observation of a new particle in the search for the Standard Model Higgs boson with the ATLAS detector at the LHC, Phys. Lett. B716 (2012) 1–29. arXiv:1207.7214. (Cited on page 1.)

[8] D. J. Gross, F. Wilczek, Ultraviolet behavior of non-abelian gauge theories, Phys. Rev. Lett. 30 (1973) 1343–1346. (Cited on page 1.)

[9] H. D. Politzer, Reliable perturbative results for strong interactions?, Phys. Rev. Lett. 30 (1973) 1346–1349. (Cited on page 1.)

[10] K. Nakamura, P. D. Group, Review of particle physics, J. Phys. G: Nucl. Part. Phys. 37 (7A) (2010) 075021. (Cited on page 1.)

[11] K. Yagi, T. Hatsuda, Y. Miake, Quark-Gluon Plasma: From Big Bang to Little Bang, Cambridge Monographs on Particle Physics, Nuclear Physics and Cosmology, Cambridge University Press, 2008. (Cited on page 1.)

[12] B. Friman, C. Höhne, J. Knoll, S. Leupold, J. Randrup, R. Rapp, P. Senger (Eds.), The CBM Physics Book, Vol. 814 of Lecture Notes in Physics, Berlin Springer Verlag, 2011. (Cited on page 2.)

[13] J. Greensite, An introduction to the confinement problem, Lect. Notes Phys. 821 (2011) 1–211. (Cited on pages 2, 23, 62, 89, 96, and 101.)

[14] S. Edwards, L. von Smekal, SU(2) lattice gauge theory in 2+1 dimensions: Critical couplings from twisted boundary conditions and universality, Phys. Lett. B681 (2009) 484–490. arXiv:0908.4030. (Cited on pages 2 and 49.)

[15] L. von Smekal, Universal Aspects of QCD-like Theories, Nucl. Phys. Proc. Suppl. 228 (2012) 179–220. arXiv:1205.4205. (Cited on pages 2, 23, and 39.)

[16] N. Strodthoff, S. R. Edwards, L. von Smekal, SU(3) Deconfinement in (2+1)d from Twisted Boundary Conditions and Self-Duality, PoS LATTICE2010 (2010) 288. arXiv:1012.0723. (Cited on pages 2 and 53.)

[17] L. von Smekal, S. R. Edwards, N. Strodthoff, Universal Aspects of Deconfinement: Interfaces, Flux Tubes and Self-Duality in 2+1 Dimensions, PoS LATTICE2010 (2010) 292. arXiv:1012.0408. (Cited on pages 2 and 38.)

[18] S. Edwards, D. B. Mehta, A. Rajantie, L. von Smekal, 't Hooft-Polyakov monopoles in lattice SU(N)+adjoint Higgs theory, Phys. Rev. D80 (2009) 065030. arXiv:0906.5531. (Cited on pages 2 and 65.)

[19] S. R. Edwards, A. Sternbeck, L. von Smekal, Exploring a hidden symmetry with electrically charged quarks, PoS LATTICE2010 (2010) 275. arXiv:1012.0768. (Cited on page 2.)

[20] S. R. Edwards, A. Sternbeck, L. von Smekal, Fractional electric charge and quark confinement, PoS LATTICE2011 (2011) 264. arXiv:1202.1477. (Cited on page 2.)

[21] J. C. Baez, J. P. Muniain, Gauge fields, knots and gravity, Series on Knots and Everything, World Scientific, Singapore, 1994. (Cited on pages 5 and 13.)

[22] C. Baker, D. Doyle, P. Geltenbort, K. Green, M. van der Grinten, et al., An improved experimental limit on the electric dipole moment of the neutron, Phys. Rev. Lett. 97 (2006) 131801. arXiv:hep-ex/0602020. (Cited on page 7.)

[23] C. Becchi, A. Rouet, R. Stora, Renormalization of gauge theories, Ann. Phys. 98 (2) (1976) 287 – 321. (Cited on page 8.)

[24] C. D. Roberts, A. G. Williams, Dyson-Schwinger equations and their application to hadronic physics, Prog. Part. Nucl. Phys. 33 (1994) 477–575. arXiv:hep-ph/9403224. (Cited on page 8.)

[25] R. Alkofer, L. von Smekal, The Infrared behavior of QCD Green's functions: Confinement dynamical symmetry breaking, and hadrons as relativistic bound states, Phys. Rept. 353 (2001) 281. arXiv:hep-ph/0007355. (Cited on page 8.)

[26] C. S. Fischer, Infrared properties of QCD from Dyson-Schwinger equations, J. Phys. G32 (2006) R253–R291. arXiv:hep-ph/0605173. (Cited on page 8.)

[27] C. Wetterich, Exact evolution equation for the effective potential, Phys. Lett. B301 (1993) 90–94. (Cited on page 8.)

[28] J. M. Pawlowski, Aspects of the functional renormalisation group, Ann. Phys. 322 (2007) 2831–2915. arXiv:hep-th/0512261. (Cited on page 8.)

[29] L. von Smekal, Landau Gauge QCD: Functional Methods versus Lattice Simulations, ArXiv e-prints (2008). arXiv:0812.0654. (Cited on page 8.)

[30] L. von Smekal, Lattice BRST without Neuberger 0/0 problem, PoS Confinement X (2012) 68. (Cited on page 8.)

[31] C. Gattringer, C. B. Lang, Quantum chromodynamics on the lattice, Lect. Notes Phys. 788 (2010) 1–211. (Cited on pages 8, 88, 99, and 102.)

[32] H. B. Nielsen, M. Ninomiya, Absence of neutrinos on a lattice (I). Proof by homotopy theory, Nucl. Phys. (1981) 20–40. (Cited on page 11.)

[33] B. Apanasov, Geometry, topology, and physics: proceedings of the first Brazil-USA workshop, held in Campinas, Brazil, June 30-July 7, 1996, [de Gruyter Proceedings in Mathematics] Series, W. de Gruyter, 1997. (Cited on page 13.)

[34] C. Nash, S. Sen, Topology and Geometry for Physicists, Dover Books on Mathematics Series, Dover Publications, 2011. (Cited on page 13.)

[35] G. S. Bali, QCD forces and heavy quark bound states, Phys. Rept. 343 (2001) 1–136. arXiv:hep-ph/0001312. (Cited on pages 15 and 16.)

[36] R. Hagedorn, Statistical thermodynamics of strong interactions at high-energies, Nuovo Cim. Suppl. 3 (1965) 147–186. (Cited on page 16.)

[37] G. 't Hooft, On the phase transition towards permanent quark confinement, Nucl. Phys. B138 (1978) 1. (Cited on page 16.)

[38] B. Svetitsky, L. G. Yaffe, Critical Behavior at Finite Temperature Confinement Transitions, Nucl. Phys. B210 (1982) 423. (Cited on pages 16, 19, and 26.)

[39] J. Liddle, M. Teper, The deconfining phase transition in D=2+1 SU(N) gauge theories, ArXiv e-prints (2008). arXiv:0803.2128. (Cited on pages 16, 17, 31, 35, 53, 54, 56, 57, 58, and 60.)

[40] K. Holland, M. Pepe, U.-J. Wiese, Revisiting the deconfinement phase transition in SU(4) Yang-Mills theory in 2+1 dimensions, JHEP 0802 (2008) 041. arXiv:0712.1216. (Cited on pages 16, 17, 56, 57, 58, 60, and 61.)

[41] P. de Forcrand, O. Jahn, Deconfinement transition in (2+1)-dimensional SU(4) lattice gauge theory, Nucl. Phys. Proc. Suppl. 129 (2004) 709–711. arXiv:hep-lat/0309153. (Cited on pages 16, 17, 55, 56, and 58.)

[42] K. Holland, M. Pepe, U. Wiese, The Deconfinement phase transition in Yang-Mills theory with general Lie group G, Nucl. Phys. Proc. Suppl. 129 (2004) 712–714. arXiv:hep-lat/0309062. (Cited on page 17.)

[43] M. Pepe, Deconfinement in Yang-Mills: A conjecture for a general gauge Lie group G, Nucl. Phys. Proc. Suppl. 141 (2005) 238–243. arXiv:hep-lat/0407019. (Cited on page 17.)

[44] K. Holland, M. Pepe, U. Wiese, The Deconfinement phase transition of Sp(2) and Sp(3) Yang-Mills theories in (2+1)-dimensions and (3+1)-dimensions, Nucl. Phys. B694 (2004) 35–58. arXiv:hep-lat/0312022. (Cited on page 17.)

[45] F. Wu, The Potts model, Rev. Mod. Phys. 54 (1982) 235–268. (Cited on page 17.)

[46] H. J. Rothe, Lattice gauge theories: An introduction, World Sci. Lect. Notes Phys. 74 (2005) 1–605. (Cited on page 18.)

[47] G. 't Hooft, A property of electric and magnetic flux in nonabelian gauge theories, Nucl. Phys. B153 (1979) 141. (Cited on pages 21, 23, 72, and 121.)

[48] L. von Smekal, P. de Forcrand, Electric and magnetic fluxes in SU(2) Yang-Mills theory, Nucl. Phys. Proc. Suppl. 119 (2003) 655–657. arXiv:hep-lat/0209149. (Cited on pages 22 and 135.)

[49] L. von Smekal, P. de Forcrand, O. Jahn, More on Electric and Magnetic Fluxes in SU(2), in: N. Brambilla, G. M. Prosperi (Eds.), Quark Confinement and the Hadron Spectrum V, 2003, pp. 303–305. arXiv:arXiv:hep-lat/0212019. (Cited on page 22.)

[50] P. de Forcrand, L. von Smekal, 't Hooft loops, electric flux sectors and confinement in SU(2) Yang-Mills theory, Phys. Rev. D66 (2002) 011504. arXiv:hep-lat/0107018. (Cited on page 23.)

[51] O. Jahn, O. Philipsen, The Polyakov loop and its relation to static quark potentials and free energies, Phys. Rev. D70 (2004) 074504. arXiv:hep-lat/0407042. (Cited on page 23.)

[52] A. Pelissetto, E. Vicari, Critical phenomena and renormalization group theory, Phys. Rept. 368 (2002) 549–727. arXiv:cond-mat/0012164. (Cited on pages 26, 27, 42, 48, and 60.)

[53] M. Hasenbusch, Monte Carlo simulation with fluctuating boundary conditions, Physica A 197 (1993) 423–435. (Cited on pages 27 and 28.)

[54] M.-C. Wu, M.-C. Huang, Y.-P. Luo, T.-M. Liaw, Coupling-anisotropy and finite-size effects in interfacial tension of the two-dimensional Ising model, J. Phys. A 32 (1999) 4897–4906. (Cited on pages 28, 30, 37, 38, 43, and 44.)

[55] K. Binder, Finite size scaling analysis of Ising model block distribution functions, Z. Phys. B43 (1981) 119–140. (Cited on page 28.)

[56] K. Binder, E. Luijten, Monte Carlo tests of renormalization group predictions for critical phenomena in Ising models, Phys. Rept. 344 (2001) 179–253. (Cited on page 28.)

[57] H. Park, M. den Nijs, Universal finite-size-scaling amplitudes of the Potts model on a torus, Phys. Rev. B38 (1988) 565–579. (Cited on pages 28, 39, 52, and 56.)

[58] K. Kajantie, L. Karkkainen, K. Rummukainen, Tension of the interface between two ordered phases in lattice SU(3) gauge theory, Nucl. Phys. B357 (1991) 693–712. (Cited on page 29.)

[59] P. de Forcrand, M. D'Elia, M. Pepe, A study of the 't Hooft loop in SU(2) Yang-Mills theory, Phys. Rev. Lett. 86 (2001) 1438. arXiv:hep-lat/0007034. (Cited on page 29.)

[60] J. Engels, E. Kehl, H. Satz, B. Waltl, Deconfinement for SU(2) gauge theory in 2+1 dimensions, Phys. Rev. Lett. 55 (1985) 2839. (Cited on pages 30 and 33.)

[61] J. Engels, F. Karsch, E. Laermann, C. Legeland, M. Lutgemeier, et al., A Study of finite temperature gauge theory in (2+1)-dimensions, Nucl. Phys. Proc. Suppl. 53 (1997) 420–422. arXiv:hep-lat/9608099. (Cited on pages 31, 33, 52, and 53.)

[62] M. Teper, The finite-temperature phase transition of SU (2) gauge fields in 2 + 1 dimensions, Phys. Lett. (1993) 417–424. (Cited on pages 31 and 35.)

[63] M. Campostrini, A. Pelissetto, P. Rossi, E. Vicari, Two-point correlation function of three-dimensional O(N) models: The critical limit and anisotropy 57 (1998) 184–210. arXiv:arXiv:cond-mat/9705086. (Cited on page 33.)

[64] M. Caselle, M. Hasenbusch, A. Pelissetto, E. Vicari, Irrelevant operators in the two-dimensional Ising model, J. Phys. A35 (2002) 4861–4888. arXiv:cond-mat/0106372. (Cited on page 33.)

[65] J. Le Guillou, J. Zinn-Justin, Accurate critical exponents from the epsilon expansion, J. Physique Lett. 46 (4) (1985) 137–141. (Cited on page 33.)

[66] M. Barma, M. E. Fisher, Two-dimensional Ising-like systems: Corrections to scaling in the Klauder and double-Gaussian models, Phys. Rev. B31 (1985) 5954–5975. (Cited on page 33.)

[67] P. Calabrese, M. Caselle, A. Celi, A. Pelissetto, E. Vicari, Nonanalyticity of the Callan-Symanzik Beta function of two-dimensional O(N) models, J. Phys. A33 (2000) 8155–8170. arXiv:hep-th/0005254. (Cited on page 33.)

[68] B. Bringoltz, M. Teper, A Precise calculation of the fundamental string tension in SU(N) gauge theories in 2+1 dimensions, Phys. Lett. B645 (2007) 383–388. arXiv:hep-th/0611286. (Cited on pages 35, 54, and 63.)

[69] R. Savit, Duality in field theory and statistical systems, Rev. Mod. Phys. 52 (1980) 453–488. (Cited on page 37.)

[70] A. I. Bugrij, V. N. Shadura, Duality of a two-dimensional nonhomogeneous ising model on a finite lattice, Phys. Rev. B55 (1997) 11045–11048. (Cited on page 38.)

[71] A. I. Bugrij, V. N. Shadura, Duality in 2D Spin Models on Torus, ArXiv High Energy Physics - Theory e-prints (1997). arXiv:arXiv:hep-th/9706045. (Cited on page 39.)

[72] J. Frohlich, J. Fuchs, I. Runkel, C. Schweigert, Duality and defects in rational conformal field theory, Nucl. Phys. B763 (2007) 354–430. arXiv:hep-th/0607247. (Cited on pages 40 and 41.)

[73] J. M. Maldacena, The large N limit of superconformal field theories and supergravity, Adv. Theor. Math. Phys. 2 (1998) 231–252. arXiv:hep-th/9711200. (Cited on page 40.)

[74] P. Ginsparg, Applied Conformal Field Theory, ArXiv High Energy Physics - Theory e-prints (1991). arXiv:arXiv:hep-th/9108028. (Cited on page 40.)

[75] N. Seiberg, E. Witten, Electric - magnetic duality, monopole condensation, and confinement in N=2 supersymmetric Yang-Mills theory, Nucl. Phys. B426 (1994) 19–52. arXiv:hep-th/9407087. (Cited on page 40.)

[76] P. Ruelle, Kramers-Wannier Dualities via Symmetries, Phys. Rev. Lett. 95 (22) (2005) 225701. arXiv:arXiv:cond-mat/0504758. (Cited on page 41.)

[77] C. Schweigert, E. Tsouchnika, Kramers-Wannier dualities for WZW theories and minimal models, Communications in Contemporary Mathematics 10 (05) (2008) 773–789. (Cited on page 41.)

[78] L. Onsager, Crystal statistics. 1. A two-dimensional model with an order disorder transition, Phys. Rev. 65 (1944) 117–149. (Cited on page 42.)

[79] R. Baxter, Exactly solved models in statistical mechanics, Academic Press, 1982. (Cited on pages 47 and 55.)

[80] J. Christensen, G. Thorleifsson, P. H. Damgaard, J. F. Wheater, Thermodynamics of SU(3) lattice gauge theory in (2 + 1) dimensions, Nucl. Phys. (1992) 225–248. (Cited on page 52.)

[81] L. G. Yaffe, Confinement in SU(N) lattice gauge theories, Phys. Rev. D21 (1980) 1574. (Cited on page 52.)

[82] N. Cabibbo, E. Marinari, A New Method for Updating SU(N) Matrices in Computer Simulations of Gauge Theories, Phys. Lett. B119 (1982) 387–390. (Cited on page 52.)

[83] C. Wozar, T. Kaestner, A. Wipf, T. Heinzl, B. Pozsgay, Phase structure of Z(3)-Polyakov-loop models, Phys. Rev. D74 (2006) 114501. arXiv:hep-lat/0605012. (Cited on pages 55 and 62.)

[84] B. Lucini, M. Teper, Confining strings in SU(N) gauge theories, Phys. Rev. D64 (2001) 105019. arXiv:hep-lat/0107007. (Cited on page 63.)

[85] M. Teper, Large N and confining flux tubes as strings - a view from the lattice, Acta Phys. Polon. B40 (2009) 3249–3320. arXiv:0912.3339. (Cited on page 63.)

[86] A. Athenodorou, B. Bringoltz, M. Teper, Closed flux tubes and their string description in D=2+1 SU(N) gauge theories, JHEP 1105 (2011) 042. arXiv:1103.5854. (Cited on page 63.)

[87] M. Caselle, P. Grinza, On the intrinsic width of the chromoelectric flux tube in finite temperature LGTs, JHEP 1211 (2012) 174. arXiv:1207.6523. (Cited on page 63.)

[88] F. Gliozzi, M. Pepe, U.-J. Wiese, Linear Broadening of the Confining String in Yang-Mills Theory at Low Temperature, JHEP 1101 (2011) 057. arXiv:1010.1373. (Cited on page 63.)

[89] A. S. Kronfeld, U. J. Wiese, SU(N) gauge theories with C periodic boundary conditions. 1. Topological structure, Nucl. Phys. B357 (1991) 521–533. (Cited on pages 63, 71, 72, 73, 74, and 129.)

[90] U.-J. Wiese, C- and G-periodic QCD at finite temperature, Nucl. Phys. (1992) 45–66. (Cited on page 63.)

[91] K. A. Milton, G. R. Kalbfleisch, W. Luo, L. Gamberg, Theoretical and experimental status of magnetic monopoles, Int. J. Mod. Phys. A17 (2002) 732–750. arXiv:hep-ph/0111062. (Cited on page 65.)

[92] C. Montonen, D. Olive, Magnetic monopoles as gauge particles?, Phys. Lett. (1977) 117–120. (Cited on page 65.)

[93] P. A. M. Dirac, Quantised singularities in the electromagnetic field, Proc. Roy. Soc. Lond. A133 (1931) 60–72. (Cited on pages 65 and 91.)

[94] R. F. Dashen, B. Hasslacher, A. Neveu, Nonperturbative methods and extended hadron models in field theory. 2. two-dimensional models and extended hadrons, Phys. Rev. D10 (1974) 4130–4138. (Cited on page 65.)

[95] A. I. Veselov, M. I. Polikarpov, M. N. Chernodub, Monopole order parameter in SU(2) lattice gauge theory, J. Exp. Theor. Phys. 63 (1996) 411–416. (Cited on page 65.)

[96] L. Del Debbio, A. Di Giacomo, G. Paffuti, Detecting dual superconductivity in the ground state of gauge theory, Phys. Lett. B349 (1995) 513–518. arXiv:hep-lat/9403013. (Cited on page 65.)

[97] J. Frohlich, P. A. Marchetti, Gauge-invariant charged, monopole and dyon fields in gauge theories, Nucl. Phys. B551 (1999) 770–812. arXiv:hep-th/9812004. (Cited on page 65.)

[98] J. Smit, A. van der Sijs, Monopoles and confinement, Nucl. Phys. B355 (1991) 603–648. (Cited on page 65.)

[99] J. Smit, A. J. van der Sijs, A Magnetic monopole in pure SU(2) gauge theory, Nucl. Phys. B422 (1994) 349–381. arXiv:hep-lat/9312087. (Cited on page 65.)

[100] A. C. Davis, T. W. B. Kibble, A. Rajantie, H. Shanahan, Topological defects in lattice gauge theories, JHEP 11 (2000) 010. arXiv:hep-lat/0009037. (Cited on pages 65, 71, and 82.)

[101] A. C. Davis, A. Hart, T. W. B. Kibble, A. Rajantie, The monopole mass in the three-dimensional georgi-glashow model, Phys. Rev. D65 (2002) 125008. arXiv:hep-lat/0110154. (Cited on pages 65 and 71.)

[102] A. Rajantie, Mass of a quantum 't Hooft-Polyakov monopole, JHEP 01 (2006) 088. arXiv:hep-lat/0512006. (Cited on pages 65 and 71.)

[103] G. 't Hooft, Magnetic monopoles in unified gauge theories, Nucl. Phys. B79 (1974) 276–284. (Cited on page 66.)

[104] G. 't Hooft, Topology of the gauge condition and new confinement phases in non-abelian gauge theories, Nucl. Phys. (1981) 455–478. (Cited on page 68.)

[105] A. S. Kronfeld, G. Schierholz, U.-J. Wiese, Topology and dynamics of the confinement mechanism, Nucl. Phys. (1987) 461–478. (Cited on page 69.)

[106] J. Ambjorn, H. Flyvbjerg, 't Hooft's nonabelian magnetic flux has zero classical energy, Phys. Lett. B97 (1980) 241. (Cited on page 72.)

[107] J. Ambjorn, J. Giedt, J. Greensite, Vortex structure vs. monopole dominance in abelian projected gauge theory, JHEP 02 (2000) 033. arXiv:hep-lat/9907021. (Cited on page 74.)

[108] M. N. Chernodub, R. Feldmann, E.-M. Ilgenfritz, A. Schiller, Monopole chains in the compact Abelian Higgs model with doubly-charged matter field, Phys. Lett. (2005) 161–168arXiv:arXiv:hep-lat/0406015. (Cited on page 74.)

[109] P. de Forcrand, M. Pepe, Center vortices and monopoles without lattice gribov copies, Nucl. Phys. B598 (2001) 557–577. arXiv:hep-lat/0008016. (Cited on pages 74 and 75.)

[110] H. Reinhardt, Topology of center vortices, Nucl. Phys. B628 (2002) 133–166. arXiv:hep-th/0112215. (Cited on page 74.)

[111] J. M. Cornwall, Center vortices, nexuses, and fractional topological charge, Phys. Rev. D61 (2000) 085012. arXiv:hep-th/9911125. (Cited on page 74.)

[112] J. M. Cornwall, Nexus solitons in the center vortex picture of QCD, Phys. Rev. D58 (1998) 105028. arXiv:hep-th/9806007. (Cited on page 74.)

[113] J. M. Cornwall, On topological charge carried by nexuses and center vortices, Phys. Rev. D65 (2002) 085045. arXiv:hep-th/0112230. (Cited on page 74.)

[114] D. Tong, Quantum vortex strings: A review, Ann. Phys. 324 (2009) 30–52. arXiv:0809.5060. (Cited on page 74.)

[115] J. Greensite, The confinement problem in lattice gauge theory, Prog. Part. Nucl. Phys. 51 (2003) 1. arXiv:hep-lat/0301023. (Cited on page 74.)

[116] J. C. Vink, U.-J. Wiese, Gauge fixing on the lattice without ambiguity, Phys. Lett. B289 (1992) 122–126. arXiv:hep-lat/9206006. (Cited on page 74.)

[117] A. J. van der Sijs, Laplacian Abelian Projection, Nucl. Phys. B (Proc. Suppl.) 53 (1997) 535–537. arXiv:arXiv:hep-lat/9608041. (Cited on page 74.)

[118] A. J. V. D. Sijs, Abelian Projection without Ambiguities, Prog. Theor. Phys. Suppl. 131 (1998) 149–159. arXiv:arXiv:hep-lat/9803001. (Cited on page 74.)

[119] L. Polley, U. J. Wiese, Monopole condensate and monopole mass in U(1) lattice gauge theory, Nucl. Phys. B356 (1991) 629–654. (Cited on page 84.)

[120] Y. Aoki, G. Endrodi, Z. Fodor, S. Katz, K. Szabo, The order of the quantum chromodynamics transition predicted by the standard model of particle physics, Nature 443 (2006) 675–678. arXiv:hep-lat/0611014. (Cited on page 87.)

[121] S. Borsányi, Z. Fodor, C. Hoelbling, S. D. Katz, S. Krieg, C. Ratti, K. K. Szabó, Is there still any T $_c$ mystery in lattice QCD? Results with physical masses in the continuum limit III, JHEPs 9 (2010) 73. arXiv:1005.3508. (Cited on page 87.)

[122] A. Bazavov, P. Petreczky, HotQCD Collaboration, Deconfinement and chiral transition with the highly improved staggered quark (HISQ) action, J. Phys.: Conf. Ser. 230 (1) (2010) 012014. arXiv:1005.1131. (Cited on page 87.)

[123] M. L. Perl, E. R. Lee, D. Loomba, Searches for Fractionally Charged Particles, Annu. Rev. Nucl. Part. Sci. 59 (2009) 47–65. (Cited on page 87.)

[124] A. Di Giacomo, Confinement in QCD: Results and open problems, Acta Phys. Polon. B36 (2005) 3723–3750. arXiv:hep-lat/0510065. (Cited on page 87.)

[125] J. Greensite, K. Langfeld, S. Olejnik, H. Reinhardt, T. Tok, Color Screening, Casimir Scaling, and Domain Structure in G(2) and SU(N) Gauge Theories, Phys. Rev. D75 (2007) 034501. arXiv:hep-lat/0609050. (Cited on page 89.)

[126] L. Liptak, S. Olejnik, Casimir scaling in G(2) lattice gauge theory, Phys. Rev. D78 (2008) 074501. arXiv:0807.1390. (Cited on page 89.)

[127] S. Deldar, H. Lookzadeh, S. M. H. Nejad, Confinement in G(2) Gauge Theories Using Thick Center Vortex Model and domain structures, Phys. Rev. D85 (2012) 054501. arXiv:1112.4963. (Cited on page 89.)

[128] T. Kugo, I. Ojima, Local Covariant Operator Formalism of Non-Abelian Gauge Theories and Quark Confinement Problem, Prog. Theor. Phys. Suppl. 66 (1979) 1–130. (Cited on page 90.)

[129] S. Elitzur, Impossibility of spontaneously breaking local symmetries, Phys. Rev. D12 (1975) 3978–3982. (Cited on page 90.)

[130] W. Caudy, J. Greensite, On the ambiguity of spontaneously broken gauge symmetry, Phys. Rev. D78 (2008) 025018. arXiv:0712.0999. (Cited on page 90.)

[131] J. Greensite, B. Lucini, Is Confinement a Phase of Broken Dual Gauge Symmetry?, Phys. Rev. D78 (2008) 085004. arXiv:0806.2117. (Cited on page 90.)

[132] J. Preskill, Magnetic monopoles, Ann. Rev. Nucl. Part. Sci. 34 (1984) 461–530. (Cited on pages 91, 93, 116, and 117.)

[133] M. Creutz, Are magnetic monopoles hadrons?, Nucl. Phys. Proc. Suppl. 140 (2005) 597–599. arXiv:hep-lat/0408013. (Cited on page 91.)

[134] C. Geng, R. Marshak, Uniqueness of quark and lepton representations in the Standard Model from the anomalies viewpoint, Phys. Rev. D39 (1989) 693. (Cited on page 92.)

[135] C. Q. Geng, Anomaly, Charge Quantization and Family, in: X.-Q. Luo, E. B. Gregory (Eds.), Non-Perturbative Methods and Lattice QCD, 2001, pp. 294–300. arXiv:arXiv:hep-ph/0101329. (Cited on page 92.)

[136] E. Witten, An SU(2) Anomaly, Phys. Lett. B117 (1982) 324–328. (Cited on page 92.)

[137] H. Georgi, S. L. Glashow, Unity of all elementary-particle forces, Phys. Rev. Lett. 32 (1974) 438–441. (Cited on page 93.)

[138] J. C. Baez, J. Huerta, The Algebra of Grand Unified Theories, Bull. Am. Math. Soc. 47 (2010) 483–552. arXiv:0904.1556. (Cited on page 93.)

[139] S. Friederich, Gauge symmetry breaking in gauge theories: in search of clarification., Eur. J. Phil. Sci. (2012) 1–26. (Cited on page 93.)

[140] J. C. Pati, Discovery of proton decay: A Must for theory, a challenge for experiment, AIP Conf. Proc. 533 (2000) 37–53. arXiv:hep-ph/0005095. (Cited on page 95.)

[141] P. de Forcrand, O. Jahn, Vortex free energies in SO(3) and SU(2) lattice gauge theory, Nucl. Phys. Proc. Suppl. 119 (2003) 649–651. arXiv:hep-lat/0209060. (Cited on page 95.)

[142] P. de Forcrand, O. Jahn, SO(3) versus SU(2) lattice gauge theory. arXiv:hep-lat/0205026. (Cited on page 95.)

[143] P. de Forcrand, O. Jahn, Comparison of SO(3) and SU(2) lattice gauge theory, Nucl. Phys. B651 (2003) 125–142. arXiv:hep-lat/0211004. (Cited on page 95.)

[144] A. Barresi, G. Burgio, M. Muller-Preussker, SO(3) Yang-Mills theory on the lattice, Nucl. Phys. Proc. Suppl. 119 (2003) 571–573. arXiv:hep-lat/0209011. (Cited on page 95.)

[145] L. von Smekal, T. Tok, P. de Forcrand, A Toy model of (grand) unified monopoles, PoS LAT2005 (2006) 314. arXiv:hep-lat/0509147. (Cited on page 96.)

[146] L. von Smekal, Confinement and unification constraints for topological defects, Nucl. Phys. Proc. Suppl. 161 (2006) 230–237. (Cited on page 96.)

[147] M. Kleman, O. D. Lavrentovich, Topological point defects in nematic liquid crystals, Philos. Mag. 86 (2006) 4117–4137. (Cited on page 97.)

[148] D. J. Callaway, A. Rahman, Lattice gauge theory in microcanonical ensemble, Phys. Rev. D28 (1983) 1506. (Cited on page 99.)

[149] N. Metropolis, A. Rosenbluth, M. Rosenbluth, A. Teller, E. Teller, Equation of state calculations by fast computing machines, J. Chem. Phys. 21 (1953) 1087–1092. (Cited on page 100.)

[150] A. Young, Spin Glasses and Random Fields, Directions in Condensed Matter Physics, World Scientific, 1998. (Cited on page 101.)

[151] M. P. Nightingale, E. Granato, J. M. Kosterlitz, Conformal anomaly and critical exponents of the XY ising model, Phys. Rev. B52 (1995) 7402–7411. (Cited on page 101.)

[152] R. Peccei, H. R. Quinn, Constraints Imposed by CP Conservation in the Presence of Instantons, Phys. Rev. D16 (1977) 1791–1797. (Cited on page 101.)

[153] T.-H. Han, J. S. Helton, S. Chu, D. G. Nocera, J. A. Rodriguez-Rivera, C. Broholm, Y. S. Lee, Fractionalized excitations in the spin-liquid state of a kagome-lattice antiferromagnet, Nature 492 (7429) (2012) 406–410. (Cited on page 101.)

[154] S. Nakatsuji, K. Kuga, K. Kimura, R. Satake, N. Katayama, E. Nishibori, H. Sawa, R. Ishii, M. Hagiwara, F. Bridges, T. U. Ito, W. Higemoto, Y. Karaki, M. Halim, A. A. Nugroho, J. A. Rodriguez-Rivera, M. A. Green, C. Broholm, Spin-Orbital Short-Range Order on a Honeycomb-Based Lattice, Science 336 (2012) 559–. (Cited on page 101.)

[155] A. Hoferichter, V. Mitrjushkin, M. Muller-Preussker, T. Neuhaus, H. Stuben, Compact lattice QED with Wilson fermions, Nucl. Phys. B434 (1995) 358–382. arXiv:hep-lat/9408014. (Cited on page 101.)

[156] N. Zverev, Algorithmic studies of compact lattice QED with Wilson fermions, Ph.D. Thesis, Humboldt University of Berlin (2001). (Cited on page 101.)

[157] J. Foley, K. Jimmy Juge, A. O'Cais, M. Peardon, S. M. Ryan, et al., Practical all-to-all propagators for lattice QCD, Comput. Phys. Commun. 172 (2005) 145–162. arXiv:hep-lat/0505023. (Cited on page 102.)

[158] J.-I. Skullerud, S. Ejiri, S. Hands, L. Scorzato, Lattice simulations of two color QCD with Wilson fermions, Prog. Theor. Phys. Suppl. 153 (2004) 60–68. arXiv:hep-lat/0312002. (Cited on page 104.)

[159] S. Aoki, New phase structure for lattice QCD with Wilson fermions, Phys. Rev. D30 (1984) 2653–2663. (Cited on page 106.)

[160] F. Wegner, Duality in generalized Ising models and phase transitions without local order parameters, J. Math. Phys. 12 (1971) 2259–2272. (Cited on page 107.)

[161] S. Datta, R. Gavai, Z(2) monopoles, vortices, and the deconfinement transition in mixed action SU(2) gauge theory, Phys. Rev. D62 (2000) 054512. arXiv:hep-lat/9909139. (Cited on pages 109, 110, and 138.)

[162] J. Greensite, K. Langfeld, private communication (2012). (Cited on pages 113 and 114.)

[163] K. Osterwalder, E. Seiler, Gauge field theories on a lattice, Ann. Phys. 110 (1978) 440–471. (Cited on page 113.)

[164] E. H. Fradkin, S. H. Shenker, Phase Diagrams of Lattice Gauge Theories with Higgs Fields, Phys. Rev. D19 (1979) 3682. (Cited on page 113.)

[165] M. Creutz, L. Jacobs, C. Rebbi, Monte carlo study of abelian lattice gauge theories, Phys. Rev. D20 (1979) 1915–1922. (Cited on page 115.)

[166] S. Kim, J. B. Kogut, M.-P. Lombardo, On the triviality of textbook quantum electrodynamics, Phys. Lett. B502 (2001) 345–349. arXiv:hep-lat/0009029. (Cited on page 116.)

[167] S. Kim, J. B. Kogut, M.-P. Lombardo, Gauged Nambu-Jona-Lasinio studies of the triviality of quantum electrodynamics, Phys. Rev. D65 (2002) 054015. arXiv:hep-lat/0112009. (Cited on page 116.)

[168] B. L. G. Bakker, A. I. Veselov, M. A. Zubkov, Standard model with the additional Z(6) symmetry on the lattice, Phys. Lett. B620 (2005) 156–163. arXiv:hep-lat/0502006. (Cited on page 117.)

[169] B. L. G. Bakker, A. I. Veselov, M. A. Zubkov, Nambu monopoles in lattice electroweak theory, J. Phys. G: Nucl. Part. Phys. 36 (7) (2009) 075008. arXiv:0809.1757. (Cited on page 117.)

[170] B. L. G. Bakker, A. I. Veselov, M. A. Zubkov, Lattice study of monopoles in the Electroweak theory, ArXiv e-prints (2007). arXiv:0708.2864. (Cited on page 117.)

[171] J. Zurita, SUSY confronts LHC data, ArXiv e-prints (2012). arXiv:1212.1662. (Cited on page 117.)

[172] S. Raby, Searching for the Standard Model in the String Landscape: SUSY GUTs, Rept. Prog. Phys. 74 (2011) 036901. arXiv:1101.2457. (Cited on page 117.)

[173] K. Hwang, T. Dodds, S. Bhattacharjee, Y. B. Kim, Three-dimensional nematic spin liquid in the stacked triangular lattice 6H-B structure, ArXiv e-prints (2012). arXiv:1212.1470. (Cited on page 117.)

[174] A. Hart, B. Lucini, Z. Schram, M. Teper, Vortices and confinement in hot and cold d = 2+1 gauge theories, JHEP 06 (2000) 040. arXiv:hep-lat/0005010. (Cited on pages 121, 122, 123, and 126.)

[175] M. Teper, The Confining string and its tension for SU(2) gauge fields in (2+1)-dimensions, Phys. Lett. B311 (1993) 223–229. (Cited on page 122.)

[176] M. Caselle, A. D'Adda, The Spatial string tension in high temperature lattice gauge theories, Nucl. Phys. B427 (1994) 273–290. arXiv:hep-lat/9403027. (Cited on page 122.)

[177] P. de Forcrand, B. Lucini, M. Vettorazzo, Measuring interface tensions in 4d SU(N) lattice gauge theories, Nucl. Phys. Proc. Suppl. 140 (2005) 647–649. arXiv:hep-lat/0409148. (Cited on page 123.)

[178] J. D. Stack, M. Stone, Elementary derivation of the universal attractive Coulomb term in the interquark potential, Phys. Lett. B100 (1981) 476. (Cited on page 125.)

[179] C. Korthals Altes, A. Michels, M. Stephanov, M. Teper, Domain walls and perturbation theory in high-temperature gauge theory: SU(2) in 2+1 dimensions 55 (1997) 1047–1071. arXiv:arXiv:hep-lat/9606021. (Cited on page 125.)

[180] P. Scior, Fractional charge and confinement of quarks, Master's thesis, Technische Universitaet Darmstadt (2012). (Cited on page 138.)

[181] C. Roiesnel, On the U(2) Lattice Gauge Theory, ArXiv High Energy Physics - Lattice e-prints (1995). arXiv:arXiv:hep-lat/9509092. (Cited on page 138.)

ACKNOWLEDGMENTS

First of all I must thank my beautiful Angela, who moved with me to Germany. Without her patience, compromises, and support, I would have never made it this far.

I also send a heartfelt thanks to Lorenz von Smekal, who has provided years of encouragement, mentoring, and friendship. Not only did he make a place for me in his research, but he also welcomed me into his home as an expatriate. When I reminisce about life in Germany, my time in Reinheim will always conjure a special affection.

A chronological thanks to my other collaborators over these years - Dhagash Mehta, Arttu Rajantie, Andre Sternbeck, Nils Strodthoff, Jeff Greensite, and Kurt Langfeld, as well as Johannes Weyrich and Philipp Scior. Our models did not always yield the results that we were hoping for, but it was always a pleasure working with you. Here I would also like to thank Philippe de Forcrand and Axel Maas for taking an interest in our work and for providing enlightening and encouraging discussions.

Thanks to Jochen Wambach, for helping me to join the institute from Adelaide and for kindly sacrificing his time to referee this dissertation. I am also grateful for the generous support provided by the Helmholtz Graduate School for Hadron and Ion Research.

Thanks to the Darmstadt crew of foreigners. We built a family, somehow. For now we've gone our separate ways - hopefully not forever. At least we'll always have a good excuse to jump on Steam.

Thanks to my Australian family for endless encouragement via Skype, especially in the dark times of thesis writing. I can't wait to see you all in person.

CURRICULUM

Name:	Samuel Ryan Edwards
Date of birth:	9. January 1985
Place of birth:	Adelaide (South Australia), Australia
Citizenship:	Australian

1998-2002	St.Ignatius College, South Australia, Australia
11/2002	High school diploma. Overall performance: 100/100
12/2005	Bachelor of Science (Theoretical Physics), University of Adelaide.
12/2007	Honors Degree of Bachelor of Science with First Class Honors (Physics), University of Adelaide.
7/2009-02/2013	Graduate study in physics, Institut für Kernphysik, TU Darmstadt.